DESIGN OF A MODULATED BEAM MASS SPECTROMETRY SYSTEM AND ITS APPLICATION TO THE PREPARATION OF ZINC SULPHOSELENIDE ALLOYS USING MBE

A thesis submitted to the University of Manchester for the degree of Doctor of Philosophy in the Faculty of Science

by

MOHAMMED BENYEZZAR B.Sc, M.Sc

September 1990

Department of Electrical Engineering

ProQuest Number: 13894539

All rights reserved

INFORMATION TO ALL USERS
The quality of this reproduction is dependent upon the quality of the copy submitted.

In the unlikely event that the author did not send a complete manuscript
and there are missing pages, these will be noted. Also, if material had to be removed,
a note will indicate the deletion.

ProQuest 13894539

Published by ProQuest LLC (2019). Copyright of the Dissertation is held by the Author.

All rights reserved.
This work is protected against unauthorized copying under Title 17, United States Code
Microform Edition © ProQuest LLC.

ProQuest LLC.
789 East Eisenhower Parkway
P.O. Box 1346
Ann Arbor, MI 48106 – 1346

Th16233

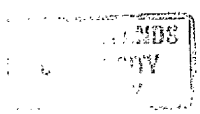

TABLE OF CONTENTS

ABSTRACT

This thesis describes the development of a computer controlled modulated beam mass spectrometry system and its application to the preparation of zinc sulphoselenide alloy films using molecular beam epitaxy.

Chapter 1 introduces the aims of the project and the background of the present work is described. The main investigations presented in the thesis are outlined.

A literature review is presented in chapters 2 and 3. The controlled vapourization of materials from effusion cells and on-line monitoring and control techniques for effusion cells are discussed. Emphasis is placed on the use of zinc sulphoselenide alloys, source temperature control, and vapour flux monitoring and control employing mass spectrometers and microbalances. The aim of these two chapters is to establish the methods adopted for vapour flux and source temperature control as well as showing the need for the work undertaken to provide facilities for the production of zinc sulphoselenide alloy films.

The design features of the modulated beam mass spectrometry system are described in chapter 4. The instrumentation constructed and the method adopted for the system computer control are outlined.

Chapter 5 discusses the characterization of the modulated beam mass spectrometry equipment and the optimum conditions for operation during a deposition are considered.

An account of an investigation into the ionization processes occuring in the mass spectrometer ionization chamber during the evaporation of ZnS and ZnSe is given in chapter 6.

Time-of-flight analysis for particles in the vapour streams emanating from the ZnS and ZnSe sources is described in chapter 7.

A study of the evaporation kinetics of ZnS and ZnSe is presented in chapter 8. The relationship between measurements on isotopic species, deposition rate and number densities are also described.

Chapter 9 outlines initial results obtained from growing zinc sulphoselenide alloy films with a pre-determined composition profile using techniques developed during the research.

A conclusion to the investigations described in the thesis is presented in chapter 10 and suggestions are made for future work.

DECLARATION

No portion of the work refered to in this thesis has been submitted in support of an application for another degree or qualification from this or any another university or institution of learning.

TO MY PARENTS

PREFACE

The author graduated from the University of Constantine (Algeria) in 1983 with a degree of B.Sc. in Physics of Solids. In 1984 he obtained the Joint Matriculation Board certificate in English. He began research in the Department of Electrical Engineering of The University of Manchester afterwards where he obtained the degree of Master of Science in 1986. In 1987 he began the research described in this thesis being financially supported by the Algerian Ministery of Higher research.

AKNOWLEDGEMENTS

The work carried out in this thesis was under the supervision of Dr. D.King whose guidance and assistance is greatfully appreciated. The author wishes to express his thanks to Professor P.G.Farrell for providing the facilities within The Electrical Engineering Department of The University of Manchester, which enabled the work described in this thesis to be conducted.

The assistance of other members of staff in particular D.Moore and D.Sutton is greatfully aknowledged as well as the assistance of S.Hibbert (Centre for Surface and Materials Analysis, UMIST) in the SIMS analysis of zinc sulphoselenide samples. The author would also like to thank the technical staff and research students for their friendship and assistance.

LIST OF SYMBOLS

Where not specified the following symbols should be assumed to represent the following quantities:

Å	:	Angstroem
a.m.u	:	Atomic mass unit
CK	:	clock
EMV	:	Electron multiplier voltage
Fm	:	Modulation frequency
fs	:	Femtosecond
Hz	:	Hertz
K	:	Boltzmann's constant
KV	:	Kilovolt
m/e	:	mass-to-charge ratio
pm	:	Picometer
q	:	Electrical charge
QMS	:	Quadrupole mass spectrometer
R	:	gas constant
RAM	:	Random-access-memory
ROM	:	Read-only-memory
rpm	:	Revolutions per minute
T	:	Temperature
TOF	:	Time-of-flight
Tm	:	Modulation period
Tw	:	Width of time window
UHV	:	Ultra high vacuum
⏚	:	Analogue ground
△	:	Difference
⏚	:	Digital ground
§	:	Refer to

CHAPTER 1

INTRODUCTION

This thesis describes the design of a computer controlled modulated beam mass spectrometry system and its subsequent use for the study of the evaporation and deposition of zinc selenide and zinc sulphide compounds on a gallium arsenide substrate using molecular beam epitaxy.

1.1 OBJECTIVES AND AIMS OF THE PROJECT

The project was started in response to the requirement for film structures suitable for integrated optic devices. Jones et al [1.1] have shown that low-loss waveguides can be produced if an optical buffer layer is placed at the interface between the wave guide and the substrate. To obtain lowest loss it proves necessary to use graded refractive index material at the interface and this introduces the requirement to prepare zinc sulphoselenide films with a composition which varies as a function of

distance from the substrate interface.

Producing a defined profile for film constituents requires high accuracy monitoring and control over the vapour species depositing on the substrate. This leads to the need for precision techniques for monitoring and controlling the system employed. Extensive use is made of computers in controlling the film composition from measurements made on number densities for vapour particles impinging on the substrate surface.

Study of the evaporant particles involved leads to the determination of the critical role of growth related parameters including substrate preparation, source conditioning, growth rate and substrate temperature. Before films with a pre-determined concentration profile can be produced the evaporation and deposition characteristics of ZnS and ZnSe compound materials have to be investigated and the information obtained exploited to obtain the wanted composition profiles. An objective of the present work is to provide a systematic approach enabling the computer controlled growth of zinc sulphoselenide alloy films using modulated beam mass spectrometry techniques.

1.2 PROBLEMS ENCOUNTERED IN PREVIOUSLY REPORTED RESEARCH

Most of the previous work undertaken by authors using

the present MBE deposition system involved the use of a single vapour source for the evaporation of zinc selenide [1.2] or the study of the thermal characteristics of the vapour sources [1.3] for temperature control purposes. This means that the study of zinc selenide and zinc sulphide using two compound sources is still required so that the growth of zinc sulphoselenide alloys can be undertaken.

During the study of zinc selenide evaporation, high background pressures for zinc particles were reported [1.4]. This interfered with the measurement of number density for particles using a quadrupole mass spectrometer.

Difficulties were also encountered in relating the measured number densities to the deposition rate measured using a quartz crystal microbalance. This can be quite detrimental when using the mass spectrometer as a sensing device and calculations of the power fed to vapour sources are used to deposit a pre-determined alloy composition profile.

The presence of substantial numbers of background evaporant particles lead to further difficulties in characterizing the evaporation of zinc selenide, including inconclusive results in observing congruency during the evaporation of ZnSe because the particle densities in the vapour stream could not be extracted from the observations made using the mass spectrometer.

Cryopanelling is used throughout the system and this helps with reducing considerably the contribution from background vapours to the measured number densities. Similar effects have been reported by Arthur [1.5] during the monitoring of arsenic vapours.

Attempts to remove the background vapour's contribution from the measured number density by comparing the measurements taken by opening and closing the source shutter proved unsuccessful because of the time elapsing between the measurements and the movement of a manually operated shutter. Interruption of the evaporant stream with a relatively slow shutter can not provide an accurate measurement of the background zinc particle density because of the relatively short lifetime of particles before they become trapped by the walls of the cryopanels. The main ion pump in the system also leads to a reduction in the concentration of background vapours but is of less significance.

It is difficult to predict whether particles other than zinc (like those of selenium) have substantial background pressures during the evaporation of compound ZnSe. The decay on the number densities for these particles may be shorter than the time taken for closing the shutter and taking the measurements.

During the study of arsenic vapour streams early workers [1.6, 1.7] did not recognize the necessity to distinguish between the vapour stream constituents and the background gases. Arthur [1.5, 1.8] suggested that some of the arsenic vapour was originating from the interaction of vapour with the walls of the vacuum system and surrounded the mass spectrometer ionization chamber with cryopanels. Improvements on his experimental method were described by Murray et al [1.9] and Pupp et al [1.10] involved the use of more efficient cryopanelling and the provision of a movable collimating slit which restricted the impinging molecular beam. By measuring the beam intensity as a function of position of the slit they were able to distinguish to some extent, between different sources of particular vapour species. Foxon et al [1.11] applied a modulated beam mass spectrometry technique to the evaporation of GaAs and helped eliminate ambiguities experienced by earlier workers because of the detection of background species.

1.3 WORK UNDERTAKEN FOR THE PRESENT INVESTIGATIONS

1.3.1 USE OF MODULATED BEAM MASS SPECTROMETRY

In the modulated beam mass spectrometry technique developed the molecular beam entering the ionization chamber of the quadrupole mass spectrometer is modulated by a mechanical chopper. The resulting time varying signal from the

spectrometer is detected synchronously using a phase sensitive amplifier. The beam of evaporant particles is modulated but the background is not since it propagates omni-directionally inside the vacuum system. This method has been extensively reviewed in previous work [1.12].

Modulation of the molecular beam is carried out using an 8 bladed stainless steel chopper with a one-to-one mark-to-space ratio driven by a synchronous motor. Similar vapour stream modulators, but with a different number of blades, have been used by other authors [1.13, 1.14]. The use of variable mark to space ratios for the chopper blades has been discussed by Aldridge [1.15]. Other molecular beam choppers involving electromagnetic reeds [1.16, 1.17] have also been described.

Mechanical modulation of particle beams has been used for numerous studies including the ionization of hydrogen molecules [1.18], a study of carbon combustion at high temperatures [1.19, 1.20] and for the measurement of particle speed distributions [1.21]. The technique has also been used for studying the evaporation of III-V compounds [1.22, 1.23], as well as for surface kinetic studies for GaAs reactions with a substrate surface [1.24]. Recent literature [1.25], [1.26] has given an account of the technique used in desorption studies.

In this thesis, the modulated beam mass spectrometry technique is used to control the vapour fluxes entering a quadrupole mass spectrometer. The spectrometer has a crossed-beam ionization chamber and this helps prevent neutral particles from reaching the quadrupole rods directly. In-situ observation of the evaporant particles in the vapour stream (measurement of particle number density after removing the background contribution) helps relate directly the observed number densities to the particles deposited on the substrate, with the overall deposition rate being measured using a quartz crystal microbalance.

1.3.2 COMPUTER CONTROL OF THE MBE SYSTEM

Control of film deposition in MBE systems using computers facilitates the handling of experimental variables and aids with the automation of the tasks to be undertaken. In the present work computers are used throughout the system. Inexpensive FORTH microcomputers are assigned to dedicated tasks. These computers control particular instruments including the mass spectrometer, a quartz crystal microbalance, a synchronous motor and the temperature of two compound vapour sources. The dedicated computers communicate with a supervisory computer which distributes data for the tasks to be carried out as well as interacting with the user.

Control systems relying on computers for UHV investigations have been discussed in the literature [1.27]. Esaki [1.28] and Chang et al [1.29] described the use of computer control in MBE studies including modulation of the molecular beam emanating from several vapour sources. The introduction of inexpensive computers has resulted in improvements in the cost-to-performance ratio so that these can be dedicated to particular tasks like controlling residual gas analysers [1.30], mass spectrometers [1.31] or vapour source temperature regulators [1.32].

Computer control is used throughout the study of evaporation and deposition of zinc sulphide and zinc selenide compounds. The information gathered about evaporation characteristics for these compounds can then be exploited to grow films with computed concentration profiles. The mass spectrometer can be used as a rate monitor for measuring the vapour stream number density for the evaporated particles. Use of the mass spectrometer as a rate monitor has been described by Terry et al [1.33]. Modulated beam mass spectrometry proves useful for monitoring number densities for particles at very low deposition rates. Control over the concentration of particles depositing on the substrate is achieved through controlling the power fed to the sources using the computer. A closed loop control system to maintain evaporation rate at a preset value from observations made by a mass spectrometer has been described by Lutz [1.34].

The use of computer control provides measurements of number density at a pre-determined set of mass-to-charge ratios and this leads to consistent monitoring of several sources. Data for controlling the deposition of a film with a particular concentration profile can then be computed and stored as an array of numbers which can then be used by the controller as a template to determine the rate of vapourizing film constituents.

1.3.3 INVESTIGATIONS DESCRIBED IN THIS THESIS

The use of modulated beam mass spectrometry coupled with computer control has facilitated an investigation of the evaporation behaviour exhibited by both zinc sulphide and zinc selenide as well as providing design data for the development of a greatly improved computer controlled film deposition system. This has helped with more advanced investigations on the vapour particles such as time-of-flight analysis for particles in transit between the rotating shutter and the mass spectrometer.

High precision measurements of number density helped with the extraction of the signals having a high signal-to-noise ratios. This has led to the development of efficient control software for the deposition system.

A theoretical review of zinc sulphoselenide alloy preparation, thermal characteristics and control of vapour sources and in-situ control techniques used during material evaporation and deposition has been combined with the following experimental investigations:

1. Design and characterization of the modulated beam mass spectrometry system. A consideration of the experimental parameters to investigate led to the development of appropriate instrumentation and the adoption of a particular architecture in the control system employed. Ways of improving the signal-to-noise ratio have been considered and the system's most appropriate settings are suggested. The ability to differentiate between vapour particles in the ambient atmosphere from those arriving directly from the vapour sources has enabled several investigations to be undertaken on zinc selenide and zinc sulphide.

2. The ionization characteristics of particles from zinc selenide and zinc sulphide vapours inside the mass spectrometer has been investigated and ion appearance potentials determined.

3. Time-of-flight analysis for ZnSe and ZnS particles at high temperature has been investigated and two methods of observation developed. Comparisons are made of the time-of-flight for different particles

leading to an effective identification of neutral particles in the vapour stream. The analysis undertaken eliminates ambiguities which may exist in identifying evaporation products.

4. The evaporation characteristics for zinc selenide and zinc sulphide compounds are described and the results obtained are compared to those in the literature.

5. Methods for differentiating zinc from sulphur have been developed and include the use of isotopic abundancy ratios, appearance potential measurements as well as time-of-flight analysis.

6. Growth of zinc sulphoselenide alloys with a pre-determined composition profile is demonstrated using the information acquired for zinc selenide and zinc sulphide. Experiments on film growth are described and the film structures obtained are characterized using a number of analysis techniques. The results are compared to the predicted profiles.

A knowledge of the deposition and evaporation kinetics of ZnS and ZnSe is of fundamental importance to understanding the growth of alloy films from the vapour phase. It is the objective of this thesis to describe studies undertaken during the evaporation and deposition of

ZnS and ZnSe aimed at improving our understanding of the evaporation processes involved. All of the work undertaken has the fundamental objective of providing an ability to grow zinc sulphoselenide alloy films with pre-determined concentration profiles for integrated optic devices.

1.4 REFERENCES

[1.1] P.L.JONES, D.MOORE, AND D.R.COTTON
J. Cryst. Growth Vol.59 p.183 (1982)

[1.2] A.J.COOPER, A.S.SAHIN, P.L.JONES, D.KING, AND D.MOORE
Vacuum Vol.34 p.925 (1984)

[1.3] R.P.GREGORY, P.L.JONES, D.KING AND D.MOORE
Vacuum Vol.38 pp.737-740 (1988)

[1.4] A.S.SAHIN
Ph.D Thesis, University Of Manchester (1983)

[1.5] J.R.ARTHUR
J. Phys. Chem. Solids Vol.28 pp.2257-2267 (1967)

[1.6] J.DROWART AND P.GOLDFINGER
J. Chim. Phis. Vol.55 p.721 (1958)

[1.7] H.GUTBIER
Z. Naturf Vol.16-a p.268 (1961)

[1.8] J.R.ARTHUR
Surf. Sci. Vol.43 pp.449-461 (1973)

[1.9] J.J.MURRAY, C.PUPP, AND .RF.POTTIE
J. Chem. Phys. Vol.58 Nb.6 pp.2569-2578

[1.10] C.PUPP, J.J.MURRAY, AND R.F.POTTIE
J. CHEM. THERMODYNAMICS Vol.6 pp.123-134 (1974)

[1.11] C.T.FOXON, J.A.HARVEY, AND B.A.JOYCE
J. Phys. Chem. Solids Vol.34 pp.1693-1701 (1973)

[1.12] M.BENYEZZAR
M.Sc. Thesis University Of Manchester U.K (1986)

[1.13] C.T.FOXON, M.R.BOURDRY, AND B.A.JOYCE
Surf. Sci. Vol.44 pp.69-92 (1974)

[1.14] R.H.JONES
Ph.D Thesis A.E.C Report LBL-104 (1971)

[1.15] V.L.HIRSCHY AND J.P.ALDRIDGE
Rev. Sci. Instrum. Vol.42 Nb.3 pp.381-383 (1971)

[1.16] G.T.W.ORMROD AND W.R.PATERSON

J. Sci. Instrum. Vol.44 pp.639-641 (1967)

[1.17] E.POHLMANN, R.HUTTL, AND H.KNECHT
J. Phys. E: Sci. Instrum. Vol.20 pp.455-456 (1987)

[1.18] W.L.FITE AND R.T.BRACKMANN
Phys. Rev. Vol.112 Nb.4 pp.1141-1150 (1958)

[1.19] D.R.OLANDER, W.SIEKHAUS, R.H.JONES, AND J.A.SCHWARZ
J. Chem. Phys. Vol.57 Nb.1 pp.408-420 (1972)

[1.20] D.R.OLANDER, R.H.JONES, J.A.SCHWARZ, AND W.J.SIEKHAUS
J. Chem. Phys. Vol.57 Nb.1 p.421 (1972)

[1.21] W.J.SIEKHAUS, R.H.JONES, AND D.R.OLANDER
J. Appl. Phys. Vol.41 Nb.11 pp.4392-4403 (1970)

[1.22] C.T.FOXON, B.A.JOYCE, R.F.C.FARROW, AND R.M.GRIFFITH
J. Phys. D: Appl. Phys. Vol.7 pp.2422-2435 (1974)

[1.23] R.F.C.FARROW
J. Phys. D: Appl. Phys. Vol.7 pp.2436-2448 (1974)

[1.24] C.T.FOXON AND B.A.JOYCE
Surf. Sci. Vol.50 pp.434-450 (1975)

[1.25] M.SAKURAI, T.HIRAYAMA, AND I.ARAKAWA
Vacuum Vol.41 pp.217-219 (1990)

[1.26] J.MURAKAMI, T.HASHIMOTO AND I.KUSUNOKI
Vacuum Vol.41 pp.369-371 (1990)

[1.27] F.M.KLINE
J. Vac. Sci. Technol. A 1 (2) pp.175-181 (1983)

[1.28] L.ESAKI
Proc. 5th Conf. On Solid State Devices Tokyo (1973)
Suppl. J. Japan Soc. Appl. Phys. Vol.43 pp.452-460 (1974)

[1.29] L.L.CHANG, L.ESAKI, W.E.HOWARD, AND R.LUDEKE
J. Vac. Sci. Technol. Vol.10 No.1 pp.11-16

[1.30] L.SHOEMAKER, J.FARDEN, AND T.WILSON
J. Vac. Sci. Technol. A 1(2) pp.184-185 (1983)

[1.31] D.DAHLGREN, J.ARNOLD, AND J.C.HEMMINGER
J. Vac. Sci. Technol. A 1(1) pp.81-83 (1983)

[1.32] R.P.GREGORY
Ph.D Thesis University Of Manchester U.K (1988)

[1.33] J.L.TERRY AND J.D.MICHAELSEN

Proc. 6th Internl. Vaccum. Congr. (1974)
Japan J. Appl. Phys. Suppl.2 Pt.1 (1974)

[1.34] H.LUTZ
J. Vac. Sci. Technol., Vol.15(2) p.309 (1978)

CHAPTER 2

ZINC SULPHOSELENIDE ALLOY EVAPORATION AND TEMPERATURE CONTROL

2.1 INTRODUCTION

This chapter reviews the literature and underlying theory for the evaporation of materials to produce alloy films using multiple vapour sources. The parameters relating to the sublimation of substances from effusion cells and the use of cell temperature control are also outlined. Emphasis is placed on the use of zinc sulphoselenide materials, their growth from the vapour phase and their potential applications.

2.2 THE NEED FOR ZINC SULPHOSELENIDE ALLOY FILMS

The production of thin alloy films using II-VI materials has been extensively reported in the literature over the past decade. Various growth techniques have been employed including vapour phase epitaxy [2.1], metalorganic

vapour phase epitaxy [2.2, 2.3] metalorganic chemical vapour deposition [2.4] and molecular beam epitaxy [2.5, 2.6]. Recently, growth experiments involving a combination of these techniques have also been reported [2.7, 2.8]. Zinc sulphide [2.9], zinc selenide [2.10], and cadmium telluride [2.11] are the major II-VI compounds which have been investigated. Mainly, the aims have been either to produce light emitting devices in the visible region [2.9, 2.12] or for the production of optical devices [2.13].

2.2.1 PROBLEMS ENCOUNTERED WITH ZINC SELENIDE FILMS GROWN ON GALLIUM ARSENIDE

The need to obtain alloy films of zinc sulphoselenide grown on gallium arsenide has proved necessary since the lattice mismatch between the zinc selenide and gallium arsenide lattices makes it difficult to obtain films with good optical and electrical qualities. The major cause of problems with preparing heteroepitaxial structures consisting of zinc selenide oriented on (100) gallium arsenide are the lattice parameter mismatch and the interdiffusion of constituents between the materials [2.14, 2.15]. These phenomena can be interdependent. Lattice mismatch between the deposited layers of zinc selenide and the gallium arsenide substrate causes stress at the interface which leads to the formation of dislocations and stacking faults [2.16]. Interdiffusion of components is

mainly caused by the migration of gallium to the layers of deposited material [2.17]. Figure 2.1 shows the lattice parameters for the materials used in the present work and their band-gap energies Eg. To compound the problems there is mismatch between the thermal expansion coefficients of GaAs and ZnSe and this induces strains on cooling the substrate. This has been observed with films of ZnSe grown on GaAs having a thickness of half a micron [2.18]. The problems with producing conducting materials using ZnSe on GaAs have led to the use of various materials for the doping process including elements like nitrogen [2.19], antimony [2.20], sodium [2.21], silver [2.22], aluminium or gallium [2.23] and chlorine [2.24]. Recent relative success has been claimed using Lithium as a dopant [2.25, 2.26].

2.2.2 SUBSTITUTION OF ZnSe BY ZINC SULPHOSELENIDE ALLOYS

The lattice mismatch effect between crystal lattices is reduced if a buffer layer of zinc sulphide is used. Zinc sulphide has been used as a barrier material between gallium arsenide and zinc selenide and shown to yield low loss structures suitable for waveguides [2.27]. A graded refractive index is produced next to the substrate surface because ZnS has a lower refractive index than ZnSe while possessing a closer match to the thermal expansion coefficient of the substrate. These properties have also lead to investigations on zinc sulphoselenide alloys for the

COMPOUND	GaAs	ZnSe	ZnS
LATTICE PARAMETER AT 300°K (Å)	5.6533	5.6684	5.4133
DIRECT BAND GAP ENERGY Eg AT 300°K (eV)	1.4	2.67	3.66

REFERENCES [2.93, 2.94, 2.95]

TABLE SHOWING THE LATTICE PARAMETER AND DIRECT BAND–GAP ENERGY FOR GaAs, ZnSe, AND ZnS.

FIGURE 2.1

production of improved wide bandgap devices [2.7, 2.28, 2.29].

The need to produce II-VI film materials with improved optical and electrical properties has led to the growth of ternary compounds like $ZnSe_{0.95}S_{0.05}$ on GaAs [2.30] or the growth of multilayered structures between substrate and epilayer. When the individual layers are below a critical thickness value [2.31, 2.32] the stress at the interface is accommodated by the strain in the layers and this reduces the propagation of dislocations and stacking faults from the substrate into the epilayer [2.33, 2.34]. The growth of these multilayered structures or (or strained layer superlattices) may help with resolving the problem of P-N junctions made of lattice mismatched materials [2.35, 2.36] or provide optoelectronic devices based on zinc sulphoselenide alloys [2.37, 2.38].

Obtaining zinc sulphoselenide alloy film structures with superior characteristics dictates the use of high accuracy techniques for the monitoring and control of the deposition process of the materials involved. During the growth of these alloy films relatively thin layers may be needed for particular composition profiles. In the growth of zinc sulphoselenide films with the concentration profile of sulphur varying from the substrate interface towards the upper layers. The molecular beam epitaxy technique offers an opportunity for controlling the growth of thin film materials because layered structures can be deposited and

the composition changed by adjusting the thickness of the layers grown [2.39, 2.40]. In situ characterization techniques can also be carried out facilitating control over the growth process including the use of mass spectrometers [2.41], electron diffraction techniques [2.42], ionization gauges [2.8], or deposition rate monitors [2.44].
Because it is possible to control the amount of evaporated and deposited materials, the performance of such a system is closely linked to the performance of the instrumentation used to monitor the depositing film. Eventually, the use of high precision control and monitoring of the film growth process may lead to the tailoring of structural, optical, and electronic film properties.

In order to grow zinc sulphoselenide alloy film materials with pre-determined composition profiles a high precision control technique has to be used. The film materials are deposited from the vapour phase and an understanding of the behaviour of the materials when they are evaporated is essential.

2.3 MATERIAL EFFUSION AND TEMPERATURE CONTROL

In the MBE process particle beams emanate from a heated vapour source towards a substrate target. Accurate control over the particles temperature is a necessity since the amount of particles emanating from the vapour cell is highly

dependent on the source temperature. Controlling the temperature of the vapour species and measuring the particle number density during the deposition experiments may help with obtaining repeatable results. Control over the vapour species temperature can be achieved once the characteristics of the effusion source are known. The effusion source temperature and source shutter are the parameters which can be acted upon to limit or increase directly the amount of vapourized materials impinging on the substrate.

To control the temperature of the evaporating material the characteristics of the effusion source must be understood and require investigating. In most temperature control systems it is assumed that at equilibrium the measured temperature of the source and the temperature of the evaporating material differ by a negligible amount.

2.4 EFFUSION SOURCE CHARACTERISTICS

Applying the thermodynamic and kinetic theory to the evaporation of a material from an effusion source, the impingement rate of particles on a surface may be shown to be given by:

$$dN / A\,dt = P (2 \Pi m K T)^{-1/2} \qquad (2.1)$$

where dN is the number of particles arriving in time interval dt, m is the particle mass, T the absolute temperature and A the material surface where the evaporation takes place. Early work on evaporation in vacuum was undertaken by Hertz [2.45]. He concluded that for every substance there is a certain maximum evaporation rate occuring when the hydrostatic pressure is nil. If the evaporant gas exerts a hydrostatic pressure p causing a return flux to the condensed phase, the number of particles evaporating becomes:

$$dN / Adt = (P - p) (2 \Pi m K T)^{-1/2} \qquad (2.2)$$

Knudsen [2.46] suggested reflection of impinging vapour particles at the evaporant surface. Hence the evaporation rate is reduced for a measured vapour pressure because a fraction of the vapour particles contribute to the evaporant pressure without being part of the flux from the condensed to the vapour phase. An evaporation coefficient ß defined as the fraction of particles arriving at the surface which remain and condense is introduced yielding the Hertz-Knudsen equation:

$$dN / Adt = ß P / (2 \Pi m K T)^{-1/2} \qquad (2.3)$$

Knudsen [2.47] found that a contaminated mercury surface

resulted in a low evaporation coefficient but with fresh clean surfaces he obtained the maximum rate of evaporation.

2.5 FREE EVAPORATION OF PARTICLES

Evaporant particles from a substance may be considered to leave the surface unimpeded in a low pressure enclosure and they are free from collisions with each other or particles in the surrounding atmosphere. Free evaporation can then take place because the evaporation process is independant of whether or not the substance is in equilibrium with its vapour phase in the vacuum. Langmuir [2.48] used these arguments and investigated the evaporation from free solid surfaces evaporation coefficient close to unity is obtained with the vapours of high molecular weight substances such as tungsten.

Free evaporation has the disadvantage of being strongly dependant on the cleanliness of the evaporant surface and the evaporation rate may be limited by the rate heat can be supplied to the evaporation site. Ruth and Hirth [2.49] proposed several mathematical treatments of evaporation mechanisms. Their calculations accounted for an evaporation coefficient of less than unity and shown good agreement with experimental observations. Measurements on evaporation coefficients have also been reported by Dushman [2.50] and Brewer et al [2.51].

2.6 KNUDSEN EVAPORATION

To overcome the problem of having a coefficient ß below unity Knudsen [2.52] suggested using evaporation by effusion through a small aperture from a vapour held in an isothermal equilibrium with its condensed phase. The internal surface area of the cell is large compared with the aperture area so that losses for effusion are replenished by the condensing material. Provided that the ratio of the particle mean free path to the cell orifice diameter (Knudsen number) is large (›› 1) and the aperture walls are vanishingly thin a non turbulent molecular beam with defined directional characteristics is emitted.

The calculation of effusion rate from a Knudsen cell is similar to that for a gas emerging from through a small aperture in the wall of a container [2.53, 2.54, 2.55]. The mean free path for a mixture of gases can be evaluated from published data [2.56, 2.57, 2.58]. The methods described by Knudsen and Langmuir have both been reviewed by Knack and Stranski [2.59] and their limitations described by Rutner [2.60] Using an M.B.E source, Delhomme [2.61] found substantially different results from those expected from Knudsen's theory.

2.7 NOZZLE SOURCES

A nozzle source incorporates a vapour exit aperture in the form of a nozzle having a converging then a diverging profile aligned with a hollow truncated cone which acts like a collimator. It can be used in evaporation processes where the formation of a molecular beam is not a pre-requisite. Shen [2.62] reviewed the use of nozzle sources in M.B.E. It is concluded from his work that the distribution of particles is too difficult to predict with the theories available and an empirical approach is necessary for each new source geometry.

2.8 EVAPORATION OF MATERIALS FROM EFFUSION SOURCES

For the evaporation of material under high vacuum conditions vapour sources of the Knudsen type may be considered. However, a true Knudsen cell is not convenient for M.B.E because wide exit apertures are needed to provide effusion rates sufficient to produce reasonable film growth rates. The effusion rate may be predicted using the equation which follows giving the density D of particles per unit solid angle at a distance r from the source:

$$D = N_a P A \cos(\theta) \left(\Pi r^2 [2 \Pi M R T]^{1/2}\right)^{-1} \quad (2.4)$$

where N_a is Avogadro's number, P the pressure of the substance, A the cell aperture diameter, M the mass of the substance, R the gas constant, T the absolute temperature and θ is an angle which is function of the evaporant particles direction.

Relationship (2.4) is known as the cosine law and has been described theoretically by Clausing [2.63, 2.64] and verified experimentally by Knudsen [2.65] and Mayer [2.66]. The effusion rate may easily be related to the temperature of the evaporating substance using The Clausing-Clapeyron equation:

$$H - Ho = (V - Vo)\, T\, dP/dT \quad (2.5)$$

Where H and Ho are the molar latent heats of vapourization at the final and initial conditions respectively. V is the volume of one gram-molecule of the vapour and Vo that at the initial conditions. P is the pressure and T the absolute

temperature.

Using the assumption that the initial volume is negligible and that the gas is ideal equation (2.5) after integration yields:

$$\mathrm{Log}(P) = A - B/T - C(T) \qquad (2.6)$$

Where A, B and C are constants of integration. This is Kirchoff's equation and it has been used by Hertz [2.45] and Knudsen [2.65]. Other equations for the evaluation of material vapour pressure have been used and are discussed in the literature [2.48, 2.53, 2.67].

2.9 RELATIONSHIP BETWEEN EVAPORATION RATE AND DEPOSITION RATE

Obtaining films with pre-determined composition profiles requires control over the material deposition rates. It has been shown for the system used for the present investigation [2.68] that the deposition rate relationship to temperature can be calculated approximately from the evaporation rate equation proposed by Langmuir [2.48] resulting in an equation similar to relationship

(2.6). The approximation involves the identification of the constants A, B and C which are specific to the material and the temperature characteristics and geometry of the source employed.

2.10 MULTISOURCE EVAPORATION

For the growth of films requiring the deposition of more than one species or compound material it is necessary to use more than one evaporant source. This offers the possibility of varying the flux concentration ratios for the evaporant materials. Multisource evaporation has been used by several workers to grow relatively complex film structures. Some of the early work using multisource evaporation has been reviewed in the literature [2.69, 2.70]. It is important to note that using several sources in M.B.E requires the empirical characterization and calibration of each source even if the sources have similar manufacturing specifications. Zinc selenide deposition using two separate sources in an MBE apparatus has been described by Park et al [2.71], and more recently zinc sulphoselenide alloy films have been grown using separate sources in various growth techniques [2.29, 2.30, 2.72]. Since there is a strong dependance between flux properties and composition it is necessary to control the growth parameters closely in MBE for graded refractive material. The use of elemental sources necessitates knowledge on the

evaporation rates, the re-evaporation rates of the vapour particles from the growing film and the elemental impingement rates.

In the present work two sources one containing ZnS and the other ZnSe are employed. Temperature control is used on both sources. Use is made of compound material sources instead of elemental sources for II-VI compounds because it is expected that the evaporation of elements from the higher atomic groups (groups V or VI in the periodic table) may lead to the production of higher order polymeric gaseous species of the same element. Some doubt also exists as to the existence of several polymeric species for selenium when compound sources are used. In group V, arsenic for example is known to produce at least dimers and tetramers when evaporated from sources containing GaAs, Mo_5As_4 or Zn_3As_2 [2.73, 2.74].

Another advantage is also reflected by the smaller number of vapour sources and therefore lower complexity in the calibration and monitoring of the cells. For the majority of II-VI group coumpounds it has been noted that most of the materials sublime in a congruent manner and lead to diatomic particles of group VI and monoatomic particles of group II vapour species [2.75] according to the equation:

$$2\ XY_{(solid)} \longrightarrow 2\ X_{(gas)} + Y_{2\ (gas)} \qquad (2.7)$$

Some doubt has been expressed about the polyatomic nature of the vapour species in the case of selenium [2.76] and to a lesser extent for sulphur.

2.11 TEMPERATURE CONTROL

Because the effusion rate is strongly dependent on the source temperature it is important to have adequate control over cell temperature. When an alloy film of continuously variable composition is required it is necessary to regulate the vapour source heater power with a high level of precision. Typically, a few percents flux density change for one degree Kelvin change in source temperature are to be expected. In the course of this thesis the magnitude of this change will be shown to depend on the absolute temperature of the source. Automatic temperature control is required for MBE work because the parameters involved in the evaporation process are highly dependant on temperature and therefore exclude any possibility of a manually controlled system where high overshoots and large variations may occur.

Selection of the appropriate temperature controller is governed mainly by the degree of accuracy required and the thermal characteristics of the evaporant source. Systems employing temperature controllers are described in the literature [2.77, 2.78].

Before a model for a temperature controller can be developed the characteristics of the process must be determined. In the present system the source is fed by a DC power supply and its temperature measured with a thermocouple. Steady-state or static calibration of the source provides information about the heating power required to produce a particular deposition rate. The parameters which need to be determined include the time taken for the temperature to start rising (delay time) and the maximum rate of change of temperature. The delay time includes the propagation delay due to heat flow velocity delay and the exponential lag caused by the process thermal time constants. Methods for determining the process time constants and delays have been discussed by Sten [2.79] and Smith [2.80].

The source has to be set accurately to a particular temperature and this can be achieved by using a feedback control system which can cope with the evaporant source characteristics and the experimental conditions in which it is employed. Several workers have used systems relying on feedback control of vapour source temperature to produce specified deposition profiles on the substrate [2.77].

Since computer control can be used in these processes and considering the computer as a time series device, time domain identification of the vapour source may produce results in the most suitable form for the design of a time sequence controller [2.81].

In most evaporation systems it is the source structure that is heated directly and not the evaporant material. An assumption which may be considered is that in equilibrium the temperature of the source walls and that of the vapourizing material are equal. Moreover, in the cylindrical M.B.E cells used for the present work it is apparent that temperature measurement is made in a location away from the heaters and the evaporant surface. This is one of the major problems absolute temperature measurements in MBE evaporation systems because of the distances between heat source and measurement point is considerable due to the distributed nature of vapour source structure. It is therefore necessary to develop a model to estimate the cell temperature with adequate accuracy.

To account for the fact that the thermocouple and the heating elements are at different locations on the source a distributed parameter model may be required [2.82]. Correcting for diffusion effects makes the model more complicated. A simplified model consisting of a single time constant with the addition of a pure delay has been described by Zeigler and Nichols [2.83]. A modification of this model is presented by Miller [2.84]. A third

alternative contrasting the last two methods has been described by Smith [2.85]. Because a second order model results in an overdamped response with a dominant first order pole or time constant indicating a significant first order effect it is simpler to postulate a discrete model for such exponential responses and the use of linear regression [2.86].

In M.B.E the heater voltage is the adjustable input variable while the crucible temperature may be considered as the measured and hence the controlled variable. If ts is the sample time, u(k) the process input at time k ts with x(k) the experimental output at interval k and X(k) the model output calculated for interval k, an error e(k) can be found such that:

$$e(k) = x(k) - X(k) \qquad (2.8)$$

Resolution on the temperature readings is dictated by that of the device used to read the thermocouple voltage (14 bit ADC converter in the present system).

In temperature control systems which employ computers truncation errors which may occur when handling the measured data have to be avoided [2.87]. The time taken for each measurement has to be related to the sampling interval [2.88]. A minimum of 12 bits was recommended [2.89] for

controlling the heating power for the vapour source.

Experimentally, use can be made of the evaporant source static temperature response curve to set initial tuning values for the control process. A sampling time much shorter than the process time constants for dominant poles and comparable to the system response time should be adopted [2.90]. High sampling frequencies may lead to undue computational efforts and high order controllers are then required to cope with the process delays [2.89]. Temperature samples can be measured in short time intervals Non-recursive filtering can be undertaken on the samples and recursive filtering can be carried out on a batch of samples because recursive filters are simpler to implement with large filter time constants [2.91].

Closed loop temperature controllers help with increasing the response speed of the evaporant source temperature. Their computer control facilitates the use of digital filters in in feedback control and processing and relating the measured data to other data like flux measurements. A detailed investigation into the design and application of a dynamic temperature controller has been submitted in a Ph.D thesis to The University Of Manchester [2.92].

2.12 CONCLUSION

A literature survey on II-VI compounds with emphasis placed on zinc sulphoselenide alloys has been described. The use of zinc sulphoselenide alloy films can provide a better substitute for zinc selenide films for the production of optical devices. Literature on the evaporation of materials and the use of feedback temperature control for vapour sources have also been reviewed.

In a MBE system using compound sources the amount of control and monitoring equipment necessary is reduced. This imposes an enhancement on the performance of the instrumentation employed in order to avoid measurement inaccuracies for the vapourized constituents and the lack of repeatability of the vapourization characteristics for the compounds used.

Some materials exhibit an evaporation coefficient close to unity and therefore the evaporation rates calculated from the equilibrium pressure and kinetic theory of gases agree with the practical observations. Other materials when vapourized in an effusion source produce evaporation coefficients less than unity and the rates of evaporation are difficult to calculate. It has been shown that when an evaporant source is employed, investigations on its characteristics have to be undertaken to acquire information about the material evaporation process and the response of the source to temperature gradients. This helps with

efficient temperature control and determination of the material evaporation kinetics by direct measurements on the vapours produced.

The literature survey carried out has outlined the methods and requirements undertaken to achieve efficient vapour source temperature control. A strategy which can be adopted is to use a combination of control over vapour source temperature and beam flux density data (from a mass spectrometer or a microbalance) to achieve and maintain the desired deposition rate for individual vapour sources.

Flux measurement is an important parameter in a MBE apparatus because the end product, which is the film material is grown from the vapour fluxes impinging on the substrate surface. An immediate conclusion would be to couple the control over the source temperature with the results from the flux measurement devices. Understanding the behaviour of the flux densities with the variation of other experimental parameters necessitates an investigation into the methods used to observe the vapour species and their related processes. This leads to a consideration of some of the phenomena involved in mass spectrometry and their influence on the design of a modulated beam mass spectrometry system.

2.13 REFERENCES

[2.1] M.UMAR-SYED AND P.LILLEY
J. Cryst. Growth Vol.66 pp.21-25 (1984)

[2.2] P.M.FRIJLINK, M.W.JONES
J. Cryst. Growth Vol.68 p.466 (1984)

[2.3] T.YODO, T.KOYAMA, AND K.YAMASHITA
J. Cryst. Growth Vol.92 pp.196-207 (1988)

[2.4] A.YOSHIKAWA, S.YAMAGA, K.TANAKA, AND H.KASAI
J. Cryst. Growth Vol.72 p.13 (1985)

[2.5] A.S.SAHIN, P.L.JONES, D.KING, AND D.MOORE
Vacuum Vol.34 p.925 (1987)

[2.6] T.YAO
J. Cryt. Growth Vol.72 pp.31-40 (1985)

[2.7] A.YOSHIKAWA, H.ONIYAMA, S.YAMAGA, AND H.KASAI
J. Cryst. Growth Vol.95 pp.572-579 (1989)

[2.8] J.LILJA, J.KESKINEN, M.HOVINEN, AND M.PESSA
J. Vac. Sci. Technol. Vol.B7(4) pp.593-598 (1989)

[2.9] S.IIDA, T.SUGIMOTO, S.SUZUKI, S.KISHIMOTO,
AND Y.YAGI
J. Cryst. Growth Vol.72 pp.51-56 (1985)

[2.10] M.UMAR AND P.LILLEY
J. Cryst. Growth Vol.88 pp.415-418 (1988)

[2.11] M.KIMATA, A.RYOJI, AND T.AOKI
J. Cryst. Growth Vol.81 pp.508-511 (1987)

[2.12] H.KUWABARA, H.FUJIYATSU, H.SHIMIZU, AND A.SASAKI
J. Cryst. Growth Vol.72 pp.299-303 (1985)

[2.13] A.J.COOPER, A.S.SAHIN, P.L.JONES, D.KING
AND D.MOORE
Vacuum Vol.34 Nb.10/11 pp.925-929 (1984)

[2.14] T.YAO
Japan. J. Appl. Phys. Vol.25 Nb.7 pp.L544-L547 (1986)

[2.15] T.YAO, Y.OKADA, S.MATSUI, K.ISHIDA, AND I.FUJIMOTO
J. Cryst. Growth Vol.81 pp.518-523 (1987)

[2.16] S. Fujita, T. Yodo, A. Sasaki
J. Cryst. Growth Vol.72 p.27 (1985)

[2.17] A.Yoshikawa, K. Tanaka, S. Yamaga, H. Kasai
Jap. J. Appl. Phys. Vol.23 p.773 (1984)

[2.18] J.E Genthe,R.E Aldrich
Thin Solid Films Vol.22 p.149 (1971)

[2.19] T.MITSUYU, K.OHKAWA, AND YAMAZAKI
Appl. Phys. Lett. Vol.49 p.1349 (1986)

[2.20] R.M.PARK, J.KLEIMAN, H.A.MAR, AND T.L.SMITH
J. Appl. Phys. Vol.63 p.2851 (1988)

[2.21] T.YAO, AND T.TAGUSHI
Proc. 13th Int. Conf. On Defects In Semiconductors
p.1221 (1984)

[2.22] N.R.J.POOLTON, J.J.DAVIES, AND J.E.NICHOLLS
AND B.J.FITZPATRICK
J. Cryst. Growth Vol.72 pp.336-341 (1985)

[2.23] W.STUTIUS
J. Appl. Phys. Vol.53 p.284 (1982)

[2.24] A.TSUSHI, T.UEMOTO, K.HIRAHARA, AND T.BEPPU
J. Appl. Phys. Vol.65 (6) pp.2561-2563 (1989)

[2.25] H.CHENG, J.M.DEPUYDT, J.E.POTTS, AND T.L.SMITH
Appl. Phys. lett. Vol.52 p.147 (1988)

[2.26] T.YASUDA, I.MITSUISHI, AND H.KUKIMOTO
Appl. Phys. Lett. Vol.52 p.57 (1988)

[2.27] P.L. Jones, D. Moore, D.R Cotton
J Cryst Growth Vol.59 p.183 (1982)

[2.28] J.ZHOU, H.GOTO, N.SAWAKI, AND I.AKASAKI
Jap. J. Appl. Phys. Vol.27 Nb.2 pp.229-234 (1988)

[2.29] H.J.CORNELISSEN, D.A.KAMMACK, R.J.DALBY
J. Vac. Sci. Technol. Vol.B6(2) pp.769-772 (1988)

[2.30] H.M.Yates, J.O.Williams
Appl. Phys. Lett. Vol.51 pp.809-810 (1987)

[2.31] J.W.Matthews, A.E.Blakeslee
J. Cryst. Growth Vol.27 p.118 (1974)

[2.32] J.W.Matthews, A.E.Blakeslee
J. Cryst. Growth Vol.32 p.265 (1976)

[2.33] S.Fujita, Y.Matsuda, A.Sasaki
Appl. Phys. Lett. Vol.47 p.955 (1985)

[2.34] I.J.Fritz, L.R.Dawson, G.C.Osbourn, P.L.Gourley, AND R.M. Biefeld
Inst. Phys. Conf. Ser. No.65 p.241 (1982)

[2.35] M.Koyabashi, N.Mino, H.Katagin, R.Kimura, M.Konagai, AND K.Takahashi
J. Appl. Phys. Vol.60 p.773 (1986)

[2.36] M.Koyabashi, S.Dosho, H.Katagin, R.Kimura, M.Konagai, AND K.Takahashi
Appl. Phys. Lett. Vol.51 p.1602 (1987)

[2.37] G.C. Osbourn
J. Appl. Phys. Vol.73 p.1586 (1982)

[2.38] G. C. Osbourn
J. Vac. Sci. Technol. Vol.A3 p.826 (1985)

[2.39] A.Y.Cho, J.R.Arthur in G.A.Somerjai and J. McCaldin (eds) " Progress In Solid-State Chemistry "
Vol.10 p.157 Pergamon (1975)

[2.40] A.Y.Cho
J. Vac. Sci. Technol. Vol.16 p.275 (1979)

[2.41] V.J.A.KORPIO
Vakuum Technik Vol.38.5-6 pp.134-142 (1989)

[2.42] P.J.DOBSON, B.A.JOYCE, J.H.NEAVE, AND J.ZHANG
Vacuum Vol.38 p.422 (1988)

[2.44] D.KING AND G.R.HOFFMAN
J. Phys. E: Sci. Instrum. Vol.4 pp.993-998 (1971)

[2.45] H.Hertz
Ann. Physik Vol.17 p.177 (1882)

[2.46] M.Knudsen
Ann. Physik Vol.34 p.593 (1911)

[2.47] M. Knudsen
Ann. Physik Vol.47 p.697 (1915)

[2.48] I. Langmuir
Phys. Rev. Vol.2 p.329 (1913)

[2.49] V.Ruth and J.P.Hirth
in E.Rutner, P.Goldfinger and J.P.Hirth (Eds)
"Condensation And Evaporation Of Solids"
Gordon and Breach Science Publishers Inc. p.99 (1964)

[2.50] S.Dushman
"Vacuum Technique" J.Wiley and Sons Inc. (1949)

[2.51] L.Brewer and J.S.Kane
J. Phys. Chem. Vol.59 p.105 (1955)

[2.52] M.Knudsen
Ann. Physik Vol.29 p.179 (1909)

[2.53] J.K.Roberts
"Heat And Thermodynamics" Blackie and Son (1960)

[2.54] E.H.Kennard
"Kinetic Theory Of Gases" Mc Graw Hill (1938)

[2.55] L.B.Loeb
"Kinetic Thery of Gases" Mc Graw Hill (1927)

[2.56] J.H.Jeans
"Dynamic Theory Of Gases" Cambridge (1904)

[2.57] J.Jeans
"An Introduction To The Kinetic Theory Of Gases"
Cambridge (1960)

[2.58] R.Glang in L.I.Maissel and R.Glang (Eds)
"Handbook Of Thin Film Technology" Mac Graw Hill (1970)

[2.59] O.Knacke and I.N.Stranski
Prog. Metal Phys. Vol.6 p.181 (1956)

[2.60] E.Rutner in E.Rutner, P.Goldfinger AND J.P.Hirth
(Eds) "Condensation And Evaporation Of Solids"
Gordon and Breach Sci. Publishers Inc. p.149 (1964)

[2.61] B.J.Delhomme, R.C.Blanchet AND J.J.Urgell
First Int. Symp. on MBE Paris (1978)

[2.62] L.Y.L.Shen
J. Vac. Sci. Technol. Vol.15 p.10 (1978)

[2.63] P.Clausing
Z. Physik Vol.66 p.471 (1930)

[2.64] P.Clausing
Ann. Physik Vol.12 p.961 (1932)

[2.65] M. Knudsen
Ann. Physik Vol.28 p.75 (1909)

[2.66] H.Mayer
Z.Physik Vol.52 p.235 (1929)

[2.67] G.J.V.Wylen and R.E.Sonntag
"Fundamental Of Classical Thermodynamics"
John Wiley and Son (1965)

[2.68] A.S.Sahin
"Microcomputer Controlled Monitoring During The MBE Growth Of Zinc Selenide On Gallium Arsenide "
Ph.D Thesis University of Manchester (1983)

[2.69] L.ESAKI
Proc. 5th Conf. On Solid State Surf. (1973)
Suppl. J. Japan Soc. Of Appl. Phys.
Vol.43 pp.452-460 (1974)

[2.70] J.TERRY AND J.D.MICHAELSEN
Proc. 6th Internl. Vacuum. Congr. (1974)
Japan J. Appl. Phys. Suppl.2 Pt.1 pp.483-485 (1974)

[2.71] R.M.PARK, H.A.MAR, And N.M.SALANSKY
J. Vac. Sci. Technol. Vol.B3(2) pp.676-680 (1985)

[2.72] J.ZHOU, H.GOTO, N.SAWAKI, AND I.AKASAKI
Phys. Status. Solidi (a) Vol.103 p.619 (1987)

[2.73] J.R.ARTHUR
J. Phys. Chem. Solids Vol.28 pp.2257-2267 (1967)

[2.74] J.J.MURRAY, C.PUPP, AND R.F.POTTIE
J. Chem. Phys. Vol.58 Nb.6 pp.2569-2578 (1973)

[2.75] M.Aven, J.S.Prener
(Eds) "Physics And Chemistry Of II-VI Compounds"
North-Holland Publishing Co.

[2.76] J.Berkowitz, W.A.Chupka
J. Chem. Phys Vol.45 No.11 p.4259 (1966)

[2.77] L.GODGREY AND J.PHILIP
J. Phys. E: Sci. Instrum. Vol.22 pp.516-518 (1989)

[2.78] J.R.YANG AND J.T.LUE
IEEE Trans. Instrum. Meas. Vol.IM-36 No.1 (1987)

[2.79] J.W.Sten
Instrum. Technol. Vol.17 No.9 p.39 (1970)

[2.80] O.J.M.Smith
ISA J. Vol.6 No.2 p.28 (Feb. 1959)

[2.81] R.P.GREGORY, P.L.JONES, D.KING, AND D.MOORE
Vacuum Vol.38 Nb.8-10 pp.737-740 (1988)

[2.82] E.M.Forgan
Cryogenics p.207 (1974)

[2.83] J.G.Zeigler ,N.B.Nichols
Trans. ASME Vol.46 No.11 p.759 (1942)

[2.84] J.A.Miller
Control Engineering Vol.14 No.12 p.72 (1967)

[2.85] C.L.Smith
"Digital Computer Process Control"
International Textbook Co.,1972

[2.86] A.Johnson
"Process Dynamics Estimation And Control"
Peter Peregrinus Ltd. London, For IEE (1985)

[2.87] A.V.Oppenheim, R.W.Schafer
"Digital Signal Processing" Prentice/Hall (1975)

[2.88] J.F.Kaiser, F.F.Kuo
"System Analysis By Digital Computer"
J. Wiley 1960

[2.89] P.Katz
"Digital Control Using Microprocessors"
Prentice/Hall Inc. London 1981

[2.90] P.Uronen, L.Ylinieme
IFAC p.457 (1977)

[2.91] S.M.Bozik
"Digital And Kalman Filtering"
E.Arnold Ltd. (1979)

[2.92] R.P.Gregory
"Digital Control Of A MBE System "
Ph.D Thesis, University Of Manchester (1988)

[2.93] W.L.ROTH
In "Physics And Chemestry of II-VI Compounds"
Eds. M.Aven And J.S.Prener North Holland
Amsterdam p.127 (1967)

[2.94] P.BARANSKI, V.KLOTCHKOV, AND I.POTYKEVITCH
"Electronique Des Semiconducteurs"
2nd Part Edition Mir Moscou p.503 (1978)

[2.95] P.L.GOURLEY, R.M.BIEFIE, G.C.OSBOURN, I.J.FRITZ
Inst. Phys. Conf. Ser. Vol.65 P.249 (1982)

CHAPTER 3

CONTROL AND MONITORING OF MATERIALS EVAPORATION AND DEPOSITION

3.1 INTRODUCTION

In-situ control and monitoring of the evaporation and deposition of film materials in a vacuum environment can be performed using a number of techniques and the commonly adopted techniques are reviewed in this chapter. Emphasis is placed on those adopted for the MBE system employed in the present work. The basic features of quadrupole mass spectrometers used for measuring the particle densities of evaporant species are discussed. Calibration of the mass spectrometer using a quartz crystal microbalance to make film deposition rate measurements is considered.

Monitoring the evaporation of materials in the experimental apparatus is of primary importance because this gives information about the quantities of material impinging on the substrate. From the measurements made control can be exercised over the composition and thickness of the

structure being grown.

3.2 IONIZATION GAUGE DETECTORS

In ionization gauges, gaseous particles are ionized by electrons emitted either from a cold cathode as in the Penning gauge [3.1] and the Redhead Magnetron Gauge [3.2, 3.3] or from a hot filament as in the Triode Ionization Gauge [3.4] and The Bayard-Alpert Gauge [3.5, 3.6]. A negatively charged electrode collects the ionized particles and the current produced gives a direct indication of the ambient gas particle density. A review of the various techniques used in ionization gauges is given by Pirani and Yarwood [3.7] and Barrington [3.8].

Because of their lower operating pressure capabilities Bayart-Alpert Gauges have been used in crystal growth systems [3.9], and other types of ionization gauges have been used in recent work on the molecular beam epitaxy of II-VI compounds for monitoring the beam pressure [3.10].

The ionizing ability of electrons of a given energy is not the same for all gases and vapours as a result measurements made with ionization gauges are liable to inaccuracy where the gas composition is uncertain. Moreover, because only total pressures can be estimated and no distinction is made between particles having different masses or charges the technique cannot be used successfully

for specific particle density measurement. This limits the application of ionization gauges considerably especially in multisource evaporation systems where not only different degrees of particle ionization and polymerization occur but also the particles themselves may be of different atomic mass.

3.3 SOURCE TEMPERATURE CONTROL

Source temperature control has been outlined previously and the phenomena relating to it discussed. Systems relying on this technique as a control means have been described in the literature [3.11]. However, the technique lacks repeatability due to the variation of evaporation profiles with the depletion of the of material in the vapour source as well as sensitivity to changes in the source operating conditions, such as movement of the temperature measuring thermocouple.

3.4 ELECTRON DIFFRACTION TECHNIQUES

These techniques involve projecting an electron beam of a defined energy and angle of incidence at the substrate surface. The information provided by the electrons diffracted from the sample is exploited to gather data about surface growth kinetics. Both low energy electron

diffraction (LEED) and reflection high energy electron diffraction (RHEED) are used for in-situ measurements.

3.4.1 LOW ENERGY ELECTRON DIFFRACTION (LEED)

The electron beam aimed at the growth surface has a low energy (conventionally from 50 to 300 eV) and is perpendicular to the substrate surface. The backscattered electron current consists mainly of inelastically scattered electrons, with a small elastically scattered component which may be separated by means of a retarding grid followed by acceleration onto a fluorescent screen. The patterns obtained are used to monitor the state of the crystal surface. Detailed experimental arrangements have been described by Pendry [3.12] and Van Hove et al [3.13] and the technique is reviewed in detail by Jones et al [3.14].

The LEED technique is highly effective as a means for determining surface fine structure [3.15, 3.16, 3.17]. Despite the obvious advantage in using a beam of low energy electrons, difficulties are encountered because low energy electron beams suffer from the effects arising from stray electric and magnetic fields. The technique is difficult to use in MBE UHV systems because it requires an electron beam perpendicular to the substrate. The difficulty arises through the MBE system geometry where the incident electron beam may interfere with the materials vapours since the

oriented particle beam is perpendicular (or nearly so) to the substrate surface.

3.4.2 REFLECTION HIGH ENERGY ELECTRON DIFFRACTION (RHEED)

This technique is quite similar to the LEED method and differs from it in that a high energy electron beam (from 3 KeV to 100 KeV) is projected towards the substrate surface at a grazing angle. Grazing angles at high energies are used to obtain electrons elastically scattered from the surface region. Normal incidence electrons pick out the well-ordered parts of the surface with orientations close to that of the average surface structure whereas grazing incidence electrons penetrate into raised areas of the surface if it is not microscopically flat.

The technique finds wide applications in MBE [3.18, 3.19, 3.20] because the recording fluorescent screen and the electron gun are almost in the plane of the substrate surface and away from the vapour beam path. RHEED allows monitoring during film growth as well as under static conditions. The substrate surface can be thermally cleaned in-situ by raising substrate temperature until a well defined spot pattern is observed [3.21]. Although RHEED has been extensively used in the study of III-V compound surfaces [3.22] it has also been applied to monitoring the growth of Zinc Sulphoselenide materials [3.23], [3.24] as

well as other II-IV compounds [3.25, 3.26].

The observation of surface growth kinetics can be extended to monitoring the number of atomic layers deposited on the substrate surface. A periodic function in reflection intensity occurs every time a layer deposits on the substrate. The oscillation period of the intensity fluctuation is exploited to deduce the deposition rate. The RHEED oscillation method has been reviewed by Dobson et Al [3.27] and Bosachi et Al [3.28] and has been used by other authors for monitoring the deposition of II-VI compounds [3.29] including zinc sulphoselenide alloys [3.23].

Although RHEED is being used extensively in MBE, most of its applications are concerned only with qualitative surface assessment and not with quantitative diffracted beam intensity analysis [3.30]. The technique is not suitable for application in growth experiments where thicknesses in excess of 1 μm are expected. Interpretation of the RHEED oscillations and recovery of data may also be difficult due to dynamical effects [3.31]. There is the the contribution from diffusely scattered electrons to the data which should be dominated by the contribution from elastically scattered electrons. It has also been reported [3.32] that the technique has not been used successfully in reconstructing surfaces like those of gallium, although attempts have now been described by other authors in the literature [3.33].

In current MBE systems employing RHEED the data are extracted by an operator who observes the patterns appearing on a fluorescent screen. Replacing the operator by using computer control, if desirable, would be difficult and costly to implement. In recent literature [3.34], use of mass spectrometry as an alternative to RHEED has been suggested by using a mass spectrometer to monitor desorbed vapour particles from the substrate surface during film growth experiments.

3.4.3 OTHER ELECTRON DIFFRACTION AND PHOTON DIFFRACTION TECHNIQUES:

Other methods used for in-situ characterization of growing film materials include auger electron spectroscopy and the detection of X rays stimulated by electron bombardment (photon techniques). Recent reviews covering most of these methods have been described in the literature [3.35, 3.36].

3.5 RESONANT QUARTZ CRYSTAL TECHNIQUES

When a quartz crystal resonator is exposed to a condensing vapour stream, its oscillation period increases as a function of the mass of material deposited on its surface. Early use of microbalances as deposition rate monitors has been reported by Sauerbrey [3.37]. The

behaviour of microbalances has been extensively reviewed in the literature [3.38, 3.39] and the use of quartz crystal microbalances for deposition rate and thickness measurement has been described by King et Al [3.40], Warner et Al [3.41], and Johnson [3.42].

Building the quartz crystal into an electronic oscillator allows the increase in the changes in the resonant period due to deposition to be measured so the increase in the mass of the deposited film can be calculated [3.43]. It is assumed that the film deposited on the surface of the quartz plate can be treated as a layer of quartz of the same mass and independant of the elastic and acoustic properties of the deposited material. For the calculation of thickness it is assumed that the density of the thin film deposit is constant and equal to the density of the bulk material. For thicker films the elastic and acoustic properties of the film must be considered but this can be dealt with by bringing the process under computer control [3.44].

3.5.1 THE QUARTZ CRYSTAL RESONANT FREQUENCY CHARACTERISTICS

The resonant frequency f_q of a quartz plate resonating in thickness shear can be related to its thickness t_q using a frequency constant C_q according

to:

$$f_q = C_q/t_q \qquad (3.1)$$

A variation $\triangle P_q$ on the oscillation period can then be related to the resulting thickness variation $\triangle t_q$ according to:

$$\triangle t_q = C_q.\rho_q.\rho_f^{-1}.\triangle P_q \qquad (3.2)$$

Where ρ_q and ρ_f are the density of the quartz and the density of the film material respectively. The term $C_q.\rho_q$ is called the mass sensitivity of the quartz crystal and is constant for the material and the type of quartz plate employed.

3.5.2 DIGITAL CONTROL AND CRYSTAL PERIOD MEASUREMENT

The technique adopted for film thickness measurements in the present work involves successive direct period measurements. In this method the signal frequency from the quartz crystal oscillator is amplified and then divided, by a factor N using a digital counter. The divided frequency is used to

gate a high frequency reference signal f_r into a binary counter. The digital count c_b at the output of the binary counter gives a measurement of the resonant period according to:

$$c_b = N.P_q.f_r/2 \qquad (3.3)$$

Using relation (3.2) yields:

$$\Delta c_b = N.f_r/2 \quad \Delta P_q \qquad (3.4)$$

Therefore, the deposition of material on the quartz plate is indicated by an increase in the count c_b of the binary counter. Supervision of the microbalance using a computer involves initiating the count sequences and reading the counts c_b after each $N.P_q$ periods of the quartz resonator. The data are then stored in the memory for subsequent processing and extraction of the deposition rate according to relation (3.4).

Digital measurement of the resonant quartz frequency using a counting process can introduce a quantization error of ±1 count [3.45]. The minimum detectable change between two consecutive counts is therefore a count equal to two. Using relationship (3.4), this yields a period resolution R_c expressed by:

$$R_c = 4.N.f_r^{-1} \qquad (3.5)$$

Normally, the resolution is expressed in terms of deposited mass per unit area. Combining relationships (3.2) and (3.5) yields the expression for mass resolution (X_m):

$$X_m = 4\ C_q.\rho_m.N^{-1}.f_r^{-1} \qquad (3.6)$$

The resolution of the measurements depends upon both the reference clock frequency and the number of stages in the counter used to divide down the quartz crystal frequency. However, increasing the number of stages of the counter-divider increases the sample time and makes the deposition control more difficult. A more attractive solution is to increase the reference frequency instead.

Measurement of resonant period is often employed in commercial deposition rate monitors [3.46, 3.47] and has been used previously in the present deposition apparatus [3.48].

Another method for extracting the deposition rate on a quartz plate has been described by Chandler [3.49]. The method involves mixing the output from the quartz oscillator with a reference frequency to produce a beat signal. Period measurement is then initiated. Despite the high resolution obtained this technique requires increased electronic complexity and computer processing of the output signal.

3.5.3 ASSESSMENT OF THE TECHNIQUE

Sources of error in the use of quartz crystal microbalances include temperature variations [3.50] and high stress in the film material [3.51]. In MBE, thermal gradients may result from energy imparted by the incident vapour particles or through radiated heat from the high temperature vapour sources. Quartz crystal monitors have been observed to suffer from transient thermal effects such as those caused by the opening of the source shutter [3.52]. The drifts in temperature introduce variations in the condensation rate causing errors in the measurements. Measurement errors can be minimized through suitable operating procedures like cooling of the quartz plate and the careful positioning of the sensor in the deposition apparatus.

Provided that the position of the quartz plate is fixed with respect to the substrate, the temperatures of both are constant, and that the evaporant distribution from the

effusion source varies negligibly between the substrate and the quartz plate, it can be assumed that the condensation rate on the quartz plate is proportional to that on the substrate surface. An initial calibration procedure can be undertaken to relate the two rates of deposition and this is essential for the determination of deposition rate on the substrate from measurement of that occuring on the quartz plate. Long term crystal loading with film material causes failure of the oscillator circuit due to the high series resistance of the quartz resonator. This can be avoided by changing the quartz plate before its series resistance rises unacceptably. Advantages in using quartz crystal microbalances in MBE include their ease of digital control and their indication of the deposited mass of material. This latter feature makes them useful for calibrating vapour flux sensitive instruments such as mass spectrometers.

3.6 MASS SPECTROMETRY FOR DETERMINING THE FLUX DENSITY OF SPECIFIC VAPOUR SPECIES

A mass spectrometer is necessary for monitoring the particle number densities of vapour stream constituents in multiple vapour source deposition systems. Other flux sensitive instruments, like microbalances, only measure the total flux density and are not species specific. Because of their compactness, minimum installation requirements and low tuning voltages [3.53] mass spectrometers of the quadrupole

type are widely employed im MBE systems where they can be brought under computer control [3.54].

3.6.1 THE QUADRUPOLE MASS SPECTROMETER (QMS)

The QMS assembly includes elements under vacuum where detection and amplification of the ion current takes place, and a part outside the vacuum chamber where electronic control and recording are undertaken. The section under vacuum includes mainly an ionization chamber where ions are produced by electrons emitted from a hot filament, a four rod assembly which acts as a mass filter by the application of a superimposed DC and radio-frequency signals, and an electron multiplier (or sometimes collector electrode) for amplifying the ion current. The section outside the vacumm chamber consists of the electronic circuitry and controls necessary for setting the different mass spectrometer parameters like the filament emission current, the electron energy, the tuning voltages, as well as scaling and recording of the electron multiplier output current. Measurement of a vapour particle density involves tuning the QMS to a given mass-to-charge ratio (a.m.u) of the required vapour species and observing the output of the instrument on a recording device.

3.6.1.1 PARAMETERS RELATED TO THE QMS OPERATION

Several parameters relate ion particle density to the output current of the QMS electron multiplier. These parameters include the ionization chamber geometry [3.55], the particle ionization cross section [3.56], the efficiency of extraction of ion species from the ion source [3.57], and sensitivity [3.55, 3.58]. A simplified approach to modelling the response of a mass spectrometer has been described by Foxon et al [3.58]. They considered the instrument as a density detector and therefore its response h(t) to a group of molecules leaving a rotating chopper placed at a distance L from the spectrometer detector at a time t=0 is the density of molecules at a time t>0 in the ionizer, and is given by:

$$h(t) = 2.L^3.e^{-(L/t.a)^2}/a^3.t^4\sqrt{\Pi}^{1/2} \qquad (3.7)$$

where

$$a = (2.R.T/M)^{1/2} \qquad (3.8)$$

R is the gas constant and M the particle gram molecular weight, and T the absolute temperature.

The QMS allows the monitoring of different vapour species

from any number of sources because it can perform selective ion monitoring. In order to relate the electron multiplier current to the partial pressure of the selected vapour constituent a calibration of the QMS is necessary. Several techniques are available including the introduction of a reference gas with a known pressure [3.59], the use of a substance with a known weight [3.60], as well as relating the QMS measurements to other flux sensitive instruments [3.48]. An overall review of quadrupole mass spectrometry and its related processes has been included in an Msc thesis submitted to The University of Manchester,1986 [3.61].

3.6.1.2 DIGITAL MONITORING AND CONTROL OF A QUADRUPOLE MASS SPECTROMETER

Quadrupole mass spectrometers are normally brought under automatic control because they are easy to drive and monitor. Computer control of the QMS operation allows rapid acquisition of data as well as preventing errors which may occur in manual control like those due to slow tuning and measurement in multiple ion monitoring. In processes requiring rapid tuning and measurement of vapour particle densities the QMS output as well as the control of other instruments used in the deposition system, computer control becomes a necessity since several measurements may have to be related quickly [3.62]. Driving the QMS externally involves applying a low DC voltage (typically between 0 to 5

volts) to tune to a gaseous species. The relationship between mass-to-charge ratio and tuning voltage is almost linear. Non-linearity which can result may be attributed to to overheating effects on the radio-frequency generating circuits in the QMS [3.48]. To have consistent accuracy and cope with the non-linearity of tuning voltage variation with the a.m.u, a high accuracy and stability in driving the spectrometer are needed. In the computer control of the QMS, a digital-to-analogue converter is normally used [3.62]. For a QMS with a mass range equal to M_R and driven with an N bit DAC, the resolution R_Q available in determining a given mass-to-charge ratio (or a tuning voltage) is given by:

$$R_Q = (M_R.2^{-N}).100\% \qquad (3.9)$$

For a QMS with a 200 mass range, a 14 bit DAC, the resolution attainable in tuning to a given mass to charge ratio is equal to 1.2% for an instrument with unit mass resolution. Monitoring the output of the QMS can be undertaken using various techniques. In a computer controlled QMS the output is normally digitized with an analogue-to-digital converter [3.63] or a voltage-to-frequency converter [3.64] before loading into the computer memory whereas if the particle beam is modulated at a particular reference frequency the output is

then monitored using an instrument sensitive to the modulation frequency such as a lock-in amplifiers [3.65, 3.66, 3.67], multichannel analyser or averagers [3.58,3.68], box-car detectors [3.69], or ion counting systems [3.70]. The accuracy of the measurements undertaken is highly dependant on the measuring instrument. Systems including on-line processing of the signal at mass spectrometer have also been described in the literature [3.71].

Relating the output from the electron multiplier to the tuning voltage requires a calibration in terms of mass-to-charge ratio of gaseous particle species. This is achieved by recognizing one or more of the peaks for gases present in the vacuum chamber which may have been introduced for the purpose of calibration. After determining the position of reference peaks the tuning for other peaks is found by extrapolation to find the approximate tuning voltage [3.61]. A search for peak maximum is then performed within a small range around the predicted peak position. The search is necessary because the relationship between tuning voltage and particle mass-to-charge ratio is not precisely linear [3.48].

Under normal operating conditions the tuning voltages are stored in the computer memory and the calibration is achieved by a search for a peak maximum [3.72] of a selected gas species knowing the approximate tuning voltage (or DAC input) from data stored in a read-only-memory [3.63] or in a

random access memory [3.61]. Another method for finding a peak maximum consists of differentiating the output current of the QMS with respect to the tuning voltage [3.73]. Instead of finding a peak maximum, the number density at a particular mass-to-charge ratio has also been represented either by the peak centroid [3.74] or by the area under the peak [3.75]. Identification of vapour species can be undertaken on-line or off-line when multiplets or overlapping peaks difficult to resolve occur in the spectrum.

Besides the occurence of instrument errors due to the DAC resolution and the resolution of the ion current measuring circuitry, there are other sources of error which should be considered. Drift in the mass tuning, probably attributable to heating effects in the high voltage radiofrequency amplifiers of the quadrupole electronics, can be minimized by lowering the tuning voltage to a minimum (0 Volt) between samples. Drift also occurs in the electron multiplier gain causing a variation in the sensitivity to particle number density. This can be overcome by not relying on the electron multiplier gain and counting the arrival of ions instead using a pulse counting technique. Inaccuracies caused by noise statistical effects at the output of the QMS can be reduced by selecting peaks with a high signal-to-noise ratio. Use of integrators [3.76] or peak discrimination techniques [3.77] where a peak is recognized when its intensity exceeds a given threshold for

a number of consecutive samples also lead to a reduction in the signal noise content. Modulation of the particle beam can be employed to reduce noise on the QMS output and this is undertaken through demodulation of the measured signal a further improvement in the signal-to-noise ratio can then be obtained using a phase sensitive averaging technique [3.58, 3.67, 3.68, 3.69].

3.6.1.3 IONIZATION PHENOMENA IN A QUADRUPOLE MASS SPECTROMETER

In a quadrupole mass spectrometer particles are first ionized by an electron beam before being filtered by the quadrupole structure. Since the evaporating particles arrive at the ionization chamber in a neutral state, it is important to determine which particles get simply ionized there and which particles fragment during the ionization process. In order to understand this phenomenon it is necessary to review the effects occuring when ions are produced by electron impact.

3.6.1.3.1 GENERATION OF IONS IN THE MASS SPECTROMETER

Collisions and interactions between gas particles inside the vacuum chamber are negligible. The particle mean free path is too long when compared to the dimensions of the UHV

chamber. Ions are not produced from the sublimation of compound materials of interest in the present investigation but it is probable that most of the compound molecules undergo dissociation in the vapour source or dissociate inside the ionization chamber of the spectrometer under electron bombardment. In the latter case ions can also be produced. The minimum energy at which ionization of a single atom takes place is known as the ionization potential of this atom. This can be represented by:

$$X_{(gas)} + e- \longrightarrow X^{+}_{(gas)} + 2e- + IP(X) \qquad (3.10)$$

where IP(X) is the ionization potential of the gaseous atom X. The subscript (gas) means that the particle is in the gaseous phase. For a molecule XY, the minimum ionization energy is given by:

$$XY_{(gas)} + e- \longrightarrow XY^{+}_{(gas)} + 2e- + IP(XY) \qquad (3.11)$$

this is represented by curves (a) and (b) in figure 3.1. When ionization is accompanied by dissociation of the molecule (curves (c)), the minimum energy required to obtain the ions X^{+} is known as the appearance potential for the ion X^{+}. This is demonstrated by:

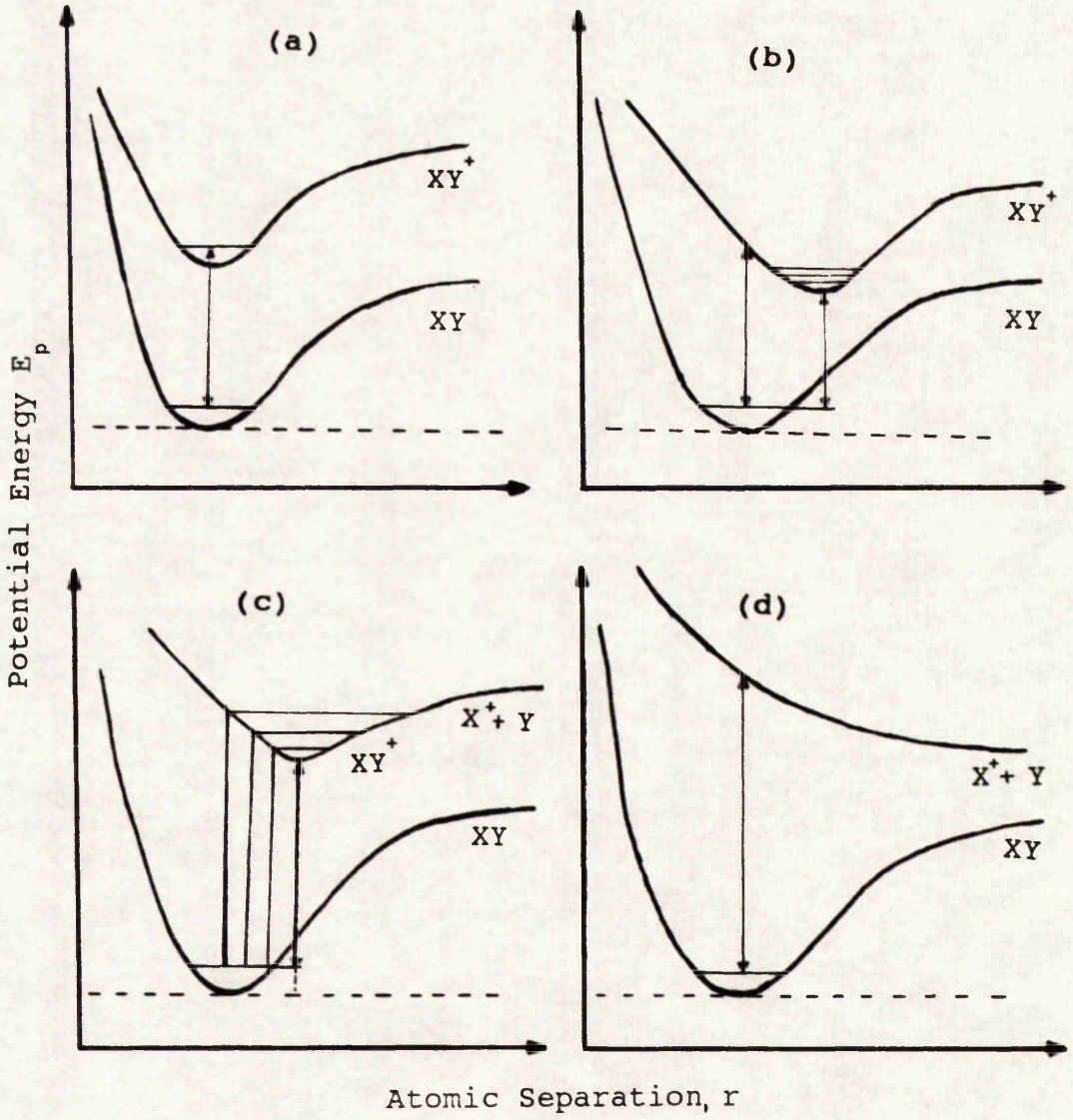

POTENTIAL ENERGY DIAGRAMS SHOWING:

(a) Equal vertical and adiabatic ionization process
(b) Vertical ionization with variation in the atomic separation
(c) Vertical ionization leading to the presence of parent and fragment ions
(d) Ionization accompanied by fragmentation

FIGURE 3.1

$$XY_{(gas)} + e^- \longrightarrow X^+_{(gas)} + Y_{(gas)} + 2e^- + AP(X^+) \qquad (3.12)$$

Curve (d) in figure 3.1 shows the case where dissociation always occurs. The appearance potential $AP(X^+)$ for the ion A^+ represents the energy $E_d(XY)$ required for the dissociation of the molecule XY plus the ionization potential of the atom X. Other sources of contribution include the molecule internal energy and kinetic energy of both X^+ and Y particles. Therefore,

$$AP(X^+) \geqslant IP(X^+) + E_d(XY) \qquad (3.13)$$

When a binary compound XZ which yields monomers X and dimers Z_2 after dissociation, the appearance potential for an ion Z^+ will then include the dissociation energy $E_d(Z_2)$ for the molecule Z_2 as well. This is shown in the successive processes:

$$XZ_{(gas)} \longrightarrow X_{(gas)} + \tfrac{1}{2}Z_{2(gas)} + E_d(XZ) \qquad (3.14)$$

If sufficient energy is supplied the molecule $Z_{2(gas)}$ dissociates and yields the ions Z^+ as shown

in equation (3.12). However, it is also possible at a lower energy that ionization of the dimer Z_2 occurs before dissociation according to:

$$Z_{2(gas)} + e^- \longrightarrow 2e^- + Z^+_{2(gas)} + IP(Z_2^+) \qquad (3.15)$$

The ion Z^+ is then obtained after the dissociation of Z_2^+ and hence from (3.12), (3.14), and (3.15):

$$AP(Z^+) \geqslant IP(Z^+) + E_d(XZ) + E_d(Z_2) \qquad (3.16)$$

The processes described can be used to demonstrate whether the particle species recorded by the mass spectrometer are due to parent molecules (or atoms) or whether fragmentation in the ionization chamber has occured. A detailed review of particle ionization processes is given by Reed [3.78].

In a QMS, control is exercised over the energy of the ionizing electrons. At low electron energies the amount of energy transfered to the molecule is equal to that of the electron beam. It is the transfer of this energy to the particle which causes its fragmentation or ionization. However, at higher energies other factors affect this assumption.

These factors include the presence of an electric field and the build up of a space charge inside the ionization chamber, the existence of a difference of potential between the filament and the ionization chamber [3.79], and the fact that only a fraction of the ions formed are collected because of the focusing fields. These factors can be minimized through careful operating procedures like regular ion source cleaning and reducing the filament emission current.

3.6.1.4 ELECTRON ENERGY AND IDENTIFICATION OF IONIZATION THRESHOLDS

For measuring the ionization potential of a particular vapour species using a mass spectrometer it is necessary for the electron energy to be set to a higher value than that expected for the sample gas, then the number density for the evaporant species is monitored while the electron energy is reduced. Given a particular QMS ionization source design, it is usually assumed that the particles under investigation are ionized by a parallel beam of constant energy electrons and that ionization cross section for the vapour particle is constant.

The variation of the ion current with the electron current yields the ionization curve of selected vapour species. A requirement in the present research is the

ability to adjust the electron energy precisely near the ionization threshold regions. Methods for the interpretation of ionization potential curves and determination of the appearance potential of the vapour species have described in the literature and including the linear extrapolation method [3.80, 3.81], Honig's method which takes into account the electron energy spread [3.82] and Morrisson's method where the ion current is derived according to the mean electron energy [3.83].

Although higher values are obtained for appearance potentials using the linear extrapolation method [3.84], it is by far the most practical technique and does not involve complex calculations. If a reference gas with a known appearance potential is introduced in a particular experiment linear extrapolation yields consistent accuracy in the measurement of appearance potential for other particles. The operating conditions of the instrument should be kept constant so that factors like the particle ionization cross-section can be assumed as constant.

An ideal ionizing electron beam should have all of its electrons confined within a small energy band. Since in electron beams emitted by (tungsten) filaments the electrons produced are not monoenergetic, monoenergetic electron impact methods have been developed by several workers [3.85, 3.86, 3.87]. A spread of energy in the beam is inherent and this spread may obscure ionization thresholds, particularly in investigations where more than one type of particle

occurs having similar mass-to-charge ratio [3.81]. This has led to the use of special techniques to make such studies feasible. These methods may include the analytical treatment of ionization curves [3.81], modulation of the ionizing electron beam and use of a retarding potential [3.88, 3.89], or the use of a monochromatic light beam [3.90] to ionize the particles. Although attractive these techniques introduce increased complexity to the system as well as requiring extensive off-line processing of the signals. The spread in the electron energy may be reduced by maintaining a constant potential between the filament and the ionization chamber. In recent QMS instruments the problems are alleviated by careful design of the ion source and the electric fields it produces.

3.7 RELATING THE QMS AND THE QUARTZ CRYSTAL MICROBALANCE OUTPUTS

A deposition rate monitor based on a resonant quartz crystal provides absolute measurements of the amount of condensed material on the quartz plate. Relating these measurements to those provided by a QMS housed in the same deposition apparatus yields a method for calibrating the QMS.

If D_m is the deposition rate measured using the quartz crystal microbalance and N_m the number density of incident particles, each of mass m, condensing on the quartz plate, then the following relationship can be written:

$$D_m = m\, N_m\, v \qquad (3.17)$$

where v is the average velocity of the particles. The particle velocity can be related to the absolute temperature using a Maxwellian distribution of gas particles yielding:

$$v = (2.K.T/m)^{1/2} \qquad (3.18)$$

where K is Boltzmann's constant and T the absolute temperature. The number density is proportional to the ion current measured at the output of the QMS. This shows that at a particular temperature the output of the QMS is proportional to the deposition rate measured using the microbalance. When the temperature is varied the resulting variation in particle velocity leads to a variation in the sensitivity of the mass spectrometer. For a small change dT in temperature, the variation in the particle velocity is:

$$dv/v = 1/2 \; . \; dT/T \qquad (3.19)$$

At a typical operating temperature of 1250 °K an increase in temperature of 40 °K yields a variation in evaporant particle velocity inducing a sensitivity variation approaching 1%. Because the variation of source temperature over the range of deposition rate used is small the assumption that the QMS output is proportional to the deposition rate incurs little error.

The QMS is sensitive not only to the material emanating from the vapour source but also to the particles in the atmosphere inside the ionization chamber. However, the microbalance output is sensitive only to the intensity of the directional flux beams which give rise to deposition on the resonant quartz plate.

Relating the mass spectrometer output to the deposition rate may then be difficult to carry out and this can be detrimental in calibrating the mass spectrometer measurements during film deposition.

3.8 CONCLUSION

The methods used for controlling and monitoring both the evaporation and deposition of film materials have been

described. The methods described included the use of ionization gauges, temperature control, electron diffraction techniques (RHEED,LEED...), microbalances, and mass spectrometry. In the present work using modulated beam mass spectrometry, flux monitoring is undertaken by using a QMS and a quartz crystal microbalance. The relevant details about the use of these instruments have therefore been emphasised. Ionization of evaporant particles inside the mass spectrometer ionization chamber has been described and a method for identifying parent molecules or atoms presented. It has also been shown that it is easier to relate the mass spectrometer output to that of the microbalance if the background vapours contribution to the QMS number density measurements are removed. This can also help with the calibration of the spectrometer since the microbalance gives a direct measurement on the mass of deposited material.

In a deposition system environment it is advantageous to digitize monitored quantities such as source temperature and vapour fluxes for subsequent analysis by computer so that changes occuring in the system parameters become apparent and can subsequently be corrected if required. This is undertaken in the present work by using a computer controlled modulated beam mass spectrometry system.

3.9 REFERENCES

[3.1] A.Guthrie And R.K.Wakerling
"Vacuum Equipment And Techniques"
Mc.Graw.Hill Inc. New York p.129 (1949)

[3.2] P.A.Redhead
1958 Fifth National Symposium On Vacuum Technol.
Trans. Pergamon Press Inc. New York pp.148-152 (1959)

[3.3] P.A.Redhead
Canadian Journal Of Physics Vol.37 p.1260 (1959)

[3.4] K.A.Spangenberg
"Vacuum Tubes"
Mc.Graw.Hill Inc. p.771 (1948)

[3.5] R.T.Bayard And D.Alpert
Rev. Sci. Instrum. Vol.21 p.571 (1950)

[3.6] D.Alpert And R.S.Buritz
J. Appl. Phys. Vol.25 pp.202-209 (1954)

[3.7] M.PIRANI and J.YARWOOD
"Principles of Vacuum Engineering"
Chapman and Hall london (1961)

[3.8] A.E.BARRINGTON
"High Vacuum Engineering"
Prentice-Hall,Inc. U.S.A p.82 (1963)

[3.9] J.LILJA, J.KESKINEN, M.HOVINEN, AND M.PESSA
J. Vac. Sci. Technol. Vol.B7 p.593 (1988)

[3.10] H.CHENG, S.K,MOHAPATRA, J.E.POTTS And T.L.SMITH
J. Cryst. Growth Vol.81 pp.512-517 (1987)

[3.11] P.G.CHILTON, W.S.TRUSCOTT, AND Y.F.WEN
J. Vac. Sci. Technol. Vol. B6 p.1099 (1988)

[3.12] J.B.PENDRY
"Low Energy Electron Diffraction: The Theory And
Its Applications To The Determination Of Surface
Structure" Academic Press London (1974)

[3.13] M.A.VAN.HOVE AND S.Y.TONG
"Surface Crystallography By LEED"
Springer Berlin (1979)

[3.14] R.O.JONES AND P.J.JENNINGS
"LEED Fine Structure: Origins And Applications"
Surface Science Reports North-Holland Amsterdam

pp.165-196 Vol.9 No 4 (1988)

[3.15] P.M.ECHENIQUE AND J.B.PENDRY
J. Phys. C Vol.11 p.2065 (1978)

[3.16] S.M.THURGATE AND P.A.JENNINGS
Appl.Surf.Sci. Vol.22/23 p.478 (1985)

[3.17] S.THURGATE AND G.HITCHEN
Appl. Surf. Sci. Vol.24 p.202 (1985)

[3.18] B.A.JOYCE, J.H.NEAVE, P.J.DOBSON And P.K.LARSEN
Phys. Rev. Vol.B29 p.814 (1984)

[3.19] J.H.NEAVE, B.A.JOYCE, P.J.DOBSON, AND N.NORTON
Appl. Phys. Vol.A31 p.1 (1983)

[3.20] B.A.JOYCE
In P.M.DRYBURGH, B.COCKAYNE And K.G.BARRACLOUGH
(eds.)"Advanced Crystal Growth. "
Prentice Hall Internl. UK Ltd. pp.337-385 (1987)

[3.21] R.M.PARK And N.M.SALANSKY
J. Vac. Sci. Technol. Vol.B3(2) pp.676-680 (1985)

[3.22] J.H.NEAVE and B.A.JOYCE
J. Cryst. Growth Vol.44 p.387 (1978)

[3.23] H.J.CORNELLISSEN, D.A.CAMMACK And R.J.DALBY
J. Vac. Sci. Technol. Vol.B6(2) pp.769-772 (1988)

[3.24] H.KUWABARA, H.FUJIYATSU, H.SHIMIZU And A.SASAKI
J. Cryst. Growth Vol.72 pp.299-303 (1985)

[3.25] J.LILJA, J.KESKINEN, M.HOVINEN And M.PESSA
J. Vac. Sci. Technol. Vol.B7(4) pp.593-598

[3.26] M.KIMATA, A.RYOJI And T.AOKI
J. Cryst. Growth Vol.81 pp.508-511 (1987)

[3.27] P.J.DOBSON, B.A.JOYCE, J.H.NEAVE, AND J.ZHANG
Proceedings Of The 7th I.S.S.C
Vacuum, Vol.38 Nb.4/5 pp.422-423 (1988)

[3.28] A.BOSACHI, S.FRANCHI, Y.O.KANTER And S.I.CHIKICHEV
J. Cryst. Growth Vol.96 pp.899-905 (1989)

[3.29] H.H.FARREL, M.C.TAMARGO And J.L.DE.MIGUEL
J. Vac. Sci. Technol. Vol.B6(2) pp.767-768 (1989)

[3.30] D.P.WOODRUFF And T.A.DELCHAR
"Modern Techniques Of Surface Science. "
Cambridge Univ. Press p.72 (1986)

[3.31] P.J.DOBSON, B.A.JOYCE, J.H.NEAVE, AND J.ZHANG

J. Cryst. Growth Vol.81 p.1 (1987)

[3.32] C.T.FOXON
J. Cryst. Growth Vol.95 pp.11-16 (1989)

[3.33] A.BOSACCHI AND S.FRANCHI
J. Cryst. Growth Vol.96 pp.899-905 (1989)

[3.34] A.J.SPRINGTHORPE AND P.MANDEVILLE
J. Vac. Sci. Technol. B.6(2) pp.754-757 (1988)

[3.35] A.W.VERE
"Crystal Growth. Principles And Progress"
Plenum Press New York pp.132-133 (1987)

[3.36] D.P.WOODRUFF AND T.A.DELCHAR
"Modern Techniques Of Surface Science"
Cambridge Univ. Press (1986)

[3.37] G.Z.SAUEBREY
Zietschrift Für Physik Vol.155 p.206 (1959)

[3.38] W.STECKELMACHER
in L.Holland "Thin Film Microbalance"
Chap.5 p.204 Chapman And Hall (1965)

[3.39] D.KING AND G.R.HOFFMAN
J. Phys. E: Sci. Intrum. Vol.4 pp.993-998 (1971)

[3.40] D.KING, R.C.F.HEYWORTH, AND G.R.HOFFMAN
J. Phys. E: Sci. Instrum. Vol.6 pp.86-89 (1972)

[3.41] A.W.WARNER AND C.D.STOCKBRIDGE
Vacuum Microbalance Techniques Vol.3 p.55 (1963)

[3.42] J.E.JOHNSON
J. Appl. Phys. Vol.36 p.3193 (1965)

[3.43] K.H.BEHRNDT
J. Vac. Sci. Technol. Vol.8 p.622 (1971)

[3.44] CHIN-SHUN LU
J. Vac. Sci. Technol. Vol.12 p.578 (1975)

[3.45] A.R.OWENS
J. Phys. E: Sci. Instrum. Vol.15 p.789 (1982)

[3.46] THICKNESS MONITOR SERIES QM-300
Veeco Instruments Inc. Terminal Drive
Plainview New York (USA)

[3.47] MODEL XTM
Inficon Inc. Syracuse New York (USA)

[3.48] A.S.SAHIN

PhD Thesis University Of Manchester UK (1983)

[3.49] P.J.CHANDLER, P.R.MEEK AND L.HOLLAND
Thin Solid Films Vol.86 p.183 (1981)

[3.50] H.K.PULKNER AND H.HILBRAND
Zeitschrift Für Angewandte Physik Vol.23 p.15 (1967)

[3.51] E.P.EER.NISSE
J. Appl. Phus. Vol.43 p.1330 (1972)

[3.52] D.KING
PhD Thesis University Of Manchester UK (1976)

[3.53] P.H.DAWSON
"Quadrupole Mass Spectrometry And Its Applications"
Elsevier Sci. Pub. Company Amsterdam (1976)

[3.54] J.R.CHAPMAN
"Computers In Mass Spectrometry"
Academic Press London UK (1978)

[3.55] V.J.A.KORPIO
Vacuum-Technik Vol.38 5-6 pp.134-142 (1989)

[3.56] A.MÜLLER, K.TINSCHERT, ACHENBACH, E.SALZBORN,
AND R.BECKER Nuclear Instrum. Ad Methods In Phys.
Research Vol.B10/11 pp.204-206 (1985)

[3.57] R.F.C.FARROW
J. Phys. D: Appl. Phys. Vol.7 pp.2436-2448 (1974)

[3.58] C.T.FOXON, B.A.JOYCE, R.F.C.FARROW, AND R.M.GRIFFITHS
J. Phys. D: Appl. Phys. Vol.7 pp.2422-2435 (1974)

[3.59] R.E.ELLEFSON, D.CAIN, AND C.N.LINDSAY
J. Vac. Sci. Technol. Vol.A5(1) pp.134-139 (1987)

[3.60] C.T.FOXON, J,A,HARVEY, AND B.A.JOYCE
J. Phys. Chem. Solids Vol.34 pp.1693-1701 (1974)

[3.61] M.BENYEZZAR
MSc. Thesis University Of Manchester UK (1986)

[3.62] D.DAHLGREN, J.ARNOLD, AND J.C.HEMMINGER
J. Vac. Sci. Technol. Vol.A1(1) pp.81-83 (1983)

[3.63] A.S.SAHIN
MSc Thesis University Of Manchester UK (1980)

[3.64] K.D.J.ROOT
In R.A.G.Carrington (ed) "Computers For
Specroscopists" Adam Hilger London UK (1974)

[3.65] D.P.BLAIR AND P.H.SYDENHAM

J. Phys. E: Sci. Instrum. Vol.8 pp.621-627 (1975)

[3.66] M.L.MEADE
J. Phys. E: Sci. Instrum. Vol.15 pp.395-403 (1982)

[3.67] R.H.JONES, D.R.OLANDER, W.J.SIEKHAUS, AND J.A.SHWARZ
J. Vac. Sci. Technol. Vol.9 No.6 (1972)

[3.68] V.L.HIRSHY AND J.P.ALDRIDGE
Rev. Sci. Instrum. Vol.42 No.3 pp.381-383 (1971)

[3.69] S.S.BANO, P.N.REDDY, B.P.N.REDDY, AND N.C.E.REDDY
Rev. Sci. Instrum. Vol.58 No.10 pp.1945-1947 (1987)

[3.70] D.A.SCHOELLER AND J.M.HAYES
Analyt. Chem. Vol.47 p.408 (1975)

[3.71] M.GROB, H.P.EGLI, A.HOFMÄNNER, G.REIS, AND G.RETTINGHAUS
J. Vac. Sci. Technol. Vol.A5(4) p.2428 (1987)

[3.72] R.BINKS, R.L.CLEAVER, J.S.LITTLER, AND J.MAC.MILLAN
Chem. In Britain Vol.7 p.8 (1971)

[3.73] A.CARRICK
Int. J. Mass Spectrom. Ion Phys. Vol.2 p.333 (1969)

[3.74] J.S.HALLIDAY
In E.Kendrick (ed.) "Advances In mass spectrometry"
Intitute Of petroleum London UK Vol.4 p.239 (1968)

[3.75] W.J.Mc.MURRAY, S.R.LIPSKY, AND B.N.GREEN
In E.Kendrick (ed.) "Advances In mass spectrometry"
Intitute Of petroleum London UK Vol.4 p.77 (1968)

[3.76] W.F.HOLMES, W.H.HOLLAND, B.L.SHORE, D.M.BIER AND W.R.SHERMAN
Analyt. Chem. Vol.45 p.2063 (1973)

[3.77] E.C.HORNING, G.M.HORNING, D.I.CARROLL,DZIDIC, AND R.N.STILLWELL
Analyt. Chem. Vol.45 p.936 (1973)

[3.78] R.I.REED
"Ion Production By Electron Impact"
Academic Press Inc. London (1962)

[3.79] J.D.WALDRON AND K.WOOD
"Mass Spectrometry Conference"
Institute Of Petroleum London p.16 (1952)

[3.80] H.D.HAGSTRUM
J. Chem. Phys. Vol.16 p.848 (1948)

[3.81] R.H.VOUGHT Phys. Rev. Vol.71 p.93 (1947)

[3.82] R.E.HONIG
J. Chem. Phys. Vol.16 p.105 (1948)

[3.83] J.D.MORRISSON
J. Chem. Phys. Vol.22 p.1219 (1954)

[3.84] R.I.REED
"Mass Spectrometry"
Academic Press London p.189 (1965)

[3.85] W.B.NOTTINGHAM
PHYS, REV. VOL.55 P.203 (1939)

[3.86] P.MARMET, AND L.KERVIN
Canadian J. Phys. Vol.38 p.787 (1960)

[3.87] E.M.CLARKE
Canadian J. Phys. Vol.32 p.764 (1954)

[3.88] R.E.FOX, W.M.HICKAM, T.KJELDAAS.Jr, AND D.J.GROVE
Phys. Rev. Vol.84 p.859 (1951)

[3.89] G.G.CLOUTHIER AND H.I.SCHIFF
"Advances In Mass Spectrometry"
Pergamon Press London p.473 (1959)

[3.90] H.HURZELER, M.G.INGHRAM, AND J.D.MORRISSON
J. Chem. Phys. Vol.28 p.76 (1958)

CHAPTER 4

DESIGN OF A MODULATED BEAM MASS SPECTROMETRY SYSTEM

4.1 INTRODUCTION

The objective of this chapter is to describe the instrumentation designed and developed for modulated beam mass spectrometry experiments. Previous measurements on the number density for the vapour species of zinc selenide have shown the presence of large background number densities for zinc particles [4.1]. The effect of the background vapours has to be investigated since it interferes with the measurements on the vapour species emanating from the sources.

The modulated beam mass spectrometry system has been developed around an existing ultra high vacuum (UHV) system. The apparatus constructed for making modulated beam mass spectrometry measurements included both mechanical and electrical hardware designs. Software has also been developed to assist with overall control of the system. Computers are used throughout the system and particular

computers are dedicated to specific tasks. A hierarchy for organizing the control and monitoring of the physical parameters has been developed which greatly enhances the flexibility and ease of use of the system.

4.2 THE UHV SYSTEM AND THE MECHANISM FOR CHOPPING THE VAPOUR STREAM

The deposition apparatus is based on a Vacuum Generators [4.2] UHV system having a work chamber of 305 mm diameter. Figure 4.1 shows a cross section of the chamber. Oil free pumps are employed throughout to avoid contamination of both the substrate and the Knudsen cell assembly. The vacuum chamber is evacuated with a 140 l/s Varian ion pump [4.3]. The base pressure of the system after an 18 hour bake at 200 °C with the sources held at 500 °C is less than 10^{-10} torr. Liquid nitrogen shrouds are used throughout the system and this helps trap background vapours and reducing contamination of the substrate.

Two Knudsen cell vapour sources are installed in the vacuum chamber and positioned symmetrically with respect to the exposed area of the substrate. The sources are loaded with ZnS and ZnSe compounds and the evaporant streams are emitted horizontally to converge on the centre of the substrate deposition area. A pyrolitic boron nitride

FIGURE 4.1

CROSS-SECTION OF THE ZnS-ZnSe DEPOSITION SYSTEM

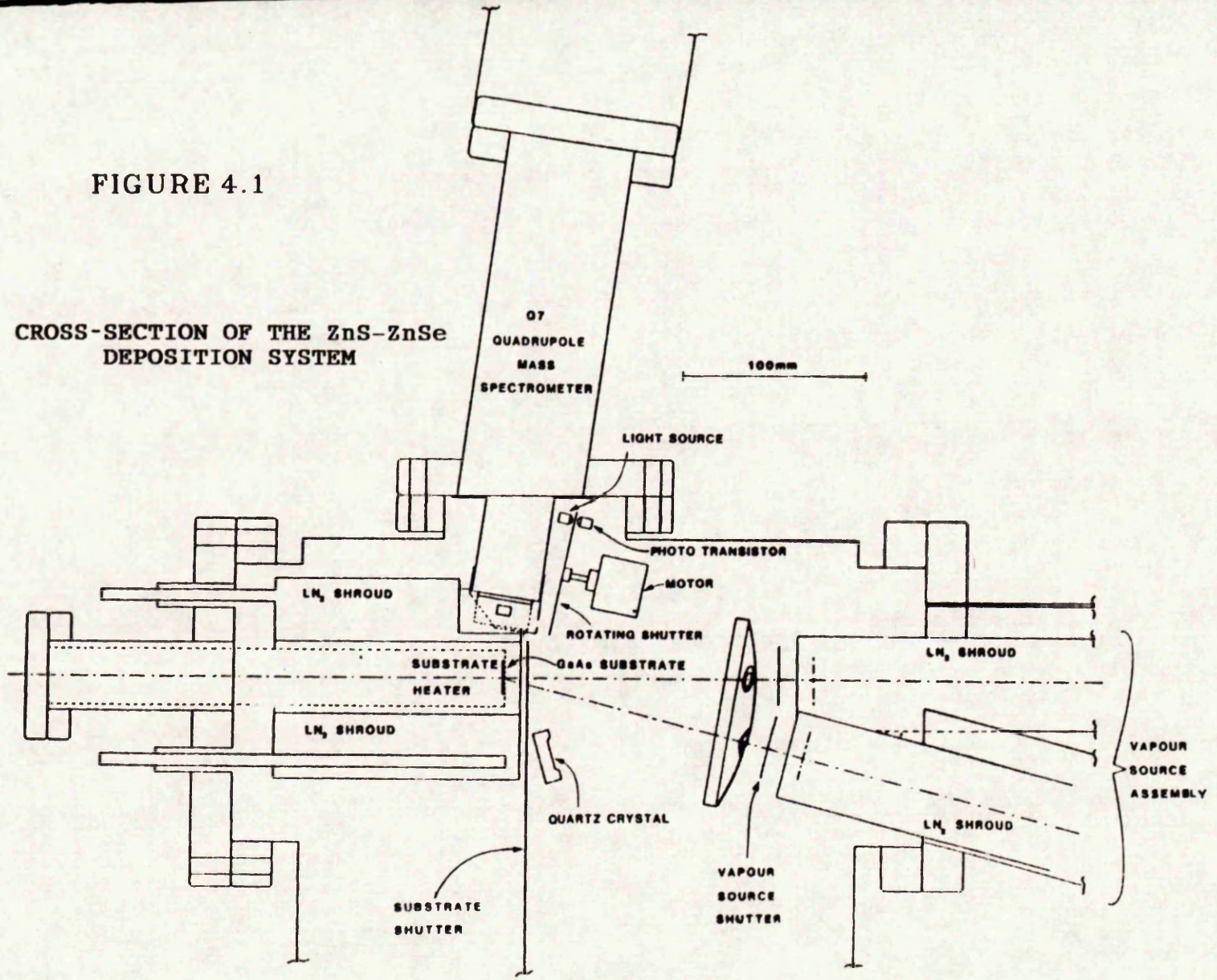

crucible is used for holding the material to be vapourized inside the ZnS source, but a cylindrical carbon crucible has been found satifactory for the ZnSe source. These crucibles are open ended and the conditions inside the cells differ considerably from those of equilibrium normally associated with Knudsen cell operation.

A Q7 quadrupole mass spectrometer (Vacuum Generators Ltd) fitted to the system for determining the number densities of evaporant species is mounted in a cross-beam configuration to separate neutral vapour species from those that have become ionized. Vapour shielding is used to minimize contamination of the ionization chamber and quadrupole rods with evaporant material. Liquid nitrogen cooled surfaces surround the ionization chamber to trap evaporant particles which may impinge on them. The electronic circuitry of the Q7 has been modified to provide a mass range of 200 a.m.u. Emission current for ionizing electrons can be measured with instruments outside the spectrometer to provide readings from 1 uA upwards and thus providing a more accurate means for emission current setting and measurement.

4.3 POSITIONING OF THE VAPOUR CHOPPING ASSEMBLY INSIDE THE UHV CHAMBER

Included in the vacuum chamber is a mechanical vapour

stream modulation device. A stainless steel structure has been designed to hold a small 3 phase synchronous motor made by Ferranti [4.4] which rotates an 8 blade shutter. Figure 4.2 shows a side view indicating the positioning of the vapour chopping assembly with respect to the vapour shield for the mass spectrometer. The rotation speed for the bakeable stainless steel synchronous motor is governed from the frequency of the sinusoidal voltages applied to the windings. The range of speeds available extends from 180 up to 7800 rpm. This exceeds the recommended maximum running speed. The stainless steel shutter is a disc 7 cm in diameter with the 8 blades 13.6 mm wide designed to provide equal on and off periods for the chopped vapour stream and the precision of the mechanical dimensions is better than 0.05 mm. The shutter is attached to the end of the motor shaft with three 8 BA pinch screws. Tightening of the screws played a crucial role in balancing the rotating shutter before placement inside the vacuum chamber. Also attached to the motor mounting bracket is a shutter position sensing device which uses a phototransistor and a filament lamp light source. A 300 micrometer wide slit is used to collimate the light emitted by the lamp towards the phototransistor. This improved on the edges of the pulses produced at the modulation frequency by the phototransistor. Figure 4.3 shows a drawing of the shutter for vapour stream modulation. The rotating shutter is positioned 24.3 mm from the centre of the QMS ionization chamber. A detailed description of the motor and rotating shutter has been

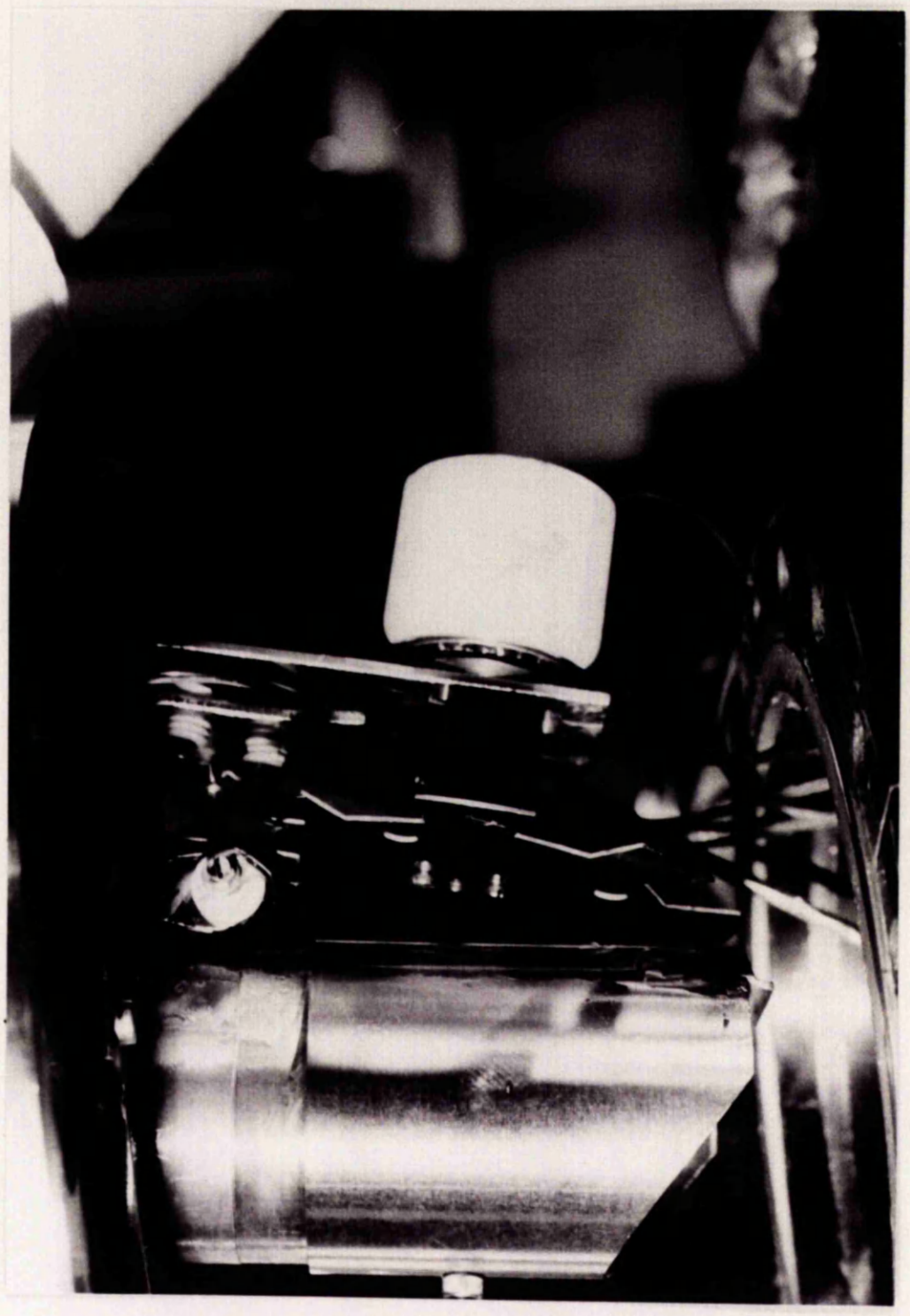

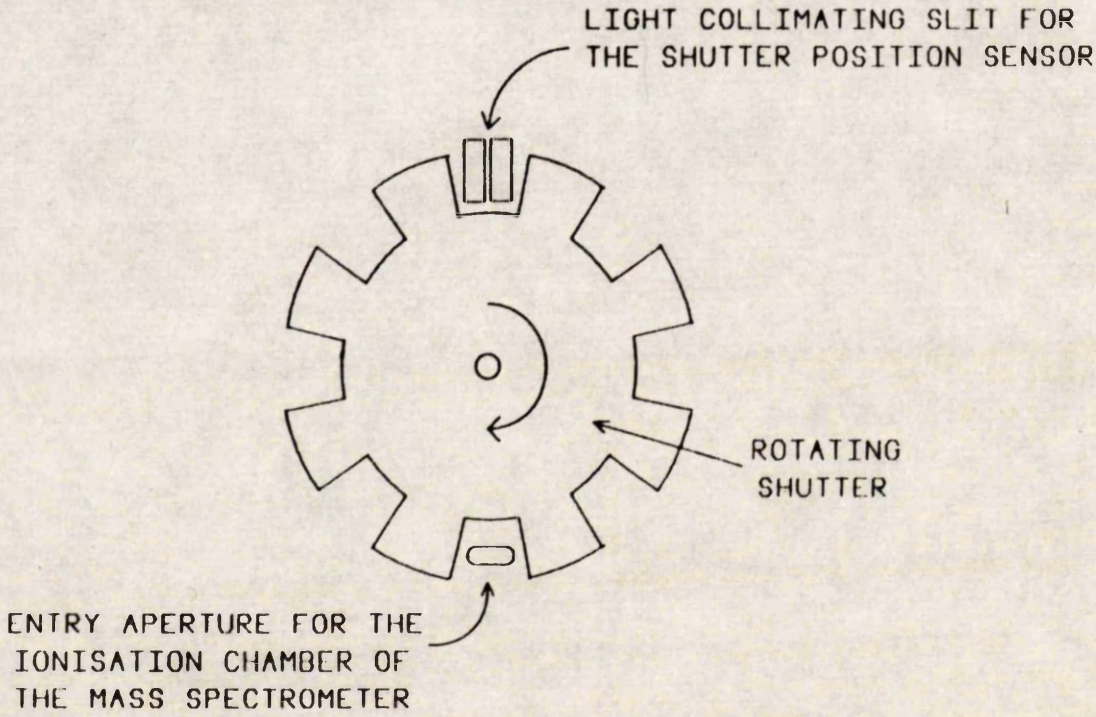

DIAGRAM SHOWING A SKETCH OF THE VAPOUR STREAM MODULATOR

FIGURE 4.3

PHOTOGRAPH SHOWING THE POSITION OF THE VAPOUR STREAM MODULATOR ASSEMBLY WITH RESPECT TO THE SHIELD OF THE MASS SPECTROMETER IONIZATION CHAMBER

FIGURE 4.2

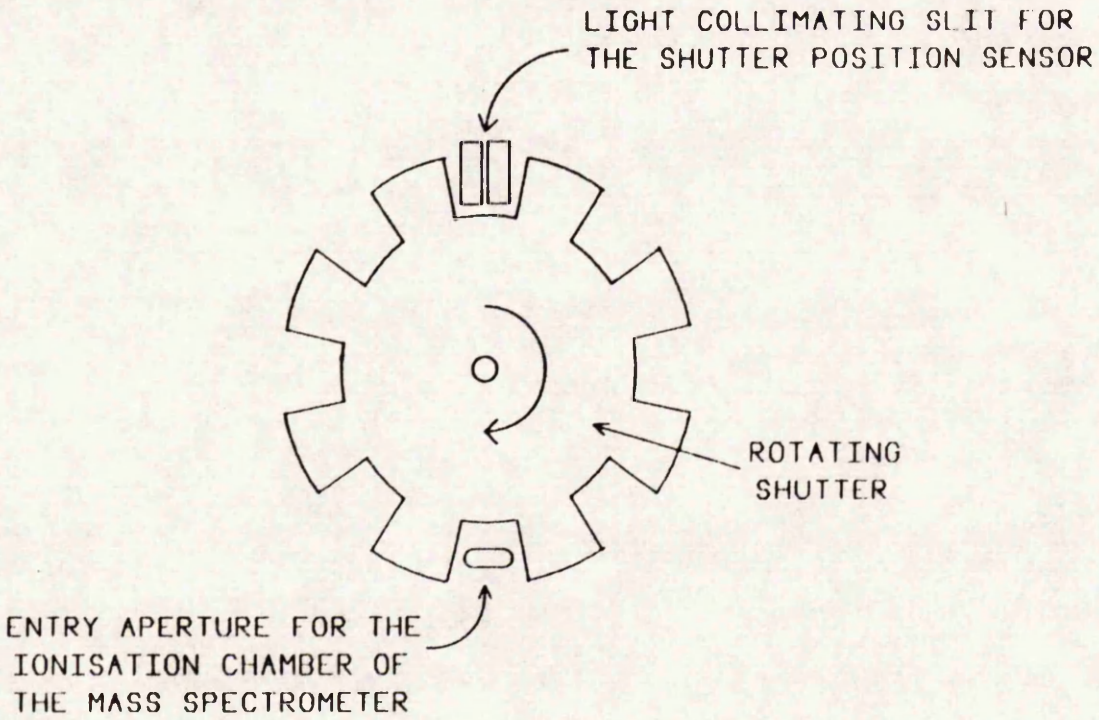

DIAGRAM SHOWING A SKETCH OF THE VAPOUR STREAM MODULATOR

FIGURE 4.3

included in an MSc thesis submitted to the University of Manchester [4.5].

A water cooled thickness-shear quartz resonator for the microbalance is sited in a position where it receives relatively less vapour flux than either the substrate or the mass spectrometer and this results from the geometry of the system precluding it being mounted in an optimum position.

Figure 4.4 contains a photograph showing the relative positioning of the rotating shutter, the microbalance quartz crystal monitor, and he entrance to the QMS ionization chamber seen through the shutter blades. The substrate holder, although not included in the picture is normally positioned vertically below the QMS entrance. In the substrate assembly, a 6.5 mm square of gallium arsenide is mounted on a tantalum disc which forms part of temperature controlled oven. The disc is heated from behind by a tantalum filament and a W/W-Re thermocouple measures the substrate temperature. Control over the substrate temperature is provided by a Eurotherm three-term temperature controller [4.6].

4.4 THE CONTROL INSTRUMENTATION USED FOR MAKING MODULATED BEAM MASS SPECTROMETRY MEASUREMENTS

An overall computer control strategy which includes a hierarchical organization of the control tasks has been

PHOTOGRAPH SHOWING THE POSITION OF MEASUREMENT DEVICES INSIDE THE UHV CHAMBER

FIGURE 4.4

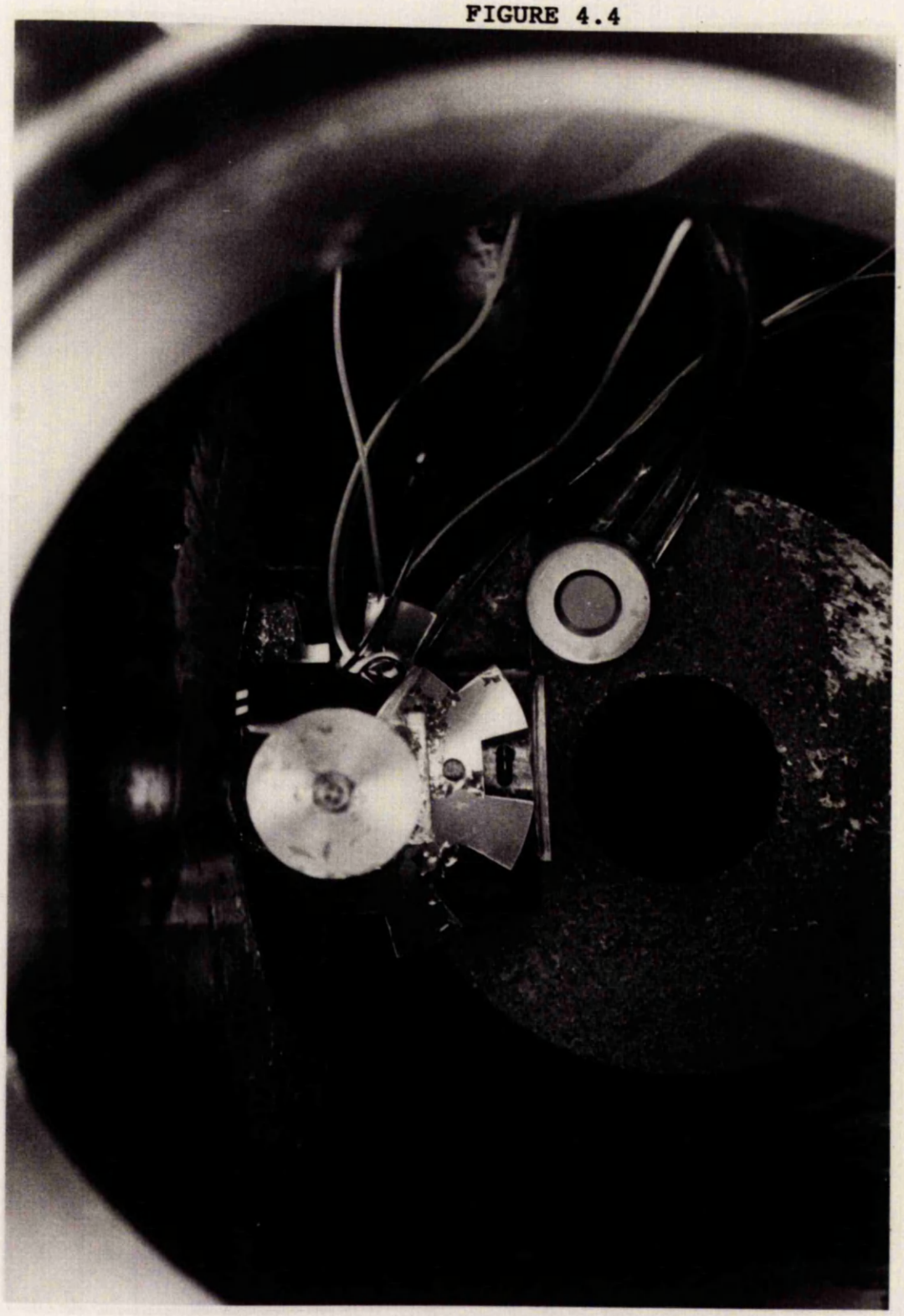

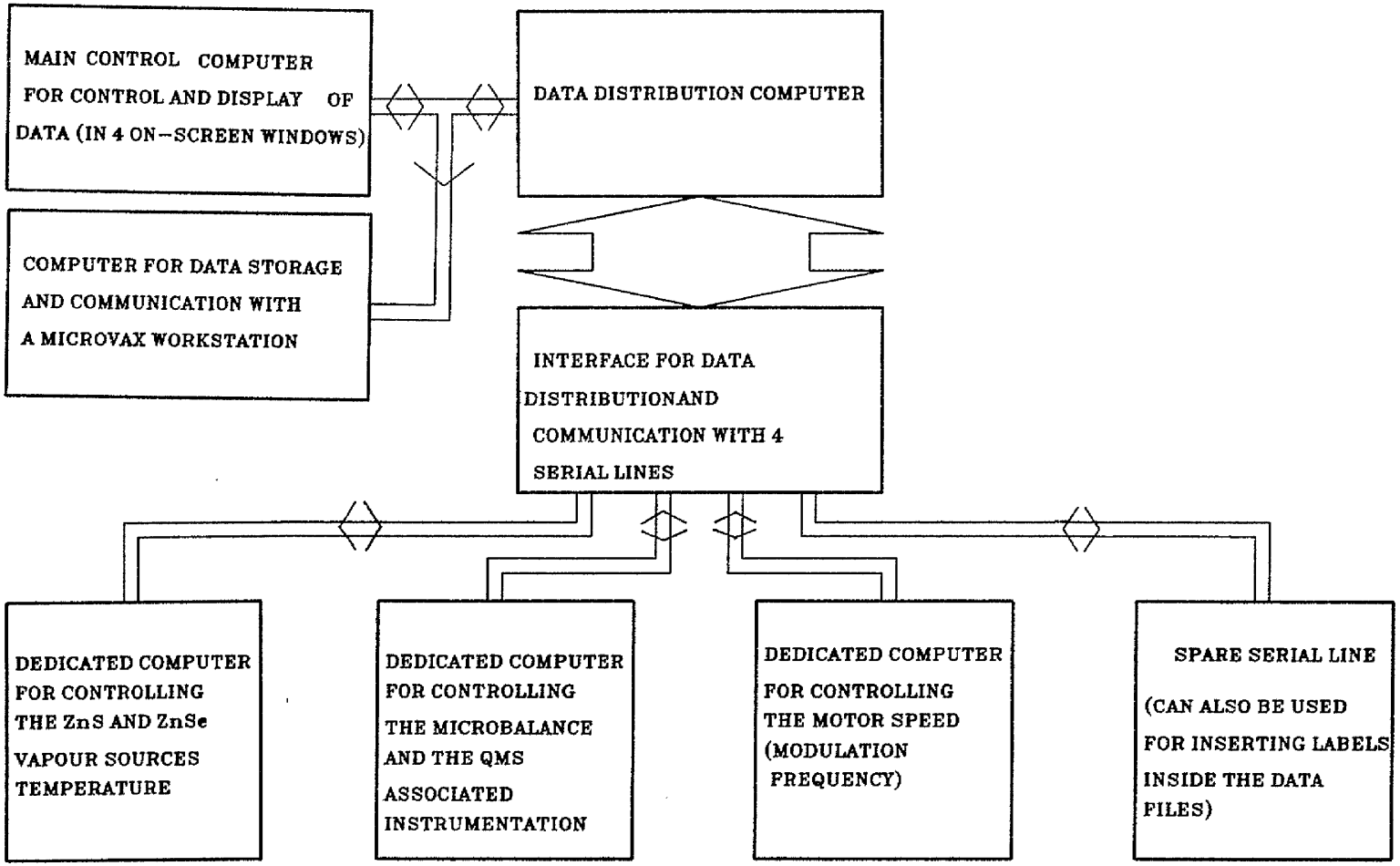

BLOCK DIAGRAM SHOWING THE ORGANIZATION OF COMPUTERS FOR DATA ACQUISITION AND CONTROL OF THE INSTRUMENTS EMPLOYED

FIGURE 4.5

adopted for the system. Figure 4.5 shows a block diagram which indicates the lines of communication for the various monitoring and control devices. At the top of the hierarchy is the main control computer which is user interactive and the processes to be monitored or the tasks to be undertaken are either read in a multiwindow display or loaded as control statements by the operator directly through addressing the target instrument. The main control computer is used as an intelligent host terminal since it allows for loading most the instrumentation control software to requisite computers. The main control computer (BBC model B 6502 microprocessor based [4.7]) connects to a data distribution computer (also a BBC model B) which takes the addressed control statements or software from the main computer and selects the appropriate destination for the information. The computers are interconnected through serial lines (RS423) using a parallel bus unit interfaced to serial line drivers. The interface handles multiplex serial line data and sorts it out for sending to the peripheral computers. Communication between the data distributing computer and the main control computer is at a Baud rate of 9600 and the exchanged data consist of a succession of singles line of bytes beginning with a channel identifier and ending with a carriage return. An auxilliary computer is used to monitor the transfer of data to and from the data distributor as well as providing a facility for storing the transferred data onto disk or for sending it to a D.E.C MicroVax workstation [4.8].

Forth microcards have been dedicated to the monitoring and control tasks of the various instruments. The dedicated computers have dedicated on ROM (read only memory) software for the tasks to be undertaken in monitoring or controlling the assigned instruments. Since the software control for the instruments is executed using the Forth language, the operator can use the main control computer directly to monitor or control particular instruments. Two Essex Forth microcards [4.9] are used, one for the control of motor speed (ie the modulation frequency) and the other for controlling the temperature of the ZnS and ZnSe vapour sources. These devices are designed as self contained microcontrollers with peripheral ports and serial communication capabilities. The central processing unit is an enhanced Rockwell 6502 microprocessor [4.10].

For controlling the mass spectrometer and the quartz crystal microbalance, a T.D.S (Triangle Digital Services) Forth microcard [4.11] is used. This device is based on a 6303 microprocessor (compatible with the 6800 family of Motorola microprocessors) and includes a serial communication channel. Parallel communication between this device and the control instrumentation dictated the development of peripheral ports for addressing and acquiring data from the assigned peripheral instruments. The developed data and address interface to this microcard is described in appendix A. A fourth serial line has been made available for future expansions and can be used to insert

BLOCK DIAGRAM OF THE OVERALL ELECTRONIC SYSTEM USED IN MODULATED BEAM MASS SPECTROMETRY EXPERIMENTS

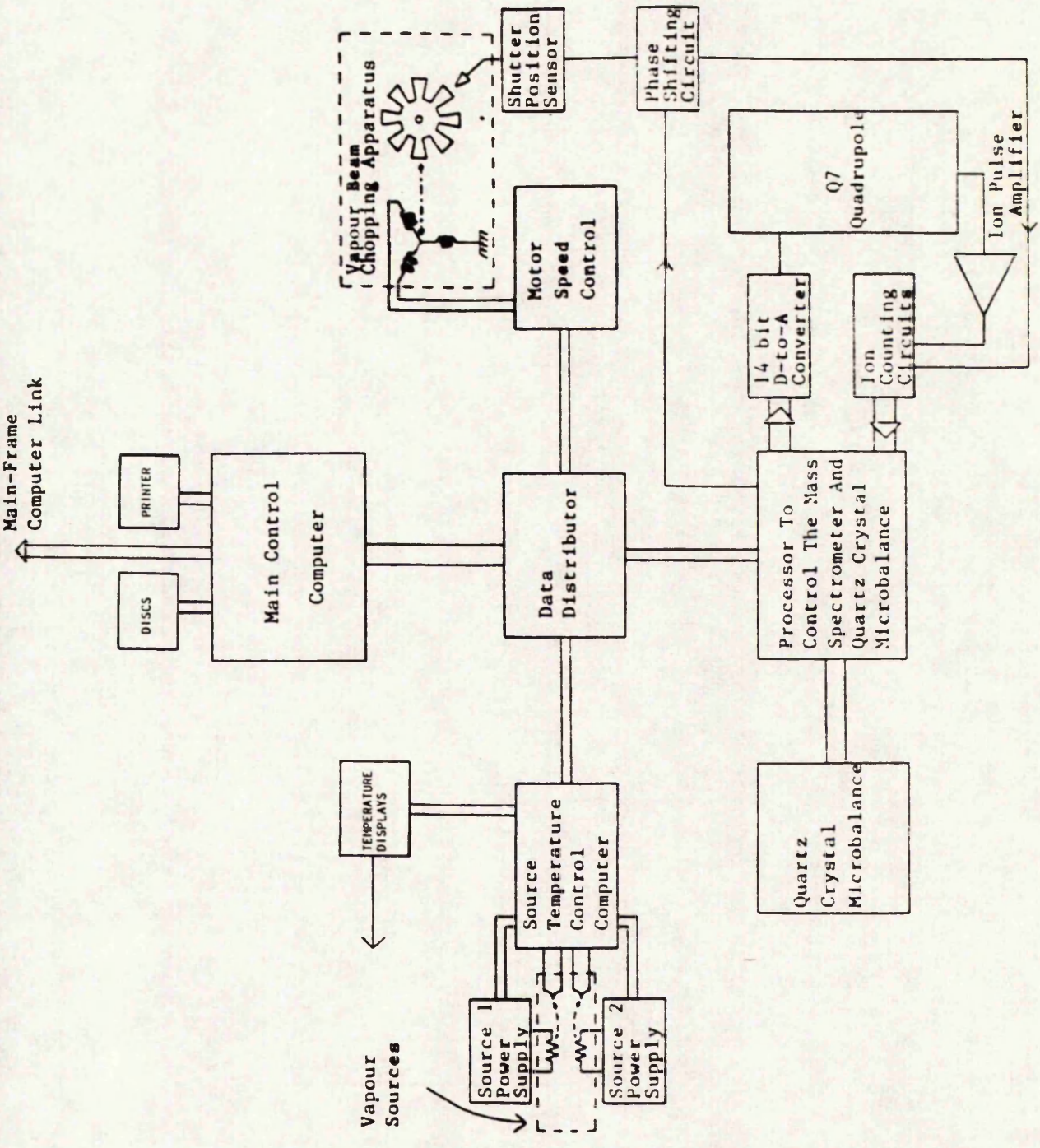

FIGURE 4.6

COMPREHENSIVE PHOTOGRAPH OF THE MBE SYSTEM

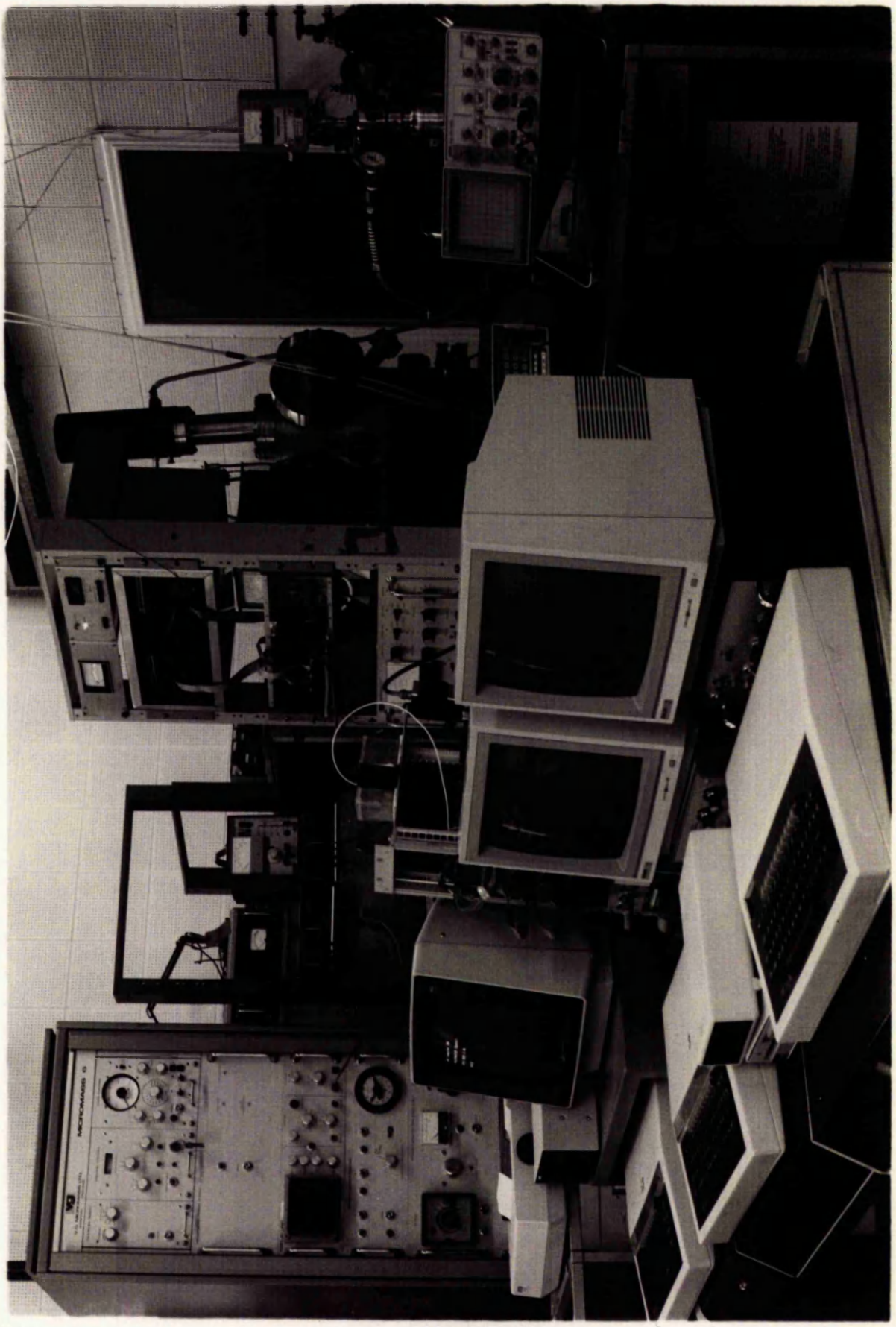

FIGURE 4.7

comments into the data files. Figure 4.6 shows an overall diagram of the control instrumentation developed for the modulated beam mass spectrometry system and figure 4.7 includes a photograph showing the full deposition and control equipment. Careful grounding procedures have been adopted in order to reduce earth loops and thus avoid oscillations in the system electronics as well as improving on signal to noise ratio [4.12,4.13].

Forth has been adopted for the system because it is well suited to control applications, has low memory usage and provides high speed. This helps the rapid development of real time software applications. The structure of Forth software programs is modular which eases the task of development whilst the simple low level routines to access the hardware provide a powerful package of easily accessible tools [4.14,4.15].

4.4.1 CONTROL OF THE MODULATION FREQUENCY

The control equipment for this process has been developed previously [4.5] and will not be reported here. However, the control software has been developed during the present work. Control over the modulation frequency is achieved using ROM based software which selects the appropriate power and excitation frequency. Only the minimum amount of power which ensures synchronous operation at the wanted speed is

delivered to the motor. At low rotational speeds the motor reluctance falls and damage due to overheating caused by the flow of large motor currents is prevented by reducing the applied voltage using data stored in a frequency based look-up table stored in the dedicated control computer.

The relationship between beam modulation frequency and the number sent to the 12 bit DAC determining motor speed has been measured over a frequency range of 20 to 1041 Hz using a Fluke counter model 23 [4.16] of 0.001 Hz resolution. A linear least squares regression has been performed and the following relationship has been obtained:

$$N_{DAC} = 3.937Fm - 0.472 \qquad (4.1)$$

Where N_{DAC} is the number sent to the DAC determining motor speed. For each modulation frequency Fm, the value of N_{DAC} is calculated from the experimental equation (4.1) and the modulation frequency is then known with an accuracy of better than 0.1 Hz. The ROM based software includes routines which feed the minimum power required for synchronous operation at the given modulation frequency, avoiding overheating of the motor. The value of the voltage delivered is displayed and can be varied while the motor is still running. Provision is made for using evaporant stream choppers with different numbers of blades. Upon resetting or switching on the dedicated control computer the motor is automatically started at 400 rpm and then the user is asked

to select the number of shutter blades in use. The range of modulation frequencies used is then displayed.

4.4.2 The ZnS AND ZnSe TEMPERATURE CONTROL EQUIPMENT

The design and performance of the instrumentation developed for controlling the temperature of the zinc sulphide and zinc selenide vapour sources has been described in the literature [4.17]. The system includes low frequency power amplifiers providing a current (0 to 5 amperes) which heats the vapour cells. The temperature is monitored using Pt/Pt-13%Rh thermocouple pressed against the bases of the crucibles holding the evaporant material. Temperature samples are taken every 5 seconds and averaged every 30 [§Chapter 2]. The measured fluctuation on a source temperature after convergence to a particular setpoint is better than 0.2 °C. Figure 4.8 shows a block diagram for the instrumentation used for vapour source temperature control. Both the ZnS and ZnSe sources have been compared to a computed model and this led to control of the sources using a first order filter algorithm [4.17]. Fast convergence of the source temperature to a computed temperature setpoint has been obtained. Figure 4.9 includes a curve which shows the convergence of the ZnS source temperature a setpoint with the ADC reading of 7000 (T=519 °C) to a setpoint at 6000 (T=457 °C). In this experiment liquid nitrogen cooling of the source has been used. The

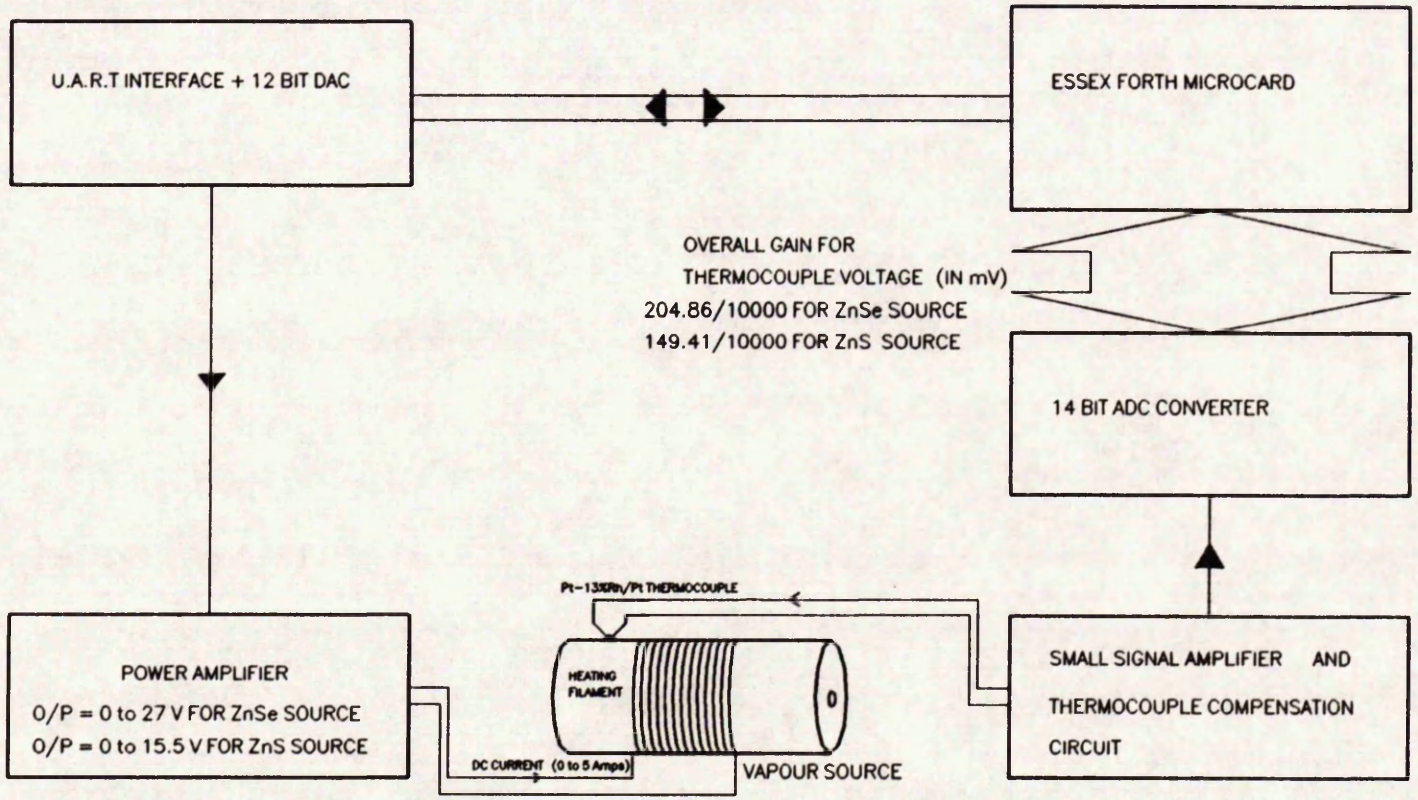

BLOCK DIAGRAM SHOWING THE INSTRUMENTATION ASSEMBLED FOR CONTROLLING THE TEMPERATURE OF ONE VAPOUR SOURCE.

FIGURE 4.8

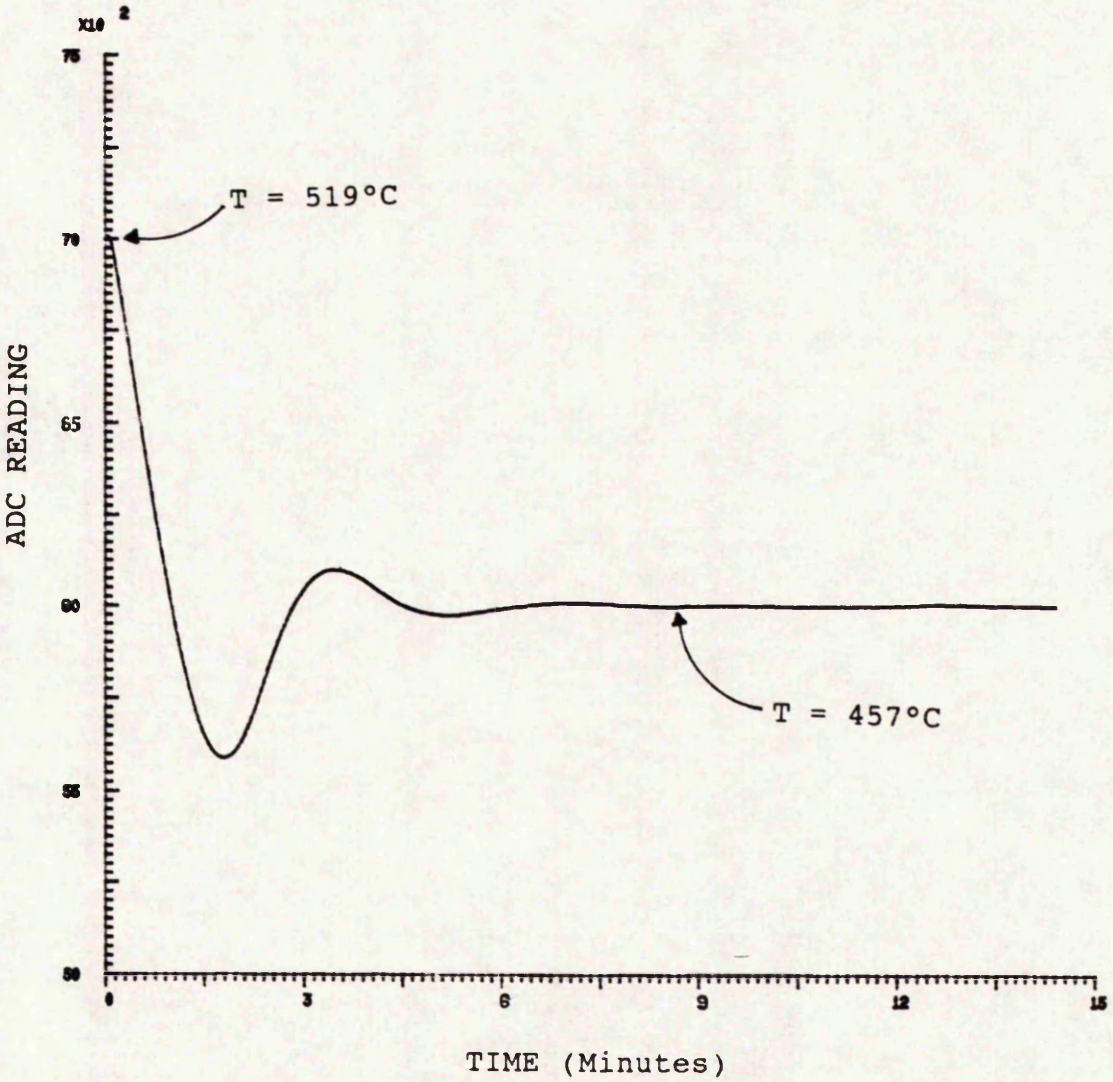

CURVE FOR THE CONVERGENCE OF THE ZnS SOURCE TEMPERATURE CONTROLLER TO A COMPUTED TEMPERATURE SET-POINT

FIGURE 4.9

curve displayed has been obtained by using equipment developed by a previous worker on the present deposition system [4.17].

A further development which has been included in the course of the present research is the provision of software which handles arrays of temperature setpoints with their instances of occurrence controlled with a real time clock. After convergence to temperature setpoint measurement of the flux number density is undertaken at a particular mass-to-charge ratio. Changes in the number density are then acted upon by varying the temperature of the source so that a constant deposition rate is obtained. This provides a powerful tool for handling programmed number density and source temperature profiles.

4.4.3 CONTROL OF THE QUARTZ CRYSTAL DEPOSITION RATE MONITOR

Control of the quartz crystal microbalance is performed through the T.D.S Forth microcomputer. Figure 4.10 shows the instrumentation used for this purpose. The control lines and addresses allocated for this instrument are included in figure A.3 of appendix A. Interface circuitry has been developed for deposition rate measurements which organizes the timing of the steering signals that supply ion pulses to the counters. The steering signal has a programmable period equal to (N+1)/Tm. As an example of

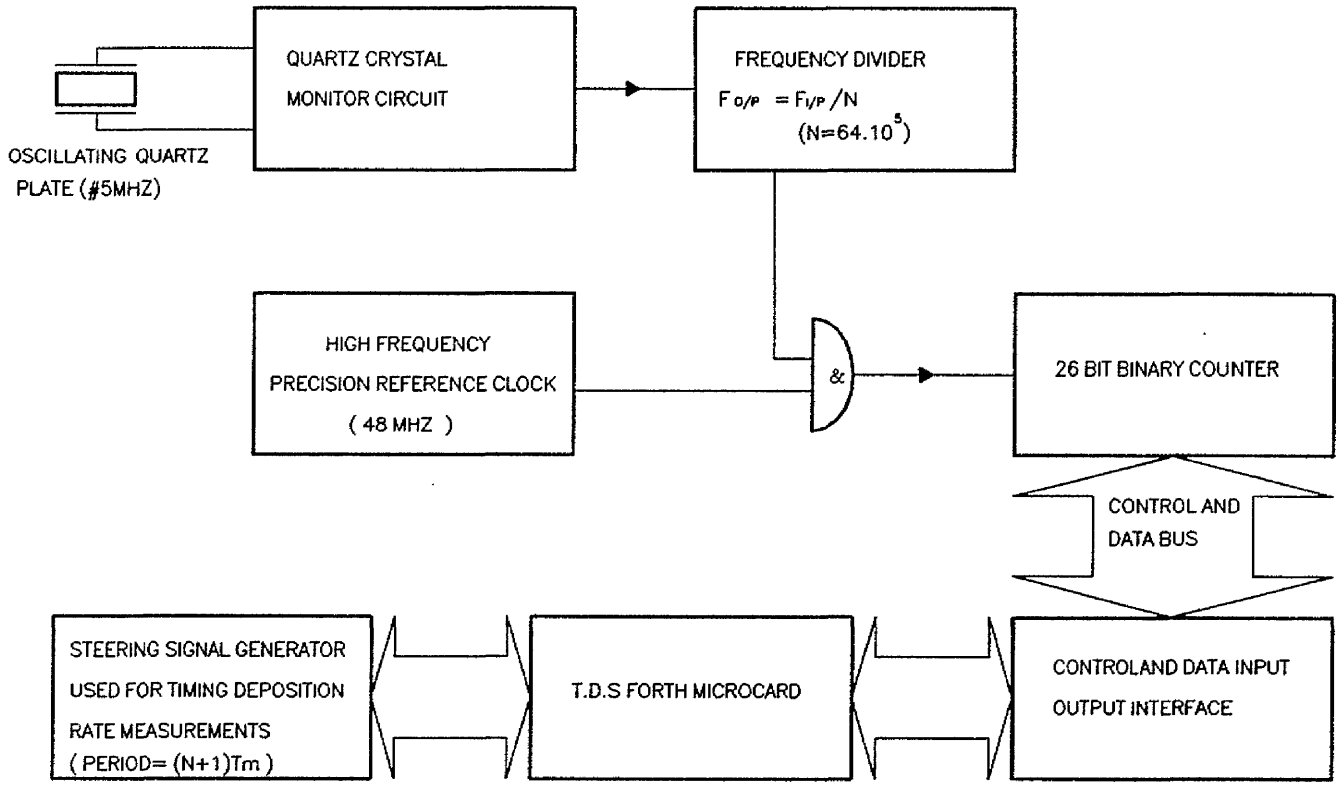

BLOCK DIAGRAM OF THE QUARTZ CRYSTAL MICROBALANCE AND ITS INTERFACING TO THE T.D.S FORTH MICROCOMPUTER

FIGURE 4.10

steering signal timing, for a modulation frequency of 122.2 Hz, N+1 is chosen equal to 200 yielding a steering signal period equal to 818.3 ms. Software control of the quartz crystal microbalance for deposition rate measurements involves generating appropriate control and the accumulation of a count proportional to the deposition rate. The count is directly related to the deposition rate using relationships (3.2) and (3.4) and this is calculated by the software used for monitoring deposition. (The control software used for the microbalance is included in appendix F). The quartz crystal monitor uses a 5 MHZ AT cut quartz resonator with a resolution on the period measurement equal to 6.5 fs and this represents an ability to detect changes in the thickness of ZnS films of 7.2 pm with a resolution on the deposition rate of 1.4 pm/s.

A 48 MHz reference clock is employed in the microbalance and the frequency of the monitoring resonator is divided by 64.10^5 using a binary counter are used. Since there is a count resolution of ±1 (§chapter 3), using equation (3.6) yields the mass resolution X_m as follows:

$$X_m = 57.2\ \mu g.m^{-2} \qquad (4.2)$$

Assuming a density for ZnS and ZnSe of 4.102 g/cm^3 and 5.42 g/cm^3 respectively [4.18], yields the

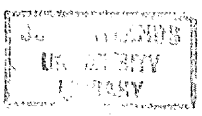

resolutions for thickness and deposition rate as follows:

	Thickness Resolution	Deposition Rate Resolution
ZnS	10.55 pm	16.5 pm/s
ZnSe	14.02 pm	21.9 pm/s

Averaging the deposition rate measurements as shown in appendix F improves on the accuracy of the measurements at low film deposition rates.

4.4.4 CONTROL OF THE MASS SPECTROMETER

A computer control system has been developed for the QMS used in the modulated beam mass spectrometry measurements and figure 4.11 shows a block diagram of the equipment produced. The various instruments used for controlling the spectrometer have been brought under computer control. Since the QMS has a 200 a.m.u range and a 14 bit DAC is used to provide mass tuning, the resolution of the tuning voltage for each peak is better than 1.2%. Details about the DAC circuit used are included in appendix B.

Ions passing through the quadrupole mass filter enter a secondary electron multiplier. A pulse of charge appears at the output of the multiplier for each ion striking the first multiplier dynode. The rate of ion arrival can be found by

either measuring the arrival rate of the charge (ie finding the average current output) or by counting the packets of charge (pulse counting). Measuring the average current output is prone to error of multiplier gain stability and as a result a pulse counting system has been developed. The signal from the electron multiplier is processed in two stages the first of which is a wide-band pulse amplifier mounted directly on the multiplier output. A 50 Ohm coaxial cable connects the amplifier to a pulse discriminator which selects pulses over a set threshold level and after amplification sends them to counters through gates which are synchronized with the evaporant stream modulation.

A description of the digital pulse counting circuitry is given in appendix C. Provision is made to perform accumulation for the ion counts over half a period of the modulation signal as well as over a time window of width t_w = 6.4μs for both on-beam (when the rotating shutter is open) and off-beam (when the rotating shutter is closed) measurements. Figure 4.12 shows the gating waveforms which are used.

A steering signal for the counting of pulses produced by dividing the modulation frequency by N+1. The steering signal controls the accumulation time for the pulses and a typical example of this is the 818.3 ms pulse used at a modulation frequency of 122.2 Hz for an accumulation taking 200 modulation periods (N+1=200). Figure 4.13 shows

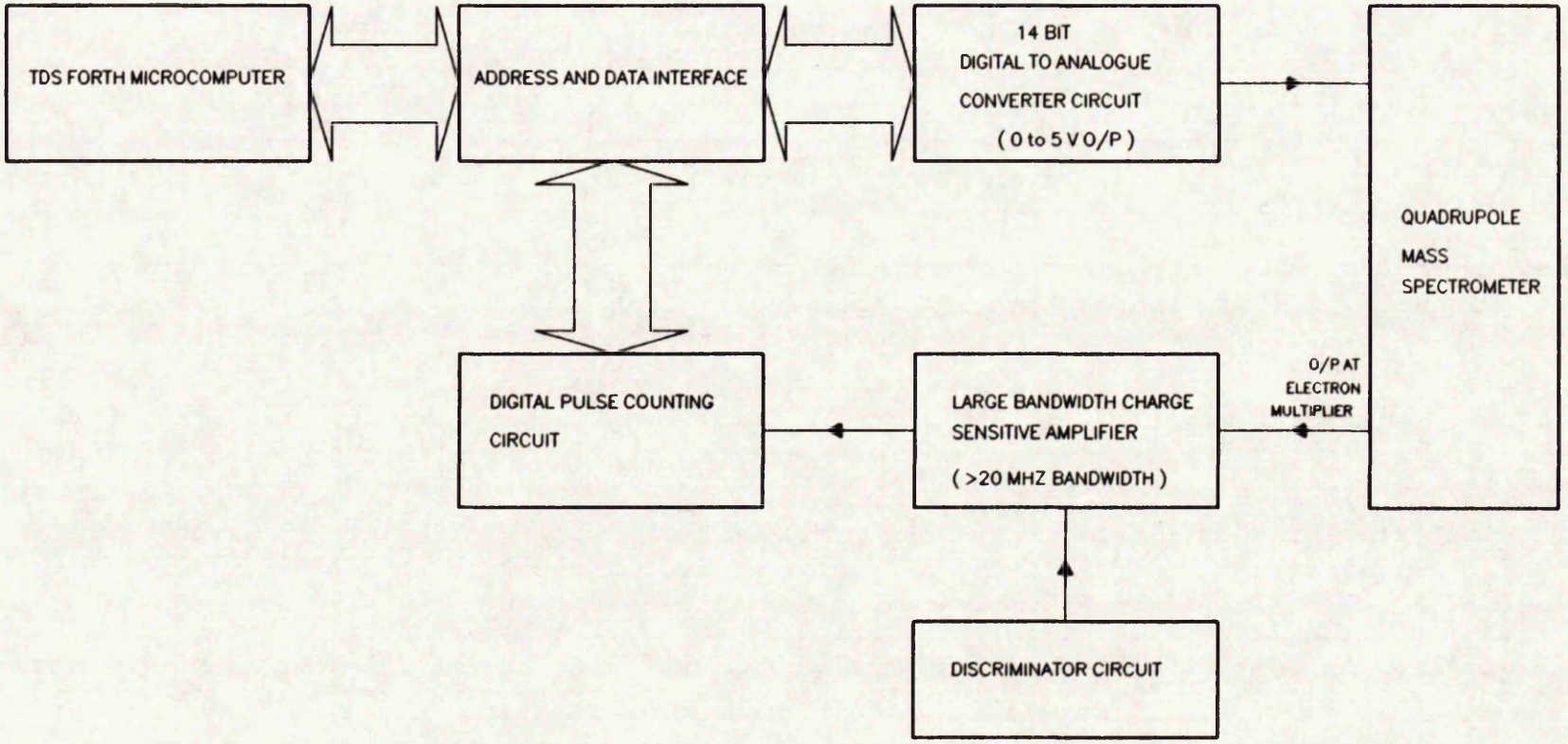

BLOCK DIAGRAM OF THE MASS SPECTROMETER CONTROL INSTRUMENTATION

FIGURE 4.11

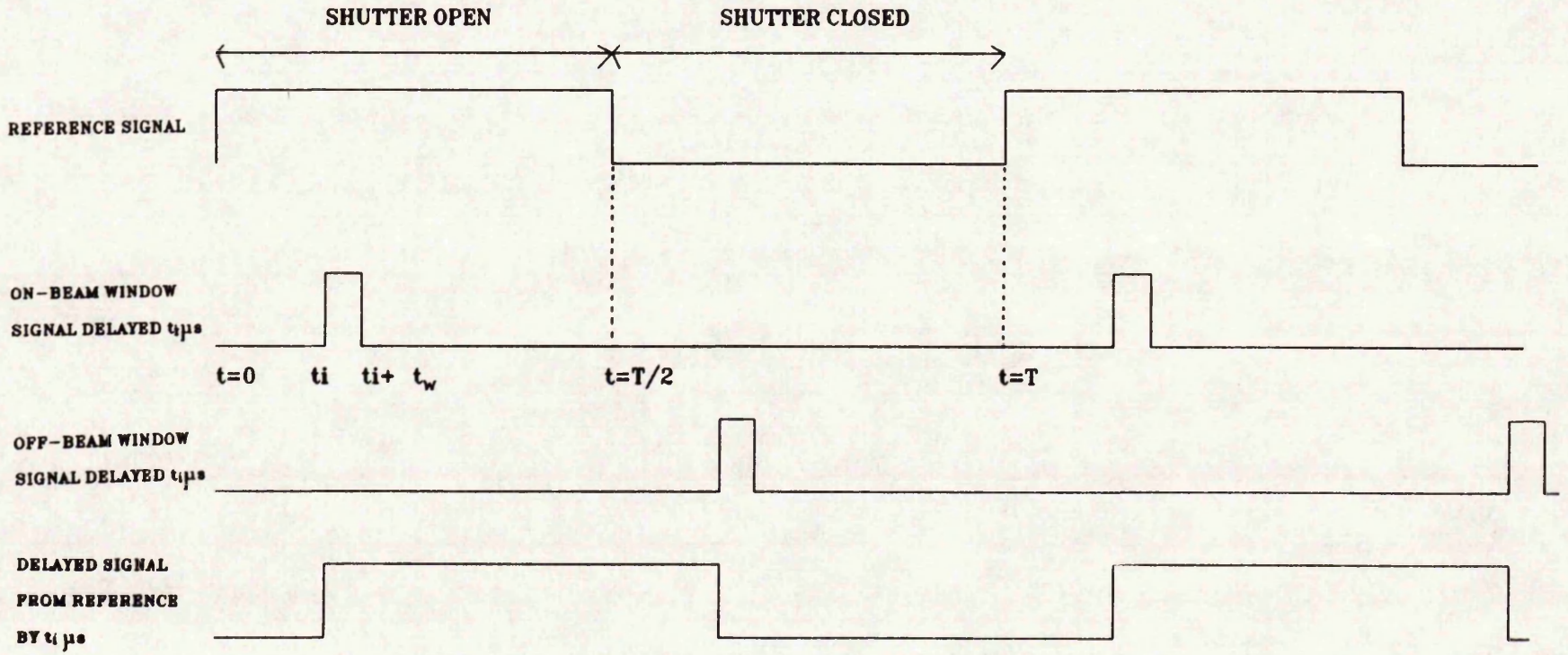

GATING WAVEFORMS USED FOR COUNTING THE EVAPORANT STREAM ION PULSES

FIGURE 4.12

the phasing of the steering signal for data acquisition in the modulated beam measurements. The reference signal used for pulse counting is obtained from a digital delay circuit since particles passing between the rotating shutter and the secondary electron multiplier experience a transit delay. Applying a similar delay to the reference signal maximizes the measured count and can be used to investigate the effect of particle transit times. Details about the digital delay circuit are included in appendix D. Figure 4.14 shows a photograph of the oscilloscope traces for the signals produced at critical points in the mass spectrometer control system. Tuning the mass spectrometer to make measurements at a specific mass-to-charge ratio during an evaporation with a fixed modulation frequency involves setting the delay for the reference signal and the steering signal accumulation time. The steering signal duration can be kept constant throughout an evaporation using a particular modulation frequency whereas the delay has to be changed when changing the spectrometer tuning between mass-to-charge ratios. Software has been developed for controlling the mass spectrometer and this is described in appendix F. The algorithm used for the control process takes into account the peak shape as well as the noise which is present on the peak.

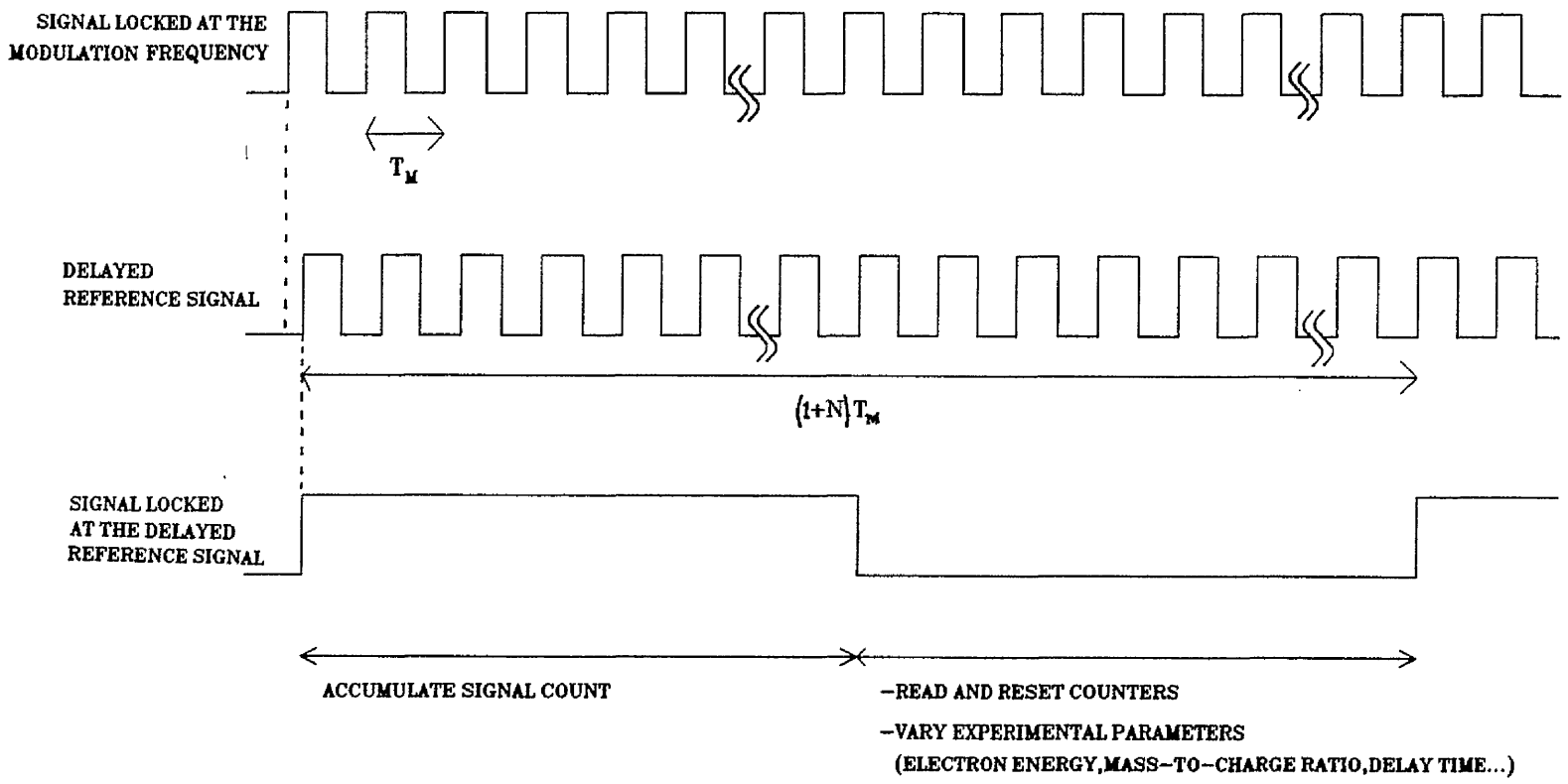

DIAGRAM SHOWING THE PHASING OF THE STEERING SIGNAL FOR DATA ACQUISITION IN MODULATED BEAM MEASUREMENTS

FIGURE 4.13

FIGURE 4.14

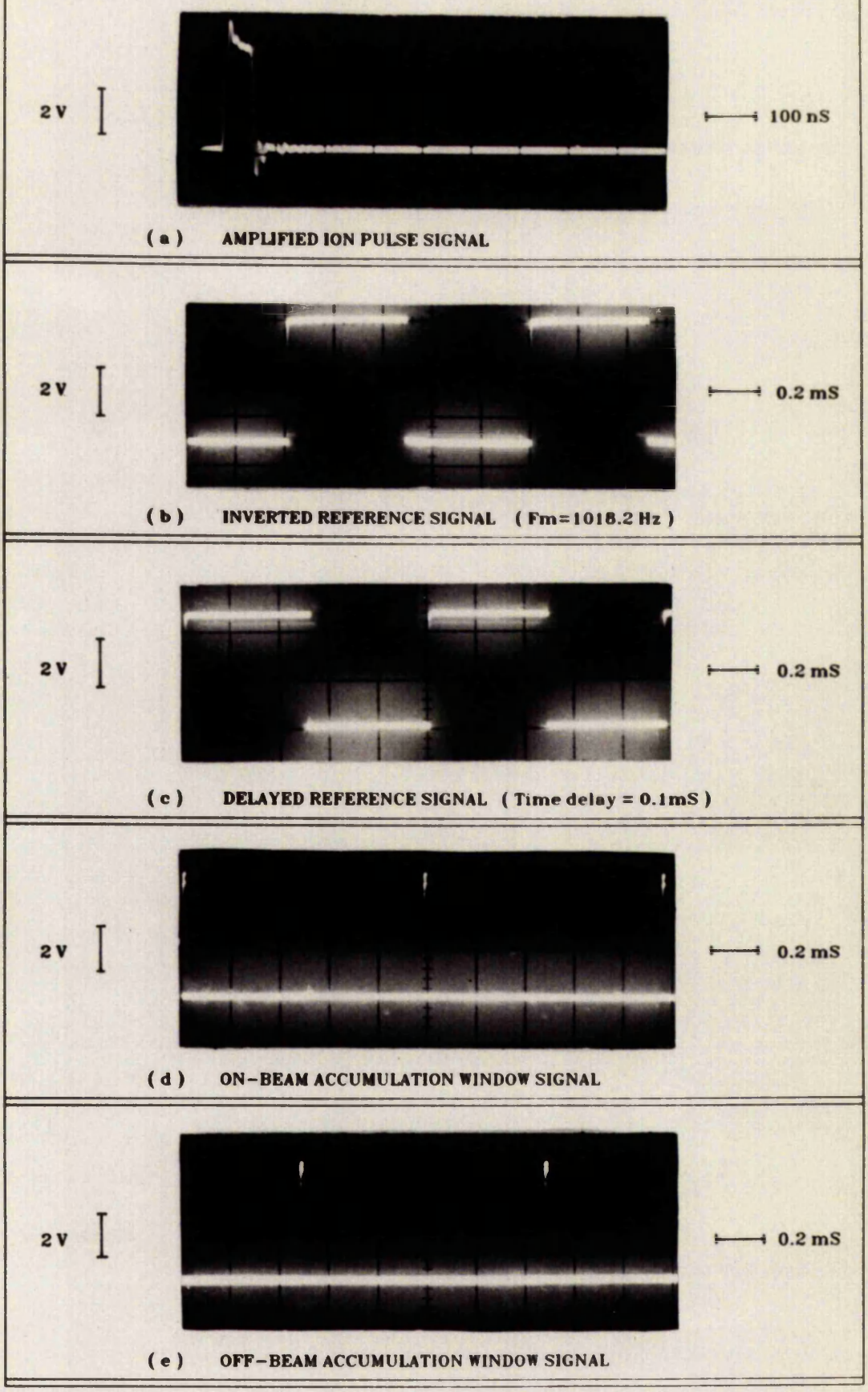

DIAGRAM SHOWING THE OSCILLOSCOPE TRACES OF THE SIGNALS USED DURING THE TIME OF FLIGHT EXPERIMENTS.

4.5 CONCLUSION

The electronic system used for modulated beam mass spectrometry experiments has been described. It has been shown that the use of computers is a necessity for the acquisition of data and control of the various instruments. Simplifying complexities inherent in the control system has been undertaken by dedicating small inexpensive computers to particular tasks. The hierarchical approach adopted in computer control of the system has provided the operator with a single console computer to control or supervise all the tasks performed by the system. The instrumentation constructed for modulated beam mass spectrometry has been described as well as the main software routines.

The decision to use Forth as the language for driving the instrument control computers has proved to be very successful because the structure favours the development of control algorithms. Another advantage of the Forth language is its operating environment which allows the execution of routines from all levels of the software hierarchy and the rapid development of new software structures to reconfigure the function of the system.

4.6 REFERENCES

[4.1] A.S.SAHIN
PhD. Thesis, The University Of Manchester U.K (1983)

[4.2] VACUUM GENERATORS LtD
Charleswood Rd, East Grinstead, Sussex (U.K)

[4.3] VARIAN ASSOCIATES LtD
Vacuum Products Division, 28 Manor Rd.,
Walton-On-Thames, Surrey (U.K)

[4.4] FERRANTI ROTATING COMPONENTS GROUP
Dalkeith, Scotland U.K

[4.5] M.BENYEZZAR
MSc Thesis University Of Manchester U.K (1986)

[4.6] EUROTHERM LTD
4/5 Cheltenham Court, Calver Road Warrington U.K

[4.7] B.B.C,
35, Marylebone High Street, London W1M 4AA U.K

[4.8] DIGITAL EQUIPMENT COPRPORATION
12 Crosby Drive BUO/E08 Bedford, MA 01730 (U.S.A)

[4.9] ESSEX ELECTRONICS CENTRE
Wivenhoe Park, Colchester (U.K)

[4.10] ROCKWELL INTERNATIONAL
Bath Rd., Cranford Hounslow Middlesex (U.K)

[4.11] TRIANGLE DIGITAL SERVICES LTD,
100a Wood St. Walthamstow, London E17 3HX

[4.12] R.MORRISSON
'Grounding And Shielding Techniques In Instrumentation'
J. Wiley & Sons Ltd (1977)

[4.13] H.W.Ott
'Noise Reduction Techniques In Electronic Systems'
J. Wiley & Sons (1976)

[4.14] L.BRODIE
'Starting Forth'
Prentice Hall Inc. (1981)

[4.15] R.GEERE
'Forth: The Next Step'
Addison Wesley Pub. Comp., (1986)

[4.16] J.FLUKE MFG. CO. INC.
Everett, Washington USA

[4.17] R.P.GREGORY
PhD. Thesis, The University Of Manchester U.K (1988)

[4.18] P.BARANSKI, V.KLOTCHKOV, And I.POTYKEVITCH
'Electronique Des Semiconducteurs'
Editions Mir Moscou (1978)

CHAPTER 5

CHARACTERIZATION OF THE MODULATED BEAM MASS SPECTROMETRY SYSTEM

5.1 INTRODUCTION

This chapter contains a description of introductory experiments undertaken in order to characterize the modulated beam mass spectrometry system.

Of interest are the operation of the QMS and the improvements in signal-to-noise ratio when vapour stream modulation is undertaken. Factors influencing the experimental system are investigated and the optimal conditions for system operation are determined. The experiments undertaken in characterizing the modulated beam mass spectrometry system involved carrying out measurements using residual gases as well as measurements during the evaporation of compound materials. For most of the investigations undertaken, the modulation frequency has been set to 122.2 Hz and the accumulation of on-beam and off-beam counts over 200 modulation periods (steering signal period

equal to 200 modulation periods) are used. Some investigations have been carried out under different conditions and these are specified when they have been used. Values which are sufficiently remote from 50 Hz (mains frequency) and its harmonics, are chosen for modulation frequencies. Other system preset conditions include an electron multiplier voltage of 3.5 KV, a filament emission current of 2 mA and a resolution setting of zero. The suitability of these system settings is discussed in this chapter.

5.2 OBSERVATIONS ON QMS PEAKS PROFILES

The profile of the peaks observed on the mass spectra for background gases and evaporated compounds at various mass-to-charge ratios has been investigated. Figure 5.1 shows the peak profile for the nitrogen ion N_2+ at m/e=28. Represented are peaks for the background, total and demodulated ion counts. The peaks are obtained by varying the tuning voltage fed to the QMS from the digital-to-analogue converter circuit and measuring the coresponding ion count for each tuning voltage. The total ion count represents the on-beam count that is, the count obtained when the shutter is open and the background count represents the off-beam count which is the count accumulated when the shutter is closed. The peak shapes for total and background ion counts are virtually identical so the

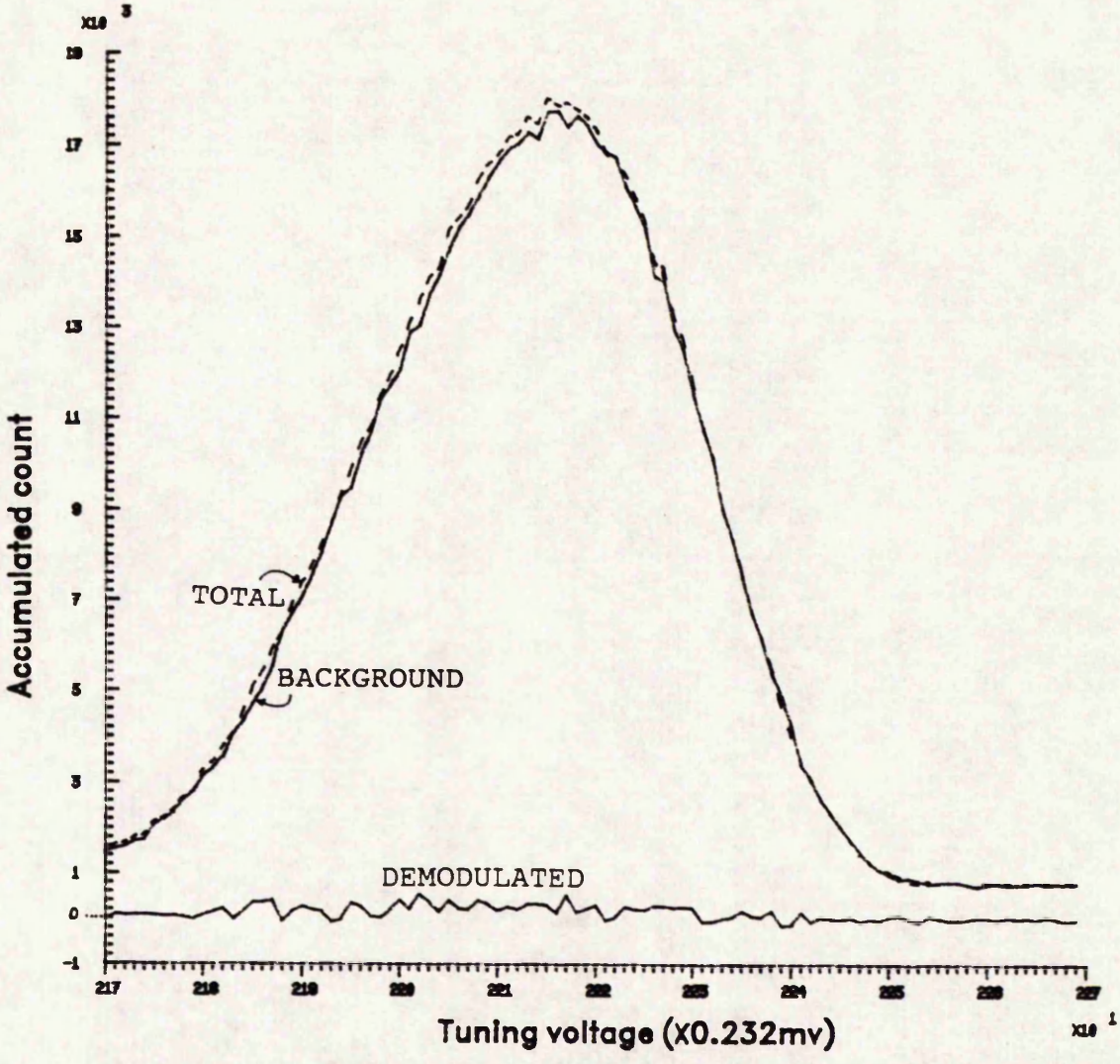

N2+ DIRECT.BACKGROUND AND DEMODULATED PEAK PROFILE AT 800 DEGREES CELSIUS AND 2MA EMISSION CURRENT

FIGURE 5.1

demodulated ion count is close to zero since N_2^+ ions are from background gases.

When the same experiment is undertaken during the evaporation of ZnSe with making measurements on the Zn+ ion at m/e=64 figure 5.2 is obtained. The demodulated and the total ion counts are larger than the background ion count and this results because most of the ions detected are from neutral particles emanating from the vapour source. The background count is formed of those particles which remain in the vicinity of the ionization chamber. Repeatable peakshapes for the evaporant particles monitored have been obtained and this helps with designing efficient peak finding software [§ appendix E].

5.3 EFFECT OF THE QMS FILAMENT EMISSION CURRENT ON THE ION COUNT

This effect has been investigated by observing the variation of the ion count for a number of vapour species with the emission current setting on the QMS (all other system variables being kept constant. Figure 5.3 shows the result for H2+ (m/e=2) indicating a high degree of linearity over a substantial range of emission current. Repeating similar experiments at other mass-to-charge ratios revealed a similar variation between the ion count and the QMS emission current setting. With a low density of ionized

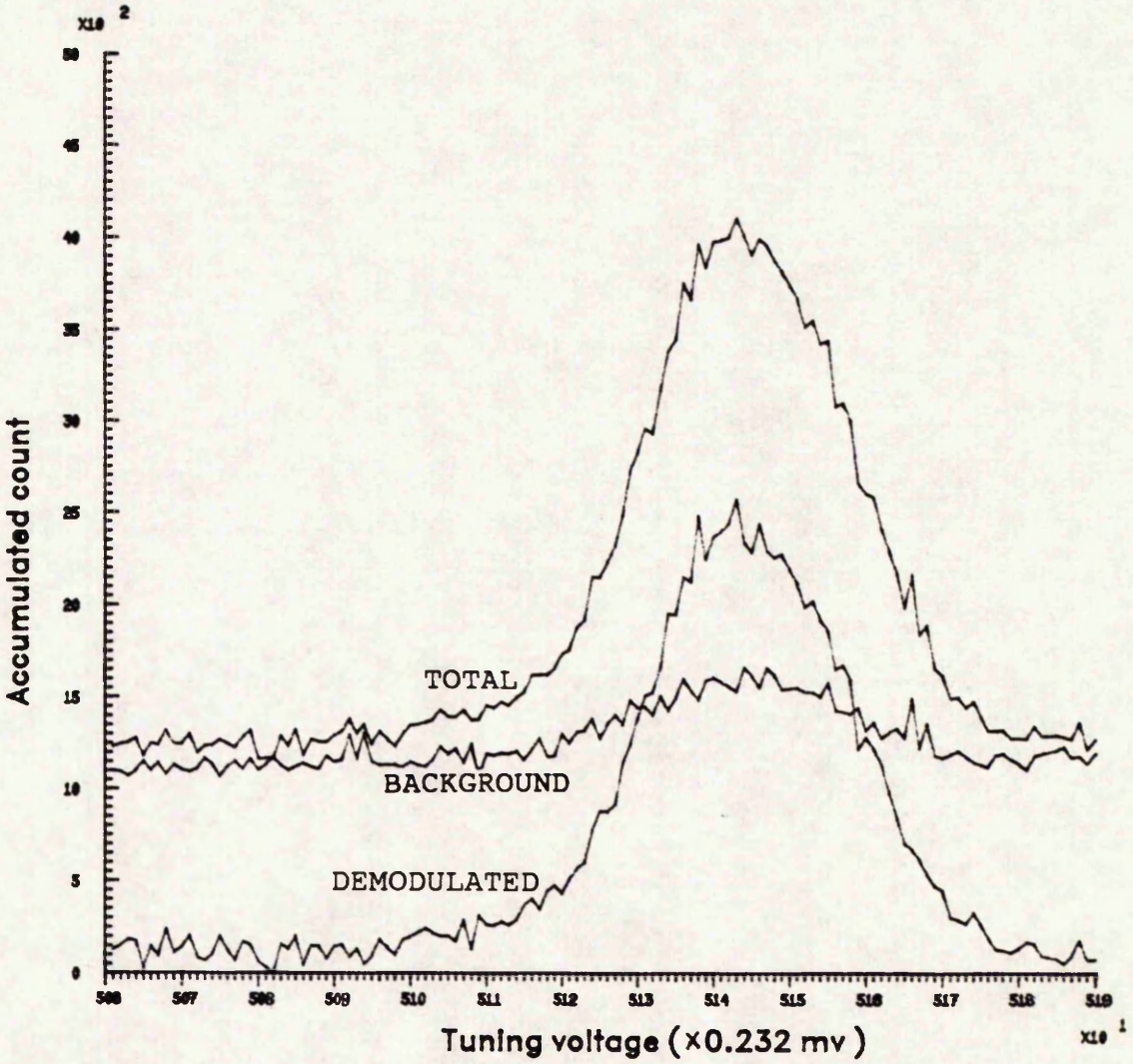

ZINC(64) DIRECT, BACKGROUND AND DEMODULATED PEAK PROFILE AT 825 °C AND 2 MA EMISSION CURRENT

FIGURE 5.2

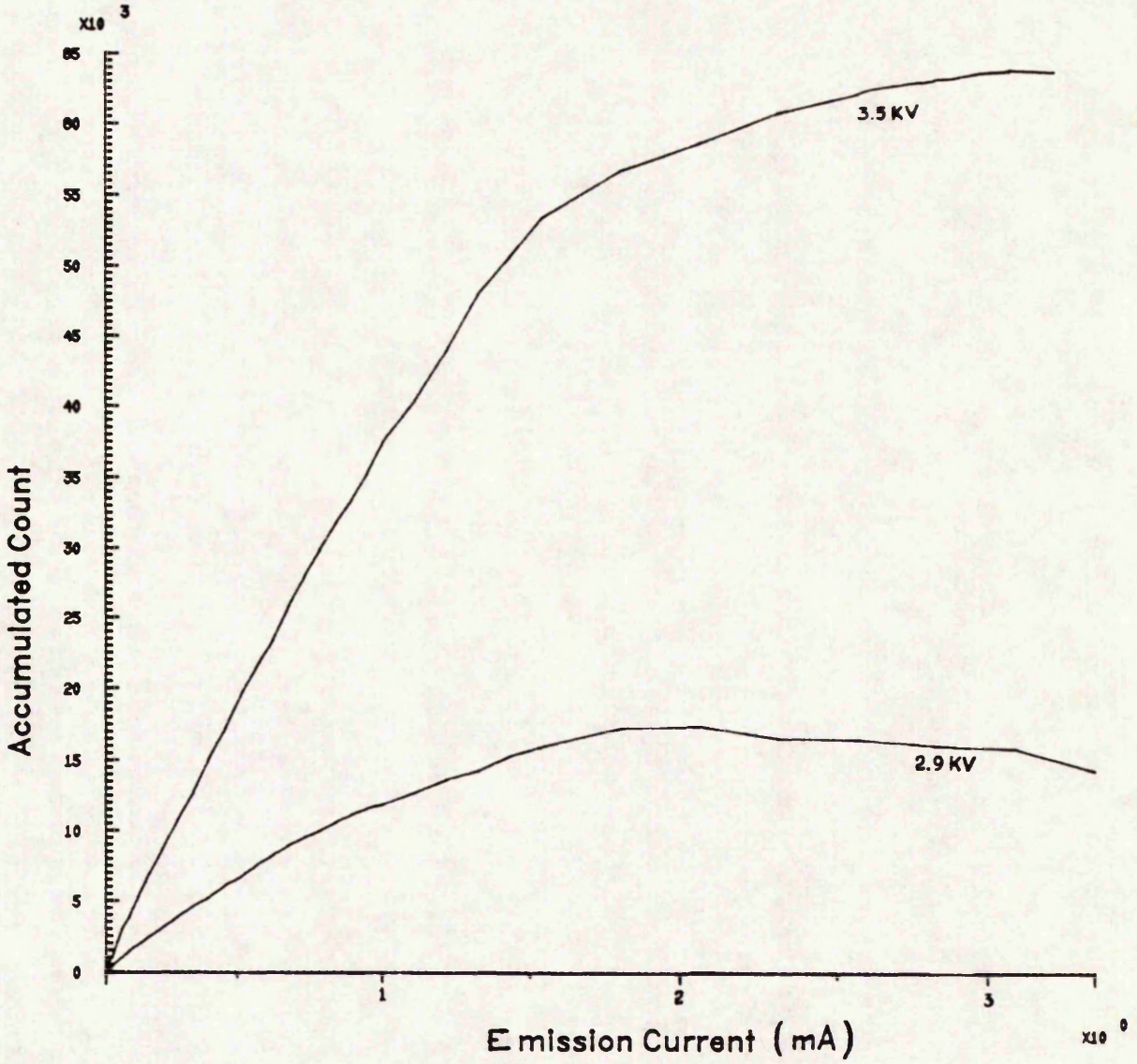

VARIATION OF H2+ PEAK INTENSITY WITH EMISSION CURRENT

FIGURE 5.3

particles in the ion chamber a linear relationship between ion and emission currents might be expected. However, the flat part on the curves obtained suggests that this is not always true. Flattening of the curves occurs at high emission currents resulting from less particles being ionized. Space charge build up may deter ions entering the quadrupole mass filter if they are bunched around the ionization chamber exit aperture and this gives rise to the fall in sensitivity.

Emission currents of up to 2 mA appear to be usable and the linearity at these current values does not suffer substantially which suggests that the space charge effects are not important at these currents. Higher emission current settings tend to suffer more from space charge effects but the signal-to-noise ratio is higher than in the case of low emission currents. This is easily justified by figures 5.4 and 5.5, where an emission current of 2 mA and an electron multiplier voltage of 3.5 KV are used for figure 5.4 whereas 200 μA and 2.5 KV are used for figure 5.5. The 200 μA emission current curve has a much higher noise content (may be explained by ion count fluctuations on the peak profile) than the 2 mA curve. Difficulties can be encountered even when searching for the peak tuning voltage at low emission currents because of noise and this consideration justifies using higher emission currents.

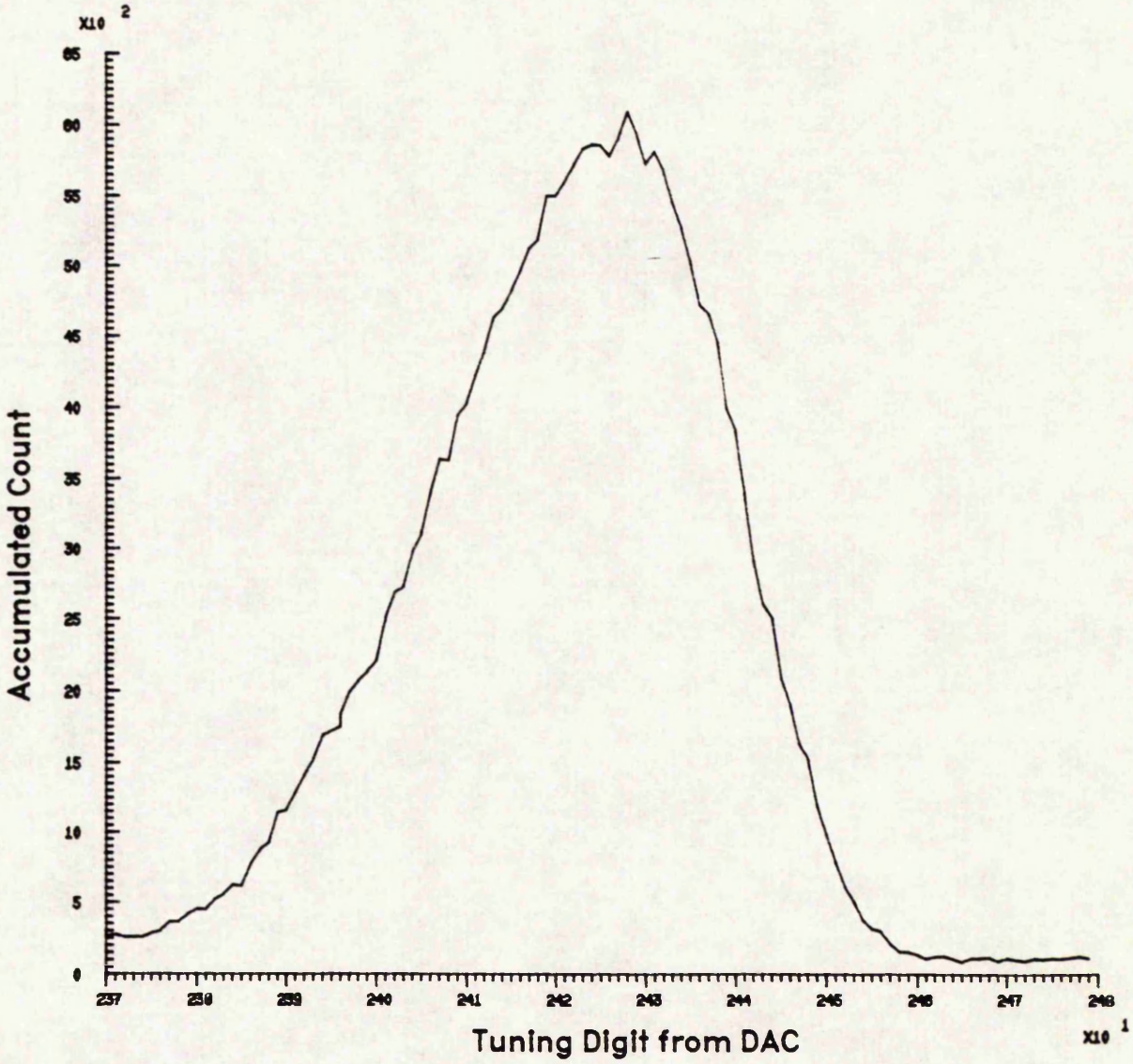

N_2^+ (m/e=28) PEAK PROFILE AT 2 mA EMISSION CURRENT AND 3.5 KV ELECTRON MULTIPLIER VOLTAGE

FIGURE 5.4

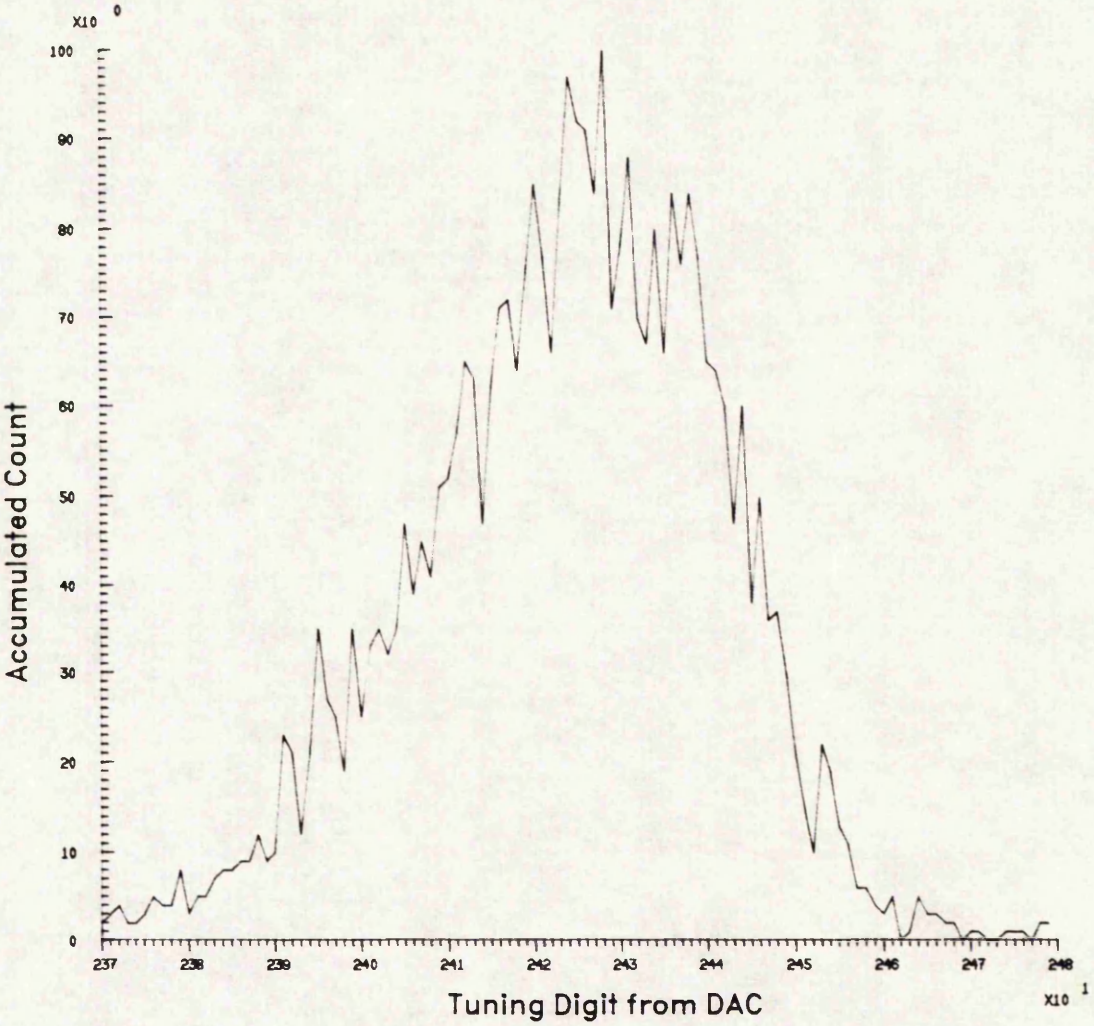

N_2^+ (m/e=28) PEAK PROFILE AT 200 μA EMISSION CURRENT AND 2.5 KV ELECTRON MULTIPLIER VOLTAGE

FIGURE 5.5

In order to relate evaporated vapour species number densities to each other, such as for determining the isotopic abundancy ratios of zinc, it is observed that the ratio between ion counts at different emission currents is constant and this is shown and used extensively in the latter part of this thesis. Where accurate isotopic abundancy ratio measurements are required there is considerable advantage in using higher emission currents where linearity between ion count and emission current is obtained and the signal-to-noise ratio is improved. As a consequence, a value for the emission current of 2 mA has been chosen for general use.

Included in figure 5.3 are curves for the ion count versus the emission current at two electron multiplier voltage settings of 2.9 KV and 3.5 KV. A comparison between the two curves leads to concluding that a setting of 3.5 KV is better and it is used throughout the present work to obtain a large ion count. Secondary electron multiplier life is reduced by large acceleration voltages but this has not proved to be a difficulty with the present system.

5.4 EFFECT OF THE QMS RESOLUTION SETTING ON THE ION COUNTS

The resolution setting determines the accuracy of tuning at any given mass-to-charge ratio. Resolution and sensitivity are inversely related parameters since high

sensitivity yields low resolution and vice-versa. The sensitivity can be defined as the smallest concentration detectable at a given mass-to-charge ratio in the presence of other vapour species [5.1]. Figure 5.6 shows the variation of the ion count at different mass-to-charge ratios as a function the resolution setting on the QMS. The curves show that when the resolution is decreased the ion counts increase sharply because of the rapid increase on the sensitivity. As the resolution is increased the ion counts decrease till reaching negligible proportions. Ions with larger mass-to-charge ratios reach a negligible ion count more rapidly as the resolution is increased.

As the mass-to-charge ratio varied the ion count varies substantially. This variation is more substantial between curves for particles having a larger difference in mass. These effects provide an explanation for the observed mass discrimination effects in the spectrometer. A low setting on the discriminator in the ion pulse counting assembly has been used in these measurements and this accounts for the large ion count at m/e = 160.

The sensitivity can be reduced and the resolution increased when making ratio measurements on isotope abundancies and it can be increased when making measurements at mass-to-charge ratios with low ion counts. For all practical purposes a resolution setting equal to zero is used in most of the work since this provides good sensitivity on most of the particles investigated. There

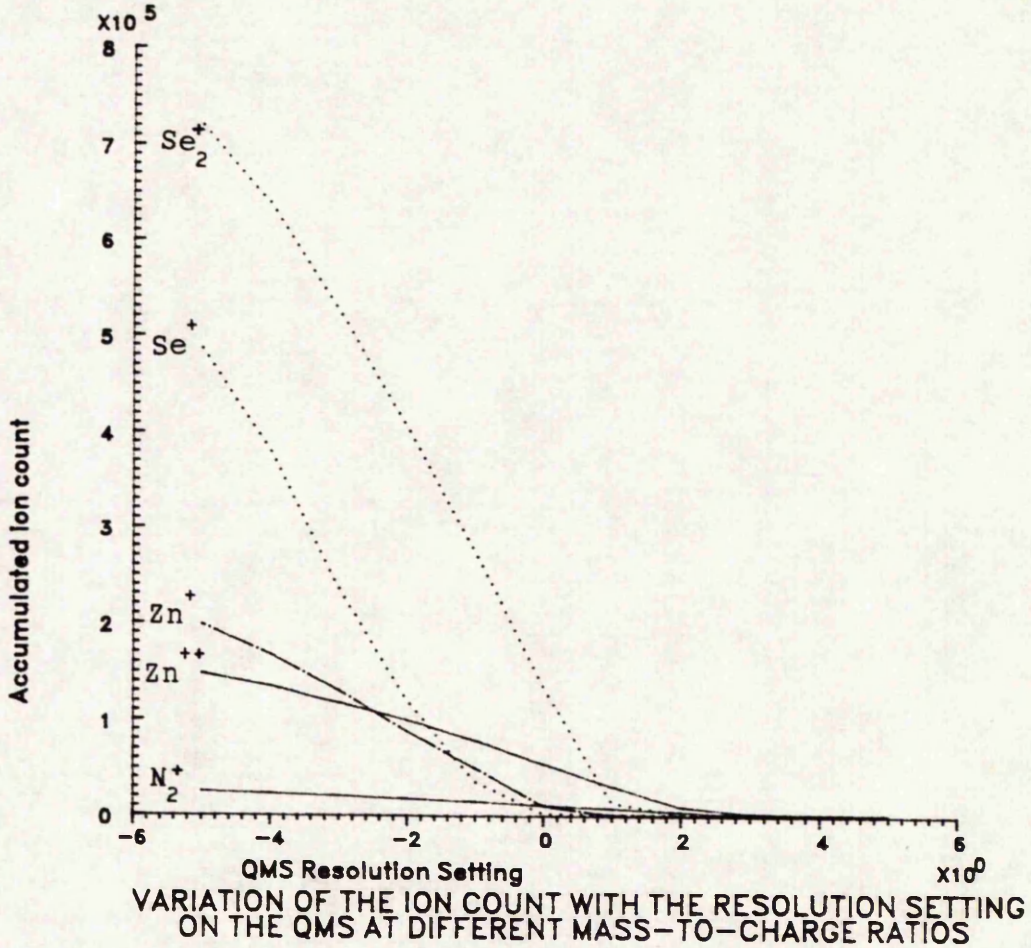

VARIATION OF THE ION COUNT WITH THE RESOLUTION SETTING ON THE QMS AT DIFFERENT MASS–TO–CHARGE RATIOS

FIGURE 5.6

is need to measure not only ion counts for isotopes only but also ion counts for vapour species at high mass-to-charge ratios (m/e=160 for Se_2) in a single set of comparative measurements and a zero resolution setting is a compromise value for all these different measurements.

5.5 IMPROVEMENT OF SIGNAL-TO-NOISE RATIO IN MODULATED BEAM MASS SPECTROMETRY

A study of the effect of modulated beam mass spectrometry on the signal noise content has been undertaken. For this purpose, measurements have been made at a number of mass-to-charge ratios. Equilibrium ion counts are measured for particles emanating from the vapour source (ZnSe source) as well as for particles in the background atmosphere. Measurements have been on vapourized particles over long periods of time but no noticeable change in the number densities has been observed.

5.5.1 OBSERVATIONS OF DEMODULATED ION COUNT FLUCTUATIONS

This set of experiments included measurements undertaken on the demodulated ion counts for hydrogen H_2+ at m/e=2 and selenium Se+ at m/e=80. A verification on the counts obtained is undertaken by counting a 5 MHz TTL signal from a generator. Forty samples in each case are taken for total

and background counts and the demodulated count extracted. The ratio of the demodulated count to the total count is calculated in percent and scaled to show the fluctuation the average value of the ratio. Here a modulation frequency of 122.2 Hz is used and the counts are accumulated over 200 modulation periods. Figure 5.7 shows the variation of the demodulated to total count ratio for hydrogen ions (m/e=2). The curve for the 5 MHz TTL signal is also included. Fluctuation on the signal generator signal is negligible as expected (below 0.1%) but the fluctuation on the hydrogen ion count is within ±5% of the average value of 0%. Figure 5.8 shows the figure obtained for selenium ions at m/e=80. Here, the fluctuation of the ion count ratios is within ±0.75% off the average value which about 82.9%. These figures show that the fluctuation in count for background gas ions are larger than those exhibited by directional beams of particles, like those for selenium obtained during the evaporation of ZnSe.

5.5.2 EFFECT OF ACCUMULATION TIME AND DEVIATION FROM THE AVERAGE ION COUNT

The effect on the ion count resulting from altering the accumulation time has been investigated. The accumulation time is altered by varying the steering signal period. It is important to have a short acquisition time coupled with good signal-to-noise ratio for the data obtained. Forty

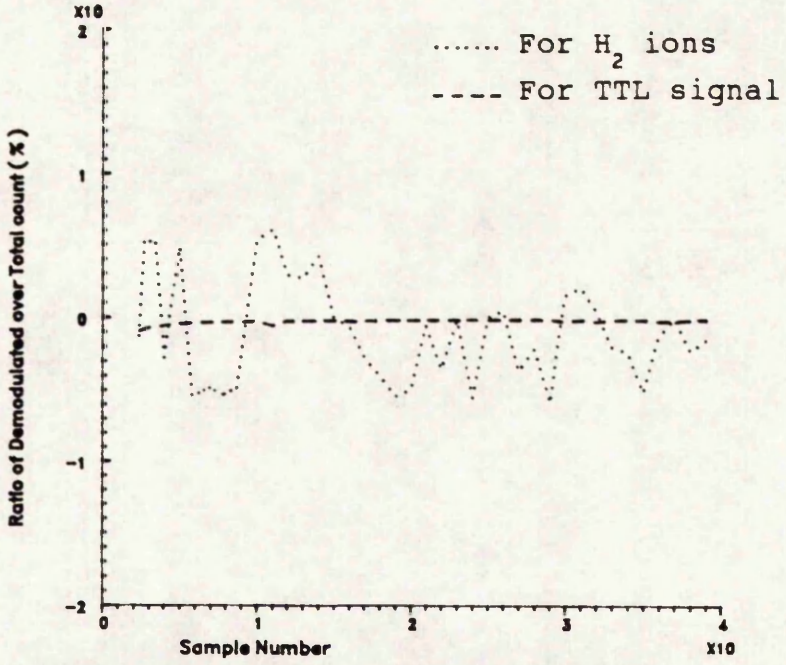

RATIO OF DEMODULATED OVER TOTAL ION COUNTS FOR H2+ IONS (m/e=2) AND PULSES FROM A TTL SIGNAL GENERATOR

FIGURE 5.7

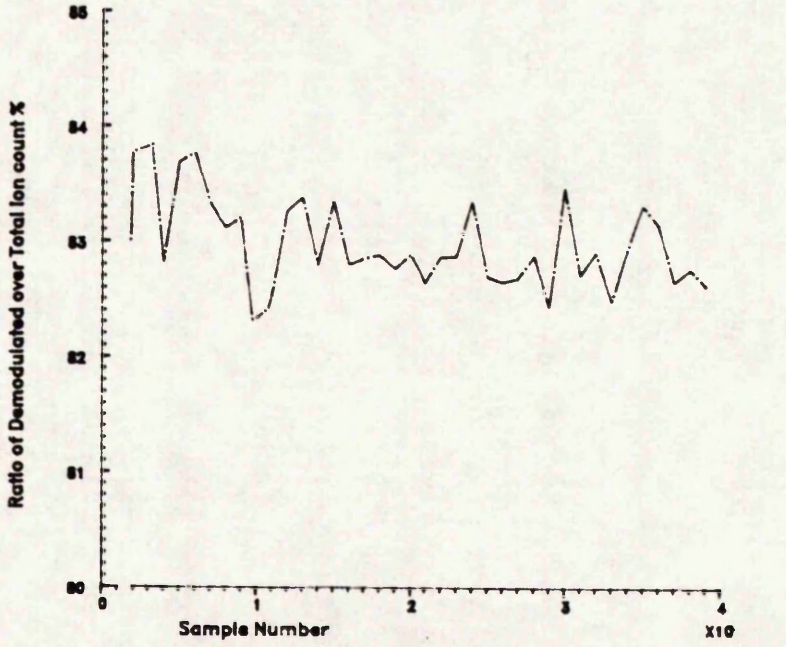

RATIO OF DEMODULATED OVER TOTAL ION COUNTS FOR SE+ IONS (m/e=80)

FIGURE 5.8

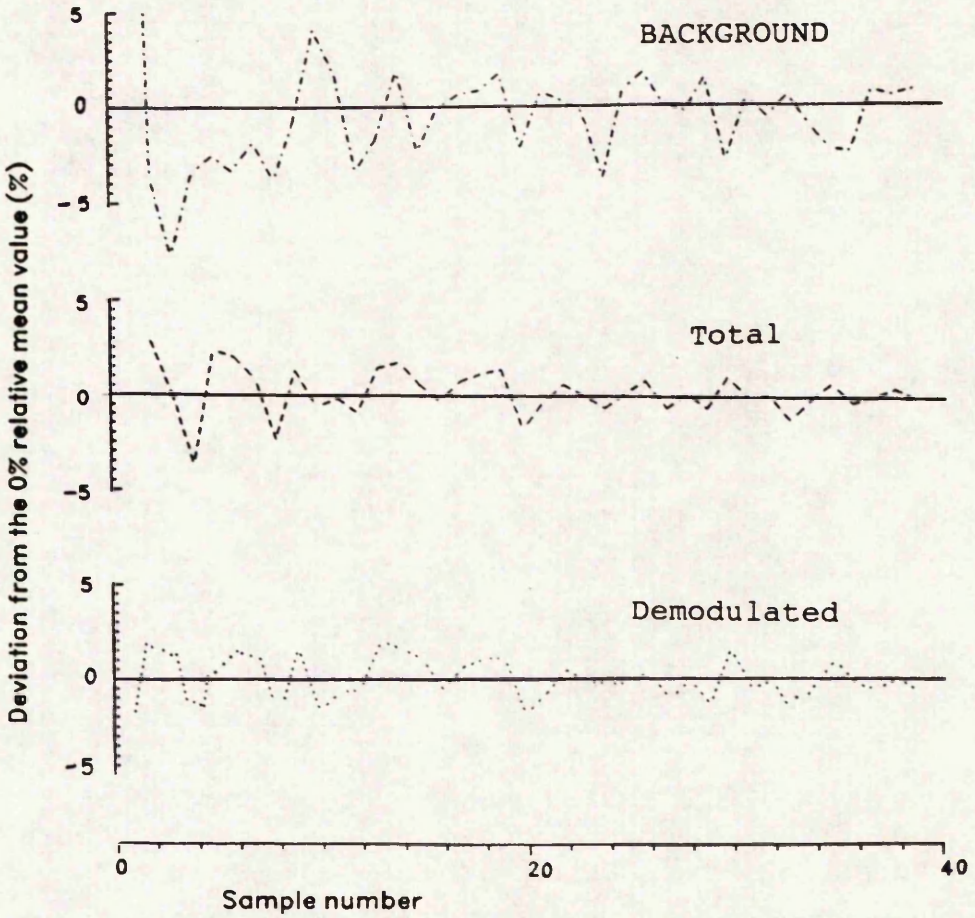

RELATIVE DEVIATION FROM THE MEAN VALUE FOR THE BACKGROUND, TOTAL AND DEMODULATED ION COUNTS FOR SELENIUM AT m/e=80

FIGURE 5.9

samples have been undertaken with the steering signal adjusted over the range from 50 to 4000 modulation periods. This yields an accumulation time for each of the background and total ion counts varying from 0.204 second to 16.366 seconds. For the representation of the results the following procedures have been undertaken:

1. The ion count is divided by the number of modulation periods included in the steering signal period. This gives equal weighting to the ion counts and produces averaged data samples which can then be compared.

2. A mean value on the averaged data samples is calculated.

3. The value of the mean is substracted from the averaged samples and the result divided by it. The ratio obtained is calculated in percent.

4. the mean value for the ion count is referenced to 0%. This helps with comparing all the results around the 0% value.

These procedures have been performed for selenium background, total and demodulated ion counts. Figure 5.9 shows the results obtained. The curves show a gradual decrease in the percentage deviation from the mean value as the sample number (and hence the steering signal period) is increased. The deviation on the background ion count

decreases from ±5% on the first samples to ±2% in the latter ones but on the total and demodulated ion counts decreases from 4% to below +1%.

5.6 THE EFFECT OF THE UHV SYSTEM TOTAL PRESSURE ON THE QMS ION COUNTS

Nitrogen gas (N_2) is introduced to the UHV chamber through a controllable feedthrough valve to raise the background pressure. The total pressure is monitored on a 5½ digit Thurlby [5.2] multimeter where the display of a voltage proportional to the system pressure is obtained. The accuracy on the voltage is better than 10 uV. The nitrogen gas is introduced into the vacuum chamber till a targetted value for the total pressure is obtained and it is then maintained at a stable value for taking measurements. At m/e=28 there is the possibility of contribution from ions other than N_2+ like CO+. Since the starting pressure inside the UHV system prior to the experiment is below 10^{-10} torr and nitrogen at much higher pressures is bled into the system, N_2+ can be considered as virtually the only contributor to m/e=28 peak. At each total pressure setting, the ion count at m/e=28 is undertaken for 12 consecutive samples. These are added together, which helps with unbiased averaging on the ion count and since N2 can be considered as a background gas, fluctuations in the ion count (as seen in previous

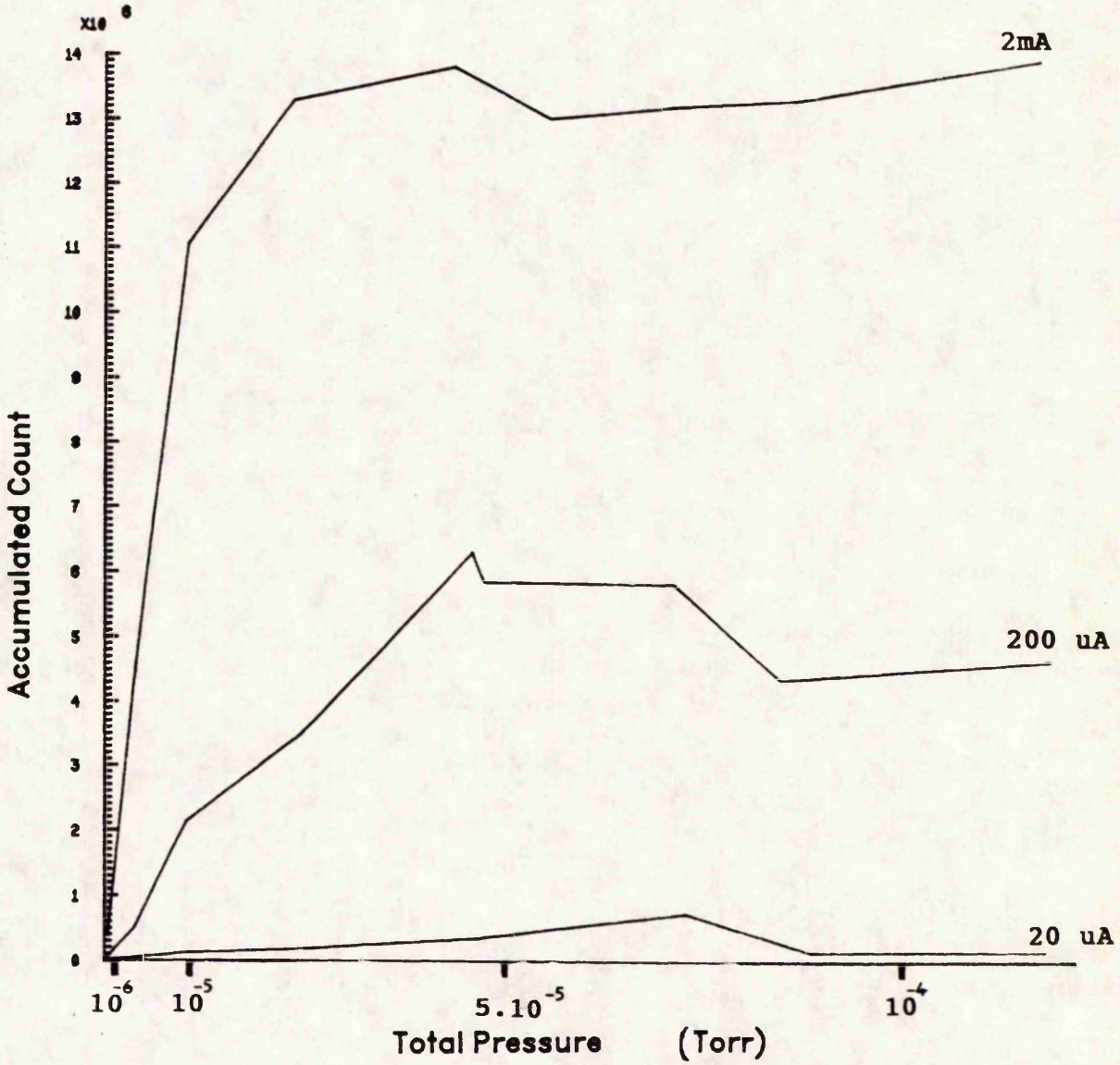

VARIATION OF N_2^+ (m/e=28) ION COUNT WITH THE UHV SYSTEM TOTAL PRESSURE

FIGURE 5.10

sections) are reduced. The measurements have been made at QMS filament emission current settings of 20 μA, 200 μA and 2 mA with a modulation frequency of 122.2 Hz and a steering signal having a cycle equal to 200 modulation periods. Figure 5.10 shows the curves obtained and they indicate that the ion count is proportional to the system total pressure until pressures in excess of 10^{-5} torr are reached. During the evaporation of zinc sulphoselenide coumpounds the system pressure must remain below this boundary if the ion counts are to be considered proportional to the partial pressure. This is of primary importance particularly if an emission current of 2mA is to be used in deposition experiments.

The observed results also show that the saturation effects occur at higher system total pressures when lower emission currents are used. The linearity between total pressure and ion count on figure 5.10 exceeds $8\ 10^{-6}$ torr for an emission current of 2 mA whereas it exceeds $3\ 10^{-5}$ torr for a 200 μA emission current and at 20 μA emission current this limit is pushed towards a total pressure of $7.5\ 10^{-5}$torr. This may mean that the limit on the linearity range is not independant of the filament emission current. The emission current helps with ionising a larger number of particles provided that the appearance potential for the vapour species investigated has been exceeded. Repeating the experiment on the variation N_2^+ with the system total pressure yielded similar

results. It may be suggested therefore that increasing the emission current and hence producing more electrons from the filament tends to produce more ions but the mass spectrometer saturates or that the spatial density of particles makes the ionization of more particles difficult after a threshold density for vapour particles is reached.

5.7 CONCLUSION

The modulated beam mass spectrometry system developed has been characterized and reliable ion count measurements demonstrated.

Simple procedures have been shown to allow for effective averaging on the ion counts. Improved signal-to-noise ratios have been obtained by using higher electron multiplier voltages and filament emission currents as well as larger steering signal accumulation times.

The effects arising from space charge build up in the mass spectrometer ionization chamber have demonstrated and found substantially negligible up to emission currents of 2 mA.

Fluctuations in the background gases as well as in the background ion counts for evaporated particles have been found much larger than those obtained from directional particle beams emanating from vapour source. Measurements

on the demodulated ion counts with fluctuations less than 1% have been demonstrated.

Proportionality between particle ion count and the UHV system total pressure has been demonstrated up to pressure in excess of 10^{-5} torr.

5.8 REFERENCES

[5.1] V.J.A.KORPIO
Vakuum-Technik 38 5-6 pp.134-142 (1989)

[5.2] THURLBY ELCTRONICS LTD
Coach Mews St. Ives, Huntingdon Cambs (U.K)

CHAPTER 6

APPEARANCE POTENTIAL MEASUREMENT FOR ZnS AND ZnSe VAPOUR PARTICLES

6.1 THE NEED FOR APPEARANCE POTENTIAL DETERMINATION

Measurement of the appearance potential for the particles detected on the mass spectrum of the QMS has been undertaken. The determination of appearance potential of the evaporant species for ZnS and ZnSe is necessary to determine the electron energy range where the magnitude of the signal at a given mass-to-charge ratio is at a maximum or where the ionization behaviour permits the separation of two or more overlapping peaks. The information about the dissociation of higher polymeric particles into lower orders can also be gathered and the ionization efficiency data can be used to separate between overlapping on the QMS spectra (zinc and sulfur at m/e=32 and 64). The method adopted for the determination of appearance potential for the vapour species relies on a linear extrapolation method [6.1]. Although this method is expected to yield higher threshold electron voltages than the actual ionization potentials [§

chapter3], a reference gas like nitrogen (or hydrogen) is used to correct for the shift towards higher energies by comparison to values reported in the literature. The appearance potential for N_2^+ is measured before and after an evaporation experiment. The use of Argon for a similar purpose has also been reported [6.2].

6.2 PRECAUTIONS ADOPTED IN APPEARANCE POTENTIAL MEASUREMENTS

In experiments to measure the appearance potentials of particles some of the parameters influencing the ionization process must be considered. The ionization cross section is assumed constant when the mass-to-charge ratio is varied. Also, the effects which may occur from the space charge created in the ionization chamber are considered minimal because it has been found that relative ion counts over the range of mass-to-charge ratios used do not vary when the emission current is varied. There is a fall in the ion count as the mass-to-charge ratio is increased and this is attributed to a fall in the QMS sensitivity In most experimental measurement the fall in sensitivity is reduced by setting the resolution on the QMS to zero [§ chapter5].

Other problems which may be encountered concern the cleanliness of the ion source. Contamination of the QMS ion source results in appearance potentials being higher than

their actual value. A difference of over 3.2 eV has been measured between the appearance potential of N_2^+ when the ion source has been freshly cleaned and after several deposition runs. It is suggested that deposits of ZnS and ZnSe on the wall of the ion source charge up and lower ionization efficiency which leads to the use of higher electron energies than are normally expected. Periodic cleaning of the source is undertaken to minimize these effects. The measurements made of the appearance potentials for vapour species in the present MBE system have been undertaken using the following steps:

1. The filament emission current on the QMS is kept at a constant setting. Other parameters which can affect the intensity of the current output from the QMS are also kept constant such as the the resolution, the secondary electron multiplier acceleration voltage (set to 3.5 KV), the discrimination level in the pulse counting assembly, the temperature of the vapour sources, and other parameters relative to the accumulation time such as the evaporant stream modulation frequency (122.2 Hz) and steering signal (200 modulation periods for each measurement).

2. The tuning voltages for the peaks to be monitored are determined using the peak finding software [§ appendix E]. Optimization of the count on each peak is obtained by compensating for the ions

arrival times from the rotating shutter to the secondary electron multiplier.

3. The QMS is adjusted to collect ions at a particular mass-to-charge ratio.

4. The electron energy is varied from 70 eV downwards.

5. Several readings are stored at each setting. This is done by either increasing the steering signal period proportionally or by issuing an instruction which adds several readings together.

6. When approaching the threshold voltages for a species predicted from the slope of the ionization curves, the electron energy is varied in steps of 0.25 eV. Outside the threshold voltage region steps of 1 to 2 eV in electron energy are used and this helps reduce the duration of the experiment.

7. The intensity of the ion count measured is then plotted as a function of the energy of the electron beam measured in electron volts. This is done off-line after storing the data in a Vax workstation.

In these experiments the electron energy is varied manually but the data acquisition as well as other parameters which must be varied (like the mass-to-charge ratio) are computer controlled. The experiment is carried out using a dedicated program which is outlined in the diagram of figure 6.1.

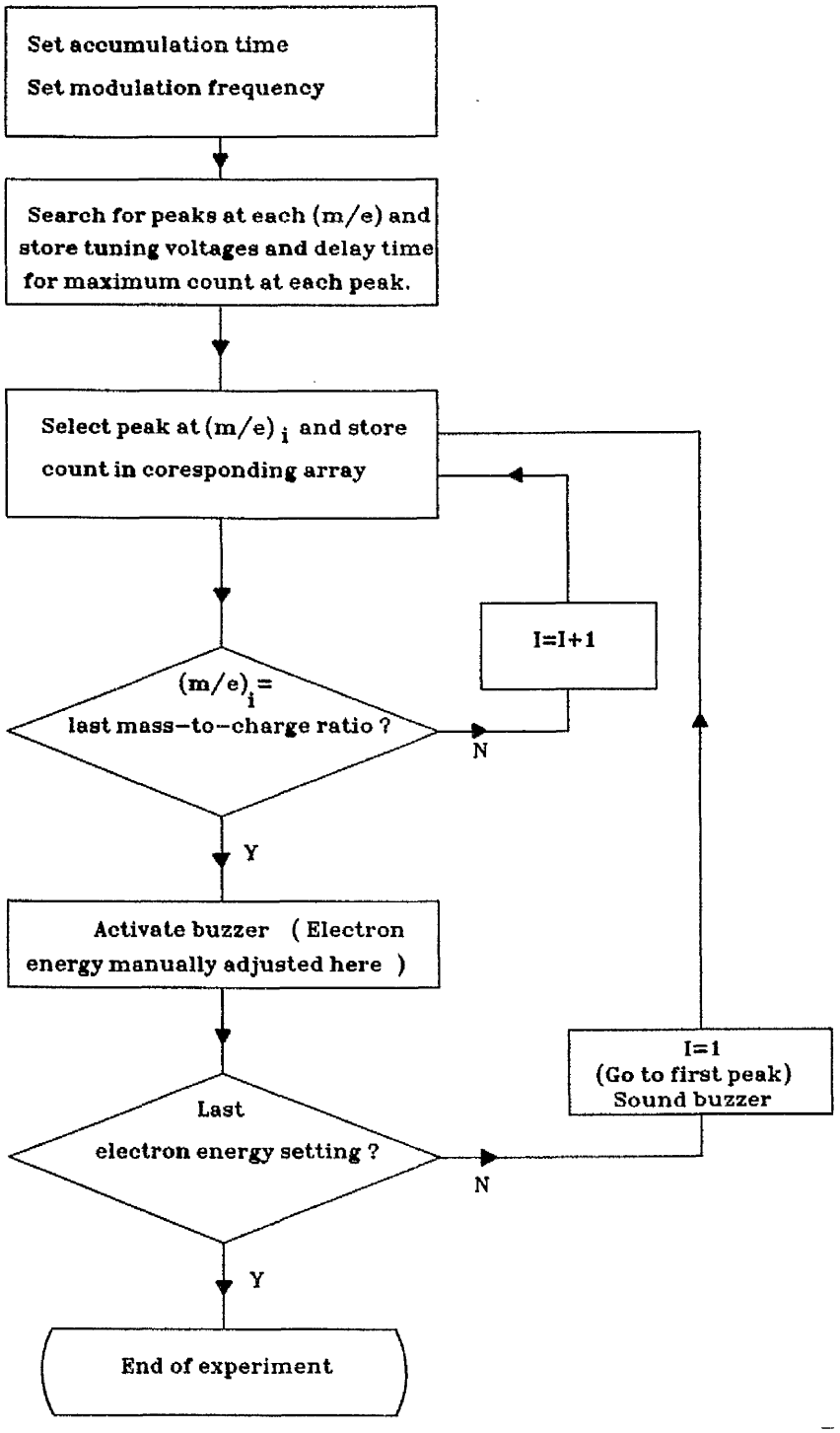

FLOWCHART SHOWING THE ACQUISITION OF DATA DURING THE IONIZATION OF PARTICLES

FIGURE 6.1

Since the electron energy is manually controlled, an audible signal is activated at the end of acquiring data at a given electron energy. A second activation of the audible signal after one period of the steering signal or 1.636 second signal the start of the acquisition of another set of data. The time of 1.636 second is large enough for manually adjusting the electron energy on the QMS control panel. This method of measurement provides for the rapid acquisition of data.

6.3 IONIZATION EFFICIENCY CURVES OF THE BACKGROUND GASES

The first investigations in the study of particle behaviour under electron impact have been carried out on the ion H_2^+ at mass-to-charge ratio 2 and the ion N_2^+ at mass-to-charge ratio 28. Figures 6.2 and 6.3 show the ionization efficiency curves of H_2^+ and N_2^+ respectively.

Determination of the appearance potential for N_2^+ is carried out after injecting nitrogen gas into the vacuum chamber so that contributions to the peak from CO+ ions is minimized. A comparison between the value obtained for N_2^+ and H_2^+ with tabulated values [6.3] show a difference of +1.4 eV for both ions and this is used for correcting the appearance potentials of the

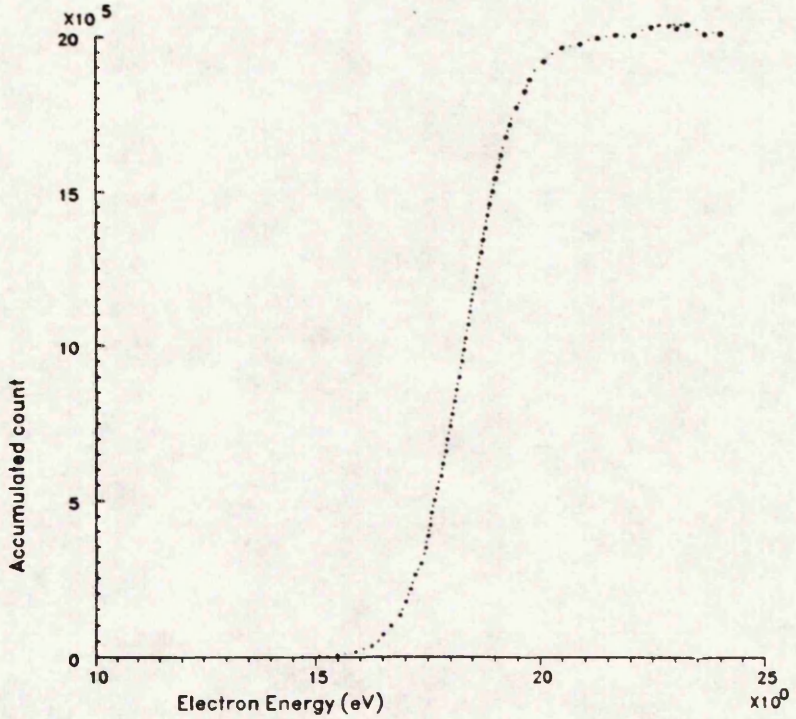

APPEARANCE POTENTIAL CURVE OF H2+ AT 900°CELSIUS

FIGURE 6.2

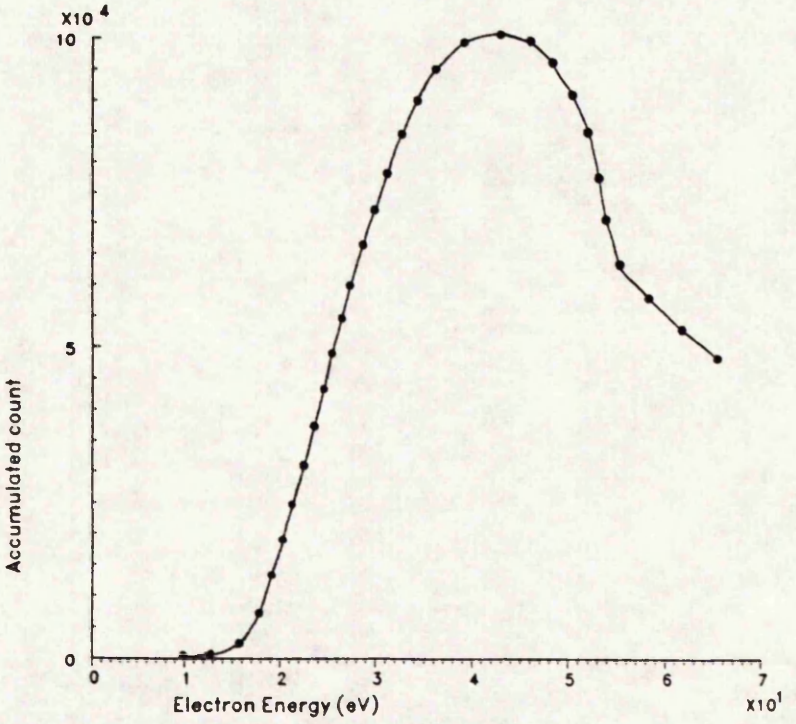

APPEARANCE POTENTIAL CURVE OF N2+

FIGURE 6.3

particles involved in the evaporation of zinc selenide and zinc sulphide compounds. The tabulated values are for ionization potentials obtained using spectroscopic methods. The error in the energy measured using the present system is estimated to be less than 0.125 eV. Since only particles from the ambient atmosphere are involved, the measurements taken are for total ion counts.

6.4 THE IONIZATION OF PARTICLES DURING ZnSe AND ZnS EVAPORATION

6.4.1 IONIZATION OF PARTICLES OBTAINED FROM ZnSe EVAPORATION

Selected particles detected during the evaporation of ZnSe compound at 900 °C are shown on a 200 a.m.u range mass spectrum in figure 6.4. The published abundancy of zinc and selenium particles [6.4] are included in the table of figure 6.5. The experimentally measured intensities have shown good agreement with the published abundancy of isotopes.

The ionization efficiency curve of zinc at mass-to-charge ratio 64 has been obtained. Figures 6.6 and 6.7 show the background, demodulated and total ion count curves for Zn+ (m/e=64) at emission currents of 200 μA and 2 mA respectively. Measurements at both emission currents show similar proportions of background-to-total ion counts

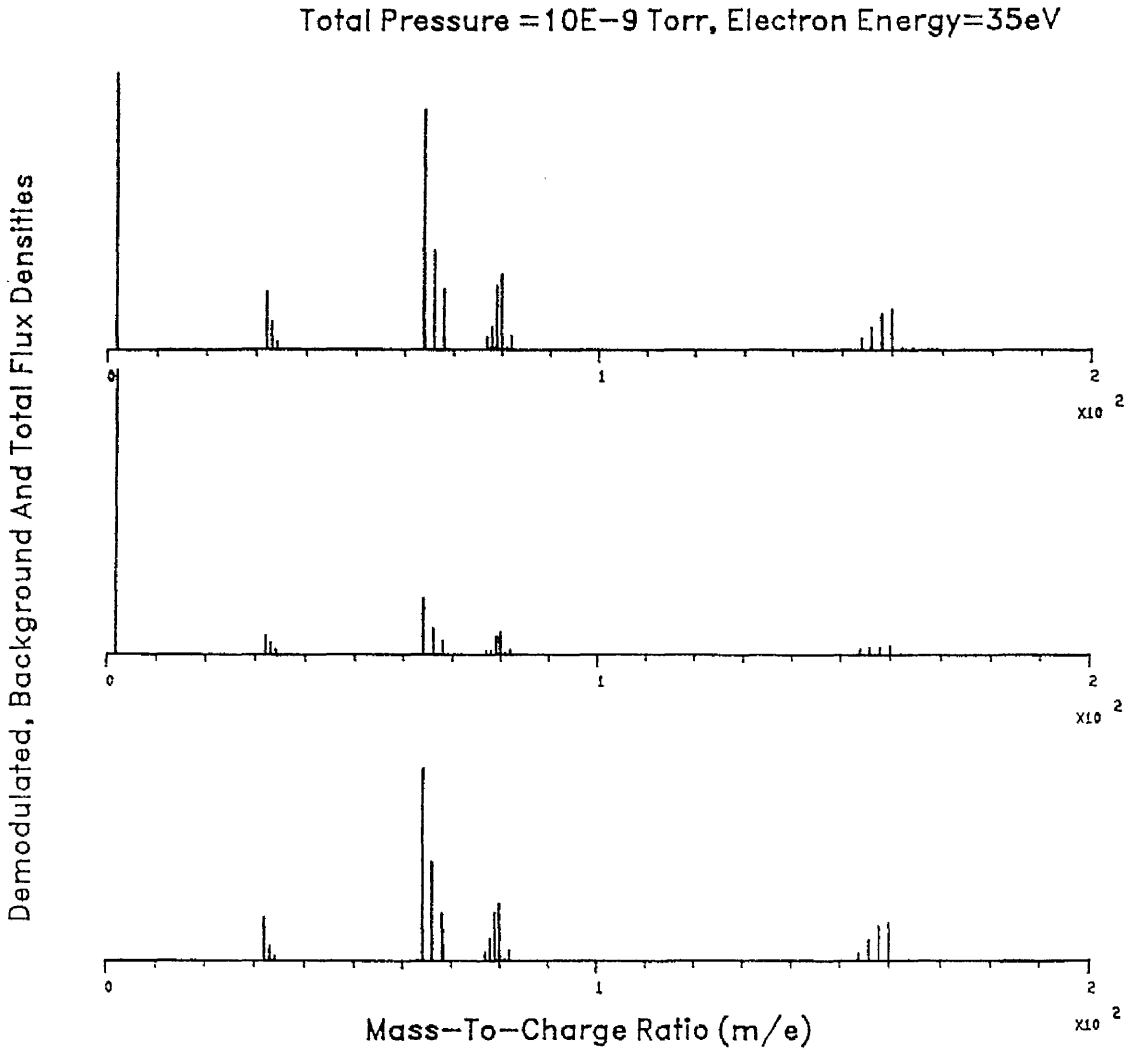

Mass Spectra Obtained During The Evaporation Of ZnSe At 880 Degrees Celsius

FIGURE 6.4

ELEMENT	SULPHUR			ZINC				SELENIUM				
m/e AT ISOTOPE	32	33	34	64	66	67	68	76	77	78	80	81
PUBLISHED ABUNDANCY (%)	95.02	0.75	4.21	48.6	27.9	4.10	18.8	9.0	7.6	23.5	49.8	9.2

PUBLISHED ISOTOPIC ABUNDANCIES FOR ZINC, SULPHUR AND SELENIUM ELEMENTS

FIGURE(6.5)

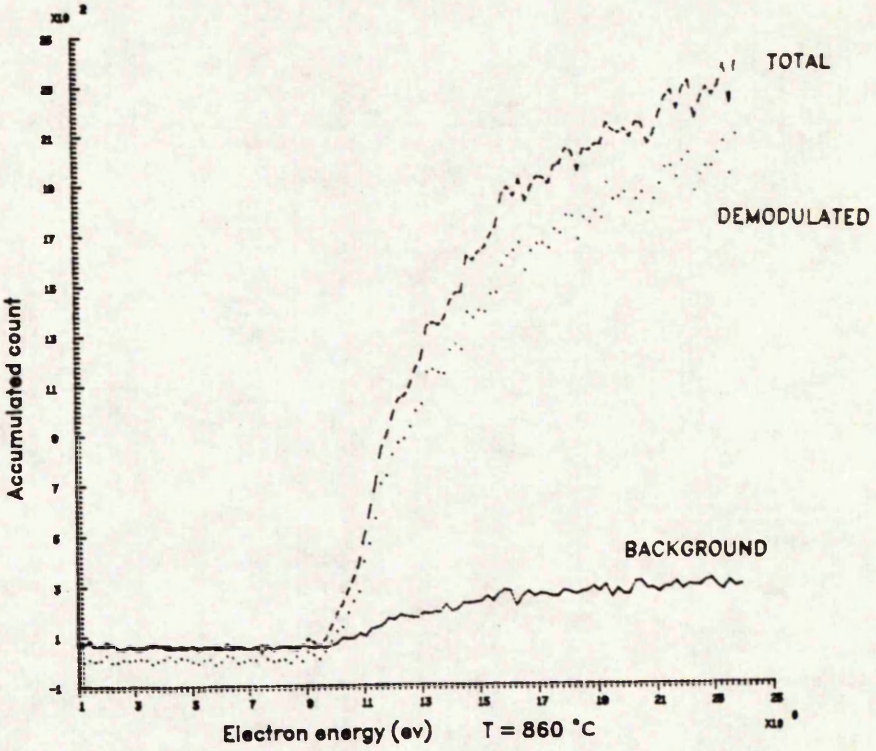

Zn^+(m/e=64) DIRECT, BACKGROUND AND DEMODULATED ION COUNTS VS THE ELECTRON ENERGY AT 200 μA EMISSION CURRENT

FIGURE 6.6

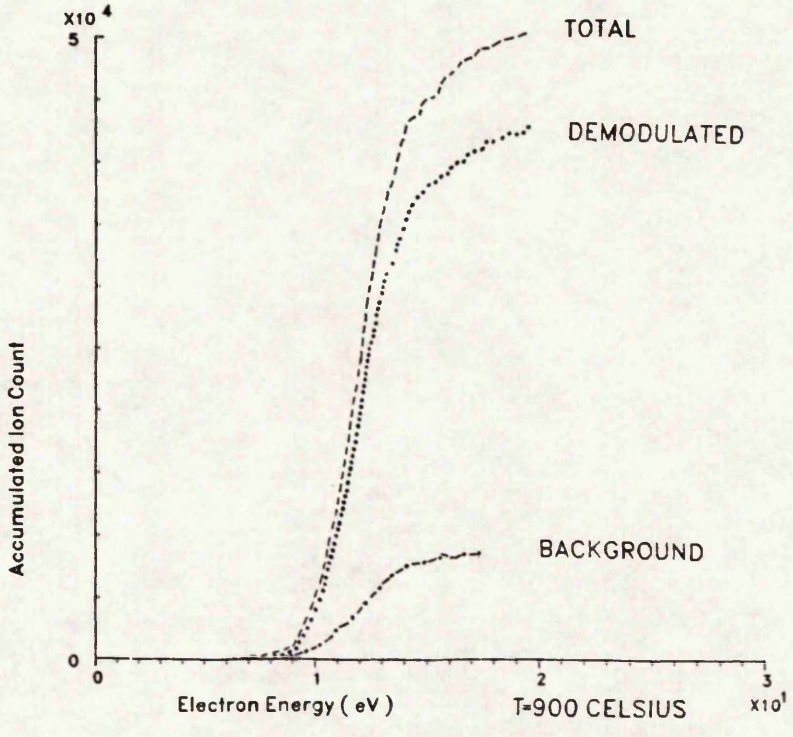

Zn^+(m/e=64) DIRECT, BACKGROUND AND DEMODULATED ION COUNTS VS THE ELECTRON ENERGY AT 2 mA EMISSION CURRENT

FIGURE 6.7

and the appearance potential is to 9.75 for both curves within the bounds of experimental error. The appearance potential curve for the zinc isotope at mass-to-charge ratio 66 shown on figure 6.8 yields a similar appearance potentials. Providing ionization data on several isotopes provides a means for verifying the obtained results on the most abundant isotope and also correcting errors which may arise from deviation from the peak maximum or drifts in the mass spectrometer tuning by calculating the isotopic abundancy ratios at any system setting (electron energy in this case). Doubly ionized zinc at mass-to-charge ratios 32 yielded the curves on figure 6.9 and the appearance potential obtained for this ion is 18.75 eV.

Figure 6.10 shows the ionization efficiency curves for selenium particles at m/e=80. The contribution from the selenium in the background to the total ion count appears to have a close similarity to that obtained on zinc. Figure 6.10 yields an appearance potential equal to 16.75 eV. Other selenium isotopes at m/e = 76, 77, and 78 have also been investigated and a appearance potential has been obtained while their ion count ratios where within 2% of the reported values in the literature [§ figure 6.5].

At m/e=160 (dimeric selenium), the appearance potential curves for the total, demodulated and background ion counts are shown on figure 6.11. Similar observations concerning the background contribution to the total ion count in the case of zinc and monomeric selenium can be made

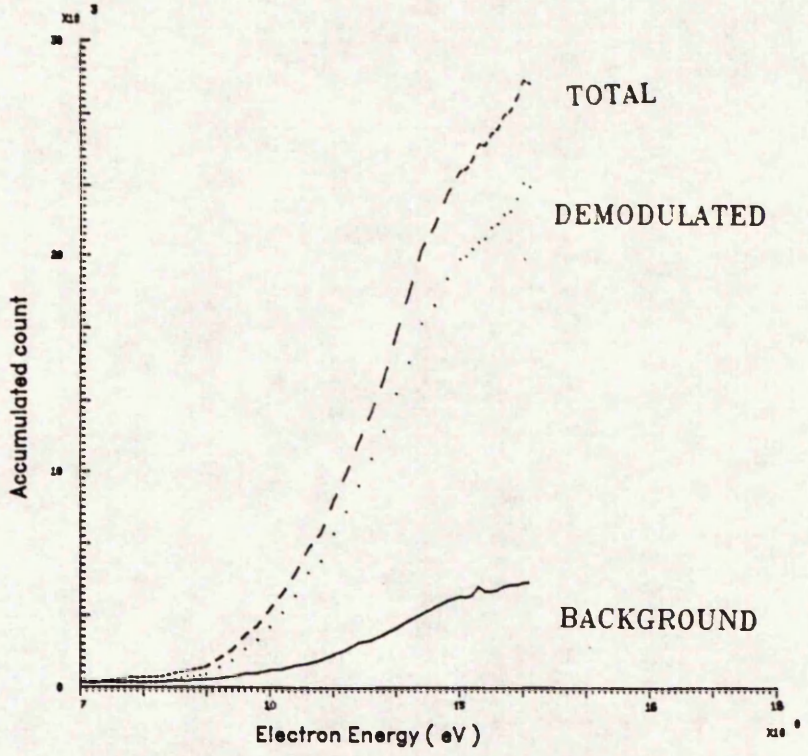

APPEARANCE POTENTIAL CURVES OF TOTAL, DEMODULATED AND BACKGROUND ION COUNTS FOR Zn+ (m/e=66) AT 900 CELSIUS

FIGURE 6.8

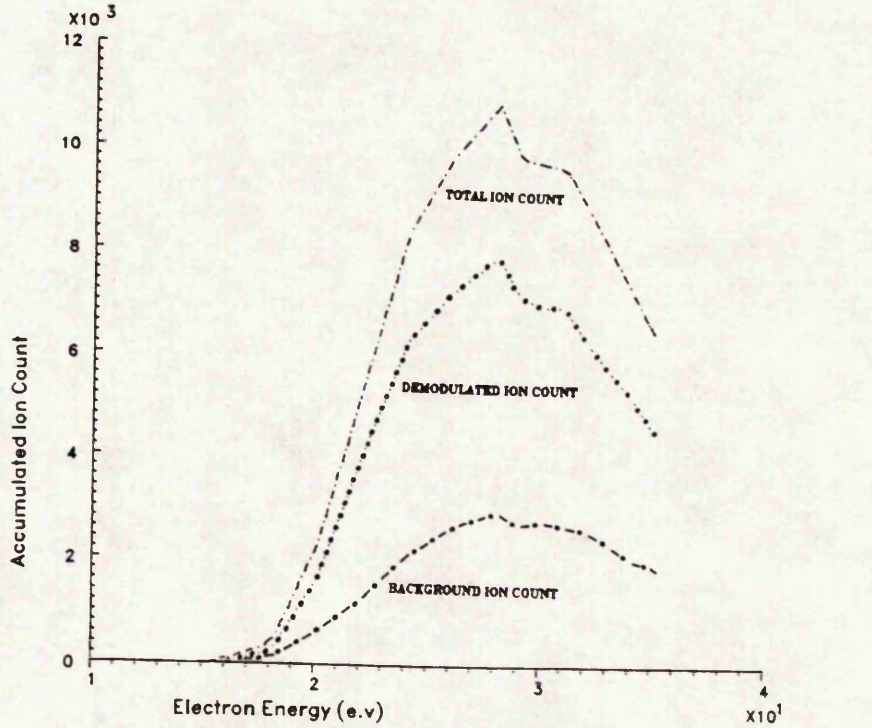

APPEARANCE POTENTIAL CURVES OF TOTAL, DEMODULATED AND BACKGROUND ION COUNTS FOR Zn++ (m/e=32) AT 880°CELSIUS

FIGURE 6.9

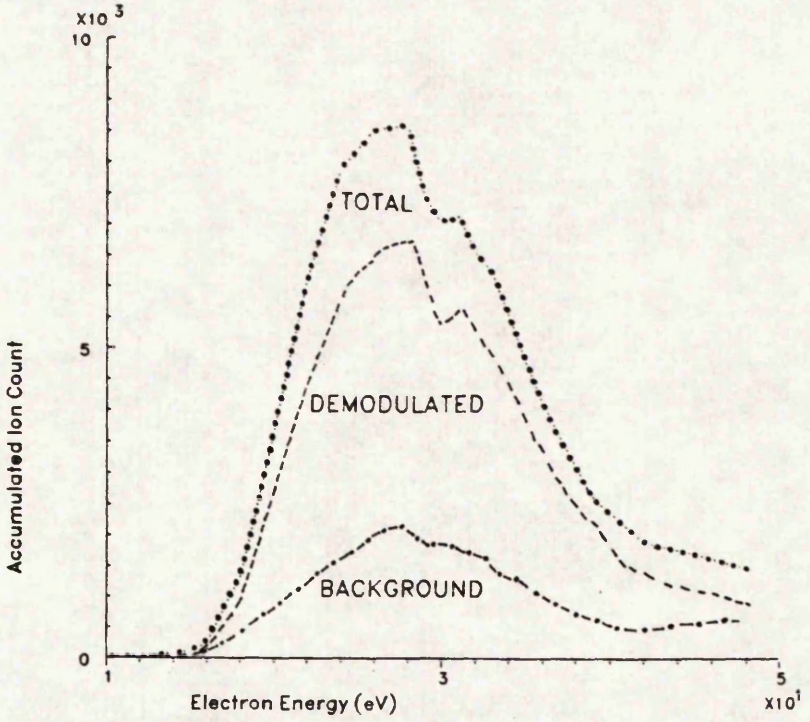

APPEARANCE POTENTIAL CURVES OF TOTAL, DEMODULATED AND BACKGROUND ION COUNTS FOR Se+ (m/e=80) AT 900 CELSIUS

FIGURE 6.10

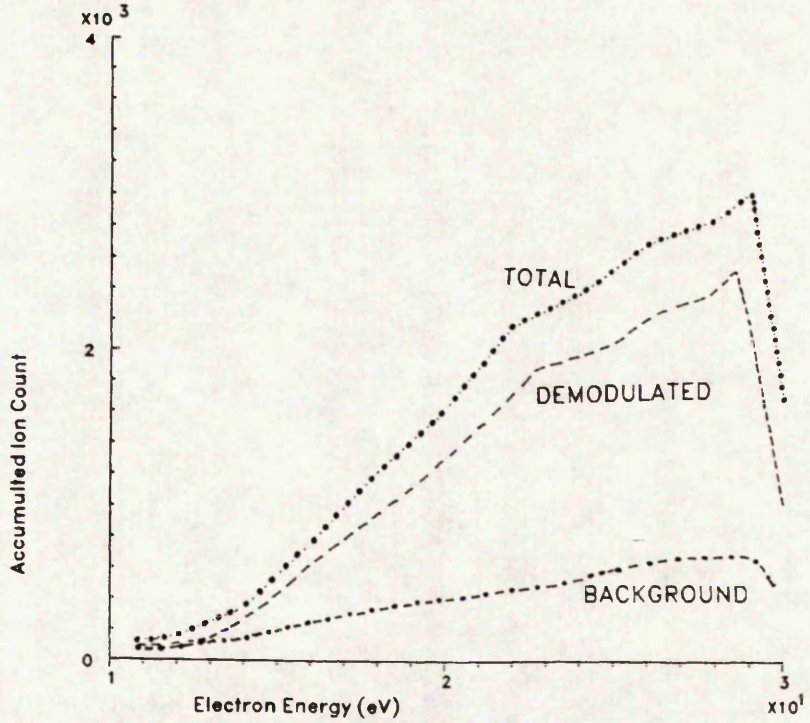

APPEARANCE POTENTIAL CURVES OF TOTAL,DEMODULATED AND BACKGROUND ION COUNTS FOR Se2+ (m/e=160) AT 900 CELSIUS

FIGURE 6.11

for Se_2+. The measured appearance potential for Se_2+ is equal to 12.75 eV. A similar value has been obtained at m/e=152, 156, and 156.

The difference between the appearance potential of Se+ and Se_2+ is equal to 4.5 eV. The number density for Se+ has been found to be higher than that of Se_2+ at higher electron energies which cannot be solely explained by the fall in sensitivity for the QMS. This is shown by plotting the variation of the ratio between the ion count on Se_2++ (m/e=160) and the ion count Se+ (m/e=80) on against the electron energy as shown on figure 6.12. The variation obtained on this figure shows the ratio reaches a maximum just after the appearance potential on Se_2+ and then decreases steadily and goes below a value of 1.0 only after the appearance potential of Se+. This suggests that at least part of the observed monomeric selenium may originate from dissociation of the dimers Se_2.

Comparing the variation of the background and demodulated ion counts with the electron energy for zinc and selenium particles shows that particles in the background and those in the direct beam have a similar probability of ionization.

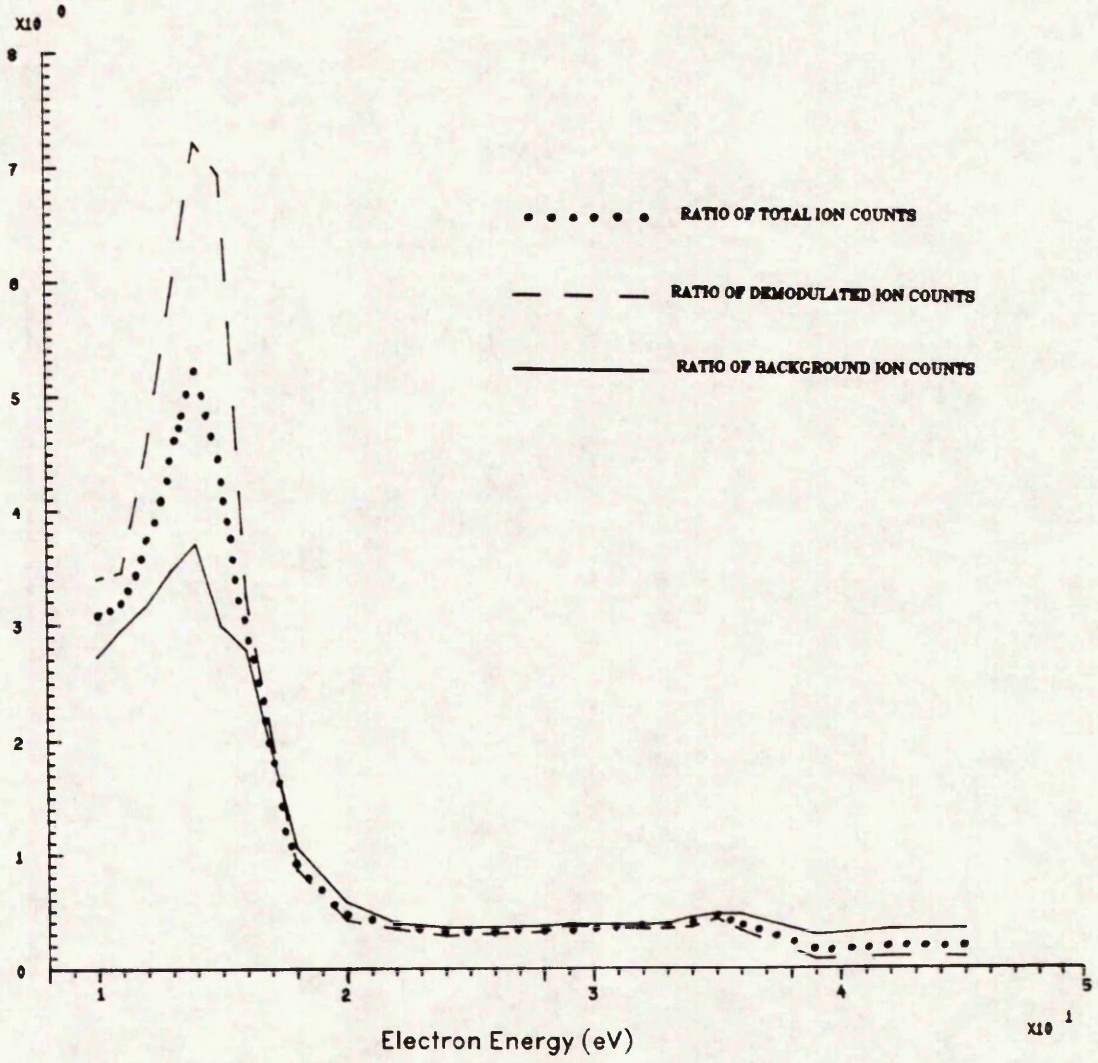

VARIATION OF THE RATIO BETWEEN THE ION COUNT FOR Se2+ (m/e=160) AND Se+ (m/e=80) WITH THE ELECTRON ENERGY AT 900 CELSIUS

FIGURE 6.12

6.4.2 IONIZATION OF PARTICLES OBTAINED DURING ZnS EVAPORATION

There is a problem with measuring the appearance potential for the component species emitted from the ZnS source because there is overlap between zinc and sulfur peaks in the mass spectrum. A comparison of the published abundancy data for isotopes shown in figure 6.5, indicates that use can be made of the peaks where sulfur content is minimal to extract data about the zinc content present [6.5]. For example, at mass-to-charge ratio 33 the sulfur content is negligible and the count measured may be considered equal to that for Zn++(m/e=33). This count can then be used to calculate the amount of doubly charged zinc ions at mass-to-charge ratio 32. Subtracting the calculated amount of zinc from the count at mass-to-charge ratio 32 leaves the count for sulfur at the same peak. A similar calculation can be undertaken on the particles at m/e = 64 and 66 during ZnS evaporation. This method has been used extensively in differentiating between the zinc and sulfur ion counts.

A mass spectrum obtained for selected masses during the evaporation of ZnS at 930 °C is shown on figure 6.13. The main peaks occuring on the spectrum are those at mass-to-charge ratios 32, 33, 34, 64, 66, and 68. Figure 6.14 shows the appearance potential curves obtained at mass-to-charge ratios 32 and 33 for the total ion counts. Examination of these curves shows that at m/e=33 the

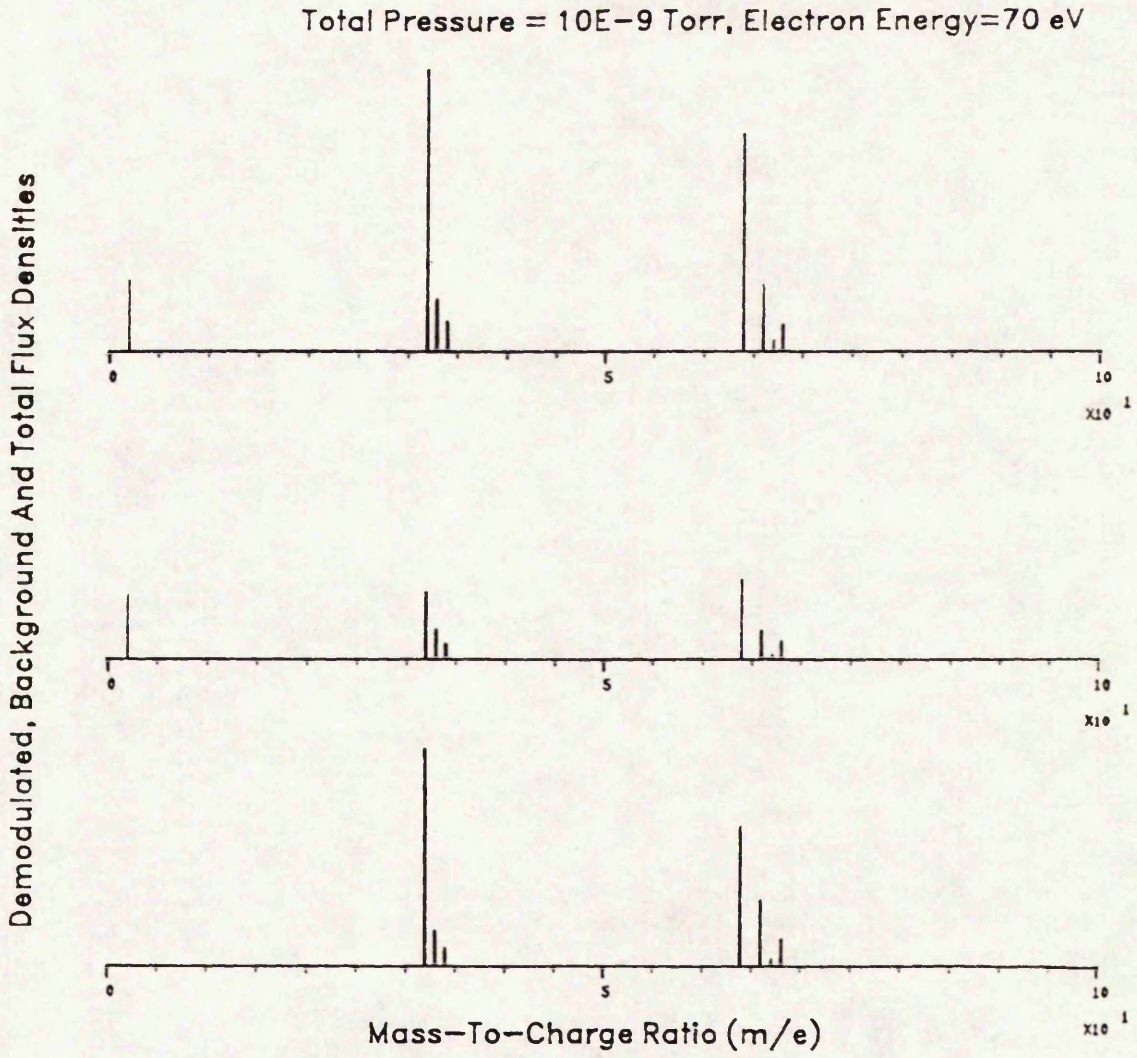

Mass Spectra Obtained During The Evaporation
Of ZnS At 1000 Degrees Celsius

FIGURE 6.13

appearance potential is equal to 18.9 eV which is equal (within experimental error) to the value obtained on doubly ionized zinc (Zn++) during the evaporation of ZnSe. This helps justifying the proposition that the amount of sulfur contributing to the peak at m/e=33 can be neglected. The appearance potential curve drawn for m/e=32 on figure 6.14 shows however that the appearance potential is equal to 12.75 eV and this may be considered as the appearance potential for monomeric sulfur ions (S+).

To confirm this argument, the sulfur content at m/e=32 is extracted by subtracting from it the ion count for zinc which is calculated by multiplying the ion count at m/e=33 by the ratio of the abundancy of the zinc isotope at m/e=32 to that at m/e=33. This ratio is used from the results obtained on ZnSe evaporation. The appearance potential curve for S+ at m/e=32 is shown on figure 6.15. The curve obtained for S+ has the same appearance potential as that for m/e=32 which contains doubly ionized zinc as well. On figure 6.16 are shown the appearance potential curves at m/e=34 for the total, demodulated and background ion counts. This figure shows that the appearance potential curve for the background ion count has a different appearance potential than that of the demodulated and total ion counts. The background curve yields an appearance potential of 18.9 eV and the demodulated and total curves yield a similar appearance potential of 12.8 eV. From the previous measurements on appearance potentials of Zn++ at m/e=33 and

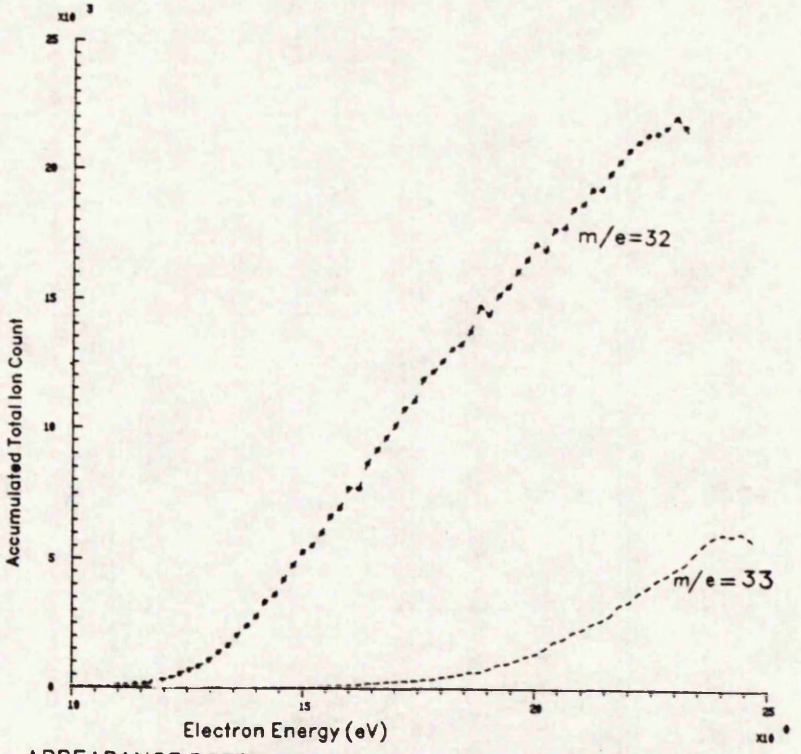

APPEARANCE POTENTIAL CURVES AT m/e=32 AND 34 DURING THE EVAPORATION OF ZnS AT 1000 CELSIUS

FIGURE 6.14

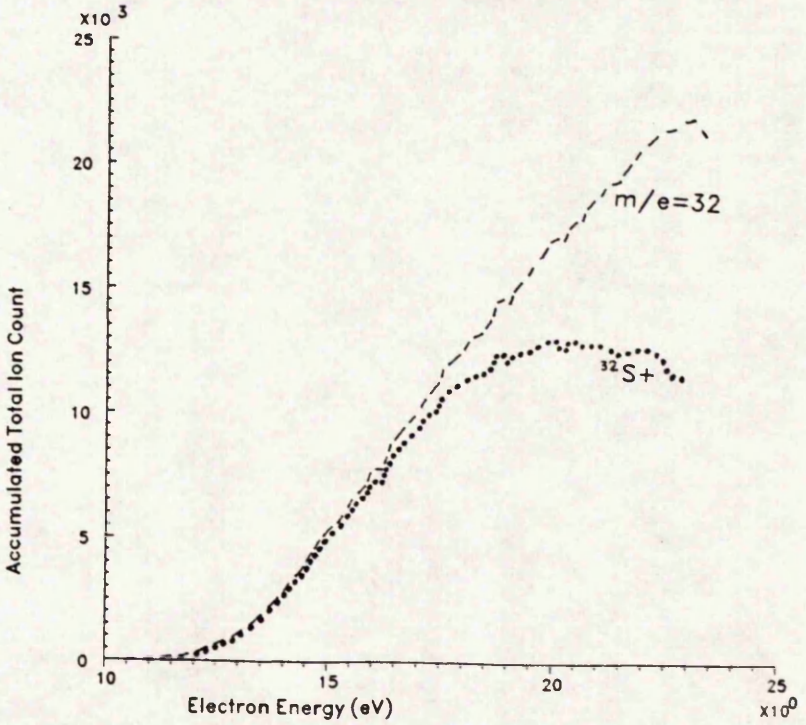

COMPARISON BETWEEN THE CALCULATED APPEARANCE POTENTIAL CURVE FOR S+ AND THAT AT m/e=32 DURING THE EVAPORATION OF ZnS

FIGURE 6.15

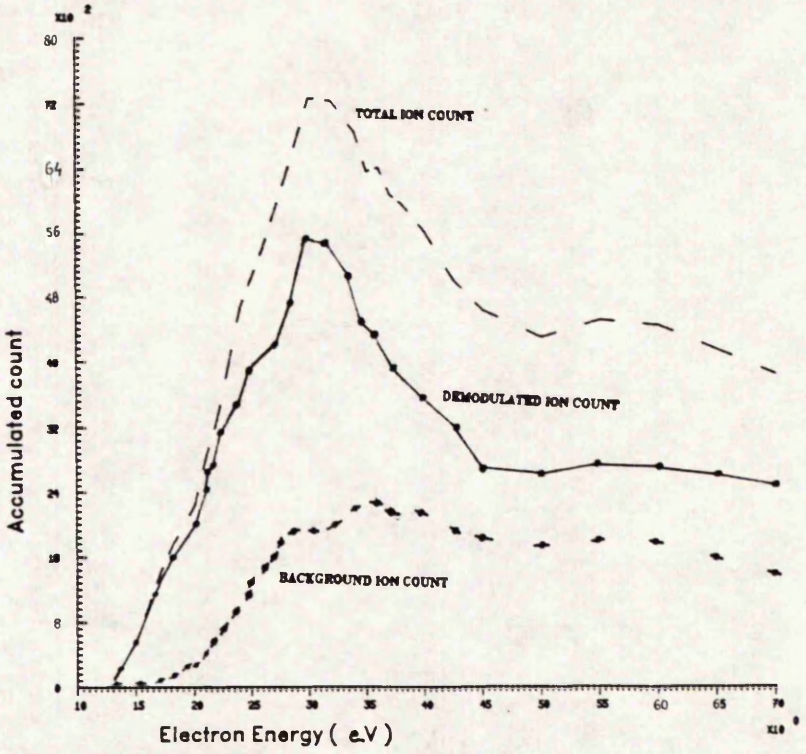

APPEARANCE POTENTIAL CURVES AT m/e=34 DURING THE EVAPORATION OF ZnS AT 1000 °C

FIGURE 6.16

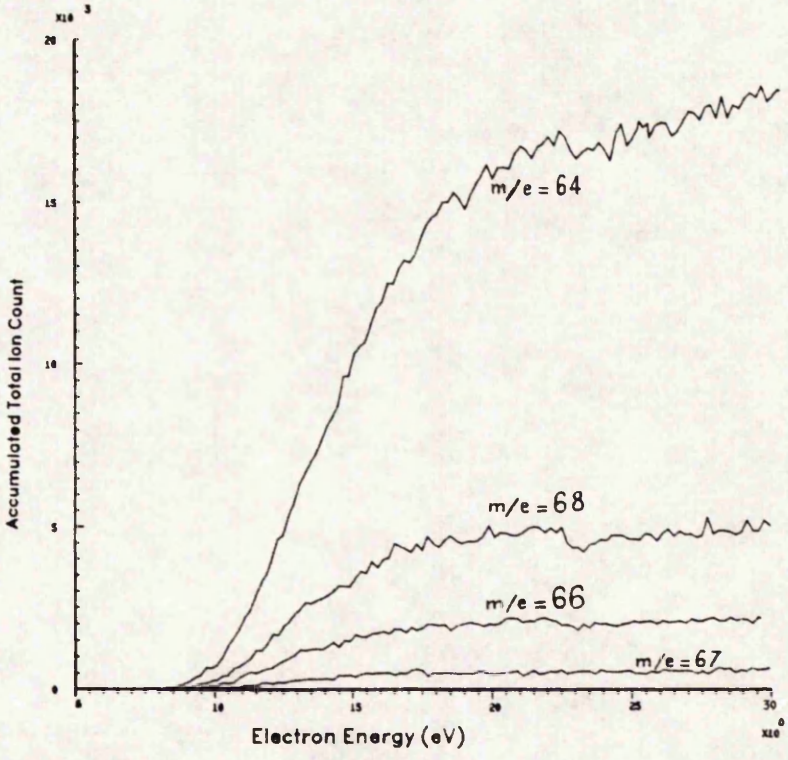

APPEARANCE POTENTIAL CURVES AT m/e=64, 66, 67 AND 68 DURING THE EVAPORATION OF ZnS AT 915 °C

FIGURE 6.17

S+ at m/e=32 and since isotopes of the same ion yield equal appearance potentials (within experimental error), it can then be suggested that the curve representing the background on figure 6.19 is that of zinc in the background and that the contribution from sulfur at this mass-to-charge ratio is negligible. With the electron energy decreasing, the total and demodulated curves decrease more rapidly after the background curve has reached a negligible value. The contribution of sulfur ion to m/e=34 is much smaller than that of Zn++. The total and demodulated ion counts yield the appearance potential of sulfur at m/e=34 which can be considered as similar to the value obtained on sulfur at m/e=32.

Observations on the appearance potentials of Zn+ and S_2+ have also been made. Figure 6.17 shows the various appearance potential curves at mass-to-charge ratios 64, 66, 67, and 68, which include zinc and dimeric sulfur. All these curves yield a similar appearance potential equal to 9.75 eV which is equal to that obtained on Zn+ during the evaporation of ZnSe. At m/e=66 and 67 the sulfur content is negligible, whereas at m/e=64 the sulfur content can be important. The equality of the different appearance potentials at these mass to charge ratios suggests that the appearance potential of S_2+ and Zn+ are equal within experimental error.

At m/e=66, the appearance potential curves for the total, the demodulated and background ion counts are shown on figure 6.18. The figure shows the contribution of the background to the zinc total ion count. This contribution is similar to that observed in the case of zinc from the evaporation of ZnSe (about 20%). A similar observation can also be made in the case of m/e=34 shown on figure 6.16.

The appearance potential of the ion S+ has been found to be equal to 12.75 eV and that of the dimer S_2+ equal to 9.75 eV. The difference of 3 eV between the two potentials may help with explaining the origin of S+ ions. On figure 6.19 is represented the variation of the ratio of demodulated ion count for S_2+ at m/e=64 to that for S+ at m/e=32 against the electron energy. The curve shows a decrease in the ratio as the electron energy increases. The decrease is more abrupt just after the appearance potential of S+. This may suggest that at least part of the monomeric sulfur is produced by the dissociation of dimers. This is also supported by the fact that a search for higher order molecules of sulfur has failed knowing that there are only zinc monomers in the vapours.

The curve on figure 6.19 shows also a step decrease in the ratio of dimeric to monomic sulfur ion counts. The decrease occurs between 21.6 and 23.5 eV. This step decrease may be due to further ionizations of the sulfur particles leading to the occurance of doubly ionized sulfur monomers S++. This can be helped by more sulfur dimers

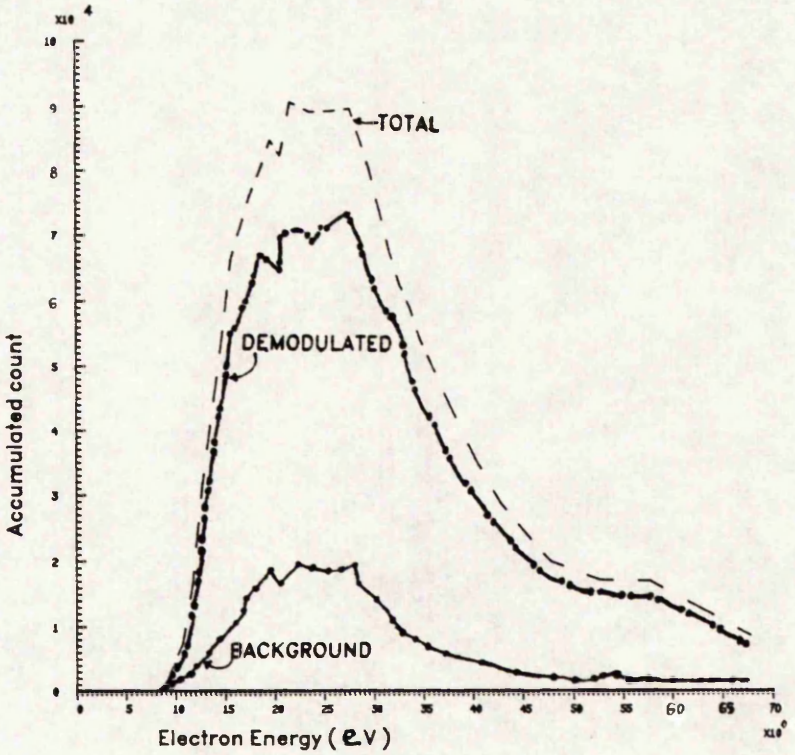

APPEARANCE POTENTIAL CURVES AT m/e=66 DURING THE EVAPORATION OF ZnS AT 1000 °C

FIGURE 6.18

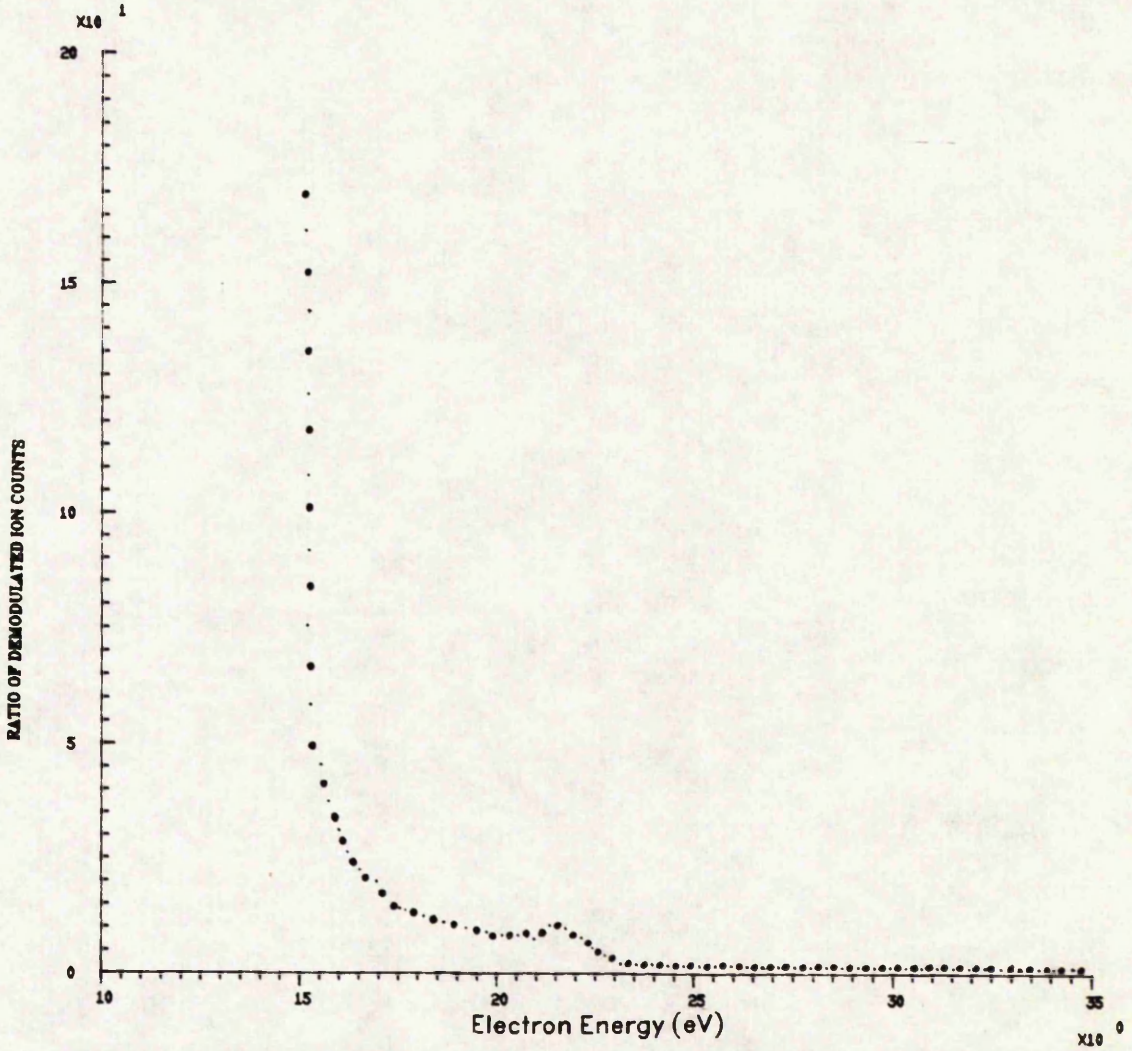

VARIATION OF THE RATIO BETWEEN THE ION COUNT FOR S2+ (m/e=64) AND S+ (m/e=32) WITH THE ELECTRON ENERGY AT 1000 CELSIUS

FIGURE 6.19

getting dissociated. The published value on the ionization potential for the ion S++ using a specroscopic technique is equal to 23.4 eV [6.6].

6.5 CONCLUSION

The appearance potentials of the particles occuring on a QMS mass spectrum during the evaporation of zinc Sulphoselenide alloys have been investigated. The results obtained on the measurements of the appearance potentials of these various particles are included in figure 6.20. The use of a supervisory computer for the control of the experiment and acquisition of data has been found invaluable for reducing the running time of the experiment as well as organizing the different measurement tasks.

The contribution of the background vapours to the ion counts of the various particles monitored has been identified. The use of modulated beam mass spectrometry with appearance potential measurements has shown the ability to identify the major contributory particles to the background vapours both in the case of ZnS and ZnSe evaporation.

It has been shown that the background ion counts for the various particles are of a similar magnitude (20% ±2%) in the ionization chamber of the spectrometer. Differences in appearance potentials between sulfur and zinc ion can

MATERIAL	SULPHUR		ZINC		SELENIUM	
VAPOUR SPECIES MASS–TO–CHARGE RATIO	32 (S+)	64 (S2+)	32 (Zn++)	64 (Zn+)	80 (Se+)	160 (Se2+)
APPEARANCE POTENTIAL (eV)	12.75	9.75	18.75	9.75	17.25	12.75

MEASURED APPEARANCE POTENTIALS OF IONS OBSERVED DURING THE EVAPORATION OF ZnS AND ZnSe.

FIGURE 6.20

help separating between their ion counts. This has been helped by explaining differences in appearance potential between total, demodulated and background particles at a single mass-to-charge ratio (m/e=34) in the evaporation of ZnS.

Use of published isotopic abundancies has helped resolve the overlap between zinc and sulfur peaks and a practical way for calculating number densities for the two components developed. The observations made on the ionization efficiency data for isotopes of sulfur, zinc and selenium suggest that their appearance potentials have equal values within an error of 0.125 eV.

The use of appearance potential measurements can prove valuable in experiments requiring a high signal to noise ratio on measured ion counts since the variation of the ion counts on the particles monitored appears to pass by a maximum threshold in the interval from 0 to 70 eV. This can be due to the occurance of consecutive ionizations at the mass-to-charge ratio investigated. The highest order polymeric species of sulfur found during ZnS evaporation have been the dimers. At least part of the selenium and sulfur monomeric ions originate from the dimers. During the evaporation of ZnS, shift to higher electron energies with the zinc content is observed on the appearance potential curves at m/e=32, 33 and 34. When the contribution of sulfur (S+) is more important the curves are shifted to lower appearance potential thresholds.

Cryopanelling of the deposition system prevents vapours from forming important background pressures but it appears that this is not consistent with the various vapour species. The decay on the zinc background is slow enough to be observed using a manual shutter because zinc is the predominant component in the vapours [§ figures 6.4 and 6.13]. It appears as though all particles emanating from the vapour sources contribute continuously to the background vapours establishing an equilibrium with those which get trapped on the cooled surfaces. Therefore it may be expected that deposition of a ZnS or ZnSe vapours onto a heated surface (substrate) may result in the formation of zinc Sulphoselenide with some particles like those of zinc reevaporating from the surface not favouring the deposited material energetically.

6.6 REFERENCES

[6.1] R.I.REED
"Ion Production By Electron Impact"
Academic Press (1962)

[6.2] A.S.SAHIN
PhD Thesis University of Manchester (1983)

[6.3] R.C.WEAST (ed.)
"The Chemical Rubber Company Handbook Of Chemistry And Physics" 70th Edition pp.E87-E88 (1989-1990)

[6.4] J.ELMSLEY (Ed.)
"The elements" Oxford Univ. Press (1989)

[6.5] M.BENYEZZAR, D.KING, P.L.JONES AND D.MOORE
Vacuum Vol.41 Nb.4-6 pp.842-846 (1990)
(Paper Included At End Of Thesis)

[6.6] R.C.WEAST (ed.)
"The Chemical Rubber Company Handbook Of Chemistry And Physics" 70th Edition p.E80 (1989-1990)

CHAPTER 7

TIME OF FLIGHT ANALYSIS OF ZnS AND ZnSe VAPOUR PARTICLES

7.1 INTRODUCTION

The time of flight for vapour particles passing between the rotating shutter and the ion detector has been investigated with the aim of determining the nature of the particles produced during the evaporation process. Also the behaviour of the particles when bombarded by electrons in the ionization chamber of the mass spectrometer has been examined. Of interest in the present study are the types of monomeric or polymeric vapour species involved in the vapourization of zinc sulphide and zinc selenide compounds prior to their deposition on the gallium arsenide substrate.

7.2 TIME DELAYS EXPERIENCED BY A VAPOUR PARTICLE AFTER LEAVING THE PLANE OF THE SHUTTER

A vapour particle of mass m leaving the plane of the

shutter at time t=0 enters the mass spectrometer after a delay time t_{d1}. Following ionization, the particles are accelerated by an electrostatic field and pass through the spectrometer quadrupole rod assembly and then this takes a time t_{d2}. These are the most important delays for providing information about the origin and characteristics of the particle species.

Other delays which must be included are inherent to the measurement system and these include a delay caused by mechanical phase shift introduced by the positioning of the photoelectronic shutter position detection device (phototransistor and lamp) in relation to the rotating shutter and the instant at which the shutter admits vapour particles to the mass spectrometer entrance. Another delay also present is caused by the complex impedance seen by the signal at the output of the spectrometer before reaching the counting circuitry assembled for digitizing the mass spectrometer ion current [7.1,7.2].

The delay caused by the mechanical phase shift can be minimized by careful positioning of the shutter assembly. However, removing this delay involves the measurement of the ion arrival time for a single vapour species at two different modulation frequencies. Since the arrival time of the ion monitored is independent of the modulation frequency, the difference in the arrival time between the two experiments is attributable to mechanical phase shift. A reference for the phase shift is established from the dual

shutter rotation speed measurements allowing corrections to be made to time of flight measurements. As for the phase shift encountered by the ion arrival signal through the complex impedance between the mass spectrometer and the counting assembly, measurement of the delay caused to a reference 10 MHz square wave has shown that this delay is less than 0.05 μs which is well below the other delay times encountered by the different particles investigated. Also, the transit of electrons through the electron multiplier structure induces a delay but this is ignorably small and does not exceed 200 ns. Figure 7.1 shows a schematic diagram for the main delays encountered by a particle of mass m between the shutter and the mass spectrometer. The total delay time t_D encountered by a particle of mass m leaving the rotating shutter at time t=0 can therefore be written as:

$$t_D = t_{d1} + t_{d2} \qquad (7.1)$$

with

$$t_{d1} = d1/v \qquad (7.2)$$

and

$$t_{d2} = d2\ (2\ n\ V\ q/m)^{-1/2} \qquad (7.3)$$

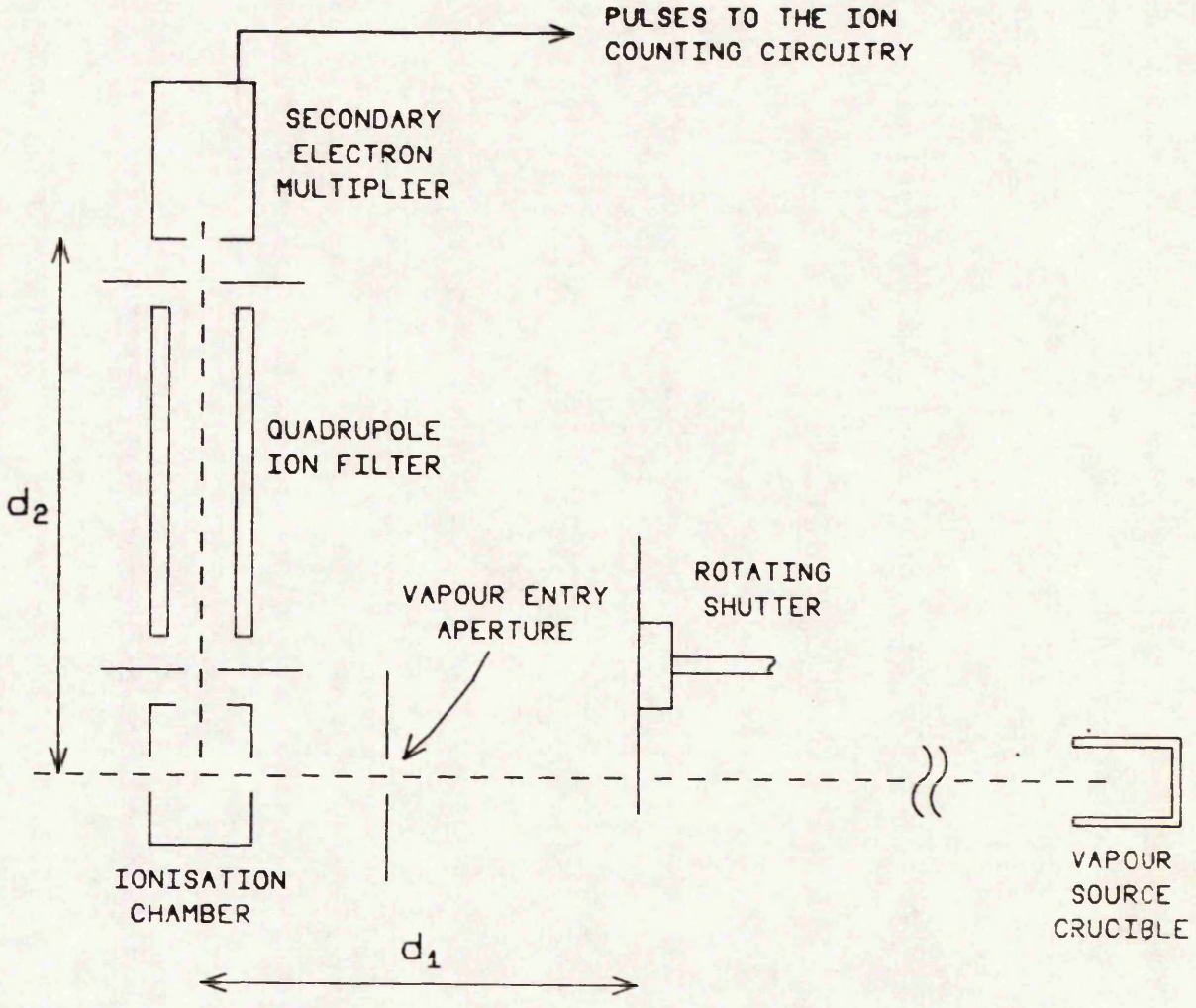

$$t_D = \frac{d_1}{v} + d_2 \sqrt{\frac{m}{2nqV}}$$

SCHEMATIC DIAGRAM FOR THE EXPERIMENTAL SET-UP SHOWING THE MAIN DELAYS ENCOUNTERED BY A PARTICLE BETWEEN THE SHUTTER AND THE ELECTRON MULTIPLIER

FIGURE 7.1

where m is the particle mass, q the electron charge, n the number of electric charges on the particles, V the QMS ion acceleration voltage (6.55 Volts), and v the particle velocity. The distances d1 and d2 are respectively equal to 24.3 mm and 128 mm. Figure 7.2 shows the calculated delays for different particles occuring during the evaporation of ZnSe and ZnS using relationship (7.1). In the rest of the text, the time delay from the chopper to the ionization chamber will be referred to as the particle time of flight (TOF) and the transit period for the ion passing through the quadrupole mass filter is to be refered to as the ion transit time (ITT). The total time t_D is called the ion arrival time (IAT). The ITT is much shorter than the TOF although d2 is longer than d2 and this is due to the magnitude of the ion acceleration voltage in the QMS imparting energies to the ions an order of magnitude, or more, higher than the thermal energies.

7.3 RESPONSE OF THE QMS TO A STEP INCREASE IN THE PARTICLE BEAM DENSITY

A pre-requisite to success in analysing the particle transit times is a theoretical analysis of the particle number density variation caused by mechanical modulation. An overall equation describing the response of a quadrupole mass spectrometer to a flux of vapour species passing through the ion source has been described by Farrow [7.3]

ION SPECY	Mass-To-Charge Ratio	Delay From Chopper To Detector (μs)	Delay Through Mass Filter (μs)
S++	16	31.124	14.400
Zn++	32	31.124	20.365
S+	32	44.017	20.365
Zn+	64	44.017	28.801
S2+	64	44.017	28.801
Se++	40	49.212	22.769
Se+	80	49.212	32.200
Se2+	160	69.596	45.538

Table a

ION SPECY	Mass-To-Charge Ratio	Delay From Chopper To Detector (μs)	Delay Through Mass Filter (μs)
S++	16	29.877	14.400
Zn++	32	29.877	20.365
S+	32	42.252	20.365
Zn+	64	42.252	28.801
S2+	64	42.252	28.801
Se++	40	47.240	22.769
Se+	80	47.240	32.200
Se2+	160	66.807	45.538

Table b

TABLES SHOWING THE ION ARRIVAL TIMES FOR PARTICLES PASSING BETWEEN THE SHUTTER AND THE ELECTRON MULTIPLIER AT 900 °K (Table a) AND 1000 °K (Table b)

FIGURE 7.2

and this has been discussed in previously reported work [7.1].

Experiments performed in characterizing the modulated beam mass spectrometry system have shown that the ionization cross section and the ion extraction efficiency can be considered as constant. As for the sensitivity, good tuning is at zero setting on the resolution [§ chapter 5]. A description of sensitivity setting for obtaining unit mass resolution is described in the literature [7.4]. The mass spectrometer can be considered as a density detector [7.5] and hence its response is proportional to the number density predicted by Maxwell-Boltzmann probability distribution for particle speeds [§ section 3.6.1.1]. After opening the shutter the distribution of particles travelling with speeds between v and v+dv towards the ionization chamber is:

$$dNv = 2\ \Pi^{1/2}\ v^{3}\ a^{-3}\ e^{-(v/a)^{2}}\ dv \qquad (7.5)$$

where $a = (2KT/m)^{\frac{1}{2}}$ is the most probable speed of the particle, K is Boltzmann's constant and T the absolute temperature.

The number of particles of mass m arriving at the mass spectrometer between times t and t+dt after opening the shutter is proportional to:

$$dNv = 4\ \Pi\ d1^{3}\ t^{-4}\ a^{-3}\ e^{-[(d1/(a\ t)]^{2}}\ dt$$

(7.6)

The symbols used in relationship (7.6) relate to the same quantities as in the previous relationships. Hence after opening the shutter there is a step increase in the flux of particles from time t=0. The number density Nv of particles of mass m at a distance d1 from the shutter is after being normalized described by:

$$N_{v} = [1 - Erfc(d1/a\ t)] + 2\ \Pi^{-1/2}\ d1/(a\ t)\ e^{-[d1/(a\ t)]^{2}}$$

(7.7)

Where Erfc is the complementary error function, which is represented by the relationship:

$$\mathrm{Erfc}(d1/(a\ t)) = 2\ \Pi^{-1/2} \int_0^{d1/at} e^{-y^2}\, dy \qquad (7.8)$$

with y used as a variable. Integrating relationship (7.7), the variation of number density with time for particles leaving the shutter plane at t=0 and arriving at the electron multiplier has been calculated . Figure 7.3 shows ion arrival curves for particles involved in the evaporation of zinc sulphoselenide alloys at 900 °C. In the calculations the complementary error function has been integrated using Simpson's rule. The time of flight for the various particles can be calculated from the curves. At t=d1/a (with a the most probable speed), relationship (7.7) yield a number density of 57.2% and this can be considered as the ion arrival time for a particular vapour species. The density of particles of mass m increases until reaching its final value dictated by the amount of material emanating from the vapour source. If the shutter is kept open the number density reaches a value which will remain constant if equilibrium conditions are achieved. The series of ion arrival curves have been calculated assuming the ions and vapour particles have the same mass.

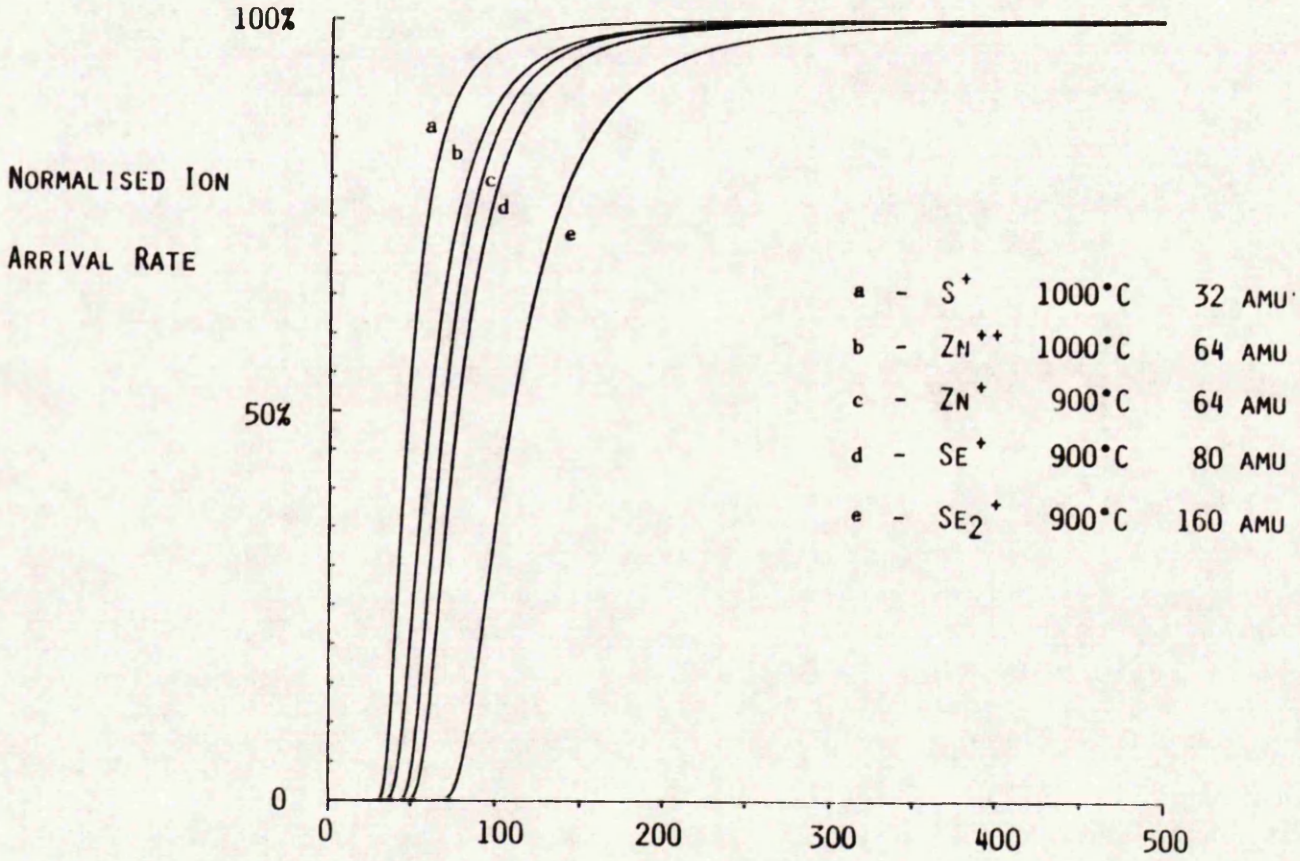

CALCULATED ION ARRIVAL CURVES

FIGURE 7.3

After closing the shutter the number density of the particles in the beam decays similar manner to the way it has risen. If f1(t)=Nv and is a normalized function on the ion count at a particular mass-to-charge ratio, therefore closing the shutter can be described by a function equal to 1-f1(t-Tm/2). This is shown on the theoretically calculated curve in figure 7.4. The total time through which the shutter has been kept open is equal to the time which has elapsed between the number density reaching 57.2% of the final value (on the rising edge of the curve) and 42.8% of the value measured on the falling edge of the curve. This may help with verifying the modulation period of the rotating shutter.

7.4 ION ARRIVAL TIME MEASUREMENTS

Experimental measurements of the ion arrival times have been undertaken. The aim here is not to verify Maxwell's theory. It is of interest however, to define particular threshold points on the ion arrival curves so that differences in the arrival times of particle species can be identified.

A high modulation frequency has been used (1018.2 Hz). The ion counts have been accumulated using a window of width tw=6.4 μs. Figure 7.5 shows the signals employed for the experiment. This window is progressively delayed throughout

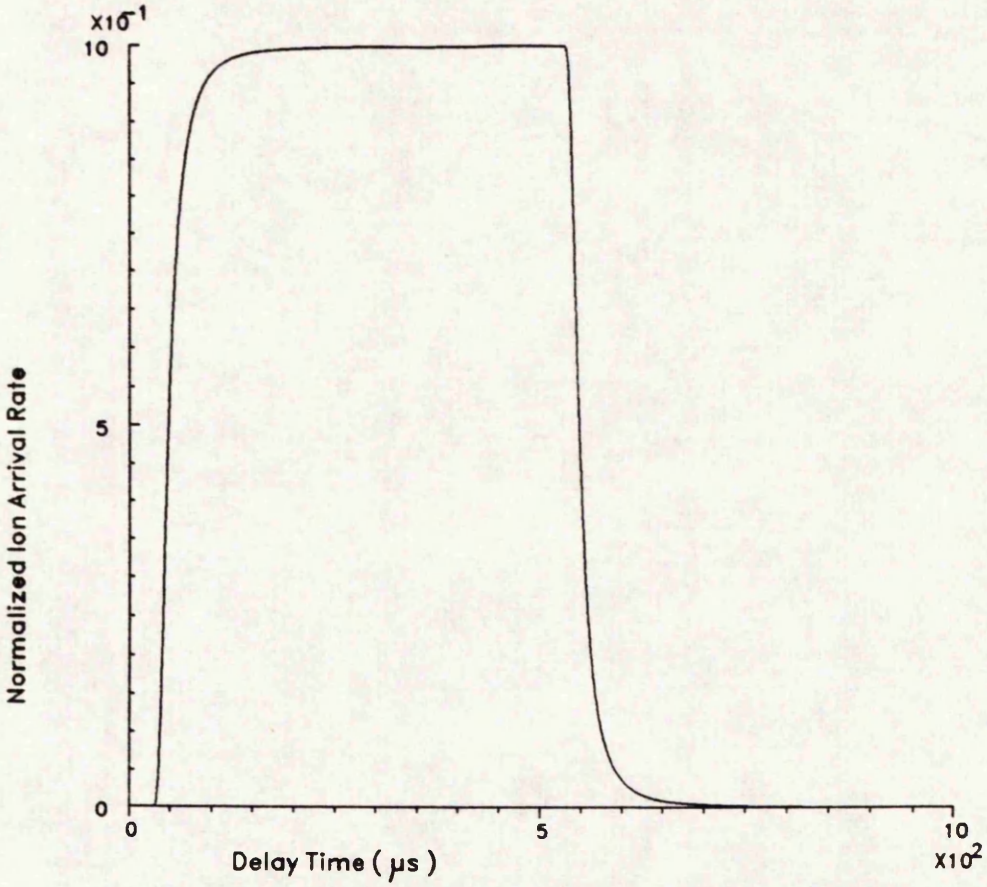

THEORETICAL ION ARRIVAL CURVE FOR SULPHUR (S+) AT A MODULATION FREQUENCY OF 1 KHz AND A TEMPERATURE OF 1000°C

FIGURE 7.4

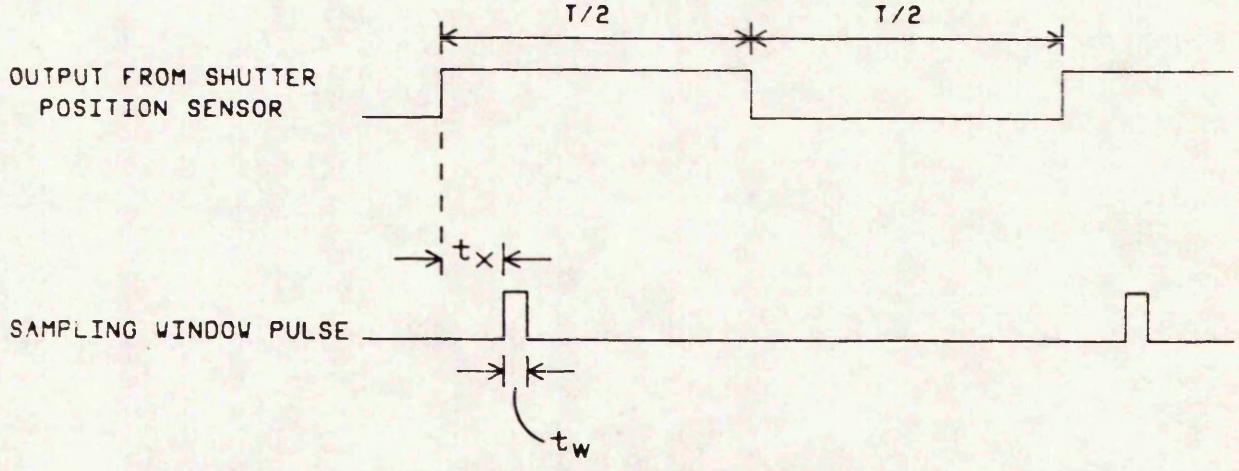

DIAGRAM SHOWING TH SIGNALS USED FOR ION ARRIVAL DATA ACQUISITION USING A TIME WINDOW EQUAL TO 6.4 μs

FIGURE 7.5

the modulation period in increments of 1 μs using the signal from the shutter position detector as a reference. At each setting of the delay a count is accumulated over a large number of window periods to achieve an acceptable signal-to-noise ratio. Typically, for a 6.4 μs window, 1000 window periods are accumulated at a modulation frequency equal to 1018 Hz. The number of window periods used to accumulate pulses at each delay time setting tx is controlled using the steering signal in the counting circuitry. The acquisition time of an ion arrival curve takes in excess of 6 minutes and the variation of flux density as a function of time has been measured and proved to be negligible over a 6 minutes period when the system is in equilibrium. This has been confirmed by other workers [7.6,7.7] using the present MBE apparatus for the evaporation of zinc selenide and zinc sulphide.

Using an accumulation window of 6.4 μs means that the signal representing the ion count is integrated over a short interval. The effect of integration is shown on figure 7.6 where a theoretically calculated curve is used for the Se+ ion showing a shift to the the left on the ion arrival curve proportional to the width of the window. For an experiment carried out using delay steps tx=0.8 μs and with a sampling window of 6.4 μs the arrival curve is shifted to the left by an interval of 5.6 μs. However, the shape of the curve remains virtually unchanged because the integration window is small compared to the modulation period (0.65% for a

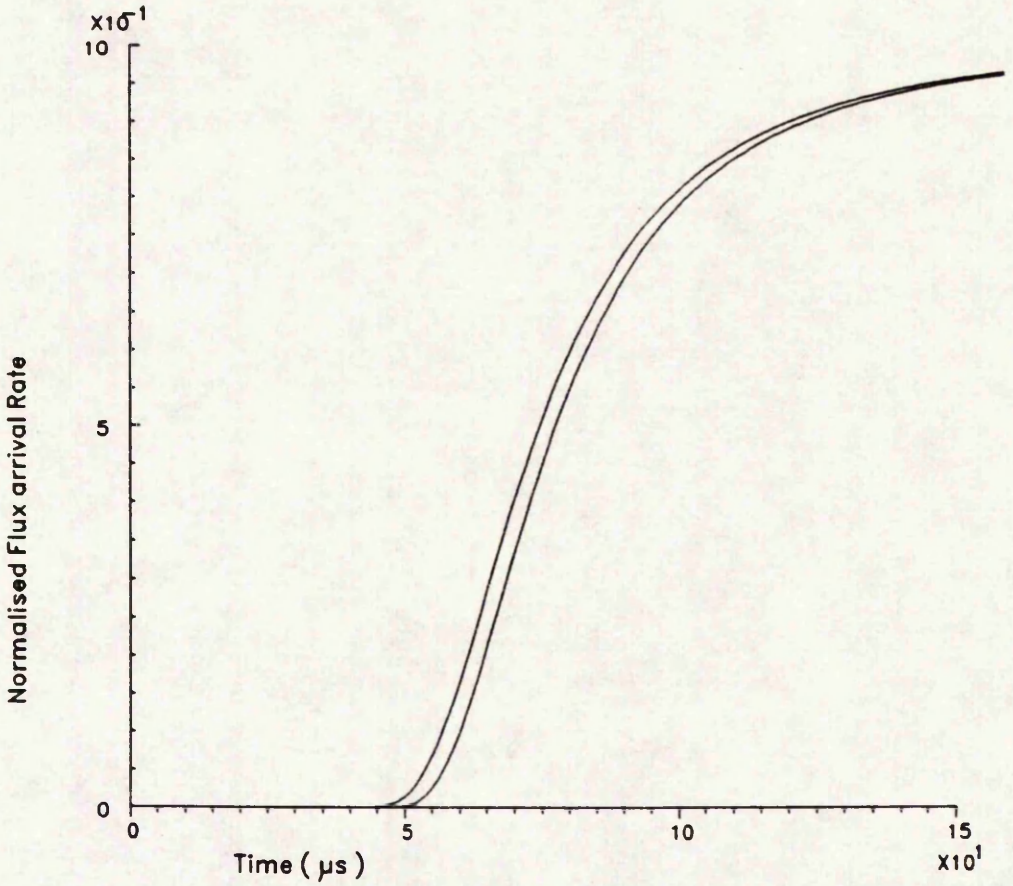

FIGURE SHOWING THE TIME LEAD INDUCED BY THE INTEGRATION OVER A 6.4 μs WINDOW FOR Se+ (a.m.u=80) AT 900 CELSIUS

FIGURE 7.6

modulation frequency of 1018.2 Hz). The time advance introduced depends on the width of the integration window and the effect on the ion arrival curve of a small window integration period can be compensated by removing the time lead from experimentally measured curves.

Figure 7.7 shows an experimentally obtained curve for selenium over a full modulation period. Figure 7.8 shows the curves obtained for the selenium dimeric ion Se_2+ and for the zinc ion Zn+ after opening the shutter. Comparing the results shown in figures 7.7 and 7.8 with the calculated ion arrival curves shows there is good agreement between theory and practice.

The experimentally obtained ion arrival curves exhibit delay times which are close to those calculated theoretically. It is the use of the delay information in these experiments which may help identifying the origin of the particles observed in the mass spectra. By measuring the ion arrival time at 57.2% of the maximum for each curve the ion arrival times for vapour species can be compared.

In the calculated curves it has been assumed the shutter uncovers the beam of particles instantaneously. However this is not the case in practice. The entrance aperture of the mass spectrometer is an 8 by 3 mm horizontal slot [§ figure 4.4] and the ionization chamber being of the cross-beam type, the electron beam ionizes the neutral particles in a direction perpendicular to the passing blade

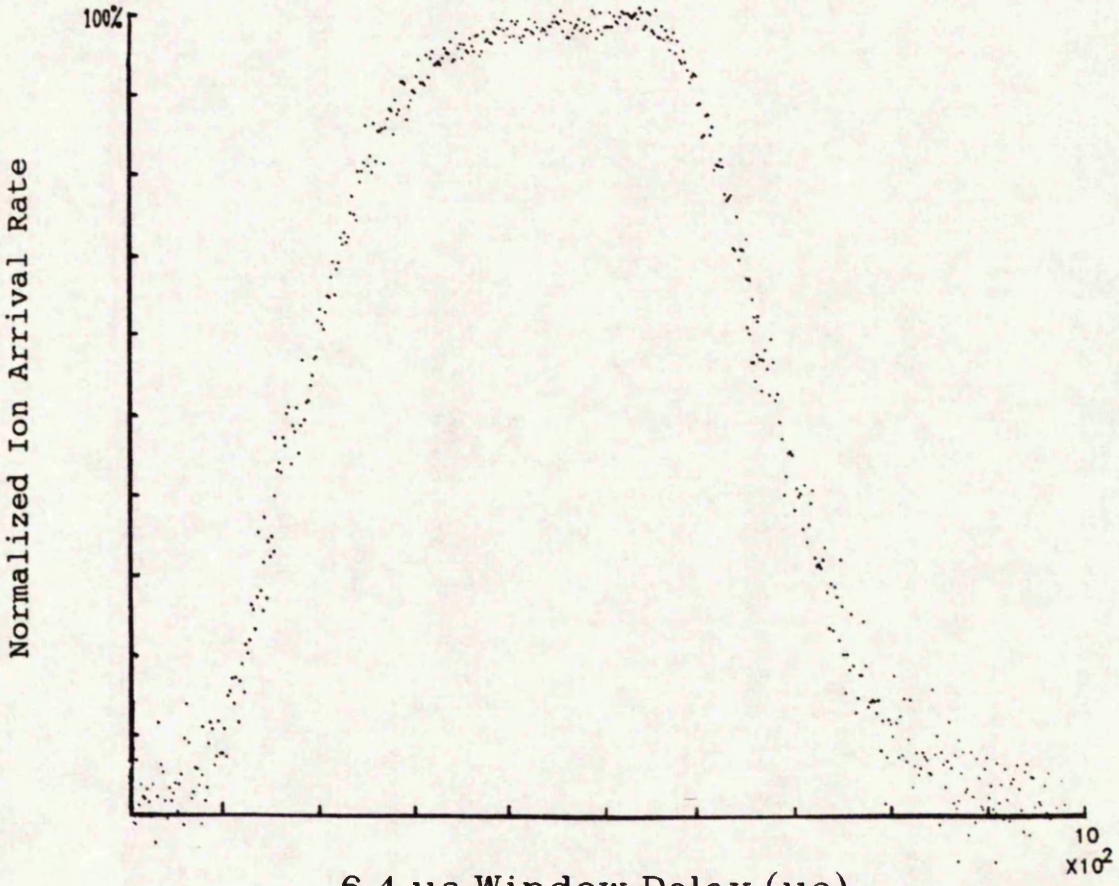

PRACTICAL ION ARRIVAL CURVE OBTAINED FOR Se+ AT A MODULATION FREQUENCY OF 1018.2 Hz, T=900 Celsius.

FIGURE 7.7

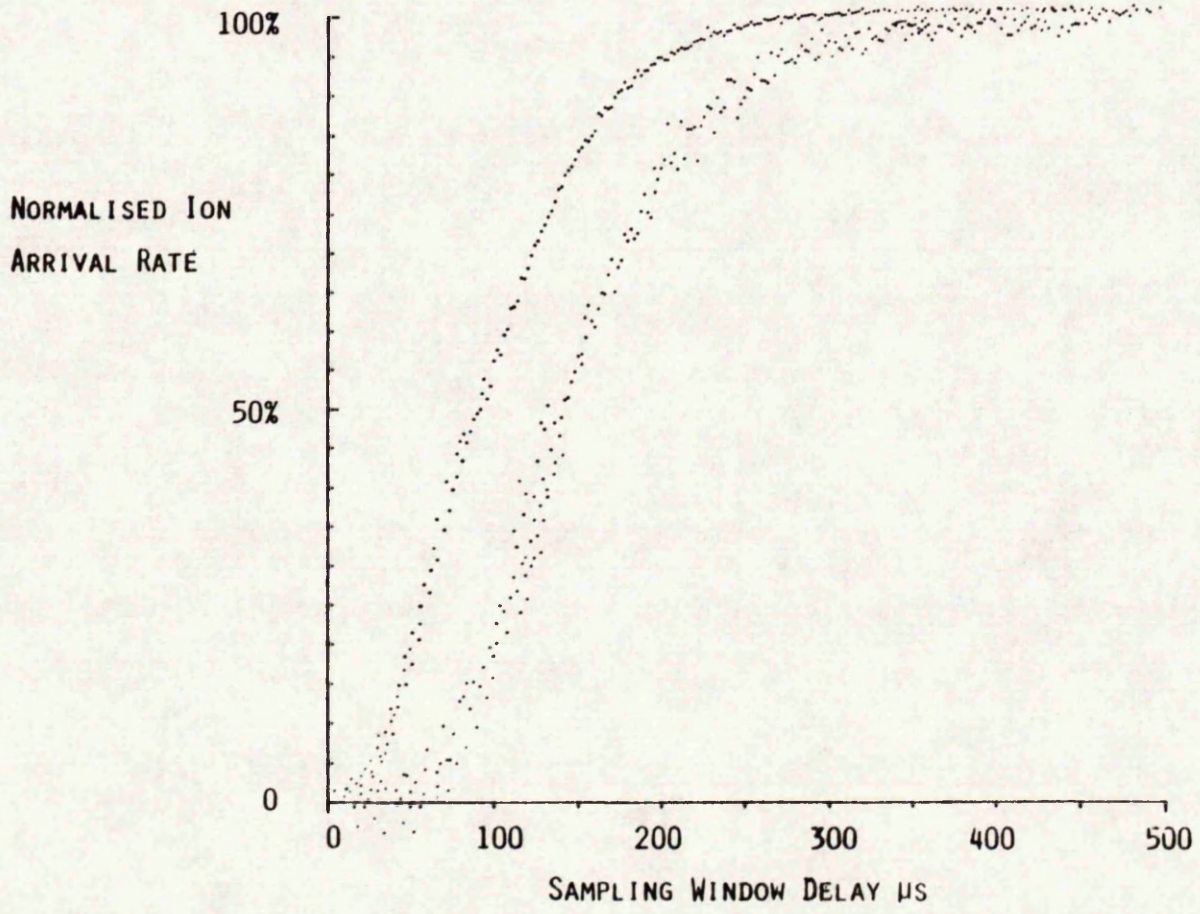

MEASURED ION ARRIVAL CURVES, SAMPLING WINDOW 6.4 µS AND SOURCE TEMPERATURE 900°C

FIGURE 7.8

of the shutter wheel. At the maximum rotation speed of 7800 rpm it takes the shutter 340 μs to uncover the mass spectrometer aperture and this would lead to expecting a considerably longer rise time on the ion arrival curves. A possible explanation of the observed results is that the volume of the ion source supplying ions which pass through the quadrupole filter successfully is very small and therefore the effective entry aperture to the quadrupole filter is considerably less than the aperture calculated from the system geometry.

7.5 AN ALTERNATIVE METHOD FOR ION ARRIVAL TIME MEASUREMENT

Using a small measurement window for TOF analysis helps verify the theoretical characteristics of a chopped beam of particles obeying Maxwell-Boltzmann's theory. A problem will arise with particles having low number densities and since large accumulation times will be required for consistent measurements to be made. Another way of obtaining time of flight information consists of using a window equal to the open period for the shutter. That is Tm/2 where Tm is the particle beam modulation period.

7.5.1 CALCULATION OF RESPONSE TO A LONG SAMPLING WINDOW

It has been demonstrated that after opening the shutter at time t=0 the flux intensity can described by the normalized function f1(t) [§ relationship (7.7)] and after closing the shutter the flux intensity is described by the function 1-f1(t+Tm/2). If f(t) is the function which represents the variation of flux intensity over a full modulation period the following relationship can be written:

$$f(t) = \begin{cases} f1(t) & \text{for } 0 \leqslant t \leqslant Tm/2 \\ 1-f1(t-Tm/2) & \text{for } Tm/2 \leqslant t \leqslant Tm \end{cases} \qquad (7.9)$$

f(t) is a periodic function and its period is Tm. Summing the number densities at a delay time tx for a particular vapour species over a sampling window of width tw us is equivalent to the following integration:

$$F(tx) = \int_{tx}^{tx+tw} f(t)\ dt \qquad (7.10)$$

The integration limits vary according to the time interval to which tx belongs. For tw equal to half the modulation period Tm/2, F(t) becomes:

$$F(tx) = \int_{tx}^{Tm/2} f1(t)\,dt + \int_{Tm/2}^{tx+Tm/2} 1-f(t-Tm/2)\,dt \qquad (7.11)$$

Extrema of F(tx) occur when the derivative with respect to the variable tx is nil.

7.5.2 THEORETICAL INTEGRATED ION ARRIVAL CURVES

Using the theoretical curves for ion arrival, an accumulation window tw=Tm/2 has been used to obtain a curve representing the function F(tx). Figure 7.9 shows the result for Se+ ions with tx varying from 0 to Tm/2. The calculation of F(t) involved the summation of the calculated data over the Tm/2 window at 1 µs intervals one modulation period. The integrated curve is put on the same time axis as the short window ion arrival curve. Examination of the figure shows that it has a maximum occuring when the ion arrival curve is at 50% of its maximum value. An integrated ion arrival curve is shown on figure 7.10 where the full modulation period is covered. The maximum on the integrated curve occurs when the flux density is at 50% of its maximum and the minimum occurs when the flux density is also at 50% of its maximum but after Tm/2

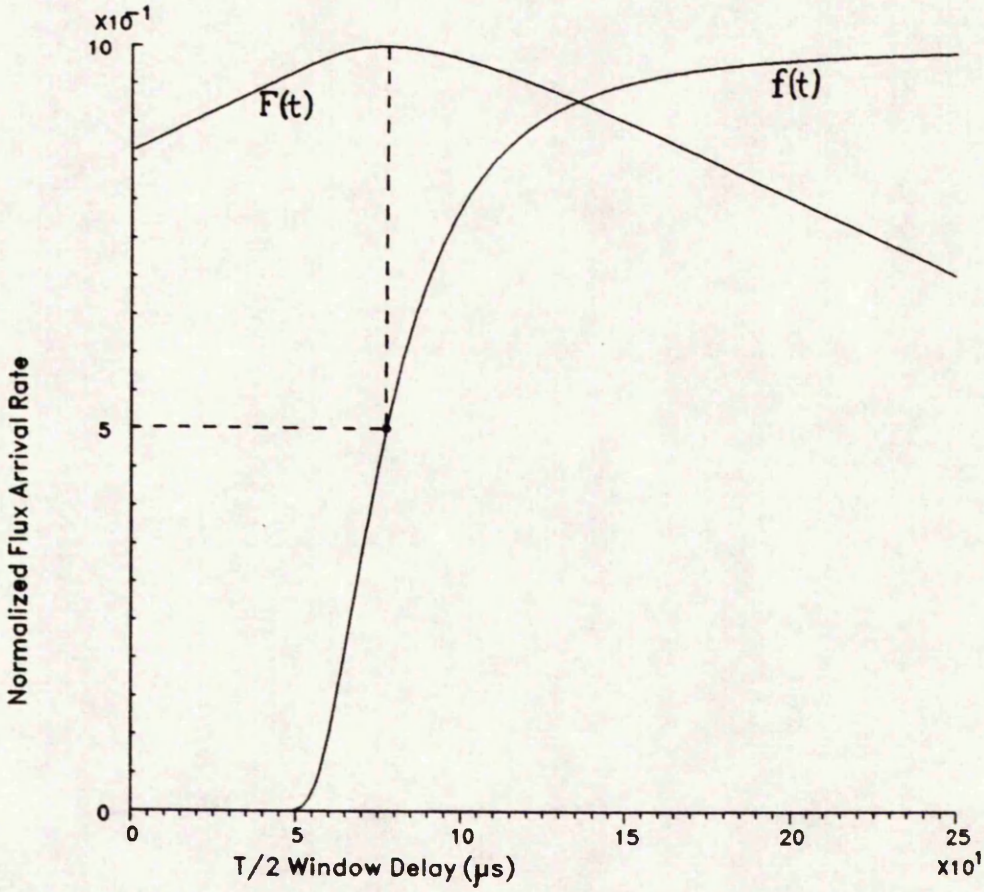

CALCULATED INTEGRATED ION ARRIVAL CURVE FROM THE ION ARRIVAL DATA FOR Se+ AT Fm=1Khz, 900 CELSIUS

FIGURE 7.9

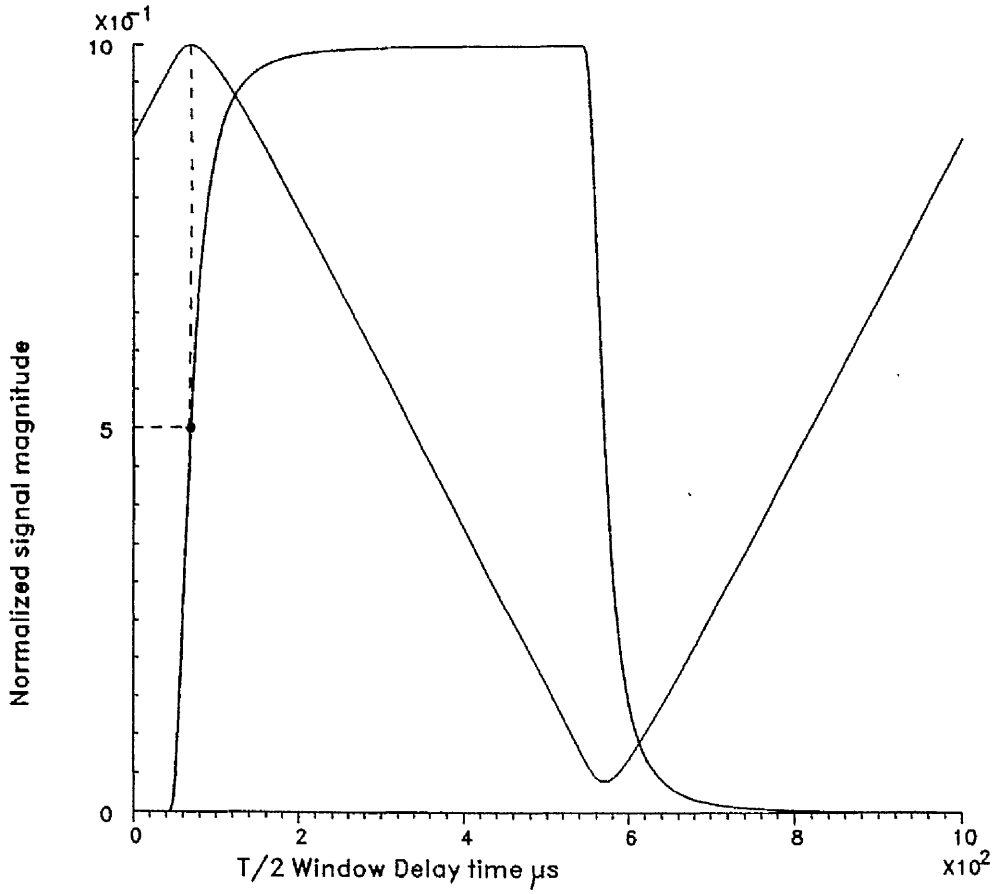

CALCULATED INTEGRATED ION ARRIVAL CURVE FOR Zn+
AT A MODULATION FREQUENCY OF 1 KHz AND 900 CELSIUS

FIGURE 7.10

from the maximum on the integrated curve. Considering a Maxwellian distribution of speeds, the maximum on the integrated ion arrival curves occurs for particles having a speed some 8.8% higher than for those possessing the most probable speed. Figure 7.11 shows two calculated ion arrival curves and the delay time between the maxima is similar to that obtained on the ion arrival curves shown on figure 7.3. This demonstrates that it is possible to differentiate between the particle arrival times by looking for the maxima of the integrated curves.

7.5.3 INTEGRATED EXPERIMENTAL ION ARRIVAL CURVES

7.5.3.1 THEORETICAL INTRODUCTION

The experimental ion arrival curves obtained earlier have been obtained by summing on ion counts accumulated using small adjacent time windows of width tx=6.4 μs. Theoretically, half a modulation period Tm/2 can be considered as the addition of number N small time windows having width tw, with the first window occuring at the delay time tx and therefore :

$$Tm/2 = N\ tw \qquad (7.12)$$

FOR Tm=982 μs and tw=6.4 μs, N=77. The ion arrival data has

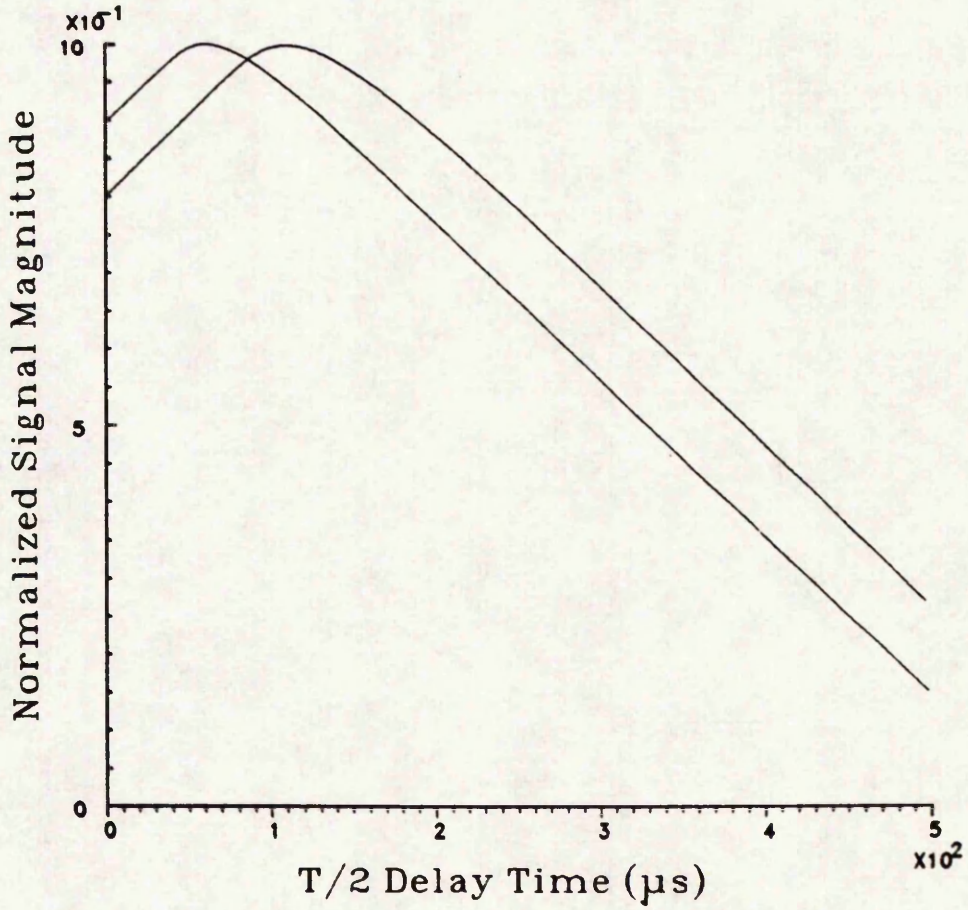

CALCULATED INTEGRATED ION ARRIVAL CURVES USING T/2 WINDOW FOR Zn++ AND Se2+ AT 900 C , Fm=1 Khz

FIGURE 7.11

been recorded for a sample window of 6.4 μs while the window delay time has been incremented in steps of 0.8 μs. If at the delay instant tx, N_{tx} represents the accumulated ion arrival count over the 6.4 μs window and N_{Ftx} represents the count accumulated from the integration of the measured ion arrival data over the period Tm/2 for the N contiguous windows, the following relationship can be written:

$$N_{Ftx} = N_{tx} + N_{tx+nt} + N_{tx+2nt} \ldots + N_{tx+(N-1)nt} \qquad (7.13)$$

and in general:

$$N_{Ftx} = \sum_{t_j = tx}^{t_j = tx + N\ nt} N_{tx + j\ nt} \qquad (7.14)$$

7.5.3.2 INTEGRATED ION ARRIVAL CURVES FROM SMALL WINDOW MEASUREMENTS

The application of the ion arrival curve integration method

to an experimental curve obtained with a 6.4 μs window is shown on figure 7.12. The curve has been obtained through a direct application of relationship (7.14) and can be considered as an integration of the small window measurements through half a modulation period. Figure 7.12 which shows this curve demonstrates the integration effect on the signal obtained using a modulation frequency Fm=812 Hz. A comparison in signal fluctuation between the two curves shows a reduction from 4% to below 0.5%. The curves obtained experimentally can be directly correlated to the theoretical ones.

Another way of representing integrated ion arrival curves is to display the on-beam signal from time t=0 and the off-beam signal from time t-Tm/2 which makes it coincide with t=0 at the start of the experiment. This is a translation of the off-beam data along the time axis equal to -Tm/2. This is shown on figure 7.13 which is drawn using the theoretical data for the ion Se+ (m/e=80). The two curves shown in this figure represent the measurements when the delay time tx is below Tm/2 (on-beam signal recorded) and when tx›Tm/2 (off-beam signal recorded). The intersection between the two curves is Tm/4 after the extrema on the curves which represent the arrival time of the ions defined in section 7.4.2.

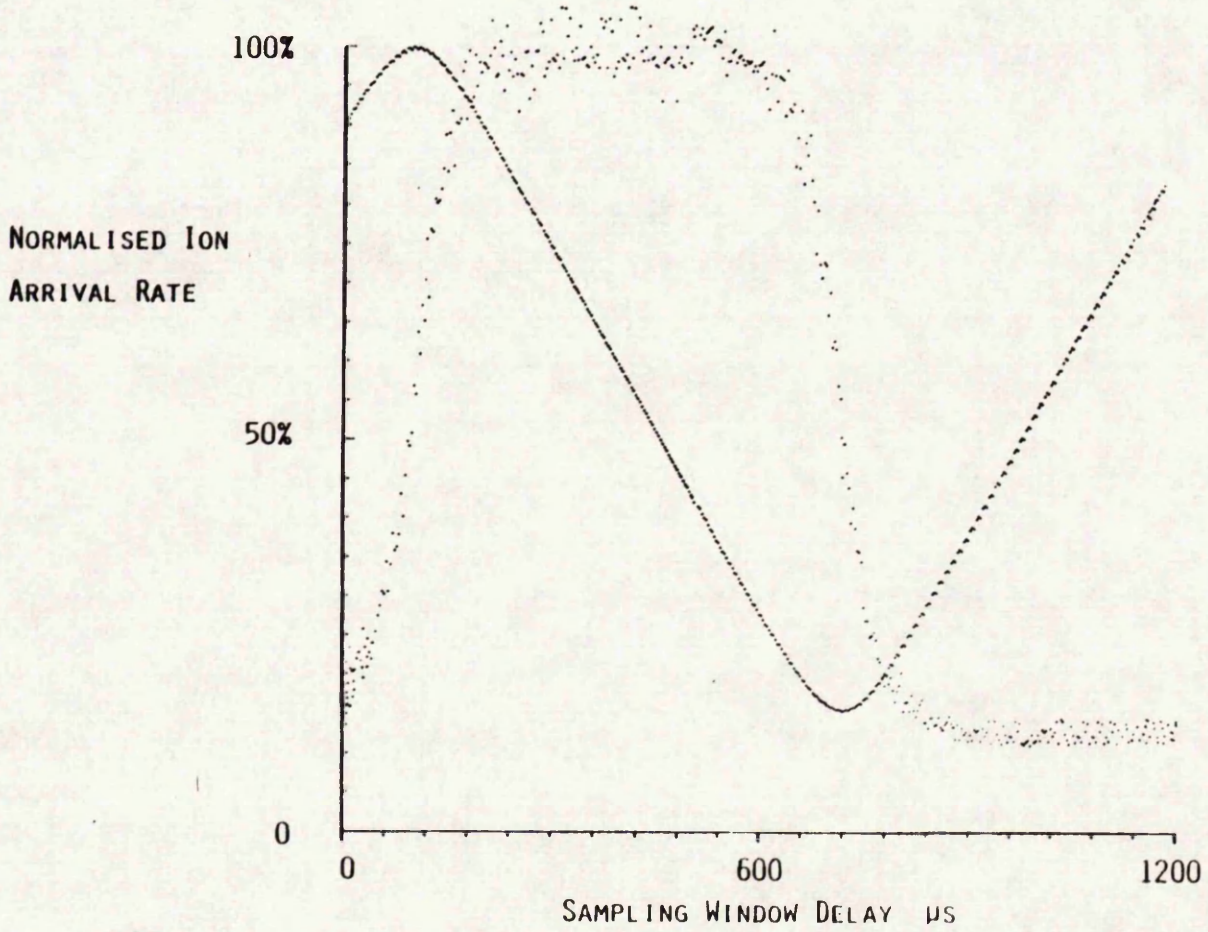

ION ARRIVAL CURVE FOR T/2 WINDOW CALCULATED FROM MEASURED 6.4 μS WINDOW RESULTS
SOURCE TEMPERATURE 925°C AND MEASUREMENTS ON Zn^{++}

FIGURE 7.12

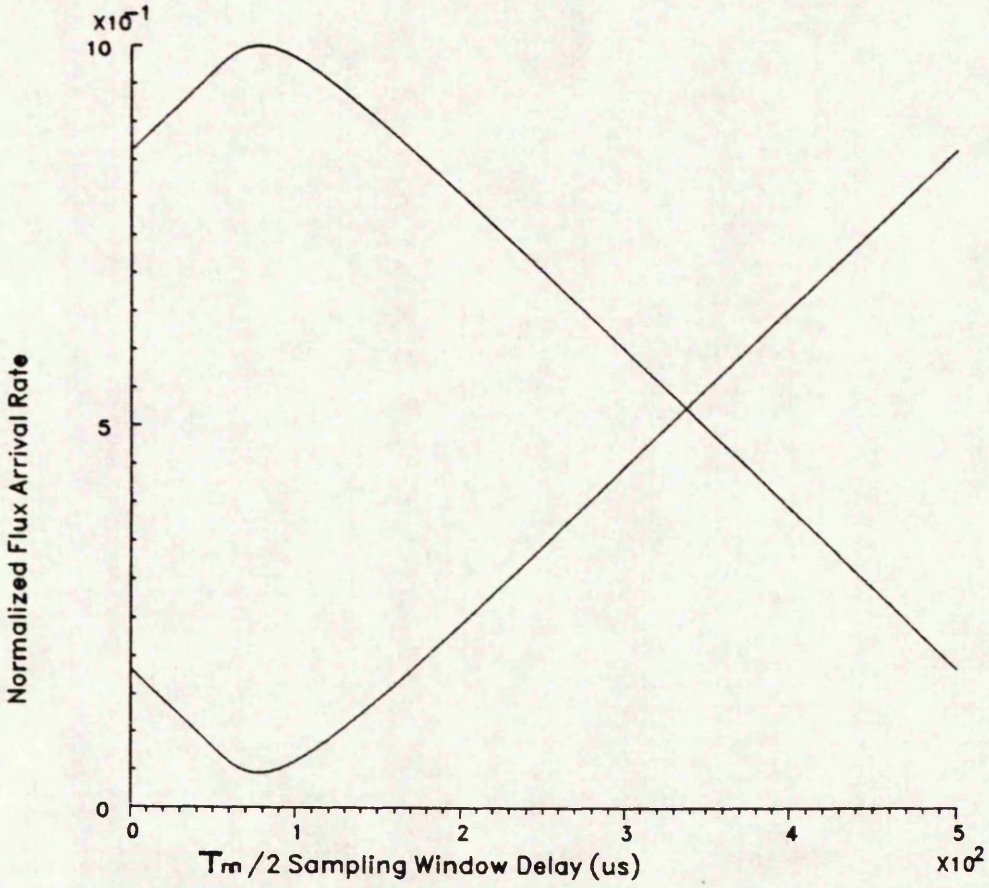

AN ALTERNATIVE REPRESENTATION FOR THE CALCULATED INTEGRATED ION ARRIVAL CURVE FOR Se+ AT Fm=1Khz, 900 CELSIUS

FIGURE 7.13

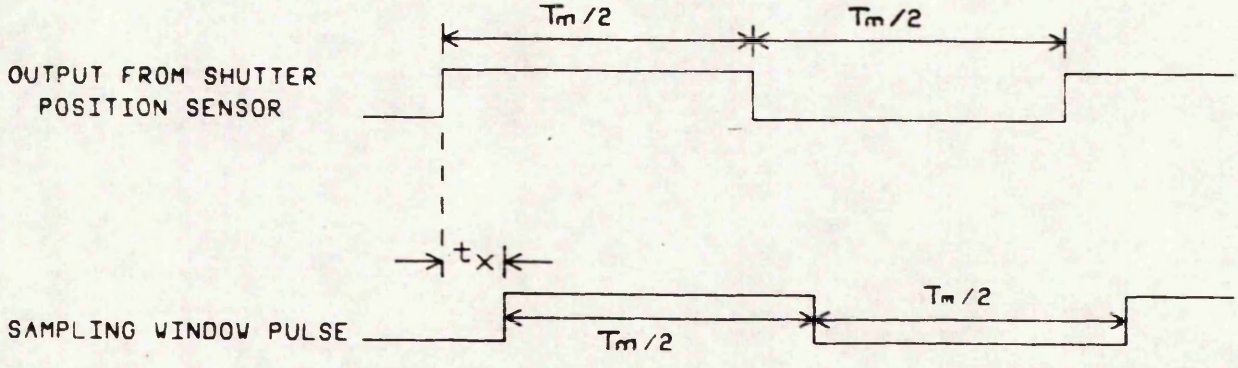

DIAGRAM SHOWING THE SIGNALS USED FOR INTEGRATED ION ARRIVAL DATA ACQUISITION USING A TIME WINDOW EQUAL TO Tm/2

FIGURE 7.14

7.5.3.3 DIRECT ACQUISITION OF INTEGRATED ION ARRIVAL CURVES

The direct acquisition of integrated ion arrival curves consists of accumulating ion pulses from the mass spectrometer over a period tw=Tm/2 where the delay time tx is taken over the whole modulation period as shown on figure 7.14. This method of acquisition reduces substantially the acquisition time from the experiments where the 6.4 μs window is used (at least by a factor of 5 better than using a 6.4 window) and figure 7.15 shows the result obtained for Zn+.

Figure 7.16 shows the results obtained by logging the data from adjacent half period sampling windows for Zn+ (m/e=64) ions and this effectively halves the acquisition time for an ion arrival curve.

The use of the direct integration over Tm/2 indicates that it is feasible to determine the arrival time of the vapour species by looking for the maximum (or minimum) on the experimental ion arrival curve. This is done by using the routines used for finding a peak in mass spectra but with the delay time adjusted automatically instead of the tuning voltage (tuning digital number to the DAC). This, further reduces the experimental acquisition time. Whenever fluctuation around a particular maximum is observed, recording of all the data points in the vicinity of the curve maximum is undertaken with small delay time steps (tx can be as low as 0.2 μs) to obtained the required accuracy.

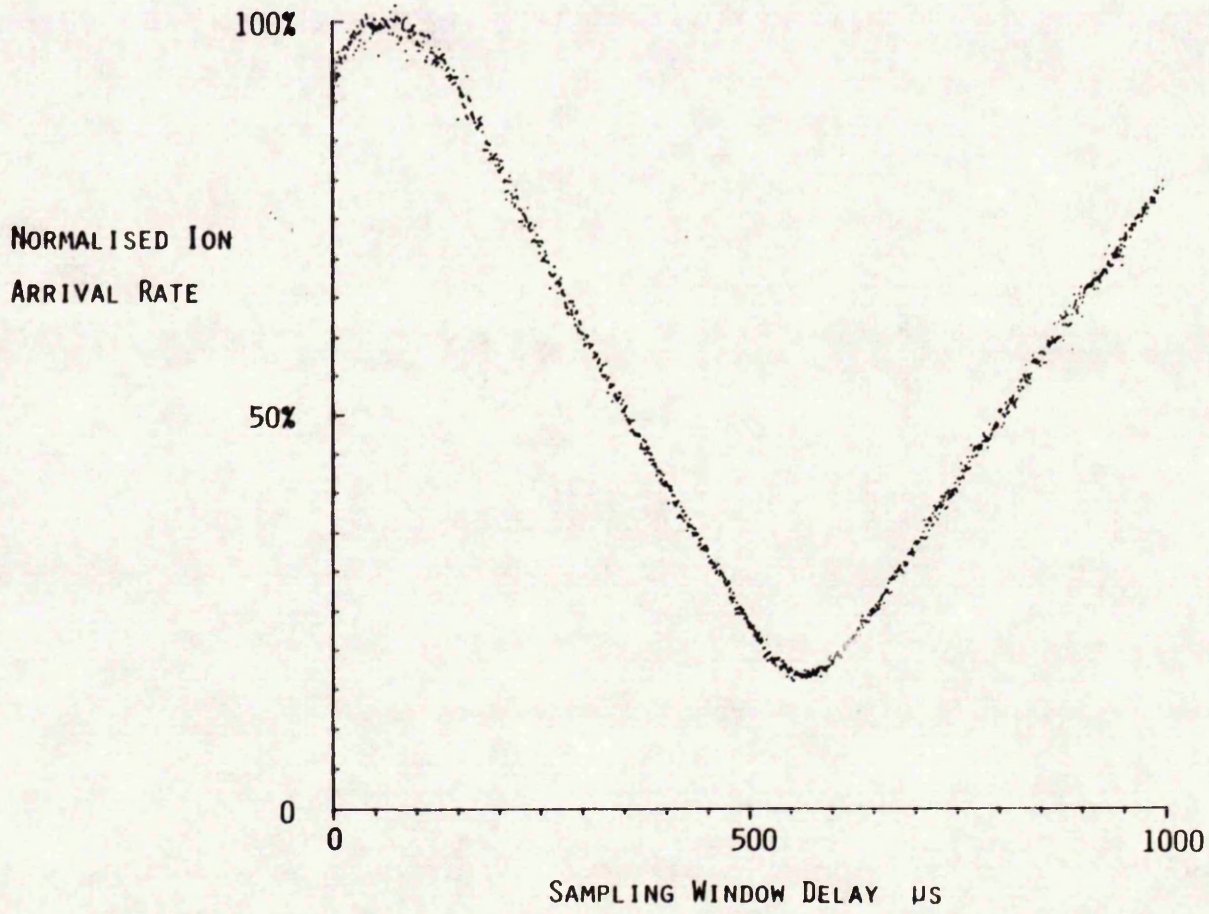

MEASURED ION ARRIVAL CURVES FOR Zn^+, T/2 SAMPLING WINDOW AND SOURCE TEMPERATURE 925°C

FIGURE 7.15

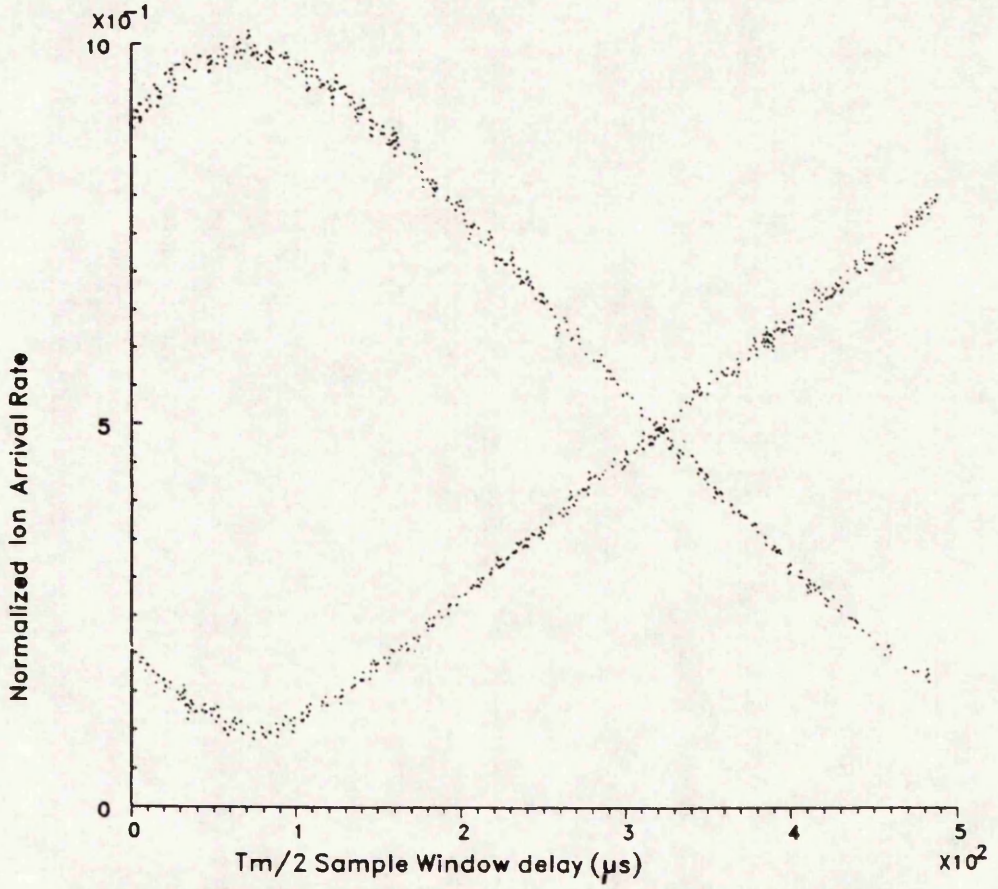

ALTERNATIVE REPRESENTATION FOR THE PRACTICAL INTEGRATED ION ARRIVAL DATA FOR Zn+ AT Fm=1018.2 Hz AND 925 CELSIUS

FIGURE 7.16

In a typical integrated ion arrival experiment 1 microsecond delay steps are implemented near threshhold points and 4 μs steps are used elsewhere. This helps reduce the acquisition time to a minimum without loss of accuracy. For a typical experiment a modulation frequency of 1018.2 Hz is used and a summation of ion pulses made over 1000 count periods. A frequency of 812 Hz has also been used and this yields a total experimental acquisition time of less than 350 seconds.

7.6 USES OF THE TOF INFORMATION

The ion arrival time determination through the use of the integrated ion arrival curves provides a means for optimizing the signal ion count. The background contribution to the ion counts and improvement in the signal-to-noise ratio are obtained in evaporation or deposition experiments by taking measurements on each of the vapour species with a fixed delay equal to its ion arrival time.

The determination of time of flight for the vapour particles can be used to identify the origin of a particular species observed in the mass spectrum. For the present study an accumulation window equal to half the modulation period has been used and measurements of arrival times have been carried out using the integrated ion arrival curves. Ion arrival curves similar to those of figure 7.16 have been

used. They show directly two extrema (a maximum at the ion arrival time and a minimum Tm/2 later) and an intersection point between the on-beam and off-beam curves which occurs at the ion arrival time plus Tm/4. A linear regression to the data in the vicinity of the intersection point on both on-beam and off-beam curves has been undertaken to determine the time delay with greater accuracy at this point. These points shift on the time axis with variation of the mass number as well as the charge of the particle selected. It is this time shift which is exploited to differentiate between the arrival times of the different particles and hence leads to their being identified at a particular mass-to-charge ratio. The integrated ion arrival time experiments have been combined with measurements of the behaviour of selenium and sulfur particles with the variation of the QMS electron energy. Results from chapter 6 are used extensively fof this study.

7.6.1 IDENTIFICATION OF THE SELENIUM PARTICLES IN THE NEUTRAL BEAM

The main particles involved during the evaporation of zinc selenide at 900 °C using ionizing electrons having an energy of 35 eV have been shown in a digital mass spectrum, figure 6.4. Since the present QMS is limited in its range to 200 a.m.u the highest mass peak that can be observed is that for Se_2^+ at mass-to-charge ratio 162. The isotopic

abundancies of the various particles present have also been shown on figure 6.5. The selenium peaks on the spectrum appear mainly around the mass-to-charge ratios 80 for Se+, 160 for Se_2+ with a small peak at mass-to-charge ratio 40 for Se++. The aim here is to determine the nature of the selenium particles which leave the vapour source.

A first approach to the problem dictates the consideration of all possible polymeric forms that selenium particles may take. An initial search for molecules of ZnSe+ at mass-to-charge ratio 144 over the range of temperatures of interest and at various electron energies suggests that there are no molecules of this type in the ionization chamber of the mass spectrometer. Over the range of temperatures from 800 to 950 °C, it is concluded that selenium particles vapourize from ZnSe compound material unbound to the zinc particles. Another conclusion which has been reached from the observations at mass-to-charge ratio 128 is that there are no dimers of zinc.

As for selenium particles a first set of experiments has been carried out at mass-to-charge ratio 160 to determine whether higher polymeric particles of selenium contribute to this peak. The ionization curves of the Se_2 particles described in chapter 6 show that appearance potential for Se_2+ is 12.75 eV. Since the arrival times of the selenium particles are strongly dependent on their mass, the measurement of TOF has been undertaken at 900 °C. The peak chosen is at mass-to-charge

ratio 160 because it is the most abundant isotope. The possibility that selenium tetramers as well as other higher polymeric species may contribute to the peak has been considered. A higher polymeric particle present in the neutral particle beam may fragment inside the ionization chamber of the QMS yielding singly ionized dimers. In this case the contribution of these polymeric vapour species would cause a larger delay time as a result of their passage between the vapour beam modulator and the detector.

Measurement of the ion arrival time at mass-to-charge ratio 160 has been undertaken over a range of electron energies. The range used is from 12.0 eV to 25 eV divided into 0.5 eV intervals and then 2 eV intervals up to 30 eV. The ion arrival times measured have remained constant within experimental error. At 900 °C the theoretically calculated ion arrival time for a Se_2^+ particle is 114 μs and the value obtained experimentally is 117 μs. This suggests that there are no higher polymeric vapour species of selenium in the beam of particles emanating from the ZnSe vapour source. The range of electron energies used could be expected to produce a range of fragments and changes would have been seen in the TOF if this had occurred.

A further set of experiments has been carried out to determine the origin of the selenium particles at mass-to-charge ratio 80. The electron energy range used in this case is from 16 eV to 30 eV in steps of 0.5 eV. The difference in appearance potential between Se_2^+ and

Se+ is 4 eV and TOF experiments carried out at this mass number have shown that the delay time remains constant, which suggests that singly ionized monomers of selenium originate from one type of selenium neutral vapour particle. Moreover, measurement of the ion arrival time shows that it is larger by 20 μs than the theoretically calculated ion arrival time for a neutral selenium monomer which is ionized inside the QMS structure. This is closer to that expected for Se_2+ particles and a total delay time for Se+ of 108 μs has been obtained. The difference between this TOF and that of Se_2 is close to the difference between their times for translation through the QMS mass filter structure. The experimentally obtained difference is 10 us and the calculated value 12 μs. The variation of the ratio of the density of Se_2^+ to Se+ as a function of electron energy has been shown on figure 6.12. The figure suggests that this ratio decreases with increasing electron energy which supports the proposition that Selenium at mass-to-charge ratio 80 originates from the dimeric species.

Therefore, selenium at mass-to-charge ratio 80 is produced by the dissociation of dimeric selenium inside the ionization chamber of the mass spectrometer and the sublimation of zinc selenide yields monomeric zinc and dimeric selenium according to:

$$ZnSe_{(solid)} \longrightarrow Zn_{(gas)} + 1/2\ Se_{2\ (gas)} \qquad (7.15)$$

and this supports the proposition that ZnSe vapourizes congruently.

7.6.2 IDENTIFICATION OF THE SULFUR PARTICLES IN THE NEUTRAL BEAM

A complication inherent in the mass spectrum for ZnS is the overlap of peaks for sulfur and zinc. Moreover, the ion arrival time of both vapour particles at a given mass peak are almost equal. Therefore a further problem to consider in this case is the extraction of the zinc contribution for a particular sulfur species during ion arrival time observations. A combination of the relative isotopic abundancy of these materials as well the difference in appearance potentials between zinc and sulfur particles has been used. From the ionization energy curves of zinc and sulfur particles and the variation of the ratio between S_2+ and S+ described in chapter 6, it has been found that the ratio of the ion count measured for S_2+ over that for S+ decreases with the increase in electron energy and at m/e=32 the appearance potential on the curve in figure 6.14 is that of sulfur. For the ion arrival curves for sulfur to be extracted from a mixture of zinc and sulfur particles, ion arrival time observations have been made at m/e=32,33,64 and 66. At each delay time tx, the amount of zinc at m/e=33 and 66 is used to calculate its number density at m/e=32 and 64. The calculated quantities

are then subtracted from the measured ones at m/e=32 and 64 leaving the contribution of sulfur at these mass-to-charge ratios. When the sulfur content is identified, a process similar to that used on selenium particles is undertaken.

A preliminary search for possible ZnS+ molecules at several electron energies and temperatures failed. Also, a search for possible polymers of sulfur other than S_2 proved unsuccessful. These searches have been carried out at relatively low electron energies (from 0 to 10 eV) since the appearance potentials of S_2+ and Zn+ are equal to 9.75 eV. This suggested ZnS molecules are not present in vapour beam or if they do exist they may undergo dissociation before their exit from the vapour source.

To demonstrate the origin of S_2+ particles observed on a ZnS mass spectrum (figure6.16), the appearance potential of the sulfur dimer is used. The ionization energy has been measured and found equal to 9.75 eV. A study using a range of energies from 9 eV to 20 eV shows that the TOF for sulfur remains constant and equal to 70 us at a source temperature of 1000 °C. This suggests that S_2+ originates from the neutral S_2 dimers and that the particles arriving at the QMS from the evaporant stream modulator do not contain higher order polymers.

A series of TOF experiments has been carried out on monomeric Sulfur. The appearance potential measurements on S+ have shown that S+ appears at a potential of 12.75 eV making it distinct from Zn++ with an appearance potential of 18.75 eV. The TOF of S+ particles has been measured with electron energy settings from 13 eV to 22 eV in steps of 0.5 eV and at higher electron energies in steps varying from 1 to 5 eV till 70 eV. The times measured reflected a similar situation to that encountered with selenium Se+. The TOF measured is 64 μs which is equal, within the bounds of experimental error, to that of S_2 neutral particles which undergo dissociation inside the ionization chamber of the mass spectrometer. When the electron energy level is below the appearance potential of Zn++ the TOF of S+ can be measured directly but at higher electron energies use of zinc isotope at mass-to-charge ratio 33 is necessary to separate the particle species. Figure 7.2 shows the theoretical TOF for the zinc and sulfur particles and helps conclude that sulfur does not enter the mass spectrometer ionization chamber as a monomer. By combining the results observed on S_2+ and S+ it can infer that only dimeric sulfur is present in the particle beam entering the mass spectrometer. This is also supported by the variation of the ratio between the ion counts on S_2+ and S+ with the electron energy (figure 6.19). And hence, the vapourization of zinc sulphide compounds in the range of temperatures used (850 to 1000 °C) occurs according to:

$$ZnS_{(solid)} \longrightarrow Zn_{(gas)} + 1/2\ S_{2\ (gas)} \qquad (7.16)$$

7.7 CONCLUSION

Modulated beam mass spectrometry has been applied to investigate the neutral particles involved in the vapourization of zinc sulphide and zinc selenide. It has been shown that the time-of-flight of the vapour species can be measured with the apparatus developed. Success in the measurement of the particle time of flight infer that only a small volume of the area in the ionization chamber supplying ions to the quadrupole filter is used and therefore it is concluded that the effective aperture is smaller than the physical one. Two methods for the measurement of the ion arrival time have been described. The first method which relies on the direct observation of the flux profile upon opening the shutter has been used to provide the second method which provides a simpler and quicker means for the measurement of the ion arrival time. The methods described have been applied to the vapour species occuring during the evaporation of ZnS and ZnSe. The results are also presented in a paper to be published [7.8] and conclude that ZnS and ZnSe evaporation leads to monomers of zinc and dimers of sulfur or selenium. The use

of the zinc isotopic abundancy ratios have been found effective in extracting the sulfur content during the analysis of the ion arrival time curves. The methods described for ion arrival time measurements can equally be applied to the evaporation of other compound materials which can be brought under mass spectrometric study.

7.8 REFERENCES

[7.1] M.BENYEZZAR
MSc Thesis, University Of Manchester (1986)

[7.2] R.H.JONES
PhD Thesis, A.E.C Report L.B.L 104, (1971)

[7.3] R.F.C.FARROW
J. Phys. D : Appl. Phys., Vol.7 p.2436 (1974)

[7.4] A.E.HOLME, W.J.THATCHER AND J.H.LECK
J. Phys. E : Sci. Instrum. Vol.5 p.429 (1974)

[7.5] C.T.FOXON, B.A.JOYCE, R.F.C.FARROW AND R.M.GRIFFITH
J. Phys. D : Appl. Phys., Vol.7 p.2422 (1974)

[7.6] A.S.SAHIN
PhD Thesis, University Of Manchester (1983)

[7.7] R.P.GREGORY
PhD Thesis University Of Manchester (1988)

[7.8] M.BENYEZZAR, D.KING, P.L.JONES AND D.MOORE
Proc. 2nd European Vac. Conf. (May 1990)
(To Be Published in Il Vuoto. Paper included at end of thesis)

CHAPTER 8

SUBLIMATION OF ZnS AND ZnSe COMPOUNDS

8.1 INTRODUCTION

A study of the evaporation characteristics of ZnSe and ZnS has been undertaken. The behaviour of these compounds with the sublimation temperature has been investigated using modulated beam mass spectrometry. Most ions occuring at particular mass-to-charge ratios in the mass spectra obtained during the evaporation process have been monitored. Mass spectra obtained during the evaporation of ZnSe and ZnS (figures 6.4 and 6.13 respectively) show that the major peaks monitored during the evaporation of ZnSe at an electron energy setting of 35 eV are Zn+ and Se+ and for ZnS the major peaks occur at mass-to-charge ratios number 32 and 64 at an electron energy of 70 eV and in this case monitoring of the number density at mass-to-charge ratio 33 and 66 is necessary to separate zinc from sulfur. However, measurements have also been made for Se_2+ and Zn++. The effect of the background vapours on the kinetics of the

ZnS and ZnSe compounds has been studied and in particular their effect on the measurement of the sublimation enthalpy for the compounds has been demonstrated.

Substraction of the measured ion counts when the rotating shutter is closed from those made when the shutter is open reduces the signal noise content and removes the contribution from the particles in the background to the measured number densities. The extraction of ion counts for particles in the vapour stream is shown to yield simple methods for monitoring particles leaving the ZnS and ZnSe vapour sources. The results presented in this chapter have been obtained using a modulation frequency equal to 122.2 Hz. Accumulation of the counts is carried out over 200 cycles of the modulation period so that the counts measured are acquired over 0.818 second. Other system presets used in the experiments include a filament emission current of 2 mA, an electron energy of 70 eV on the QMS and a total system background pressure not exceeding 10^{-8} torr.

8.2 TOTAL DEPOSITION RATE AND ABSOLUTE SOURCE TEMPERATURE

The variation of deposition rate with absolute source temperature has been investigated for ZnSe and ZnS. The quartz crystal microbalance is used as the deposition rate monitor and with temperature and amount of heat supplied to

the vapour cells determined using the temperature controller electronics. Since the amount of material deposited onto the water cooled surface of the quartz plate is a fraction of the total amount of material evaporating from each cell, it may be assumed that the deposition rate can be directly related to the total vapour pressure. Figure 8.1 shows this variation for both compounds measured in separate experiments. The curves show that ZnS requires a higher temperature for a given deposition rate when compared with ZnSe. This suggests that ZnS requires a higher energy for sublimation than ZnSe.

Relating the deposition rate to the source temperature as in equation (2.6) [§ chapter 2] requires the determination of the constants A, B and C. The mass m of material striking unit area per second can be related to the total pressure p according to Langmuir's relationship :

$$m = p\,(2\,\Pi\,R\,T/M)^{-1/2} \qquad (8.1)$$

where M is the particle mass, R the gas constant and T the absolute temperature [8.1]. Hence if Dm is the deposition rate then:

$$\mathrm{Log}(Dm) + 1/2\ \mathrm{Log}(T) = \mathrm{Log}(p) - 1/2.\mathrm{Log}(2\,\Pi\,R/M) \qquad (8.2)$$

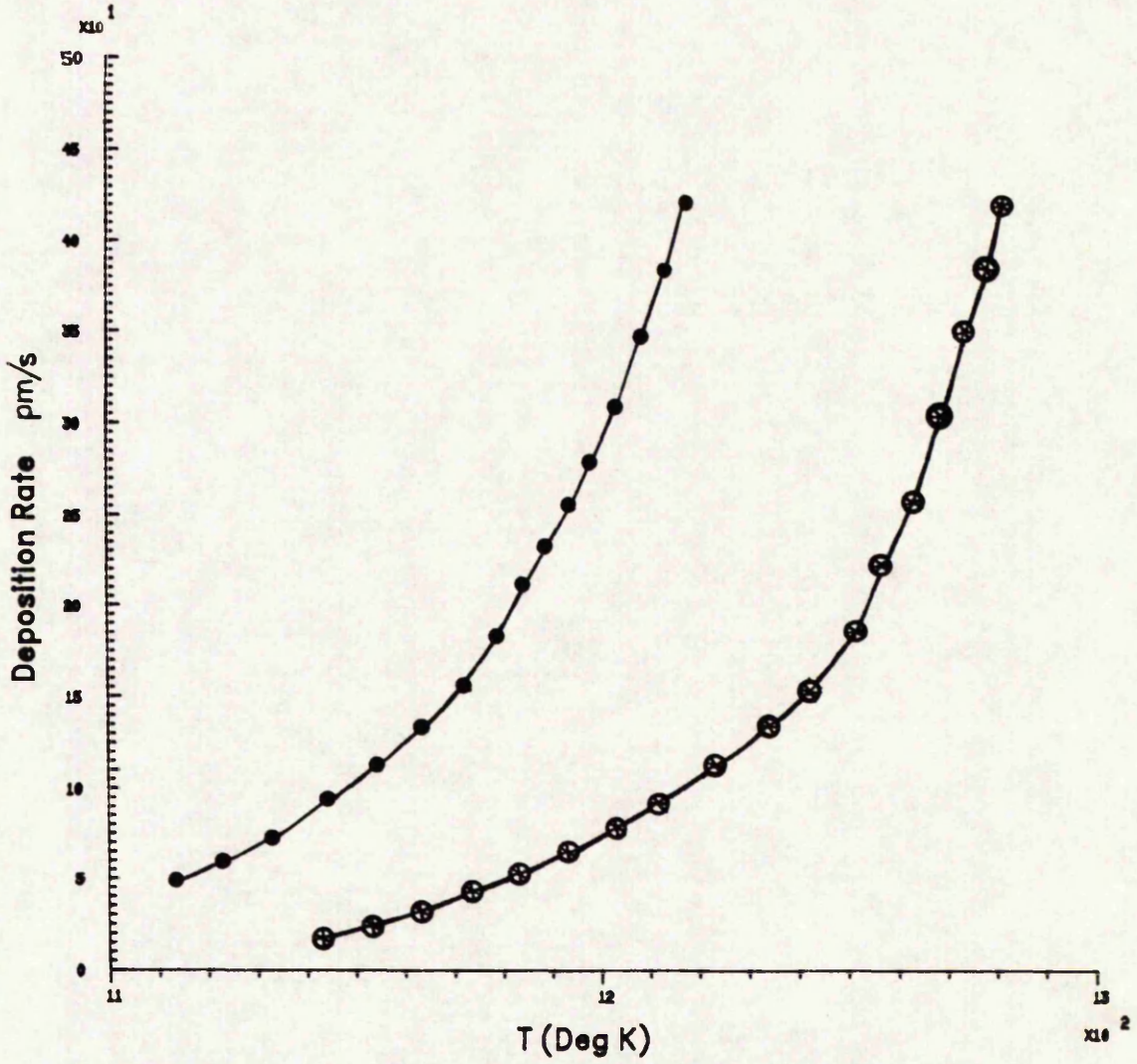

VARIATION OF THE DEPOSITION RATE WITH THE ABSOLUTE TEMPERATURE FOR ZnS (◉) AND ZnSe (●).

FIGURE 8.1

Measurements made by Korneeva et al [8.2] show that the total vapour pressure p of the vapour constituents is related to the absolute temperature according to:

$$\mathrm{Log}(p) = A - B/T \qquad (8.3)$$

Relationships (8.2) and (8.3) yield after substitution:

$$\mathrm{Log}(Dm) + 1/2\ \mathrm{Log}(T) = A - B/T \qquad (8.4)$$

When measuring the deposition rate Dm of the vapourized material onto a cooled surface it is assumed that the condensation coefficient for the vapour hitting the surface is constant and the spatial distribution of evaporant material from the source is not dependent upon the rate of effusion.

Hence it can be seen from equation (8.4) that C = -1/2. The constant A takes into account the fraction of the emitted vapour hitting the surface and this depends on the geometry of the system and the vapour emission characteristics of the source. B is the slope of the curve Log(p) = f(1/T) and is characteristic of the kinetics for evaporation of the substance under investigation. Figure 8.2 shows the variation of Log(Dm) + 1/2 Log(T) as a function of the inverse of temperature for ZnS and ZnSe. The curves' constants A and B are determined from a least

squares regression to a straight line. The resulting empirical equations for ZnS and ZnSe, showing the relationship between vapour cell temperature and deposition rate, are as follows:

For ZnS:

$$\text{Log}(Dm) + 1/2\ \text{Log}(T) = -15655/T + 36.11 \qquad (8.5)$$

For ZnSe:

$$\text{Log}(Dm) + 1/2\ \text{Log}(T) = -14484/T + 35.54 \qquad (8.6)$$

Tabulated in figure 8.3 is a comparison between the published values for the constant B for both ZnS and ZnSe and those from the present work. The values obtained in this work are higher than the values obtained by other authors who have used the present vacuum system (5.3% higher than the value obtained by Cooper et al [8.3] on ZnSe and 9.1% higher than obtained by Gregory et al [8.4] on ZnS). The difference may be due to the fact that the geometry of the system has been affected as well as to the extensive averaging undertaken on the deposition rate measurement in the present work. The value for ZnSe is close to that published by Korneeva (within 1.9%) and on ZnS the value is within 7.9% of that given by Mc Cabe [8.5]. The range of temperatures used (1060 to 1220°K on ZnSe and 1020 to 1260 °K on ZnS) is different from that described by other

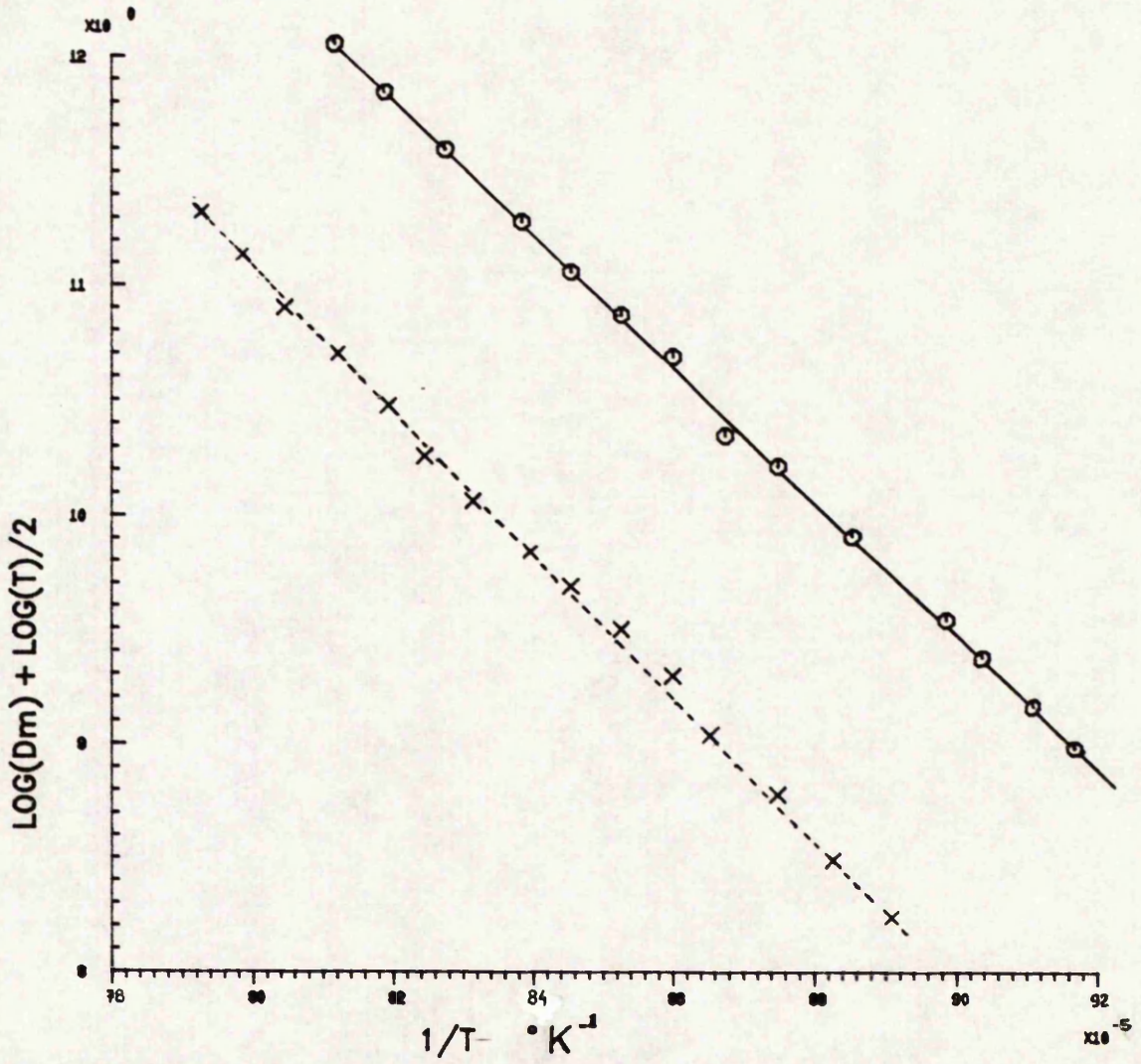

GRAPH OF LOG(Dm)+(LOG(T))/2 vs THE RECIPROCAL OF ABSOLUTE TEMPERATURE FOR ZnS (+)AND ZnSe (⊙).

FIGURE 8.2

COMPOUND	ZnSe			ZnS		
AUTHORS	KORNEEVA Et Al	COOPER Et Al	PRESENT WORK	Mc CABE	GREGORY Et Al	PRESENT WORK
SLOPE -B	14,202	13,715	14,484	14,405	14,222	15,655

TABLE SHOWING A COMPARISON BETWEEN THE EMPIRICAL VALUES OF THE SLOPE B FROM DIFFERENT AUTHORS AND METHODS .

FIGURE 8.3

authors.

The value for the geometry factor A is nearly constant when measured on both materials (1.5% difference) and this may suggest that the spatial pattern of vapour evolution is almost identical the two separate vapour sources.

8.3 VAPOUR SPECIES NUMBER DENSITY VERSUS ABSOLUTE TEMPERATURE

Measurement of the individual vapour species number density with varying source temperature has been undertaken on ZnSe and ZnS. Figure 8.4 shows the variation of the ion count for selenium Se_2+ and zinc Zn+ as a function of the absolute source temperature. Similar variations have also been observed during ZnS evaporation for zinc Zn+ and sulfur S_2+ ions and these are shown on figure 8.5. The behaviour of the particle densities show close agreement with that predicted from the variation of the total deposition rate with the source temperature. Figures 8.4 and 8.5 have been obtained by allowing the source temperature to converge to a preset value using the temperature controller followed by measurement of number densities.

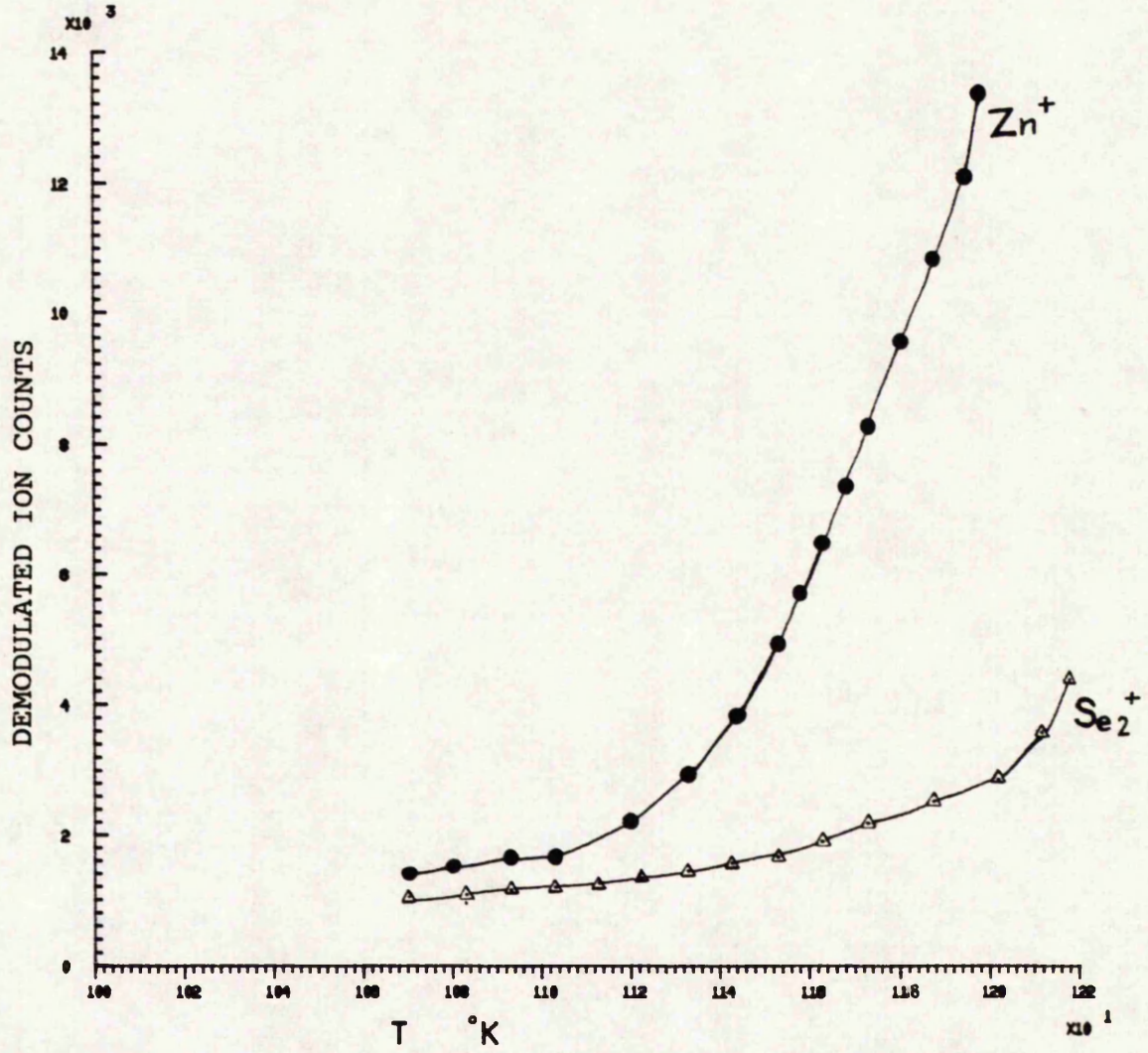

GRAPH OF Se2+ AND Zn + MEASURED NUMBER DENSITIES vs THE ABSOLUTE TEMPERATURE OF THE SOURCE

FIGURE 8.4

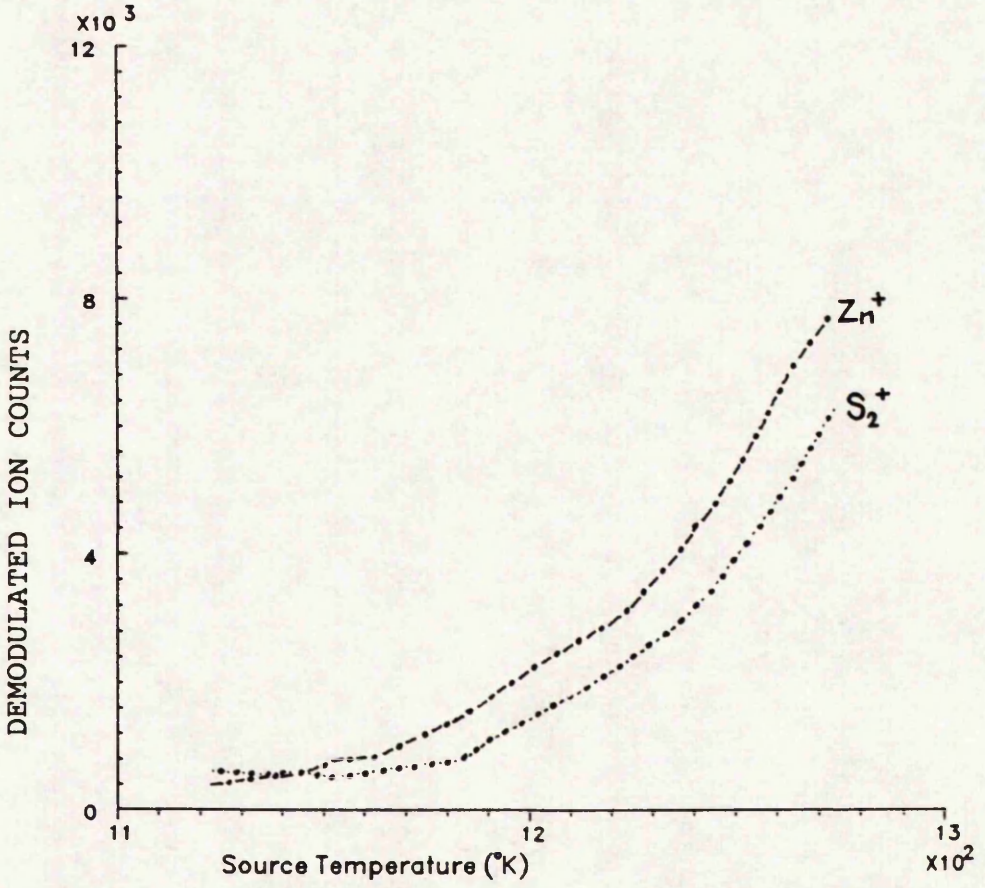

VARIATION OF S2+ AND Zn+ ION COUNTS (m/e=64) WITH THE ABSOLUTE SOURCE TEMPERATURE (MEASUREMENTS MADE USING EQUILIBRIUM SOURCE TEMPERATURES)

FIGURE 8.5

Since the data acquisition time in the present system is relatively short it allows rapid measurements of number densities. Because both temperature measurement and flux measurement can be carried out simultaneously, a dynamic measurement on the variation of abundancy at selected mass-to-charge ratios have been undertaken. Temperature samples are taken every 5 seconds and an average temperature reading is taken every 6 samples or 30 seconds [§ section 4.4.2]. The 30 second temperature reading has been associated with a measured number density. This has been done by programming the temperature controller to converge slowly to a high temperature set-point and while the temperature is rising measurements of the density for zinc and sulfur are undertaken. The delay between the 30 second temperature measurement and number density reading is less than 0.5 second. Since both quantities are controlled with two separate computers the measurements are made as close in time as possible removing problems which may occur from delays induced by computer and instrumentation wait states.

Figure 8.6 shows the measurements obtained during the evaporation of ZnS. The count on S_2^+ is lower than that for Zn+ because a higher electron energy has been used leading to more sulfur dimers getting dissociated. The results show that the curves obtained are similar to those obtained by converging to particular temperature set-points and then measuring the particle number densities. However, the time taken in the dynamic experiment is much shorter

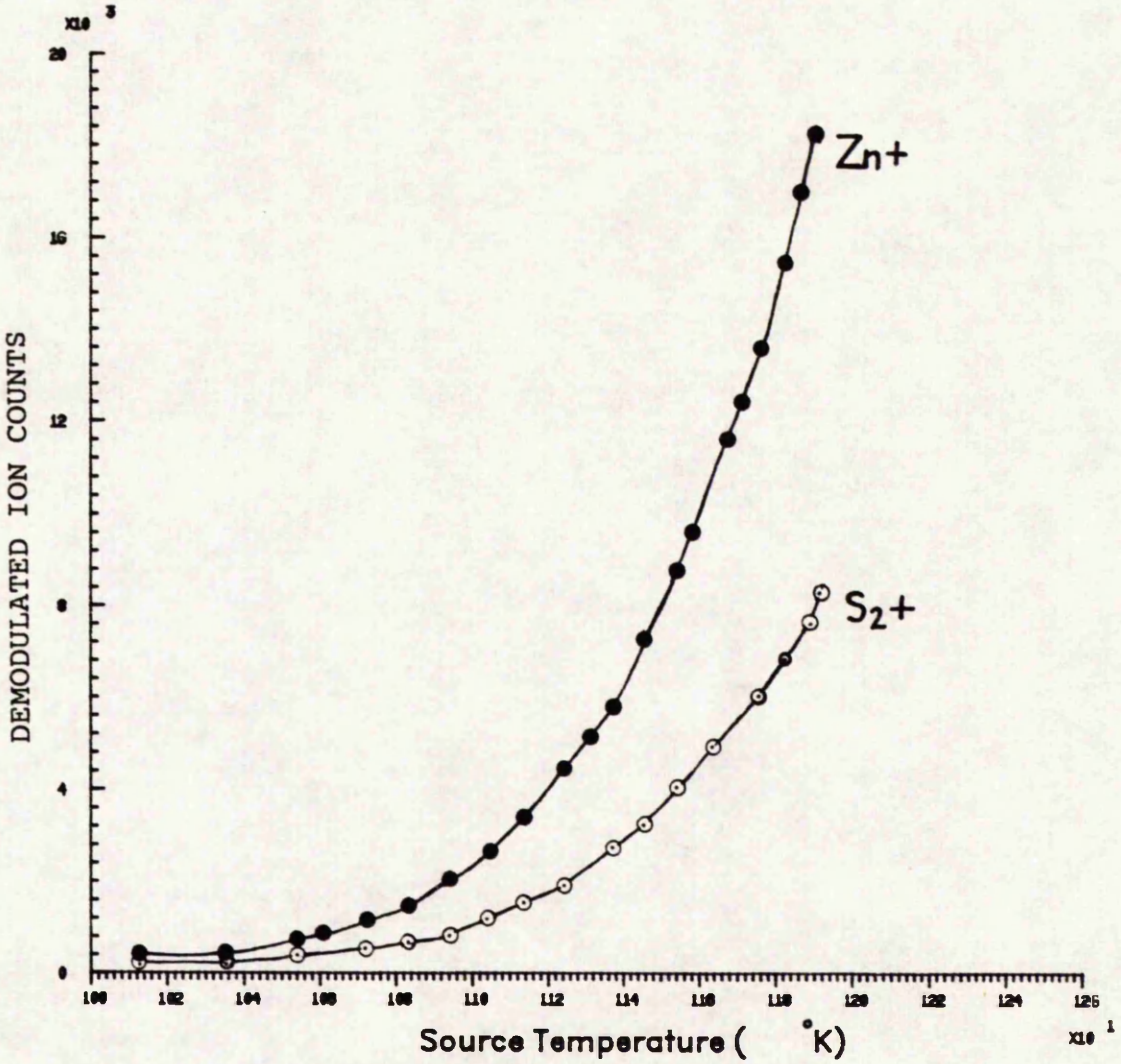

VARIATION OF THE INTENSITY OF Zn+ AND S2+ NUMBER DENSITY AS A FUNCTION OF THE ABSOLUTE SOURCE TEMPERATURE

FIGURE 8.6

than that obtained by using equilibrium temperatures. For a typical dynamic experiment the time taken is equal to that required for convergence of the controller to a high temperature set-point (10 minutes). Using equilibrium conditions up to 10 minutes elapse for each point taken and this consumes considerable time for a complete curve.

8.4 TOTAL DEPOSITION RATE AND INDIVIDUAL VAPOUR SPECIES NUMBER DENSITY

The variation of number density for vapour species with deposition rate has been measured. The variation is recorded by allowing the vapour source to reach equilibrium temperature set-points before taking measurements deposition rate and number density. The results obtained for Zn+ and Se+ are shown in figures 8.7 and 8.8. These exhibit a linear relationship between the demodulated number densities and deposition rate. The relationship between number density and deposition rate is closer to a linearity on the demodulated curve than on the curve representing the total number density. The background contribution to the observed number densities are similar for Zn+ and Se+ although Zn+ has a larger ion count than Se+ which may be due mainly to a fall in the QMS sensitivity as the mass-to-charge ratio rises. Further observations have been made during the evaporation of ZnS and figure 8.9 shows the variation of S_2+ ion count with the deposition rate.

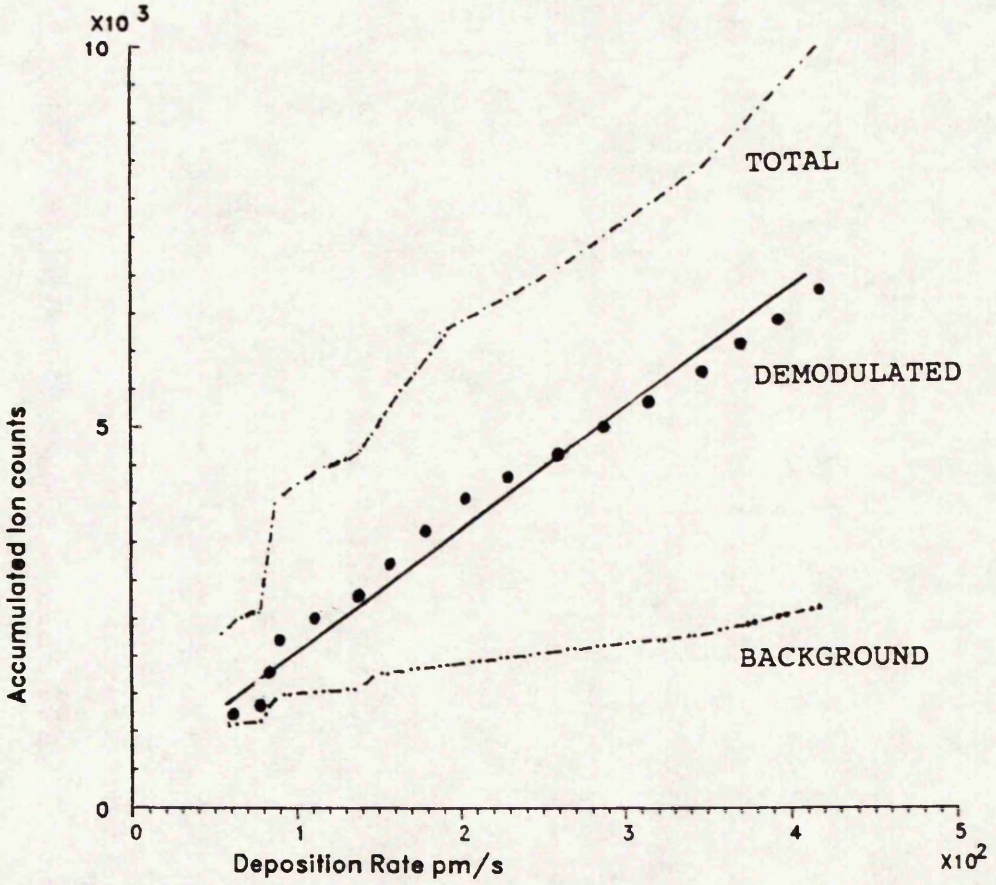

VARIATION OF Zn+ (m/e=64) ION COUNTS WITH THE TOTAL DEPOSITION RATE

FIGURE 8.7

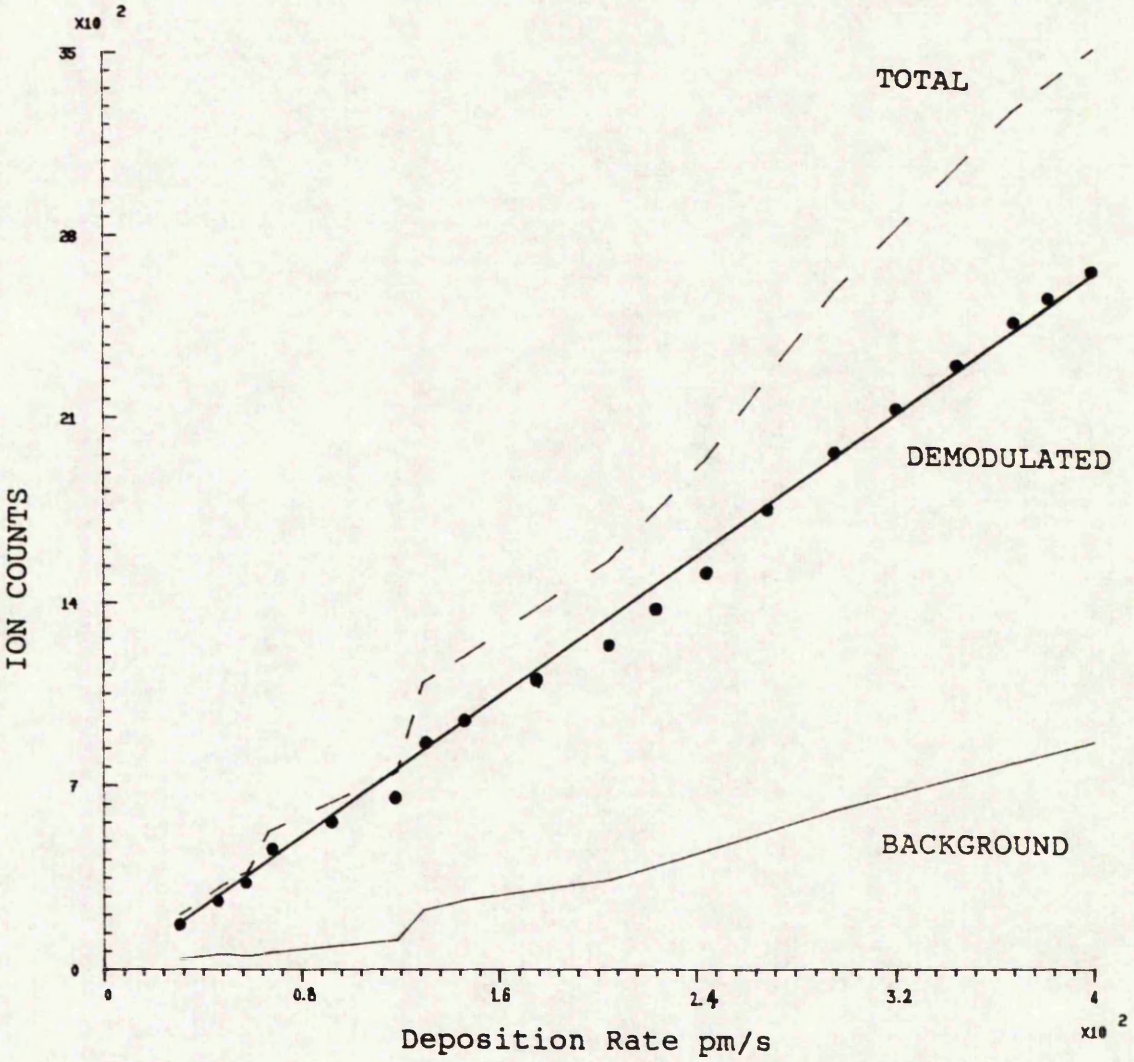

VARIATION OF Se^{+}(m/e=78) ION COUNTS WITH THE TOTAL DEPOSITION RATE

FIGURE 8.8

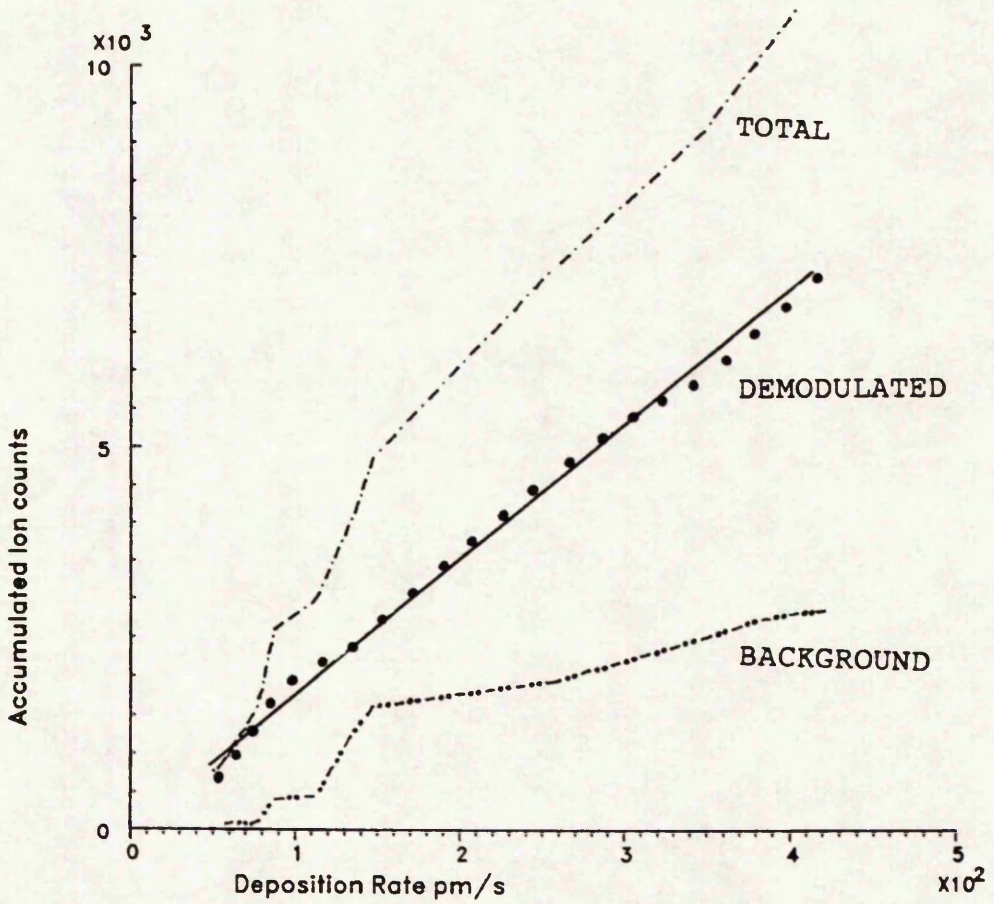

VARIATION OF S2+ (m/e=64) ION COUNTS WITH THE TOTAL DEPOSITION RATE

FIGURE 8.9

Contributions from the background ion count in the case of S_2+ are similar to those in the case of Zn+. Therefore, the evaporation of ZnSe and ZnS leads to the vapourized particles displaying similar proportions of background to total number densities. The results reported in chapter 6 support these observations.

Figure 8.8 and 8.9 show that when the deposition rate approaches zero the background ion count either tends to zero or is already negligible (because on-beam and off-beam ion counts can be very close at low deposition rates). However, in the figure representing zinc (figure 8.7), the background count appears to remain above zero when the deposition rate is nil. Experiments performed by measuring the ion counts for different particles during the evaporation of ZnS and ZnSe have shown that upon closure of the vapour source shutter the number densities for selenium and sulfur decay quickly whereas the count on zinc remains high for a longer period and a measurable number density may still be evident after a system bake at 200 °Celsius. This has also been reported in previous work on the present system [8.6]. It is possible that zinc contaminates the ionization chamber and/or escapes to the spectrometer quadrupole structure leading to appreciable background pressure.

8.5 ION COUNT RATIOS FOR ZnSe AND ZnS VAPOUR PARTICLES

It has been shown in chapter 7 that the evaporation of ZnS and ZnSe is congruent and yields monomers of zinc and dimers of sulfur or selenium. Measurements on the ion count using the mass spectrometer can support these results if the ratios between the number densities for various ions (from the vapourized compounds) observed on the mass spectra are constant with temperature or the deposition rate. Previous results based on observations using a mass spectrometer and obtained using the present MBE system suggested that the evaporation of ZnSe may be non-congruent and that zinc exhibits a high background pressure [8.6]. In the present work observations on the ion count ratios for the various ions using the mass spectrometer are undertaken.

Constant ion count ratios for the various ions are of high importance in controlling the number densities during film deposition experiments because the controls are then simplified owing to the reduction in the number of variables to monitor using computers. Figure 8.10 shows the variation of the ratio of Se+ to Zn+ with deposition rate on the quartz crystal monitor. The ratio curves of total and background densities for both vapour species are clearly non-linear which might suggest non-congruency. However, an examination of the curve showing the ratio of the demodulated counts suggests the ratio of Se+ to Zn+ is

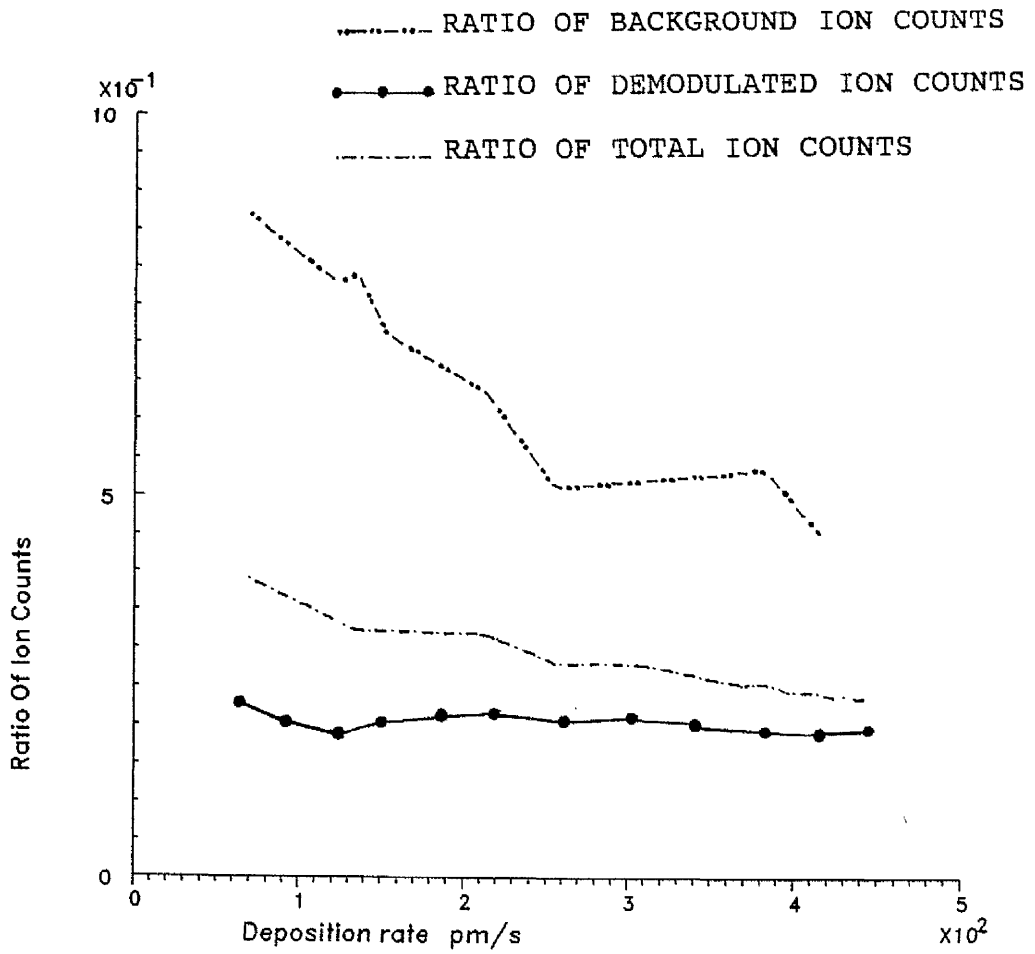

VARIATION OF THE RATIO OF BACKGROUND, DEMODULATED AND TOTAL ION COUNTS FOR Se^{+}(m/e=80) OVER Zn^{+}(m/e=64) WITH THE DEPOSITION RATE

FIGURE 8.10

constant over a range of deposition rates and hence over a range of vapour source temperatures. This supports the results suggesting that the evaporation of ZnSe occurs congruently. A similar approach to ZnS also supported congruency and figure 8.11 shows the ratio of S_2+ to Zn+ ion counts as a function of the absolute source temperature. Figure 8.12 includes the ratios of demodulated ion counts for S+ (m/e=32) over Zn++ (m/e=32), S_2+ (m/e=64) over Zn+ (m/e=64) and Se+ (m/e=78) over Zn+ (m/e=64) and shows that the evaporation of ZnS and ZnSe occurs congruently throughout the range of source temperatures employed [8.10]. The use of time-of-flight analysis has already determined the sublimation behaviour of ZnSe and ZnS and the obtained constant ion count ratios when the source temperature (or deposition rate) is varied reinforce the observations made on the evaporation process.

Because the effect of background particle number density as well as noise in the measurements may lead to erroneous conclusions about the compounds evaporating congruently, measurements of total, demodulated and background ion counts have been undertaken on zinc isotopes. Figure 8.13 shows the ratios for Zn+ (m/e=66) and Zn+ (m/e=64). The curves displayed show that it is difficult to obtain accurate measurements on these ratios when demodulation of the ion counts is not employed particularly towards lower deposition rates. The ratio of ion counts for Zn+ (m/e=66) over that for Zn+ (m/e=64) is close to the

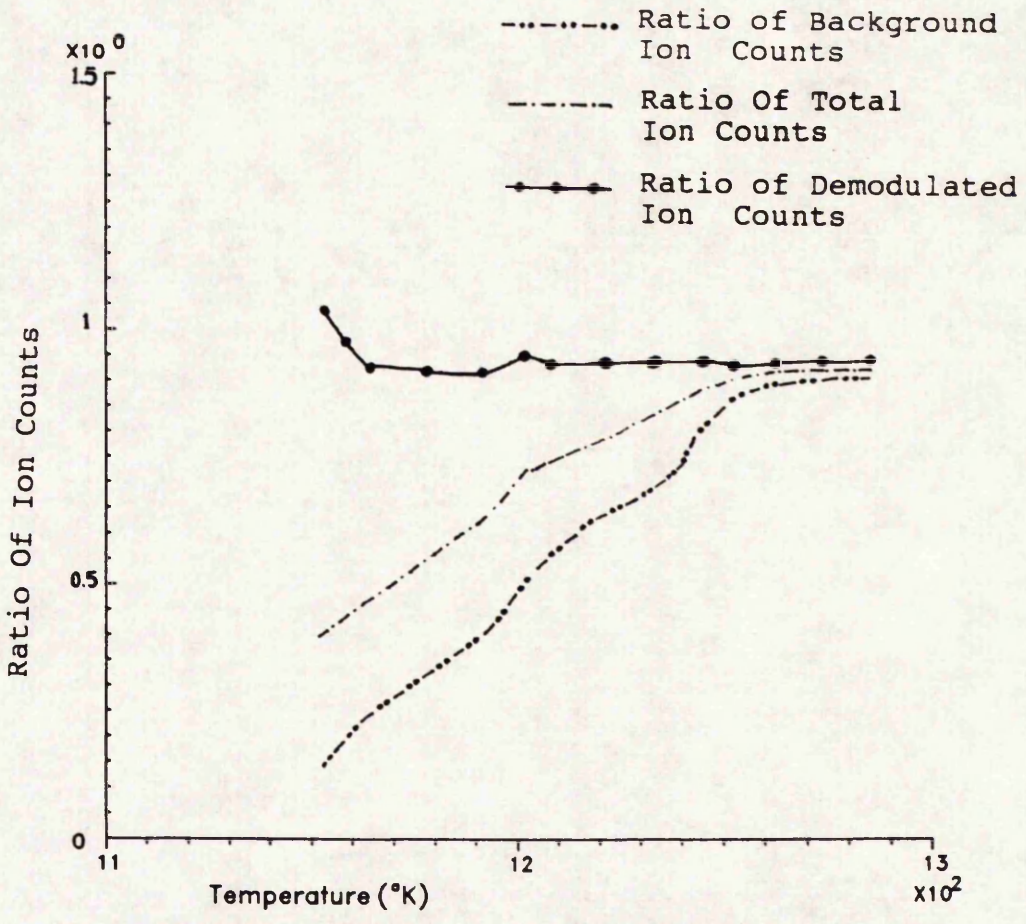

VARIATION OF THE RATIO BETWEEN S2+(64) AND Zn+(64) NUMBER DENSITIES WITH THE ABSOLUTE SOURCE TEMPERATURE

FIGURE 8.11

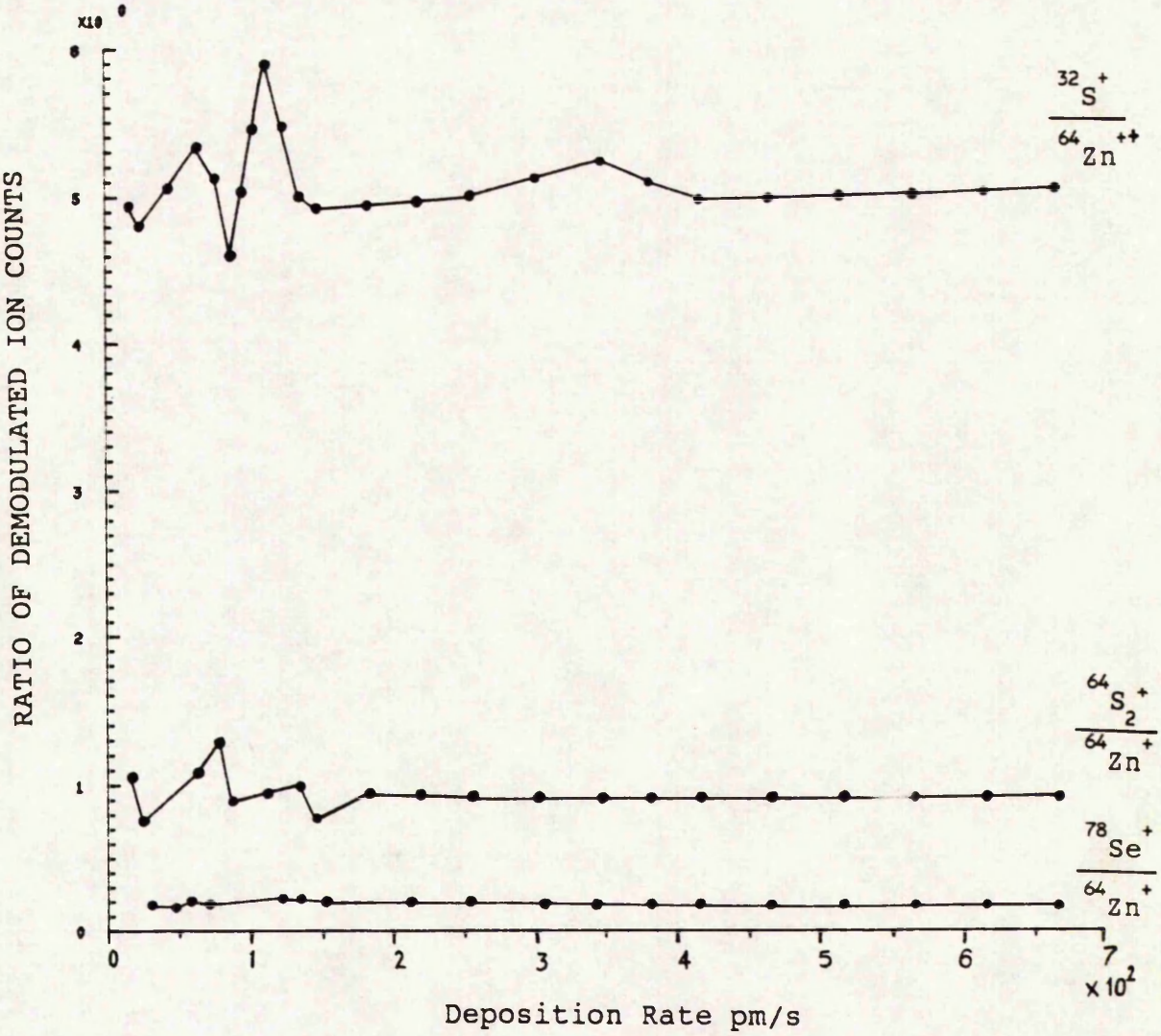

RATIOS OF ION SPECIES CONCENTRATIONS DURING THE DEPOSITION OF ZnS AND ZnSe

FIGURE 8.12

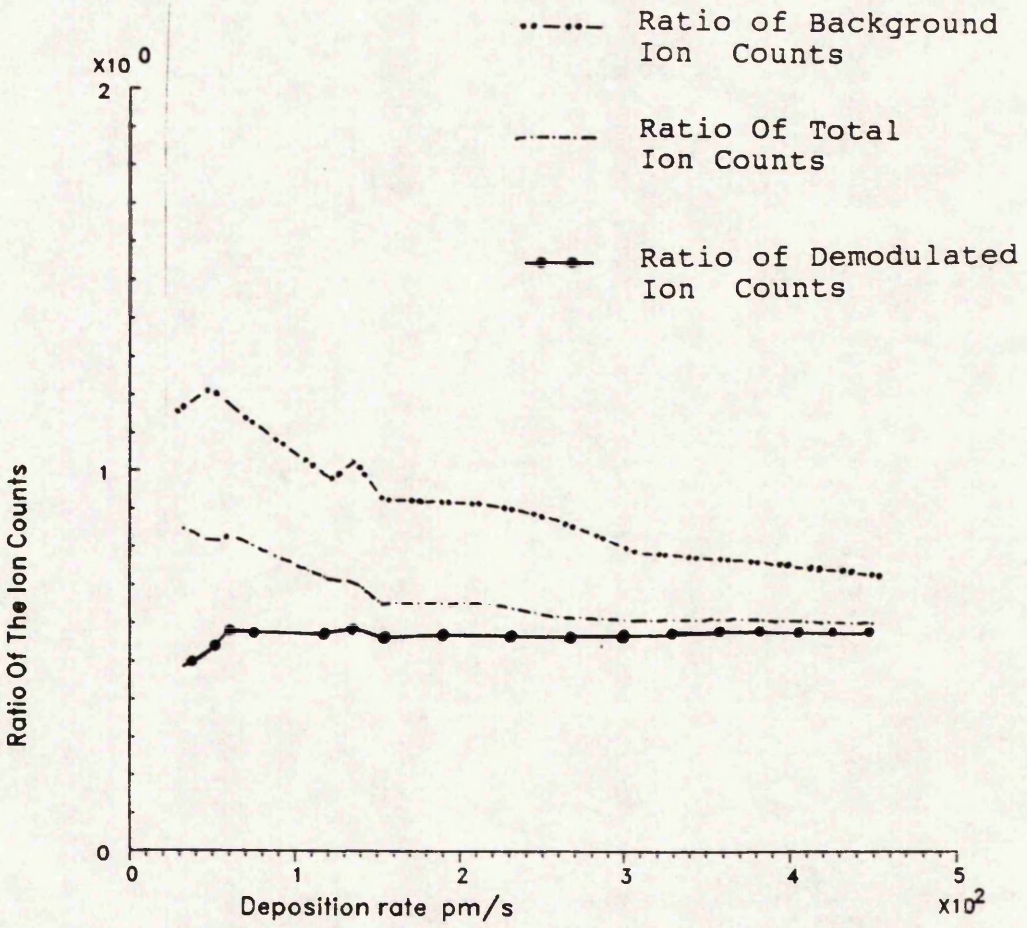

VARIATION OF THE RATIOS OF BACKGROUND, DEMODULATED AND TOTAL ION COUNTS FOR Zn+ (m/e=66) OVER Zn+ (m/e=64) WITH THE DEPOSITION RATE

FIGURE 8.13

published value 57.4% [§ figure 6.5] on the demodulated curve. The effect of noise on these measurements can be seen by comparison of figures 8.14 and 8.15. Both figures display the ion count ratios for Zn++ (m/e=33) and Zn+ (m/e=64) at 200 μA and 2 mA respectively. The signal noise content is greater when the spectrometer filament emission current is reduced (200 μA) as well as when the ion count for a particular vapour species is low (zinc isotope at m/e=33). This is demonstrated on the curves representing the ratios for total and background ion counts. However, the ratios for the demodulated ion counts show close variations in both cases. This suggests that since the isotopic or ion count ratios are not dependent on the spectrometer emission current, demodulation of the ion counts reduces the signal noise content substantially and aids the accurate measurement of low ion counts. It should be noted that the ion count ratios can change if some of the other experimental parameters are varied, such as the electron energy, the discriminator level in the pulse counting circuitry or the sensitivity setting of the spectrometer.

8.6 APPLICATION OF ION COUNT RATIOS FOR MONITORING THE EVAPORATION OF ZnSe AND ZnS COMPOUNDS

Since the aim of the present work is to control alloy composition during the growth of ZnS_xSe_{1-x} films,

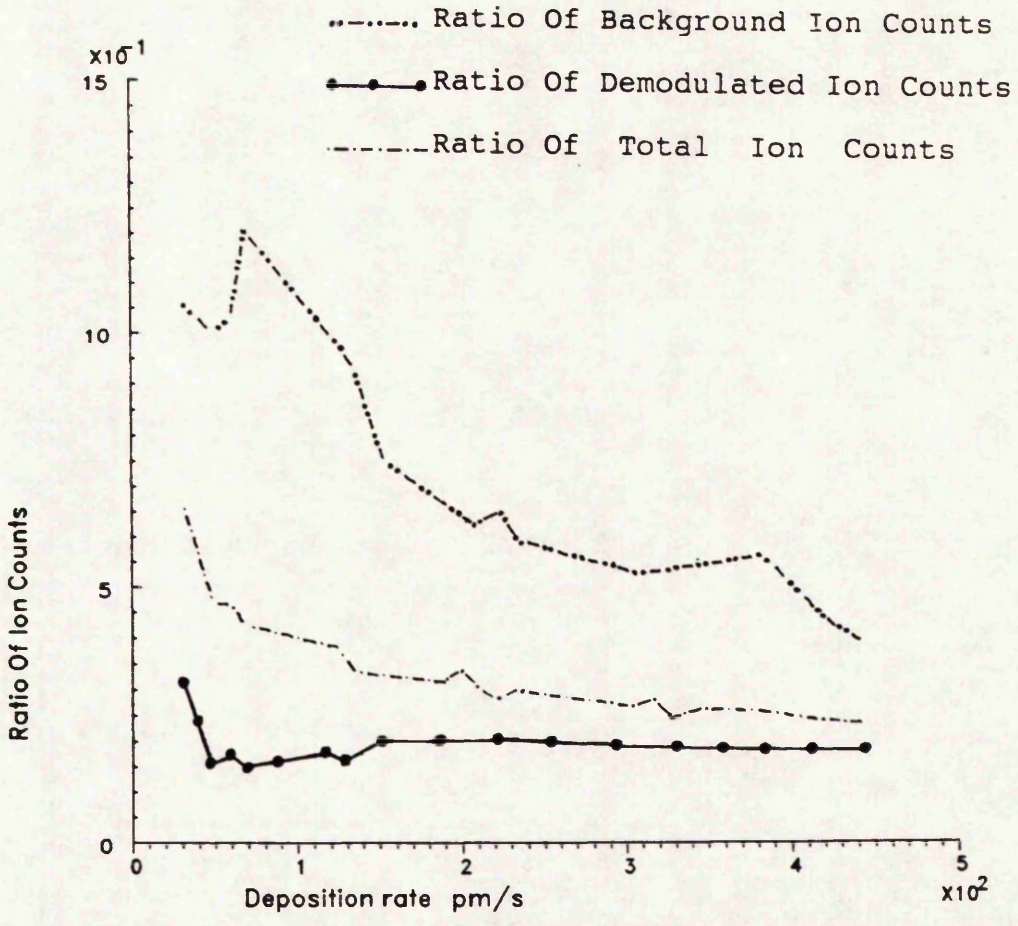

VARIATION OF THE RATIO OF BACKGROUND, DEMODULATED AND TOTAL ION COUNTS FOR Zn^+(m/e=33) OVER Zn^+(m/e=64) WITH THE DEPOSITION RATE

(AT 200 μA Emmission Current)

FIGURE 8.14

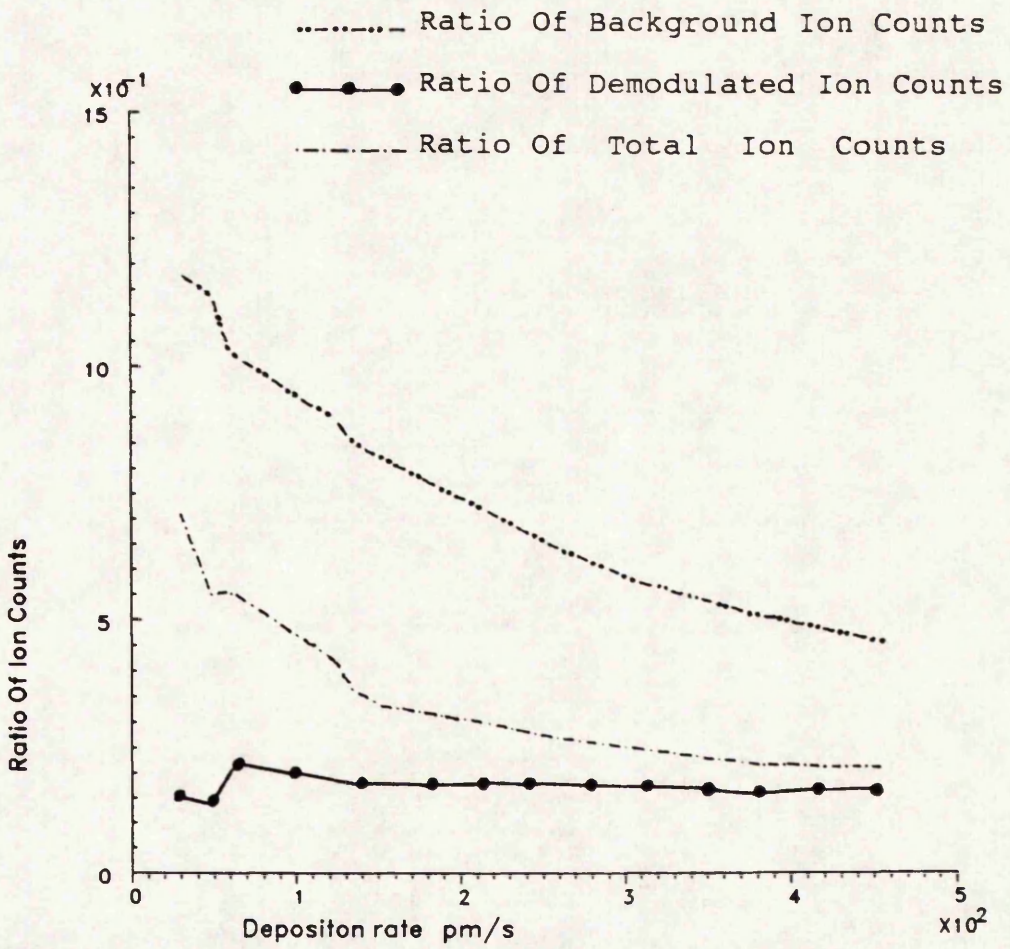

VARIATION OF THE RATIO OF BACKGROUND, DEMODULATED AND TOTAL ION COUNTS FOR Zn^{+}(m/e=33) OVER Zn^{+}(m/e=64) WITH THE DEPOSITION RATE

(AT 2 mA Emmission Current)

FIGURE 8.15

use of the ion count ratios can help with accurate monitoring of the vapours depositing on the substrate surface. Simple monitoring procedures may be undertaken over a large range of temperatures by exploiting initially measured evaporant species ion counts (or number densities).

8.6.1 SINGLE COMPOUND SOURCE MONITORING

When only one source is in use, the calculation of the number densities from measurements at a single mass-to-charge ratio is direct. This can be undertaken after determining the ratio between the number densities for specific particles (ion count ratios) at a single source temperature. The congruency ratios when ZnSe is used are directly measurable but in the case of ZnS, initial use has to be made of isotopic abundancy of zinc and sulfur for calculating the ion count ratios between zinc and sulfur evaporant particles.

8.6.2 DUAL SOURCE MONITORING DURING THE DEPOSITION OF ZINC SULPHOSELENIDE ALLOYS

The main problem in determining the flux densities for particle species while evaporating zinc sulphoselenide from the two compound sources is the separation of the ion count for zinc emanating from the ZnS source from that occuring

from the ZnSe source. There is need to combine the congruency results with the measured isotopic abundancies on zinc since the main peaks of zinc and sulfur overlap in the mass spectra.

During dual source evaporation including zinc selenide and zinc sulphide, if the measured ion counts at m/e=64 and 66 are represented by I(64) and I(66) respectively, the following relationships can be written:

$$I(64) = I(Zn64)_{ZnSe} + I(Zn64)_{ZnS} + I(S_2)_{ZnS} \qquad (8.9)$$

and

$$I(66) = I(Zn66)_{ZnSe} + I(Zn66)_{ZnS} \qquad (8.10)$$

where $I(Zn64)_{ZnS}$ is the ion count for zinc at m/e=64 which has originated from the ZnS vapour source, $I(S_2)_{ZnS}$ is the ion count for sulfur dimers at m/e=64...etc

If Ri represents the ratio between the zinc isotopes at m/e=66 and 64 , and Rc1 represents the measured ratio between the number densities of zinc (from the ZnS source) and sulfur S_2+ at the same m/e=64, a system of two

linear equations is obtained from equations (8.9) and (8.10). Solving these equations yields:

$$I(Zn64)_{ZnSe} = (1+1/Rc1)\ I(66) - (Ri/Rc1)\ I(64) \qquad (8.11)$$

$$I(Zn64)_{ZnS} = (1/Rc1)\ I(64) - (1/RiRc1)\ I(66) \qquad (8.12)$$

Ri is measured for the ZnSe evaporation after closing the ZnS source and Rc1 can be measured by closing the ZnSe source shutter and taking measurements at m/e=64 and 66.

In a typical experiment involving the evaporation of ZnS and ZnSe the constants Ri and Rc1 are first determined. At the starting temperature the ratios of number densities at the peaks to monitor $I(Zn64)_{ZnS}$ or or $I(Zn64)_{ZnSe}$ are calculated and stored. For subsequent temperature settings, only the particle densities at m/e=64 and m/e=66 are monitored and the stored ratios are recalled for calculating the number densities of other particles. A similar experimental technique can be adopted using the mass-to-charge ratios m/e=32 and m/e=33 instead of measurements at m/e=64 and m/e=66 and this is justified by the observations made previously on ion count ratios [§ section 8.5]. Constituents of the flux produced during dual

source evaporation of zinc selenide and zinc sulphide can therefore be measured through making measurements at two mass-to-charge ratios. The presented method can also be used for closed loop control of flux densities during the growth of zinc sulphoselenide alloy films since the number of variables to monitor is reduced to a minimum (monitoring at two mass-to-charge ratios for the two vapour sources). A major requirement is to be able to extract the number densities for particles in the vapour stream and this can be performed using modulated beam mass spectrometry.

8.7 EVAPORATION KINETICS OF ZnSe AND ZnS COMPOUNDS

During the evaporation of ZnS and ZnSe it has been observed that the total background pressure does not exceed 10^{-8} torr. Results obtained on the variation of the measured number density for nitrogen (N_2+) as a function of total pressure have established that a linear relationship exists over a large pressure range. Since it can be assumed that the measured ions number density using the QMS is proportional to the partial pressure of the monitored particles (from below 10^{-10} to 10^{-8} torr). Moreover, the results obtained from chapter 5 show that vapourizing ZnS or ZnSe yields monomers of zinc and dimers of sulfur or selenium. Therefore, the sublimation enthalpy of ZnS or ZnSe compounds can be estimated by calculating the energy (or enthalpy) required

to produce the monomers of zinc and dimers of sulfur or selenium from the solid phase.

Since the behaviour of the ion count with source temperature for the predominant vapour species in the spectra of ZnSe and ZnS has been observed, Arrhenius plots for these vapour species have been produced. The plots shown in figure 8.16 for Se_2^+ and Zn+ on ZnSe (m/e= 160 and 64 respectively) and figure 8.17 for S_2^+ and Zn+ (m/e=64 for both) on ZnS. The mean dissociation enthalpy for ZnSe or ZnS is obtained from the slope of the Arrhenius plots using the Clausius-Clapeyron equation [8.7, 8.8]:

$$\Delta H^T = -R \frac{d\ln(I^+)}{d(1/T)} \qquad (8.13)$$

where

R is the gas constant = 1.987 $cal.K^{-1}.mole^{-1}$

I^+ is the ion count of a particular vapour species

ΔH^T is the dissociation enthalpy at the average absolute temperature T.

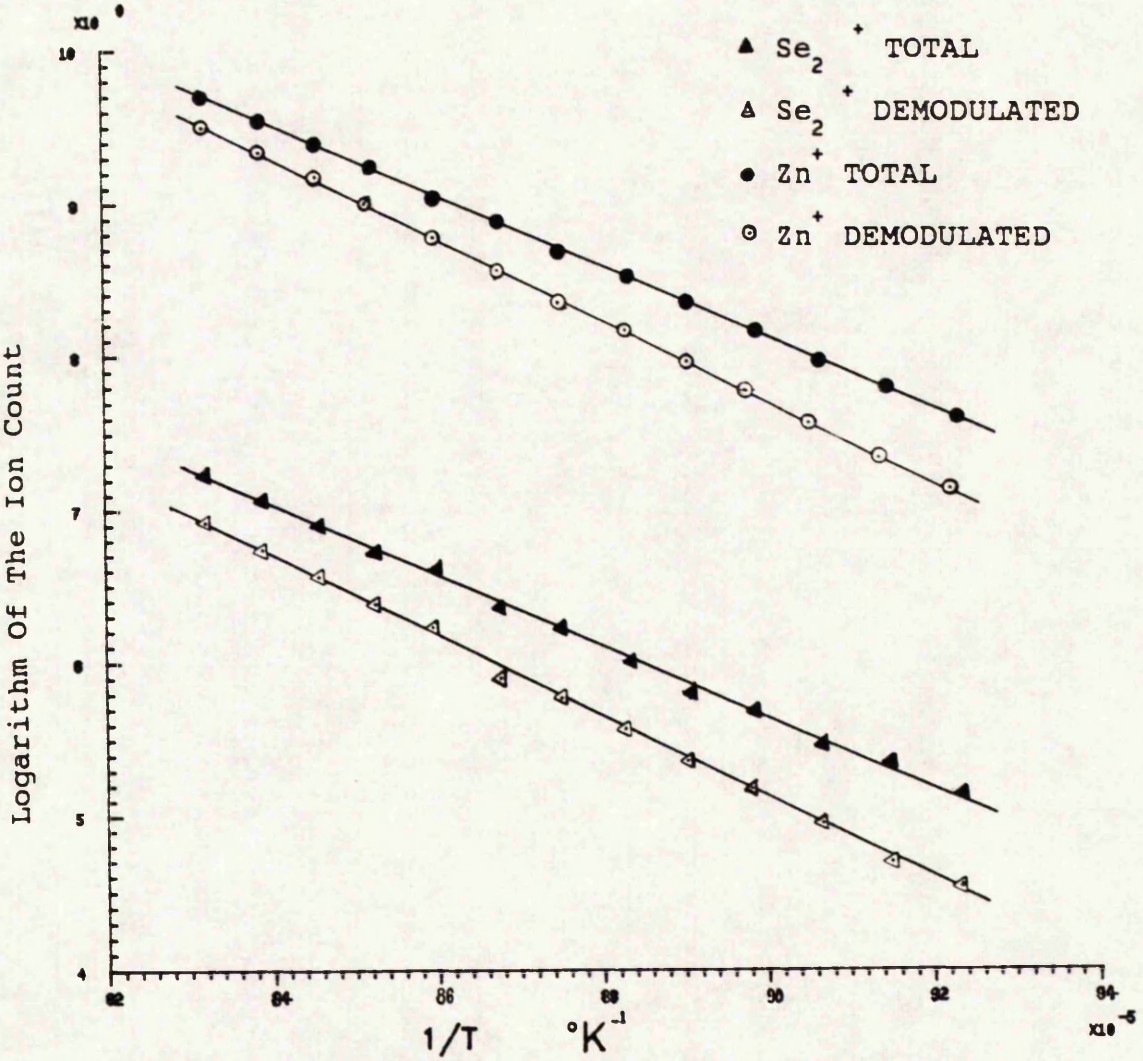

VARIATION OF THE LOGARITHM OF THE ION COUNT FOR Zn^+ (m/e=64) AND Se_2^+ (m/e=160) WITH THE INVERSE OF THE ABSOLUTE SOURCE TEMPERATURE

FIGURE 8.16

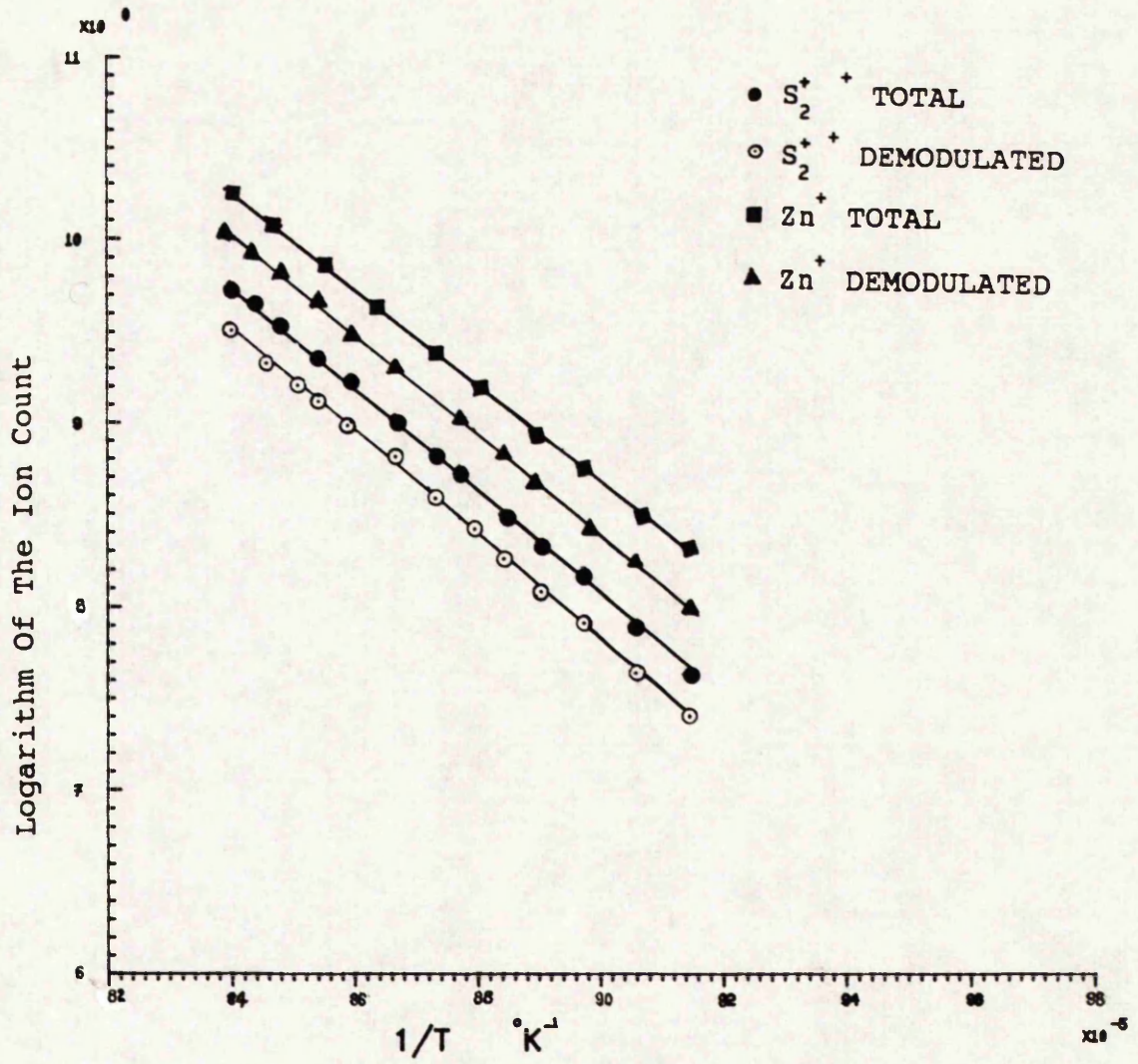

VARIATION OF THE LOGARITHM OF THE ION COUNT FOR Zn^+ (m/e=64) AND S_2^+ (m/e=64) WITH THE INVERSE OF THE ABSOLUTE SOURCE TEMPERATURE

FIGURE 8.17

8.7.1 SUBLIMATION ENTHALPY OF ZnSe

By measuring the slope of the Se_2^+ Arrhenius plot the vapourization enthalpy of Se_2^+ is obtained. A similar procedure is used for Zn+. Since the evaporation of ZnSe occurs according to relationship (7.15), then:

$$ZnSe_{(solid)} \longrightarrow Zn_{(gas)} + 1/2\ Se_{2(gas)}$$

yields:

$$\triangle H_{(ZnSe\ solid)} = \triangle H_{(Zn\ gas)} + 1/2\ \triangle H_{(Se_2\ gas)} \qquad (8.10)$$

with T the average temperature equal to 1110 °K which is halfway through the temperature range investigated. The Arrhenius slopes are obtained from a least squares linear regression to the variation of the logarithm of ion count versus the reciprocal of absolute source temperature. These slopes have been calculated for total ion counts which contain contribution from the background ions and also using demodulated ion counts where the background contribution is removed.

The obtained slopes on the demodulated data yielded the vapourization enthalpies of Zn and Se_2 as follows:

$$\triangle H^{1110}(Se_2) = 54.32 \text{ Kcal/mole} \qquad (8.11)$$

$$\triangle H^{1110}(Zn) = 55.10 \text{ Kcal/mole} \qquad (8.12)$$

and yields the mean vapourization enthalpy of ZnSe as:

$$\triangle H_{vap\ ZnSe} = 81.88 \text{ kcal/mole} \qquad (8.13)$$

A measurement of the enthalpy of dissociation of ZnSe has been reported by Goldfinger and Jeunehomme [8.9] and the value they propose (84.5 Kcal/mole at an average temperature of 1084 °K) is within 1.1% of that for the present work. The range of temperatures used by Goldfinger et al was quite large (1000 to 1600 °K). Although a third of this range has been used in the present work close agreement has been obtained for results where the background contribution to the fluxes is removed. Figure 8.18 tabulates the calculations carried out on the sublimation enthalpies. Also included in the table are calculations of the sublimation enthalpy of ZnSe using total ion counts which include the contribution from the background. A substantial decrease (20%) in the measured enthalpy is observed when the total ion counts are used. It is observed that the vapours in the background tend to reduce the slope of the Arrhenius curve and this will lead to the lower

COMPOUND MATERIAL		ZnSe		ZnS	
VAPOUR SPECIES		Zn	Se_2	Zn	S_2
MEASUREMENTS MADE ON THE TOTAL ION COUNT	$Log(I^+)$	$27.8 - \frac{21892}{T}$	$26.2 - \frac{22797}{T}$	$32.1 - \frac{26909}{T}$	$33.9 - \frac{28780}{T}$
	VAPOUR SPECIES VAPOURIZATION ENTHALPY	43.49	45.29	53.46	57.18
	COMPOUND SUBLIMATION ENTHALPY	66.14		82.06	
MEASUREMENTS MADE AFTER REMOVING THE BACKGROUND ION COUNT	$Log(I^+)$	$32.2 - \frac{27342}{T}$	$30.8 - \frac{27732}{T}$	$32.9 - \frac{29120}{T}$	$34.3 - \frac{29828}{T}$
	VAPOUR SPECIES VAPOURIZATION ENTHALPY	54.32	55.10	57.86	59.26
	COMPOUND SUBLIMATION ENTHALPY	81.88		87.50	
ENTHALPIES MEASURED BY GOLDFINGER ET AL		84.70		88.50	

* The enthalpies are measured in Kcal/mole.

TABLE SHOWING THE CALCULATION OF THE SUBLIMATION ENTHALPY OF ZnSe AND ZnS FROM THE MEASUREMENT OF INDIVIDUAL VAPOUR SPECIES NUMBER DENSITY USING THE QMS.

FIGURE 8.18

value for the measured enthalpy.

8.7.2 SUBLIMATION ENTHALPY OF ZnS

A similar approach to that used on ZnSe has been adopted for ZnS. The following values are obtained from data using the demodulated number densities measured at Zn(m/e=64) and S_2(m/e=64):

$$\triangle H^{1130}(S_2) = 59.26 \text{ Kcal/mole} \qquad (8.14)$$

$$\triangle H^{1130}(Zn) = 57.86 \text{ Kcal/mole} \qquad (8.15)$$

Using equation (7.16) yields:

$$\triangle H^{1130}(ZnS) = \triangle H^{1130}(Zn) + 1/2\ \triangle H^{1130}(S_2) \qquad (8.16)$$

and this gives

$$\triangle H^{1130}(ZnS) = 87.50 \text{ Kcal/mole} \qquad (8.17)$$

This value of the sublimation enthalpy is within 1.1% of that suggested by Goldfinger et al [8.9] which was 88.5

Kcal/mole at a temperature of 1075 °K. Their measurements were made over the range of 1000 to 1600 °K which is much larger than the range used in the present work. The various measurements made on the sublimation enthalpy of ZnS in the present work are tabulated in figure 8.18. Included in the table is an estimate of sublimation enthalpy for ZnS based on the use of number densities which include the contribution from background vapours. A reduction of 6.2% on the enthalpy is observed on measurements which include contribution from the background vapours.

8.8 CONCLUSION

The sublimation of ZnS and ZnSe has been investigated using modulated beam mass spectrometry. It has been shown that the evaporation process for both ZnS and ZnSe compound materials can be described by relating the absolute source temperature to material deposition rate. The variation with temperature of the demodulated particle density for the vapour species observed on the spectra of a QMS has been found similar to that for the total deposition rate measured on the quartz crystal monitor.

The effect of noise and the background vapours on the the number density measurement for fluxes emanating from the vapour cells have been investigated. Including the contribution of the background vapours and failing to reduce

the signal noise content from the measured number densities has been shown to have lead in the past to incorrect conclusions concerning the congruent evaporation of ZnSe.

The sublimation enthalpies of ZnS and ZnSe have been calculated using modulated beam mass spectrometry. It has been shown that including the background vapour leads to a lowering of the values for sublimation enthalpy. The values measured for the enthalpies of ZnS and ZnSe are in close agreement with those described in the literature, although a smaller range of temperatures has been used in the present work.

Constant ion count ratios for evaporant species in the vapour stream have been observed when the source temperature is varied. The measurement undertaken support the congruent evaporation for ZnS and ZnSe compounds. Relying on ion count ratios and measured isotopic abundancies, a simple method for measuring flux densities and controlling the composition of films of zinc sulphoselenide alloys (ZnS_xSe_{1-x}) has been proposed.

8.9 REFERENCES

[8.1] I.LANGMUIR
The Phys. Review Vol.11 p.329 (1913)

[8.2] J.V.KORNEEVA, V.V.SOKOLOV, AND A.V.NOVASELOVA
Russ. J. Inorg. Chem. Vol.5 p.117 (1960)

[8.3] A.J.COOPER, A.S.SAHIN, P.L.JONES, D.KING and D.MOORE
Vacuum Vol.34 p.925 (1984)

[8.4] R.P.GREGORY, P.L.JONES, D.KING and D.MOORE
Vacuum Vol.38 p.737 (1988)

[8.5] C.L.Mc.CABE
J. Metals Vol.6 p.969 (1954)

[8.6] A.S.SAHIN
PhD Thesis Univ. Manchester (England 1983)

[8.7] C.KITTEL AND H.KROEMER
"Thermal Physics" 2nd Edition
W.H.Freeman And Comp. pp.281-282 (1980)

[8.8] M.W.ZEMANSKY AND R.H.DITTMAN
"Heat And Thermodynamics" 6th Edition
Mac Graw Hill Pub. Comp. pp.253-261 (1981)

[8.9] P.GOLDFINGER AND M.JEUNEHOMME
Trans. Faraday Soc. Vol.59 p.2851 (1963)

[8.10] M.BENYEZZAR, D.KING, P.L.JONES AND D.MOORE
Proceedings Of The 11th International Vacuum Congress
Vacuum Vol.41 Nb.4-6 pp.842-846 (1990)
(Paper included at end of thesis)

CHAPTER 9

PRODUCTION OF ZINC SULPHOSELENIDE EPITAXIAL FILMS

9.1 INTRODUCTION

Zinc sulphoselenide thin epitaxial films have been grown on silicon doped n type GaAs substrates. The slice orientation is (100). Gallium arsenide has been chosen for its compatibility with ZnSe and ZnS in terms of crystalline structure and lattice spacing [§ section2.2]. Depositions have been performed using closed loop temperature control. Flux densities have also been controlled using the particle beam modulation apparatus. The aim is to grow layers of zinc sulphoselenide alloys with pre-determined concentration profiles. The work presented in this chapter introduces the procedures undertaken for growing crystals with pre-determined concentration profiles.

9.2 PREPARATIONS FOR THE GROWTH EXPERIMENTS

Relatively low substrate temperatures (275 °C) have been used and this reduces the effects of thermal mismatch in the process employed. Before a film is grown, several procedures are undertaken and these include:

1. The substrate is chemically cleaned using the following steps:

    1. Immersion in boiling hydrochloric acid for 2 minutes.

    2. Agitation in an ultrasonic bath filled with hot hydrochloric acid for 3 minutes.

    3. Drying in an oven at 200 °C.

    4. The substrate is loaded into the vacuum chamber.

2. The two vapour sources are loaded, one with a ZnS charge and the other and the other with ZnSe.

3. The vacuum system is evacuated and baked for 16 hours at 250 °C to produce a vacuum pressure of 2.10^{-10} torr or less. During bake, the temperature of each source is initially raised to 500 °C and this removes possible contaminants which might have been introduced during source charging.

4. After stabilizing the required vacuum liquid nitrogen is fed to the shrouds surrounding the vapour source and substrate holder.

5. Prior to opening the substrate shutter, the substrate is cleaned in-situ by raising its temperature to 590 °C for ten minutes after which the temperature is lowered to 275 °C and maintained during the whole of the deposition experiment. The temperature of the sources is also raised to 500 °C for 1 hour before initiation of the growth process.

6. The vapour sources temperatures are raised to the first growth temperature and one or both sources shutters (depending on the film required) are opened immediately before opening the substrate shutter.

7. When the desired source temperature program is completed or film thickness is achieved, the shutters are closed and the system is shut down.

Films with variable concentration profiles for zinc sulphide and zinc selenide have been deposited. To exercise the equipment the growth of films with a linear concentration profile on sulfur and selenium has been undertaken. Use has been made of the information gathered during the evaporation and deposition of these materials [chapters 6,7 and 8]. The main impetus for the present experiments is to show an ability to grow films with pre-determined concentration

profiles using the modulated beam mass spectrometry system. Included in this chapter are example for films with a pre-determined composition profile which have been grown using the present system.

Before the growth of films with pre-determined concentration profiles, the parameters to be fed to the control computers are determined using results obtained from previous measurements on vapour species number densities and on deposition rates for the compounds. Then, while the growth experiment is in progress, the total deposition rate, the particle densities and temperatures are controlled. When the growth run was terminated, the films obtained were characterized . It is relating the characteristics of the grown film structure to the pre-determined and in-situ measurements on the film materials which helps with assessing the ability to deposit films having pre-determined concentration profiles.

9.3 PRE-DETERMINATION OF THE FILMS COMPOSITION PROFILE

9.3.1 DETERMINATION OF THE SOURCE TEMPERATURE PROFILES

The profile of the source temperatures for such an alloy has been evaluated. The temperature setting is one of the major factors influencing the growth conditions and the temperature program for the vapour sources is of primary importance in determining the profile obtained [9.1]. Besides congruency of evaporation for both ZnS and ZnSe compounds, it has been seen in sections 8.2 and 8.3 that the number densities of sulfur and selenium as well as the total deposition rate, have a near exponential dependence on the absolute source temperature. A logarithmic variation of source temperature setting with growth time has been adopted to produce a linear variation of deposition rate with film thickness. The aim of this work is to show that a particular temperature profile can be selected and that the alloy composition profile can be predicted. A linear profile can be chosen for ZnSe or ZnS by selecting data from the curves in figure 8.1 particular deposition rate on the substrate as in the data from figure 8.1. In the growth of alloy films with variable concentration profiles of the constituents using ZnS and ZnSe, a range of temperatures can be chosen for each of the compounds. For an increasing concentration of selenium from the substrate an initial temperature is chosen where the deposition rate is very low. The increases in deposition rate undertaken over equal time intervals, can be undertaken by selecting multiples of the initial deposition rate using data from figure 8.1. For a

decreasing concentration profile, it is submultiples of an initial high deposition rate which are selected.

To produce varying concentration profiles ten temperature steps have been chosen for each source. For the ZnS source the temperature varies logarithmically in ten steps according to the equation:

$$T_{ZnS} = 971 - 131 \, Log_{10}(j) \ ^{\circ}C \qquad (9.1)$$

j=1,2,...,10

resulting in and the temperature being lowered from 971 °C down to 840 °C for a deposition rate from 256 pm/s down to negligible levels.

For the ZnSe source, the temperature also varies logarithmically from 810 °C to 908 °C in ten steps according to:

$$T_{ZnSe} = 810 + 98 \, Log_{10}(j)^{\circ}C \qquad (9.2)$$

and this yields a deposition rate from 0 to 295 pm/s. The temperature settings for both sources are loaded into the computer memory as a two dimensional array with their instants of occurrence timed with a real time clock. At each setting growth is maintained for 10 to 15 minutes. The temperature profile obtained on the ZnS source versus time during the deposition experiment is shown on figure 9.1.

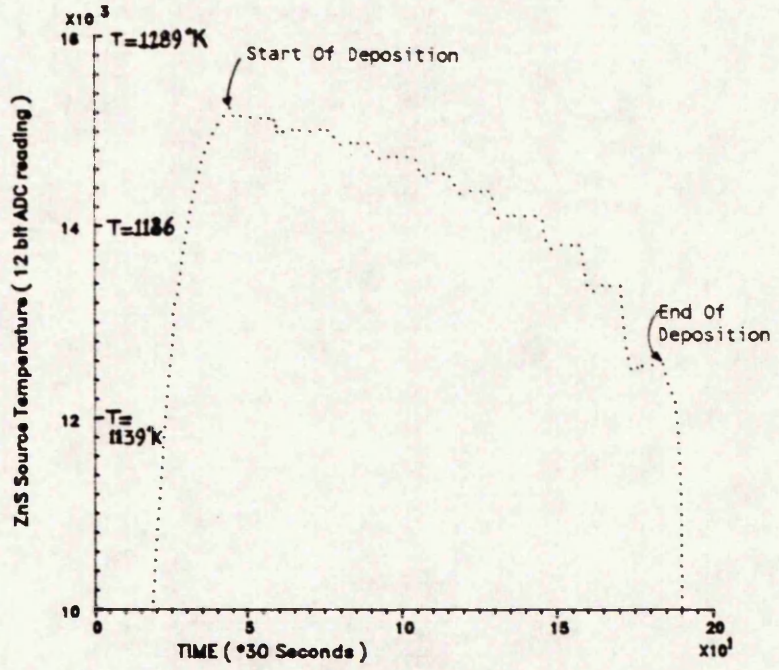

ZnS SOURCE TEMPERATURE PROFILE WITH TIME DURING THE DEPOSITION EXPERIMENT

FIGURE 9.1

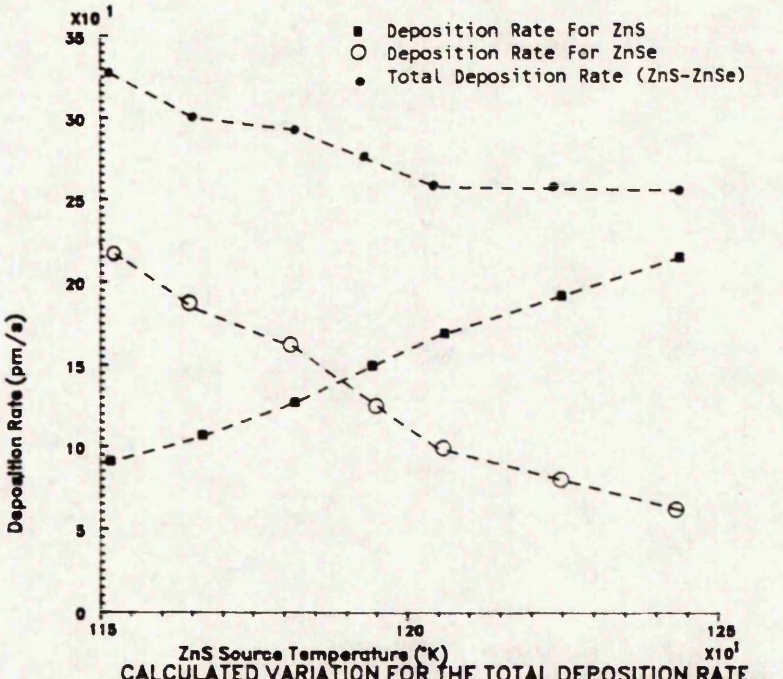

CALCULATED VARIATION FOR THE TOTAL DEPOSITION RATE DURING THE ZINC SULPHOSELENIDE GROWTH EXPERIMENT

FIGURE 9.2

When the temperature controllers converge to the first computed set-point, the substrate shutter is opened and the substrate is exposed to the vapour streams.

9.3.2 TOTAL DEPOSITION RATE PROFILE

In order to pre-determine the total deposition rate profile the measurements presented in figure 8.1 are used.

The deposition rates versus temperature represented on figure 8.1 have been obtained for temperatures increased in steps of 5 °C. Therefore the temperatures prescribed by equations (9.1) and (9.2), although within the range of those in the figure, can differ by up to 2.5 °C from them. The deposition rates coresponding to the temperatures prescribed by the equations (9.1) and (9.2) have therefore been obtained by interpolation of the data represented in figure 8.1. The interpolation procedure has been carried out using Neville's algorithm [9.2]. Data is calculated for each of the compounds' deposition rate and the results combined knowing that in the solid state, the densities for ZnS and ZnSe materials are 4.102 and 5.42 g/cm^3 respectively [9.3]. It is assumed that both compounds contribute according to their densities to the thickness of zinc sulphoselenide film deposited on the quartz crystal. The calculated profile is shown in figure 9.2. The data is presented with one measurement at each temperature setting

only. The figure shows an approximately linear profile for the total deposition rate. The total deposition rate decreases with time because the initial ZnSe deposition rate is higher than the final rate.

From the calculations made on the total deposition rate, it is estimated that films of 2.38 μm in thickness are expected with ZnSe contributing 1.78 and ZnS 0.6 μm to the film. This calculation has been made for the film thickness deposited on the quartz crystal microbalance.

9.3.3 CALCULATED PROFILE FOR THE MONITORED VAPOUR SPECIES

From equations (9.1) and (9.2) giving the sources temperature profiles and figures 8.4 and 8.5 giving the variation of the ion counts for selenium and sulfur with temperature, films relying these temperature profiles are to have sulfur concentration to decrease and selenium to increase with thickness from the surface of the GaAs substrate. Similar calculations to those performed on deposition rate can be made on Se+,Zn+ or S2+ flux densities. As an example, Figure 9.3 shows the obtained ion count variation for Se+ ions after interpolation of the ion counts coresponding to the temperatures prescribed by equations (9.1) and (9.2) using Neville's algorithm. Although the ion counts may vary due to changes in the experimental detection system settings (such as electron

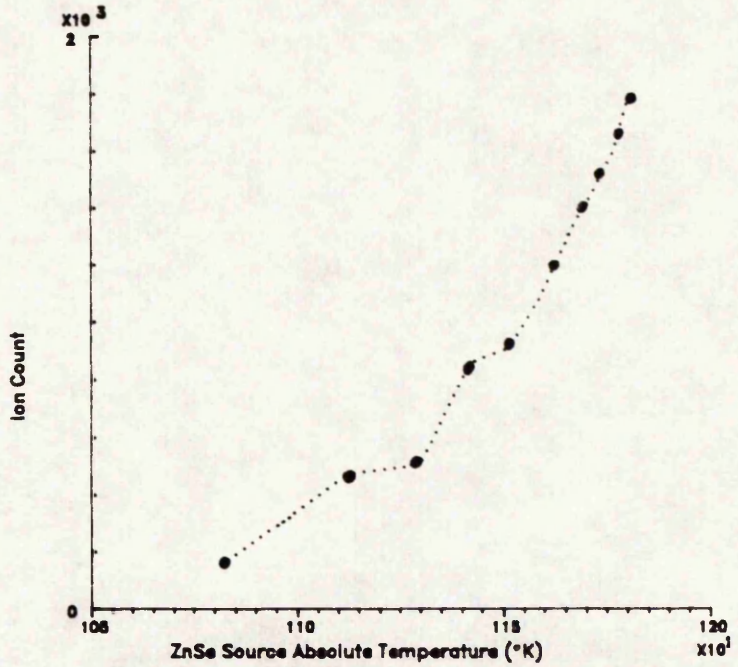

CALCULATED PROFILE VARIATION FOR THE ION COUNT ON Se + WITH THE ABSOLUTE TEMPERATURE OF THE ZnSe SOURCE

FIGURE 9.3

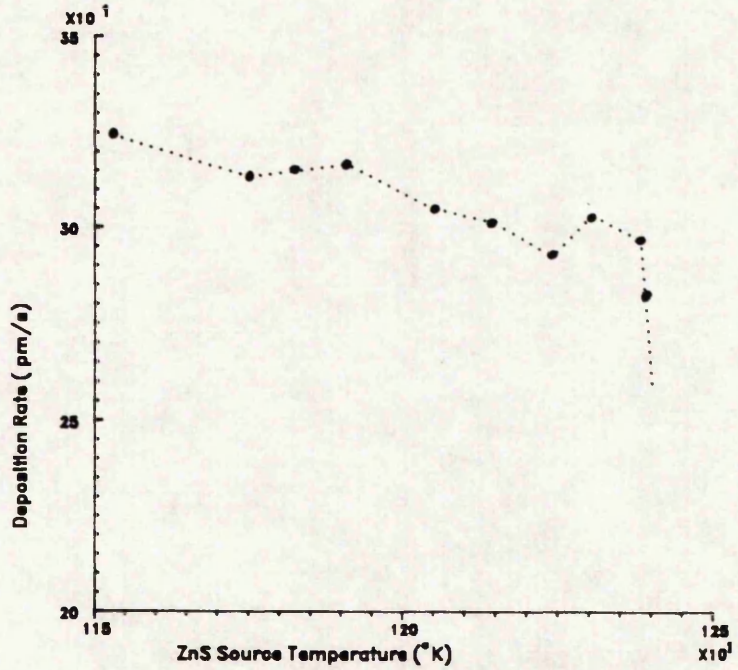

VARIATION FOR THE TOTAL DEPOSITION RATE WITH THE ZnS SOURCE TEMPERATURE DURING THE ZnS–ZnSe FILM GROWTH EXPERIMENT

FIGURE 9.4

energy, discrimination level on the pulse amplifier, accumulation time for ions etc...[§ chapter 5]), the profile for the ion counts variation with temperature should not be affected. The ion counts can be related to the deposition rate for calibration purposes.

9.4 IN-SITU OBSERVATIONS OF THE MATERIALS DEPOSITED

The variation of the total deposition rate with time during growth experiments for films where the vapour sources temperature profiles are prescribed by equations (9.1) and (9.2) is shown on figure 9.4. It can be observed that measurements using the quartz crystal microbalance are highly repeatable. The in-situ variation of the total deposition rate can be easily related to the calculated variation shown on figure 9.2. A decrease in overall deposition rate is observed and this is due to the temperatures chosen for the two compound sources.

The variation of the major vapour species ion counts with time obtained by continuously monitoring the vapour species at the different mass-to-charge ratios has been undertaken. After convergence of the temperature controllers to a temperature set-point, the flux densities measured using the mass spectrometer are continuously monitored. When a change in flux rate occurs action is taken by the control system to adjust the power fed to the

source heaters according to insure a constant deposition or flux density rate. Figure 9.5 shows the profile for zinc at m/e=64. The observed variation is comparable to that for the total deposition rate. In chapter 8 it has been shown that the ion counts for individual vapour species observed on the mass spectra of ZnS or ZnSe are proportional to the deposition rate of the associated compound. A comparison between Figures 9.4 and 9.5 indicates proportionality exists between the ion count for zinc and the total deposition rate when ZnS and ZnSe are evaporated simultaneously.

Figure 9.6 shows the variation of the ion count for Se^+ (m/e=78 and m/e=80) monitored during the deposition of ZnS and ZnSe. This profile compares well with that calculated (figure 9.3).

9.5 CHARACTERIZATION OF GROWN ZINC SULPHOSELENIDE ALLOY FILMS

There are a number of characterization method for film materials. In the present work use has been made of some the facilities within the Department as well as in other establishments and the results are outlined in the sections which follow. The characterizations are for zinc sulphoselenide alloy films which have been grown with concentration profiles for selenium and sulfur prescribed deposition rate calculated from equations (9.1) and (9.2).

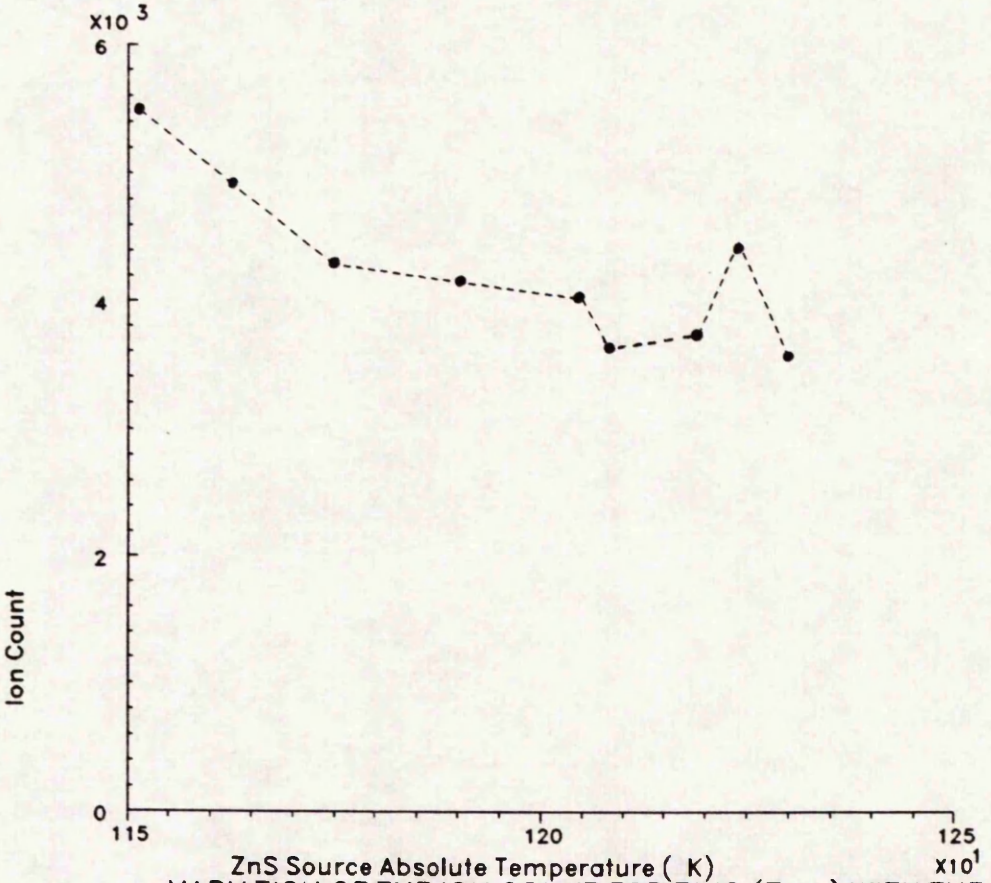

VARIATION OF THE ION COUNT FOR ZINC (Zn+) WITH THE ZnS SOURCE TEMPERATURE DURING THE DEPOSITION EXPERIMENT

FIGURE 9.5

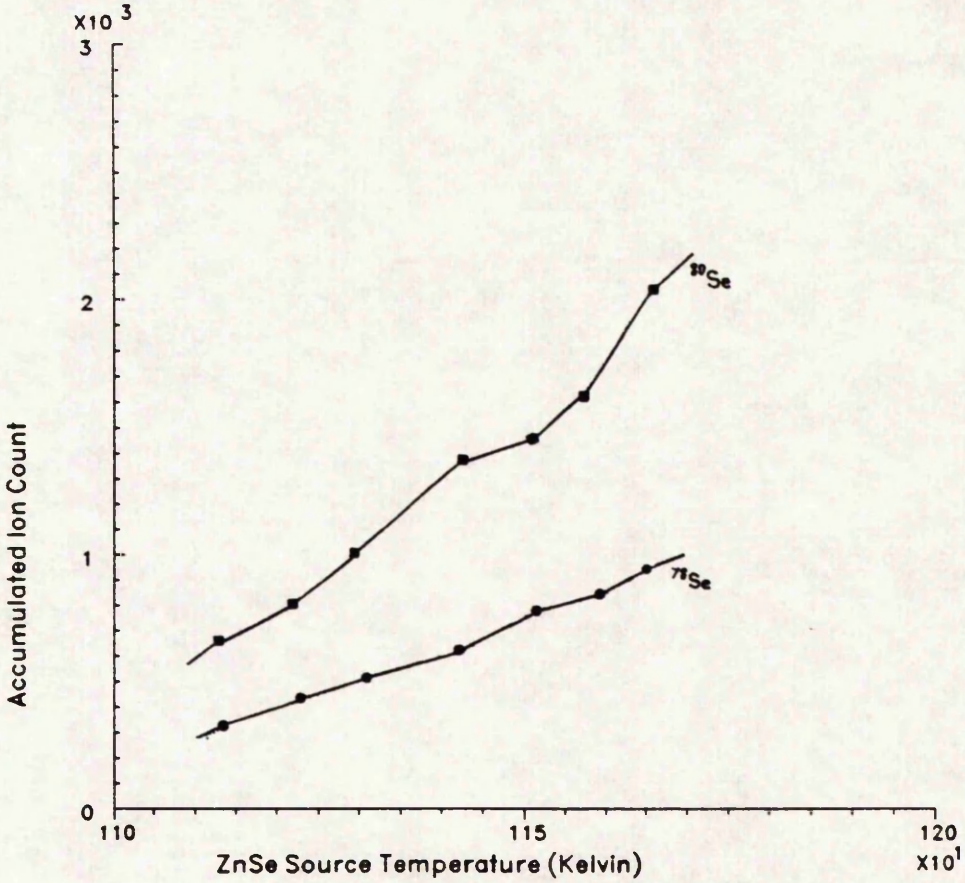

ION COUNTS VARIATION WITH THE ABSOLUTE SOURCE TEMPERATURE AT m/e= 78 AND 80 DURING THE DEPOSITION ZINC SULPHOSELENIDE

FIGURE 9.6

9.5.1 FILM THICKNESS MEASUREMENT

9.5.1.1 THE FRINGE MEASUREMENT METHOD

The thickness of the crystals has been measured with a fringe displacement technique using A Watson Interference Microsystem. The reference monochromatic light source is a Sodium lamp with the wavelength equal to 0.59 μm. Using this instrument the boundary of the film is observed so that the height of the surface can be compared with the base surface where growth took place. When the instrument is set up line fringes are obtained. The position of the central fringe for the base surface is found on an eyepiece graticule and the number of monochromatic fringes between the base surface and the top surface of the film is counted. The fringes are shifted by one fringe spacing for each height increment of half a wave length. A refractive index of 2.4 has been used for zinc sulphoselenide alloy films. The displacement caused by the GaAs substrate is compared to that caused by the grown crystal so that the grown layer thickness can be found

9.5.1.2 RESULTS FROM THE THICKNESS MEASUREMENT

The thickness determined using the fringe measurement method on several grown samples of zinc sulphoselenide alloys which have undergone similar growth conditions is equal to 1.18

±0.1 μm. In the present samples, at each source temperature setting, measurements have been made on the deposition rate and the main peaks in the mass spectrum. The final thickness of a crystal is calculated by adding the thicknesses obtained from the deposition rates observed for each temperature setting and growth time interval.

The thicknesses measured is found to be 45.3% of the overall thickness of 2.6 μm displayed by the quartz crystal microbalance. This may be due to the condensation coefficient on the heated substrate being less than unity. The temperature of the water cooled resonant quartz crystal is also different from the temperature of the substrate which may account for the difference in condensation coefficients on the two surfaces. Moreover, a non uniform distribution of evaporant, rising to a peak on the axis, may help explain the discrepancy. For a more accurate measurement of the condensation coefficient, the quartz crystal plate should be placed at the site of the substrate so that the particle spatial beam distribution and the temperature gradient effects are minimized [9.4].

9.5.2 DETERMINATION OF THE CRYSTALS QUALITY

Reflection electron diffraction (R.E.D) has been used to determine the nature of the grown crystals. Diffraction patterns have been obtained on a Metrovic model EM6. An

electron beam of energy 100 KeV energy is directed towards the substrate surface at a glancing angle which can varied. The diffraction pattern is recorded on a fluorescent screen. The operation is similar to that used in the R.H.E.E.D technique [§ section 3.4]. Figure 9.7 shows the spot patterns obtained at different glancing angles. Figure 9.8 shows the pattern obtained from an uncoated GaAs substrate. A direct conclusion from these patterns is that the grown structure displayed has a smooth surface and is an epitaxial single crystal film.

9.5.3 ENERGY DISPERSIVE ANALYSIS OF THE ZINC SULPHOSELENIDE FILMS

9.5.3.1 THE E.D.A.X TECHNIQUE

In energy dispersive analysis by Xrays (E.D.A.X), a specimen region of the film is chosen for analysis and an electron beam focused onto it. A solid state detector and a multi-channel analyser (M.C.A) are set to collect the X-rays over a given energy range yielding an energy spectrum. The collected data are displayed on a fluorescent display or a monitor and the final spectrum is examined by identifying each peak and ascertaining its position in the energy range [9.5]

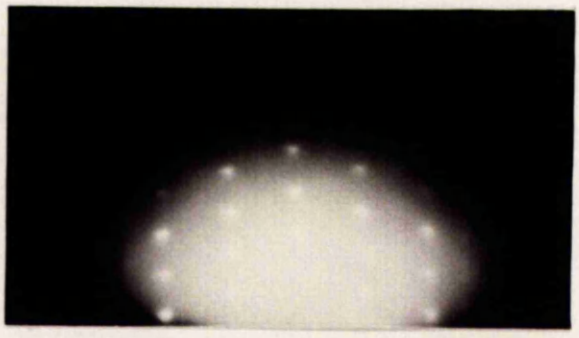

(a) 0 3 $\bar{1}$ GLANCING AZIMUTH (18.4° ANGLE)

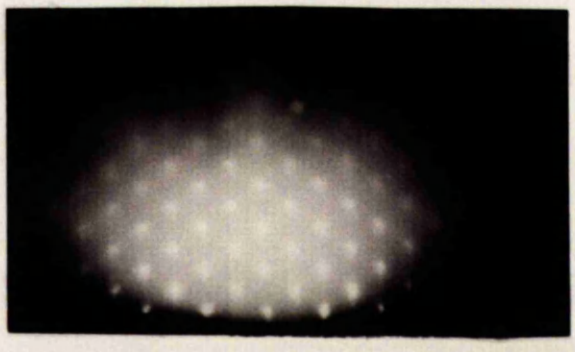

(b) 0 1 $\bar{1}$ GLANCING AZIMUTH (45° ANGLE)

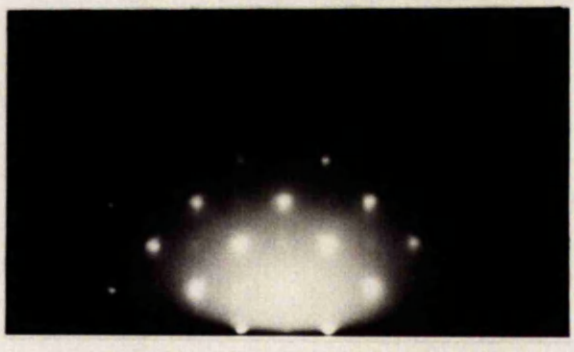

(c) 0 1 0 GLANCING AZIMUTH (Near 0° angle)

REFLECTION ELECTRON DIFFRACTION PATTERNS OBTAINED FROM A CRYSTAL WHERE ZINC SULPHOSELENIDE HAS BEEN GROWN ON A (100) ORIENTED GALLIUM ARSENIDE SUBSTRATE.

FIGURE (9.7)

0 1 $\bar{1}$ GLANCING AZIMUTH (45°ANGLE)

REFLECTION ELECTRON DIFFRACTION PATTERN OBTAINED FROM A CRYSTAL OF GALLIUM ARSENIDE (SUBSTRATE).

FIGURE (9.8)

Most systems employing the E.D.A.X technique have a fixed mechanical geometry. However, other parameters are adjustable like the dead-time and the energy range. The dead-time is the period when the detector is receiving or has just received an X-ray and is 'dead' to other incoming X-ray photons. The dead time is reduced by setting the instrument to count in the live-time mode, that is, the time for which the detector processes the X-ray photons. The time for which the analysis proceeds can also be used (clock time) for a similar purpose.

Variation of the energy range is a necessity since the energy of the X-ray lines to be detected determines the energy range selected for analysis [9.6]. The height of a peak for an element in the spectrum allows a quantitative evaluation to be made. A more accurate means for measuring peak intensity is to integrate the area under the peak. The energy band is selected on the M.C.A such that all the X-ray counts are within two particular energies which are functions of the peak width. A control computer for the instrument facilitates substraction of the background contribution to the observed energy spectra [9.7].

9.5.3.2 APPLICATION OF THE E.D.A.X TECHNIQUE TO ZINC SULPHOSELENIDE FILMS

The E.D.A.X technique has been applied to zinc

sulphoselenide samples grown with the concentration profiles described previously [§ section 9.3] using a Cambridge Instruments E.D.A.X system. Figure 9.9 shows the energy spectrum obtained. The peaks contributing to the observed spectrum have been identified. A qualitative assessment of the spectrum obtained reveals the main constituents of the crystal under test.

The counts on the different peaks show their quantitative contribution. The integration of the different peaks observed has been undertaken and the background substracted.

The obtained ratio of sulfur to selenium from the analysis is found equal to 29.08%. This is in accordance with the in-situ observations made on the integrated deposition rate which had increased when the temperature on the ZnS source was decreasing while that on the ZnSe source was increasing. The ratio between the calculated deposition rates for ZnS and ZnSe is equal to 33.7%. This observation may suggest that the material grown in ten layers of zinc sulphoselenide with different layer compositions may be described by the following averaged overall chemical formulae: $ZnS_{0.239}\ Se_{0.761}$.

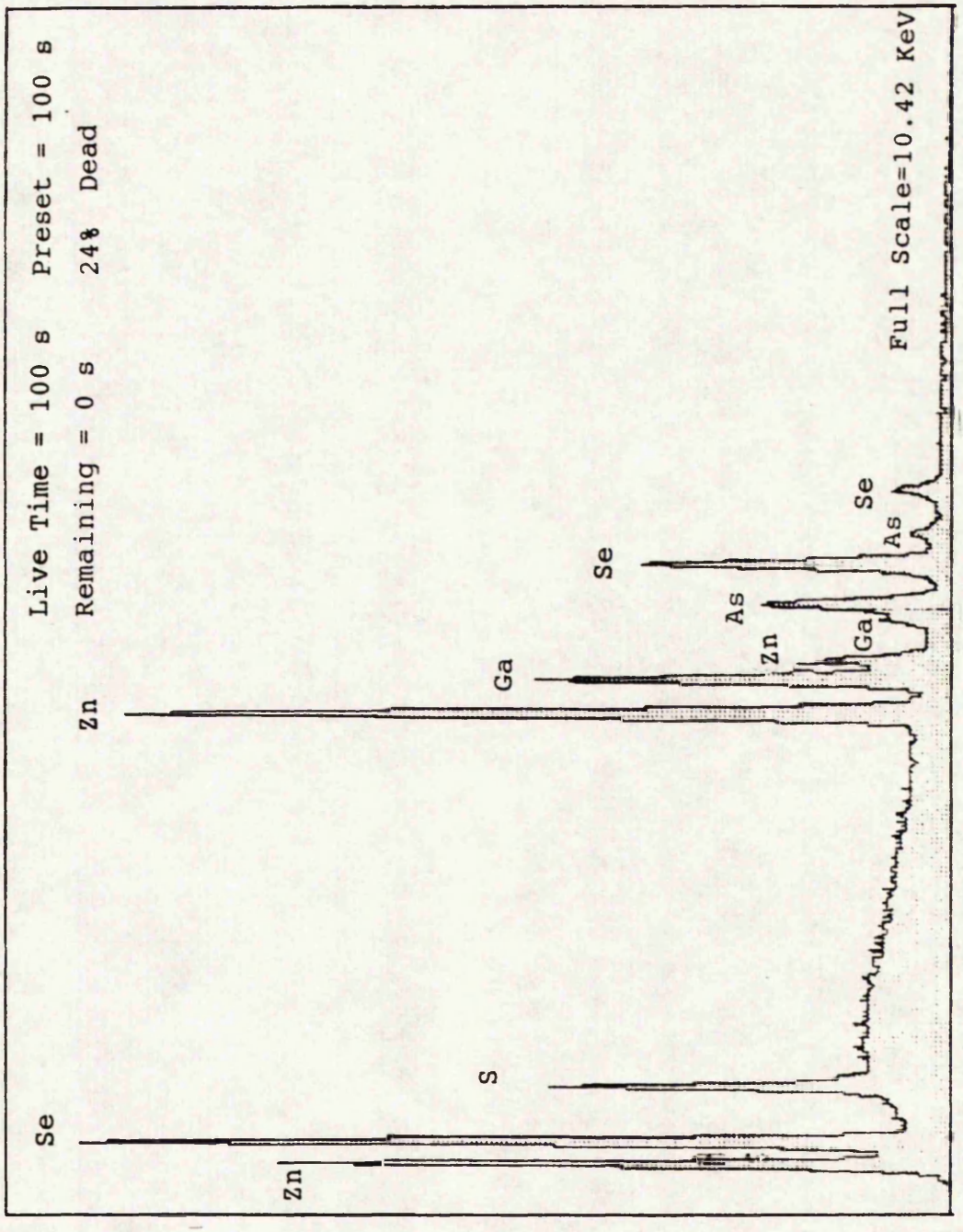

ENERGY DISPERSIVE SPECTRUM BY X-RAYS OBTAINED FROM THE DISPLAY OF A M.C.A FOR THE ZINC SULPHOSELENIDE FILM

FIGURE 9.9

9.5.4 MEASUREMENT OF ALLOYS COMPOSITION PROFILE

9.5.4.1 SECONDARY ION MASS SPECTROMETRY (S.I.M.S)

This technique is based on the bombardment of a solid surface by ions and mass analysis of the sputtered ions and neutral particles. The results are displayed as a function of depth into the film for monitored elements after data processing. The fraction of sputtered particles emitted as positive or negative ions depends on the measurement conditions. A primary ion beam of electro-negative elements tends to produce large numbers of negative ions whilst a primary beam of electro-positive elements yields a greater profusion of positive ions.

The use of this technique has been discussed in the literature [9.8, 9.9] and the factors which determine how well the S.I.M.S depth profile reflects the actual materials' composition include depth resolution, dynamic range and sensitivity. These factors have been reviewed by Magee et al [9.10]. Improvements on the dynamic range are obtained by acquiring the concentration profiles from a well defined narrow sample depth. A low energy ion beam is to improve on the depth resolution by reducing the atomic mixing effects between the primary ions and the substrate lattice atoms. Sensitivity is improved by using chemically active primary ions like O_2+. It is also improved by raising the energy of the ion beam but this reduces the

depth resolution.

9.5.4.2 APPLICATION OF S.I.M.S ANALYSIS TO ZINC SULPHOSELENIDE ALLOY FILMS

The secondary ion mass spectrometry technique (S.I.M.S) has been applied to samples of zinc sulphoselenide alloys grown with the condition described in section 9.3. A Vacuum Generators Simslab instrument has been used operating between 0-10kV with O_2+ (positive S.I.M.S) or Cs+ (negative S.I.M.S) primary ions to obtain depth profiles. A positive S.I.M.S profile with depth has been obtained using using a primary beam of oxygen with a 200 nA ion current intensity and an acceleration voltage of 10 KV.

Of interest are the profiles for sulfur and selenium with sample thickness. The results obtained are shown in figure 9.10 and are plotted directly from the S.I.M.S apparatus data acquisition system. The data (or curves) show very high counts at m/e=64 and 66 compaired to the count at m/e=78. It is suggested that the contributions from oxygen at these mass-to-charge ratios leads to not only to a higher count but more importantly to the profiles for sulfur and zinc being difficult to define.

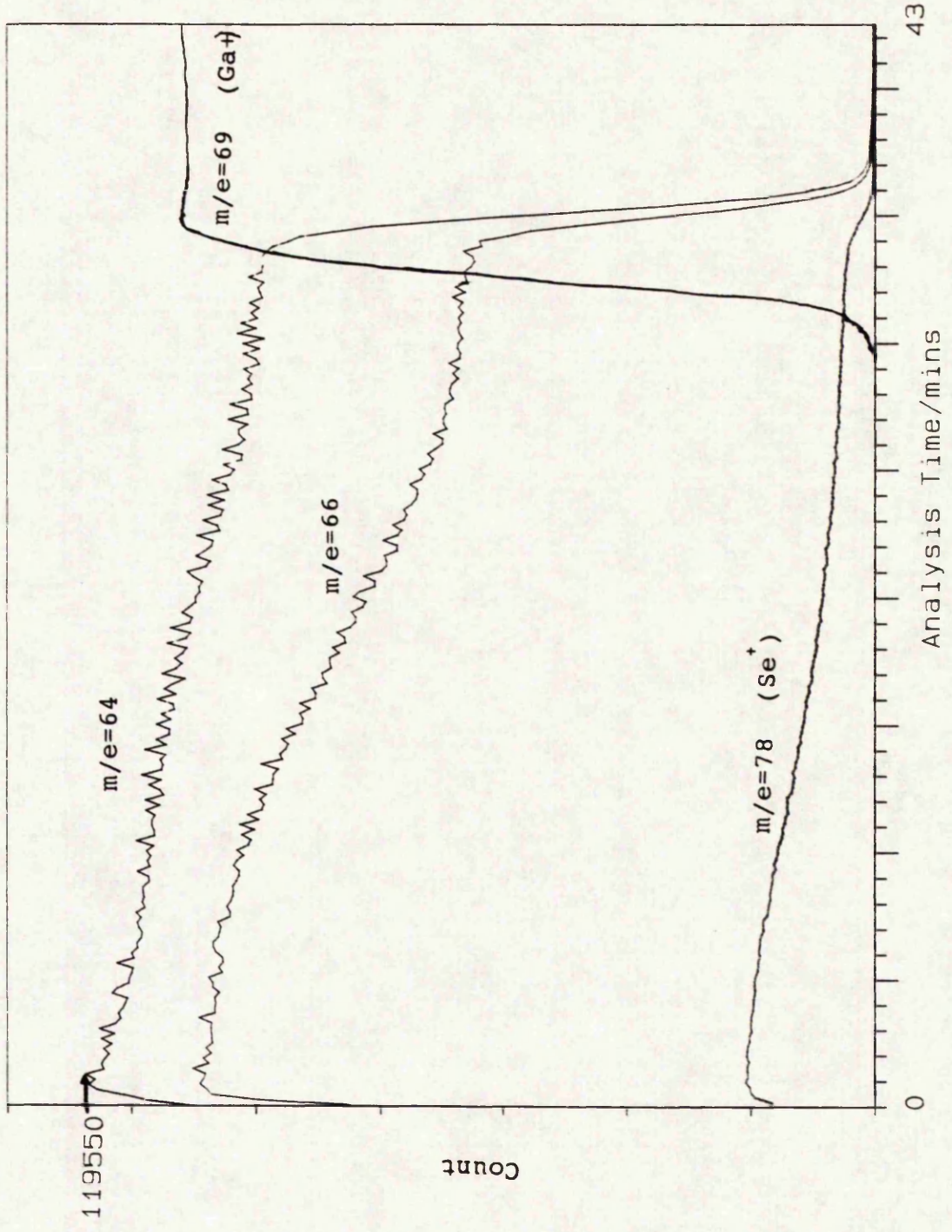

DIAGRAM SHOWING THE VARIATION OF THE PROFILE OF MATERIALS AS OBTAINED FROM A S.I.M.S ANALYSIS FOR THE ZINC SULPHOSELENIDE FILM AT 5 MASS-TO-CHARGE RATIOS

FIGURE 9.10

At m/e=78, no substantial contribution from other materials is expected apart from that of selenium ions Se+. Therefore the profile at this mass-to-charge ratio can be related to the in-situ observations. The profile variation is easily related to that obtained in-situ [§ figure 9.6]. A comparison between the curves for gallium (m/e=69) and selenium (m/e=78) suggests that the count on gallium is substantial before that on selenium becomes negligible and this can be explained by some of the gallium diffusing into the zinc sulphoselenide layers which are close to the substrate boundary.

Observation of figure 9.10 shows that at m/e=64 and 66 the ion counts have different profiles. There is a stronger decrease in the ion count at m/e=66 than at m/e=64. Since the amount of ZnSe deposited is larger than that of ZnS, it is therefore to be expected that going towards to GaAs interface, the decrease in the ion count at m/e=66 is stronger than that at m/e=64 (sulfur present at m/e=64). The sulfur contribution is negligible at m/e=66. Assuming that the sputter gas oxygen makes constant contribution to the measured ion counts at m/e=64 and 66, the interference to the measurements caused by ions like O_4+, ZnO_2++, SO_2+,...etc, and their isotopes, can be minimized.

Obtaining the profiles for Zn+ and S_2+ from the S.I.M.S analysis has required the use of isotopic abundancy ratios for zinc and sulfur and these are then combined with scaling down the intensities measured at m/e=64, and 66. Similar scaling numbers have been used on Zn+ and S_2+ and this aids comparison between the two materials. Of interest are the profiles for these materials and the way they vary between the GaAs interface and the zinc selenide top layer. The extracted profiles are shown in figure 9.11 and they indicate profiles which are similar to those predicted before the deposition.

The same curve for Se+ on figure 9.10 has redrawn on figure 9.11. The profile on Zn+, S_2+ and Se+ demonstrate consistently distribution for these materials in the zinc sulphoselenide alloy film. The profile on S_2+ shows a sudden increase near the interface with GaAs and this may be due to the presence of oxides at the substrate boundary.

Results shown in figure 9.11 are supported by those obtained from the E.D.A.X technique. The ratio of 29.08% between the amount of suflur and selenium is in accordance with the 30% decrease in zinc content from the top of the film to the substrate interface and the near linear variation of the profiles in figure 9.11 shows that the overall ratio between sulfur and selenium is close to 30%.

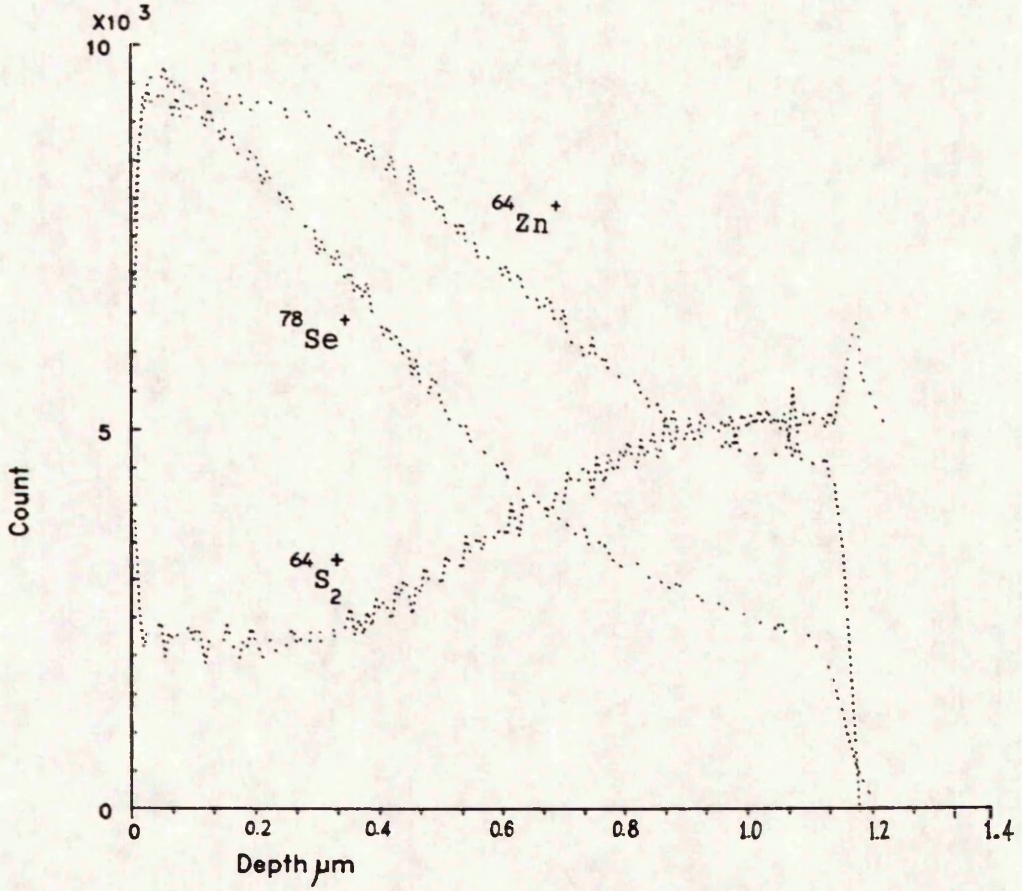

POSITIVE SIMS PROFILE FOR A ZINC SULPHOSELENIDE FILM INCLUDING Zn+ AT m/e=64, S2+ AT m/e=64 AND Se+ AT m/e=78

FIGURE 9.11

Comparing the profiles for zinc and selenium shown in figures 9.5, 9.6 and 9.11 may suggests that the composition profiles for zinc sulphoselenide alloy films may be predicted by monitoring the flux densities for particles emanating from the vapour sources using a mass spectrometer.

9.6 CONCLUSION

The growth of zinc sulphoselenide alloys with a pre-determined composition profile has been demonstrated and the factors influencing the growth process have been outlined. The use of modulated beam mass spectrometry has been found to be necessary for identifying the vapour species emanating from the sources and there is good correlation between the measurements and the composition profile of the materials deposited on the substrate.

The importance of removing the background contribution to the ion counts measurements has been outlined. The total deposition rate variation with temperature when both ZnS and ZnSe are evaporated has been shown to be proportional to the ion count on zinc and this is in accordance with the results obtained previously on separate evaporations of the two compounds.

The profiles predicted from measurements during growth are very close to those obtained in the deposited films. The measurements on the films' thickness and the thickness indicated on the quartz crystal microbalance have been shown to help with determining the amounts of materials deposited on the substrate and will aid with growing films where in-situ observations of flux densities can be directly related to the finished film composition.

Pre-determination of film composition profile can be undertaken if the characteristics of the vapourized materials are known. Modulated beam mass spectrometry has been shown to yield accurate in-situ measurements and the use of computers on-line computers has proved flexible for programming composition profiles for the vapour species depositing on the substrate.

The close agreement between results obtained for measurements made using the QMS during the experiments and the results obtained from subsequent analysis suggest that the vapour species (Zn, S_2, and Se_2) have close sticking coefficients. Further experiments on the growth of zinc sulphoselenide alloy films may help with assessing these quantities as well as optimizing the approach towards the growth of zinc sulphoselenide films with pre-determined composition profiles.

9.7 REFERENCES

[9.1] N.J.SAUER, T.Y.CHANG, A.H.DAYEM, and E.H.WESTERWICK
J. Vac. Sci. Technol Vol.B5 Nb.3 (1987)

[9.2] W.P.PRESS, B.P.FLANNERY, S.A.TEUKOLSKY, AND W.Y.VETTERING
'The Art Of Scientific Computing (Fortran Version)'
C.U.P p.81 (1986)

[9.3] P.BARANSKY, V.KLOTCHKOV AND I.POTYKEVITCH
'Electronique Des Semiconducteurs. 2eme Part.'
Edition Mir Moscou (U.R.S.S) p.366 (1978)

[9.4] D.CALLAGHAN
Ph.D Thesis University Of Manchester (1978)

[9.5] J.A.CHANDLER
'X-Ray Microanalysis In The Electron Microscope'
Elsevier/North Holland Pub. Comp. p.456 (1987)

[9.6] J.A.BEARDEN
'X Ray Wavelengths'
N.Y. 0-10586 U.S A.E.C Tennessee U.S.A (1964)

[9.7] D.B.WILLIAMS
'PRACTICAL ANALYTICAL ELECTRON MICROSCOPY IN MATERIALS SCIENCE'
p.66 PHILIPS Elect. Inst. Elec. Optics Pub. Group
Library Of Congress Cat. Nb.83-83128

[9.8] H.W.VERVER
Surf. Sci. Vol.47 pp.301-323 (1975)

[9.9] C.W.MAGEE, W.L.HARRINGTON, AND R.E.HONIG
Rev. Sci. Instrum. Vol.49(4) pp.477-485 (1977)

[9.10] C.W.MAGEE and R.E.HONIG
Surf. and Interf. Analys. Vol.4 Nb.2 pp.35-41 (1982)

CHAPTER 10

CONCLUSION

10.1 CONCLUSIONS ON THE WORK DESCRIBED IN THIS THESIS

This thesis has described the design and characterization of a computer controlled modulated beam mass spectrometry system. The application of the modulated beam mass spectrometer to controlling the evaporation and deposition of zinc sulphide and zinc selenide compounds has also been discussed. Information acquired from the evaporation and deposition experiments on the compounds has been exploited for the growth of zinc sulphoselenide alloys with pre-determined composition profiles using molecular beam epitaxy. The need for the work undertaken arose from difficulties encountered during controlled film depositions in previous research. Literature surveys have been undertaken on II-VI compounds (with emphasis placed on zinc sulphoselenide alloys), effusion sources, temperature control, and in-situ monitoring and control techniques (with

emphasis placed on the use of mass spectrometers and microbalances for the purpose of vapour flux control purposes).

In the modulated beam mass spectrometry system developed it has been proved necessary to use computers for data acquisition and control of the various instruments during the deposition of ZnS or ZnSe. Small and inexpensive Forth microcomputers have been dedicated to various tasks to provide an efficient control capability where several processes are controlled via a main supervisory computer. The dedication of computers to specific tasks has allowed several processes to be continuously monitored or controlled simultaneously.

The use of the Forth language has led to structured software development coupled with high speed task execution. Simple algorithms have been developed for tuning the mass spectrometer and as well as for setting setting the necessary for each particle species during time-of-flight analysis. Other software has been employed for deposition rate monitoring, array handling in temperature control, synchronous motor speed control and routines to relate the deposition rate to the particle number density. The Forth computer language is ideally suited to the development and measurement control tasks because it allows for the rapid development of subprocesses. Short data acquisition time has allowed some of the measurements to be dynamically related as in the case of the variation of the zinc number

density with ZnS source temperature. Optimal operating conditions for the developed control system have been suggested.

The use of computer controlled modulated beam mass spectrometry technique yields high signal-to-noise ratio. Using an ion pulse counting technique for the signal from the secondary electron multiplier of the mass spectrometer results in signal fluctuations on the demodulated ion count below 1%.

The improvements made in controlling and monitoring the various processes involved with mechanical particle beam modulation has lead to an ability to separate consistently ion counts for vapour particles in the background from those in the vapour stream. High accuracy on the measurement capability has led to measurements being made on most isotopic vapour species reported for zinc, sulfur and selenium. The isotopic abundancy ratios obtained for various particle species are close to those reported in the literature. Separation of overlapping peaks has proved viable using isotopic abundancy ratios and is invaluable for separating zinc from sulfur components. Measurements on several isotopes for a particular vapour species number density have been undertaken in various experiments since the acquisition time of the system is short enough to allow these measurements to be made and stored for subsequent analysis.

During a study of the ionization process for particles resulting from the evaporation of ZnS and ZnSe, substantial background pressures have been observed for all particles. The appearance potentials for most species in the mass spectra obtained during film deposition have been determined and this information has helped with identifying the origin of monomeric ions resulting from fragmentation of polyatomic particles in the ionization chamber of the mass spectrometer. Values for appearance potentials have also proved useful for separating overlapping peaks of zinc and sulfur.

Modulated beam mass spectrometry has also been used to investigate the neutral particles present in the vapour stream. It has been shown that the system developed is capable of measuring time-of-flight for particles over the relatively short distance from the evaporant stream chopper and the ionization chamber of the mass spectrometer. Two methods for time-of-flight measurement have been described and comparison made between theoretical and practical results.

The first method consists of directly observing particle number density variation as a function of time after the rotating shutter allows the molecular beam to pass through to the ionization chamber. Results obtained from the measurements show close agreement with the kinetic theory of gases. Success of the method suggests that ions getting through the quadrupole structure originate from a

very small volume of the ionization chamber. This conclusion is arrived at from observations of the rise time for the particle count which is substantially smaller than that calculated using the dimensions of collimating aperture at the entrance to the mass spectrometer.

The second method for time-of-flight measurements involves integrating the ion counts accrued over half a modulation period. Time-of-flight data for particles is obtained by measuring the delay of the extrema from the datum signal provided by the shutter position sensor. This method yields high signal-to-noise ratios and proves to be a powerful technique for time-of-flight measurement. Comparison of the times measured for the various particles during the evaporation of ZnS and ZnSe have helped conclude that these compounds vapourize giving monomers for zinc and dimers for sulfur and selenium.

Determination of the neutral particle species in the vapour stream helps with establishing the evaporation characteristics exhibited by ZnS and ZnSe. Previous research had suggested that zinc selenide did not vapourize congruently from the effusion cells used in the system. Repeating the measurements using modulated beam mass spectrometry to determine the vapour flux emanating directly from the cells shows that congruent evaporation takes place for both ZnSe and ZnS. The observations made previously included the effect of background vapour pressures for the constituents and lead to an incorrect deduction about

non-congruency.

Investigating the kinetics of ZnSe and ZnS evaporations has led to the measurement of their sublimation enthalpies. The effect of including the background ion count contribution to the enthalpies measured has been demonstrated and shown to yield lower values for the sublimation enthalpies. The results obtained on the demodulated number densities for ZnS and sublimation enthalpies compare well with measurements undertaken by other authors although a smaller range of temperatures has been used in the present work.

The variation of demodulated particle number density as a function of total deposition rate observed during evaporation of ZnS and ZnSe has been shown to be linear. It has been suggested that observed deviation from linearity is mainly caused by background vapours in the mass spectrometer ionization chamber and by noise effecting the signals measured at low deposition rates. The linearity obtained confirmed that the mass spectrometer can be used as an evaporation rate monitor. This allows control to be exercised over the heating power fed to the vapour sources from mass spectrometer measurements.

Controlling the composition of zinc sulphoselenide from measurements of vapour flux particle density measurements is complicated by the overlap of spectra for zinc and sulfur. A means for overcoming the problem has been devised which

involves using isotopic abundancy ratios and the knowledge that the materials evaporate congruently from the vapour sources. As a result the flux densities for vapour species can be determined by monitoring the particle number densities at two mass-to-charge ratios. Programmed control over the spectrometer measurements facilitates the determination of particle number densities and subsequent control of effusion cell heating power from calculated flux densities.

The information acquired from the study of evaporation and deposition kinetics of ZnS and ZnSe has been applied to the growth on GaAs substrates of zinc sulphoselenide alloys with pre-determined composition profiles.

The films obtained have been characterized and the composition profiles shown to relate well to those computed using the demodulated ion counts for the in-situ measured number densities. The modulated beam mass spectrometry system employed has been shown to be essential to the controlled deposition of zinc sulphoselenide help with the production of zinc sulphoselenide alloy film with pre-determined composition profiles.

10.2 SUGGESTIONS FOR FUTURE RESEARCH

For further research several areas of investigation on ZnS and ZnSe growth kinetics can be suggested including the

following :

1. A comparison of arrival times for zinc vapour from the ZnS and the ZnSe effusion cells might be used to determine the particle densities emanating from each of the cells.

2. The present system can also be used to investigate the products of the vapourization of other materials or compounds. For example, individual sources for selenium or sulfur will help with determining the products of their vapourization using time-of-flight analysis. It is expected that high order polymers may occur for these materials.

3. Surface kinetics studies using modulated beam mass spectrometry during deposition of ZnS or ZnSe on GaAs. This may provide an insight into the growth mechanisms for zinc sulphoselenide alloys. For this purpose only the positioning of the devices inside the vacuum chamber would have to be changed. Information about the desorption from the substrate could be obtained by placing the substrate at a glancing angle to the evaporant flux and observing the desorbed particles using modulated beam mass spectrometry.

Work is in progress to include the use of convolution techniques in the time-of-flight analysis for particles in transit between the rotating shutter and the mass

spectrometer. This process of convolution will provide an insight into the behaviour of the mass spectrometer's ionization chamber and delineate the capabilities of the modulated beam mass spectrometry system.

APPENDIX A

ADDRESS AND DATA INTERFACE FOR THE T.D.S MICROCARD

Address decoding and data bus interfacing has been undertaken on the TDS card in order to use this computer for the control of the mass spectrometer and the quartz crystal microbalance. Figure A.1 shows the schematic diagram for the address decoding and data bus interface circuitry. The circuit has been constructed with a view to controlling instruments requiring more than 16 eight bit addresses. The address and control lines from the 6303 microprocessor are buffered to increase their drive capability. The two way exchange of data between the microprocessor and the peripheral instruments is undertaken using a 74LS245 two way 8 bit buffer. The microprocessor R/$\overline{W}$ control line determines the direction of data flow and the two way buffer is enabled whenever one of their addresses is decoded. Address strobes are produced using two 4 to 16 line decoders (type 74LS154) and addresses in the range 0400HEX to 040FHEX and 0420HEX to 042FHEX are decoded.

FIGURE A.1

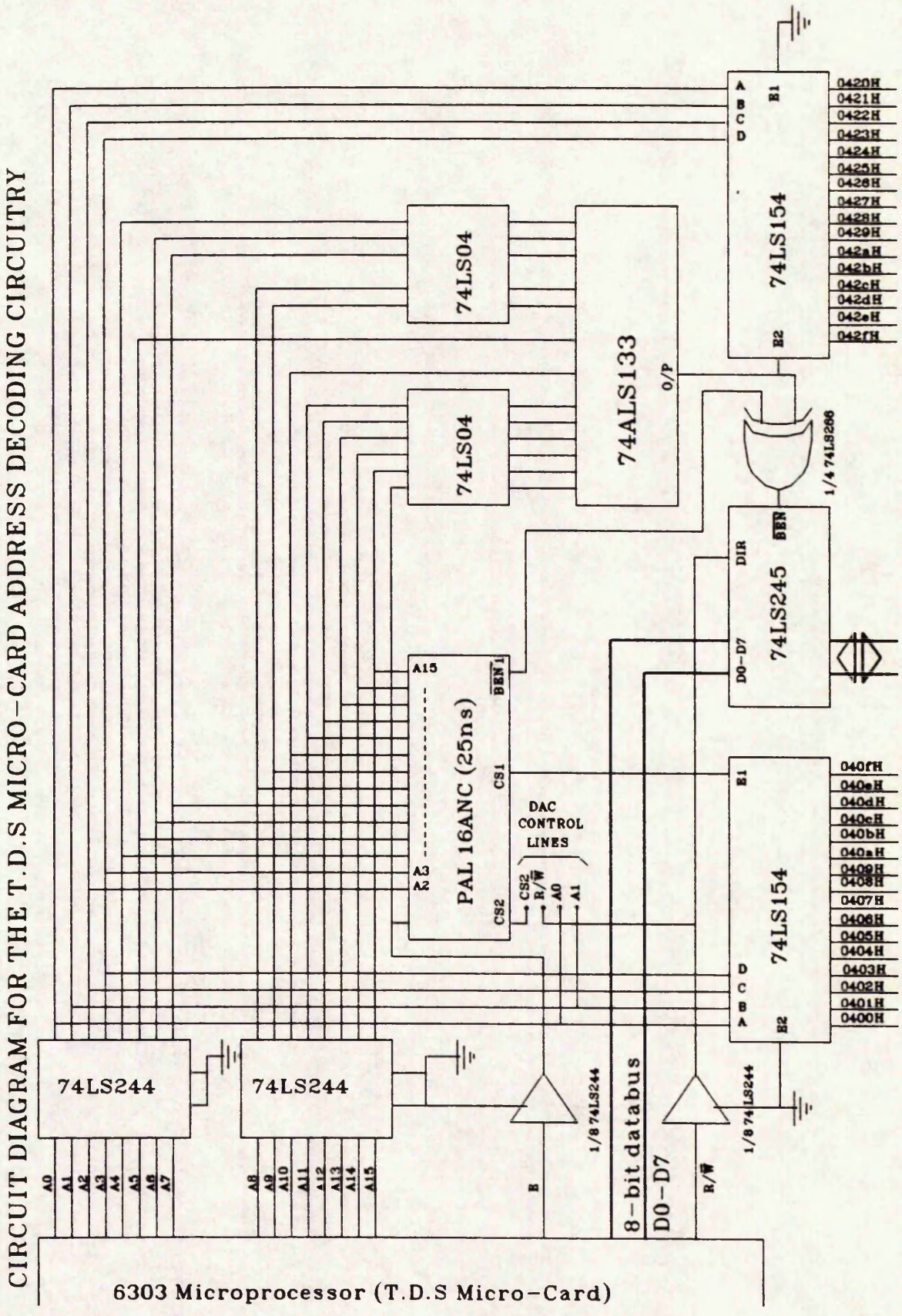
CIRCUIT DIAGRAM FOR THE T.D.S MICRO-CARD ADDRESS DECODING CIRCUITRY
74LS154
0420H
0421H
0422H
0423H
0424H
0425H
0426H
0427H
0428H
0429H
042aH
042bH
042cH
042dH
042eH
042fH
74LS04
74LS04
74ALS133
O/P
1/4 74LS266
74LS245
DIR
DO-D7
PAL 16ANC (25ns)
A15
A3
A2
CS1
CS2
DAC CONTROL LINES
R/W
A0
A1
74LS154
040fH
040eH
040dH
040cH
040bH
040aH
0409H
0408H
0407H
0406H
0405H
0404H
0403H
0402H
0401H
0400H
74LS244
74LS244
1/8 74LS244
1/8 74LS244
8-bit databus
D0-D7
A0
A1
A2
A3
A4
A5
A6
A7
A8
A9
A10
A11
A12
A13
A14
A15
E
R/W
6303 Microprocessor (T.D.S Micro-Card)

A programmable logic array device type PAL16ANC with a delay time less than 25 ns has been used to produce the following signals:

1. CS1 signal which is active when an address in the range 0400HEX to 040FHEX or from 0410HEX to 0413HEX is decoded.

2. CS2 signal which is used for the DAC and is active when one of the four addresses from 0410HEX to 0413HEX is called.

3. BEN1 signal which is asserted for addresses ranging from 0400HEX to 040FHEX.

Figure A.2 shows the circuit programmed into the PAL. This device has been used because a large number of address lines are needed for the decoding process and this allowed a reduction in the overall circuit complexity. Programming of the PAL has been carried out by using a STAG [A.1] programmer controlled by an IBM PC. Figure A.3 shows a timing waveform diagram obtained on a Hewlett Packard [A.2] logic analyser when decoding of the address 0400HEX. The strobes produced for the addresses from 0400HEX to 040FHEX are used for controlling the microbalance as well as reading the steering and the digitized mass spectrometer signals. Figure A.4 shows the allocation of addresses used for reading data and sending control information. The DAC circuit (appendix B) is controlled using CS2, address lines A0 and A1, and the microprocessor R/$\overline{W}$ control line.

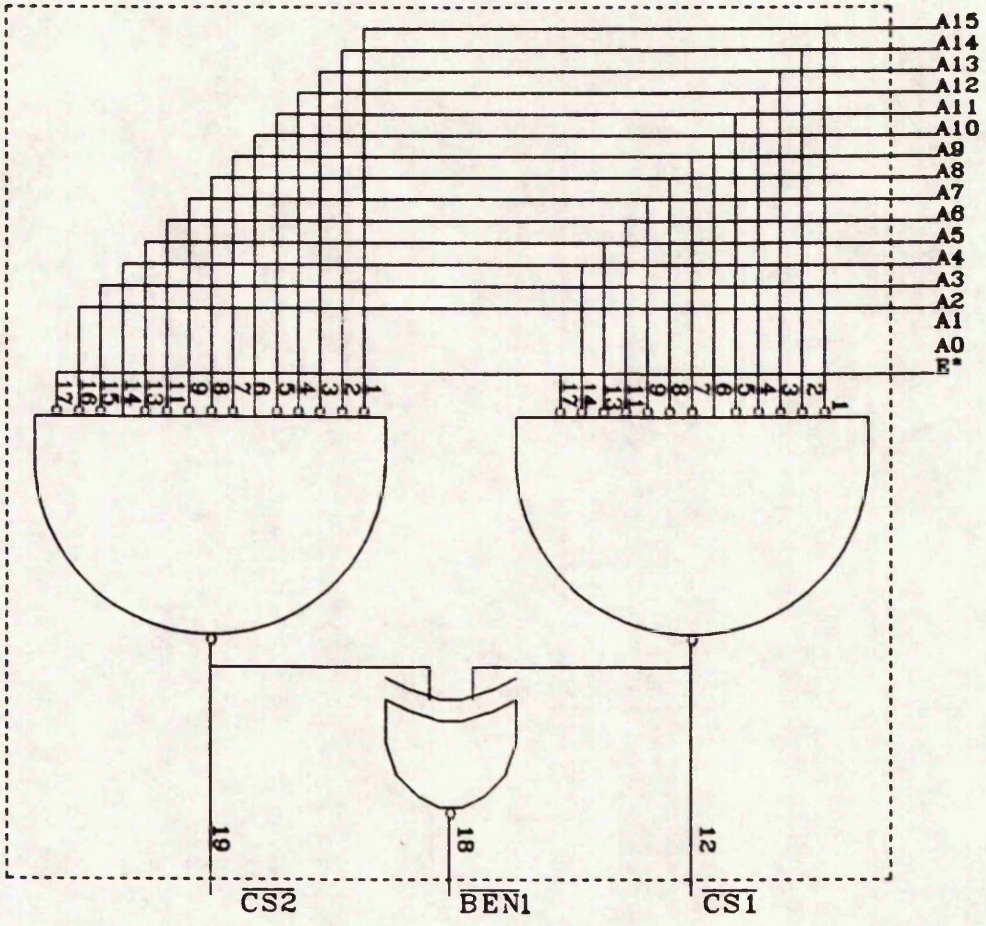

Logic Equivalent circuit to the PAL Used.

FIGURE A.2

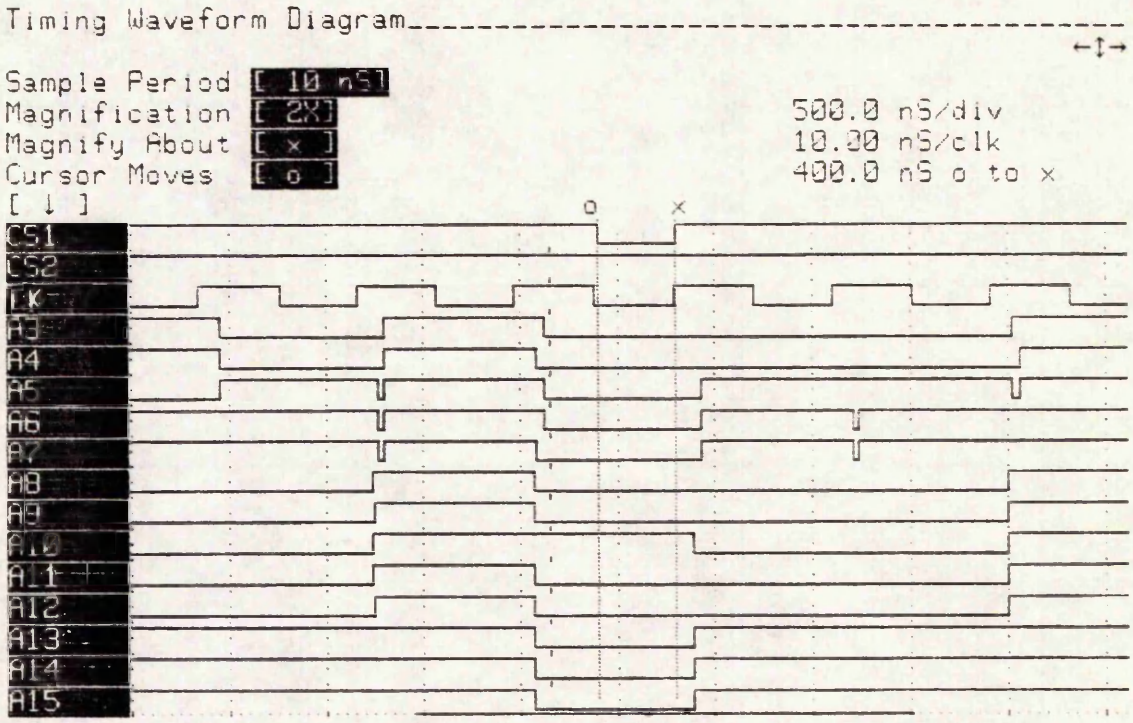

TIMING DIAGRAM OBTAINED BY DECODING ADDRESS 0400HEX

FIGURE A.3

INSTRUMENT	ALLOCATED DATA LINES	HEX ADDRESS
PULSE COUNTING CIRCUIT	ON-BEAM COUNT DATA BITS D16-D23 (INPUT)	0400
	ON-BEAM COUNT DATA BITS D8-D15 (INPUT)	0401
	ON-BEAM COUNT DATA BITS D0-D7 (INPUT)	0402
	OFF-BEAM COUNT DATA BITS D16-D23 (INPUT)	0403
	OFF-BEAM COUNT DATA BITS D8-D15 (INPUT)	0404
	OFF-BEAM COUNT DATA BITS D0-D7 (INPUT)	0405
	COUNTERS RESET (OUTPUT) D0 FOR ON-BEAM D1 FOR OFF-BEAM	0406
	NOT USED	0407
	STEERING SIGNAL STATUS D0 OVERFLOW SIGNAL (INPUT) D1 ON-BEAM COUNTER D2 OFF-BEAM COUNTER	0408
MICRO-BALANCE	DATA BITS D0-D7 (INPUT)	0409
	DATA BITS D8-D15 (INPUT)	040A
	DATA BITS D16-D23 (INPUT)	040B
	DATA BITS D24-D25 (INPUT)	040C
	COUNT OVERFLOW SIGNAL D0 CRYSTAL FAILURE SIGNAL D1 (I/P)	040D
	INTERRUPT SIGNAL STATUS D0 (INPUT)	040E
	RESET SIGNAL D0 STROBE SIGNAL D1 (INPUT)	040F
DAC CIRCUIT	ADDRESS LINES A0,A1 USED D0-D7 AT 0412HEX D8-D13 AT 0411HEX 0413HEX CALLED FOR LOADING DATA (O/P)	0410-041F
DIGITAL DELAY CIRCUIT	DATA BITS D16-D19 (OUTPUT)	0420
	DATA BITS D8-D15 (OUTPUT)	0421
	DATA BITS D0-D7 (OUTPUT)	0422
	DELAY ENABLE D0 (OUTPUT)	0424
STEERING SIGNAL CIRCUIT	DATA BITS D8-D15 (OUTPUT)	0425
	DATA BITS D0-D7 (OUTPUT)	0426

FURTHER ADDRESSES (0427 to 043F HEX) ARE FOR FUTURE EXPANSIONS

MEMORY MAP FOR THE INSTRUMENTS CONNECTED TO THE T.D.S MICROCOMPUTER.

FIGURE A.4

Addresses 0410HEX to 0413HEX are used for the transfer of a 16 bit data word into the internal circuitry of the 14 bit DAC.

For addresses from 0420HEX to 042FHEX, a 74ALS133 NAND gate is used with its output passed with the signal BEN1 through an XOR gate to enable the two way data buffer (figure A.1). The address strobes produced for this memory area are for controlling circuitry associated with the mass spectrometer, including a 20 bit digital delay circuit (appendix D) and a 16 bit circuit which generates the steering signal for ion count accumulation (appendix C). Figure A.3 includes detail of address allocation. Expandability in using the TDS microcard for the control of further instruments has been provided through the availability of strobes for addresses ranging from 0427HEX to 042FHEX.

APPENDIX B

THE QMS DRIVER CIRCUIT

Driving the Q7 QMS requires the generation of a voltage varying from 0 to 5 V for an a.m.u range of 0 to 200. An Analog Devices [A.1] 14 bit digital to analogue converter type AD7534 has been used for this purpose. The circuit constructed around the DAC is shown in figure A.1 A precision reference circuit based around a high stability Ref05 integrated circuit is used and a -5 V reference is obtained through the use of operational amplifier (A1 type (OP77). The 200 KOhms potentiometer allows setting the value of the Ref05 voltage to 5 V and the 100 Ohms potentiometer adjusts the reference of the DAC. A 1 bit resolution on the DAC means that the generated output voltage is within 0.3 mV of the value defined by the input number. Offsets on the output voltages are corrected after connection to the mass spectrometer with all the equipment switched on. The 200 KOhms potentiometer connected to the operational amplifier A2 (type OP77) permits offset voltage correction. This is further aided by the use of the

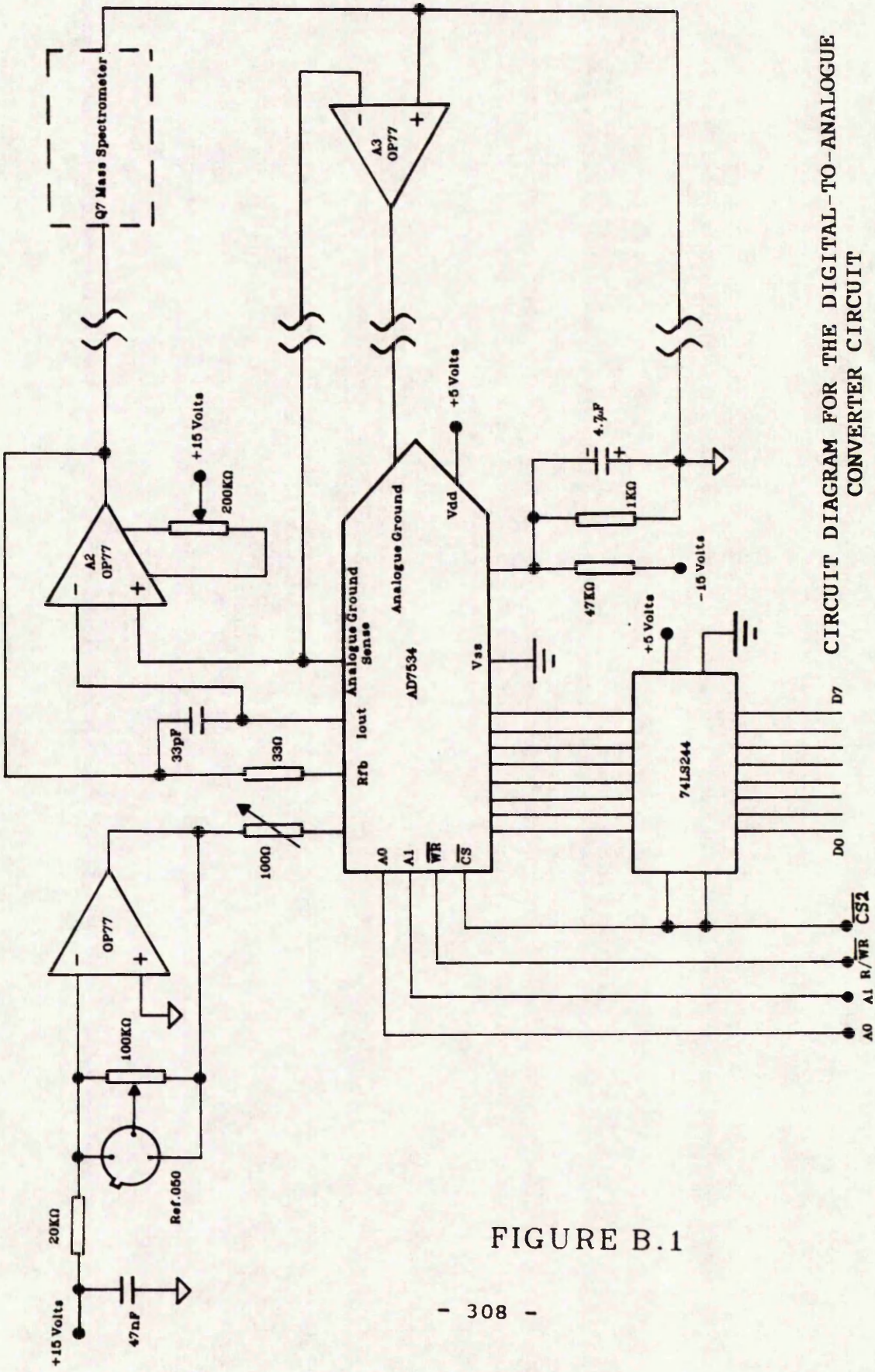

CIRCUIT DIAGRAM FOR THE DIGITAL-TO-ANALOGUE CONVERTER CIRCUIT

FIGURE B.1

operational amplifier A3 (type OP77) which forces the grounds of the DAC circuit and that of the mass spectrometer to similar levels. The circuit A3 is used because the QMS is situated away from from the DAC circuit. The necessity to account for possible differences in voltage between the QMS ground and the DAC analogue ground dictated the use of the circuit A3 which is connected at the site of the spectrometer ground to reduce the effect of track resistance of the path between the DAC and the QMS. Practically, the use of the ground forcing circuit helped effectively to reduce the difference in potential between the two grounds from 200 µV to below 10 µV. The voltages have been measured using a 5½ Thurlby precision multimeter. The 7534 DAC has internal latches and data is sent from two addresses decoded out of the TDS microcomputer memory. The 14 bit number is provided to the DAC circuit using the following simple Forth instructions:

```
‹14 bit number›   HEX 411 ! 0 413 ! decimal
```

The 14 bit number is in fact sent to the two addresses 411HEX for the most significant byte and 412HEX for the least significant byte. The data is first loaded to the latches by sending the 16 bit number to 411HEX. This enables the DAC control lines A0, A1 and CS. Afterwards, address 413HEX is called for transferring the data from the buffered input register to the DAC.

APPENDIX C

THE DIGITAL PULSE COUNTING CIRCUITS FOR THE MASS SPECTROMETER

The digital pulse counting circuit has been developed to count the pulses at the output of the ion pulse amplifier. Provision is made to count on separate channels pulses received when the shutter is open as well as when it is closed. The window through which the count is accumulated can be of different time widths, depending upon the objective of the measurement. Two pulse accumulation modes are available which either use an accumulation window equal to half the modulation period (obtained directly from the delayed modulation period) or a time window preset to 6.4 us and synchronous with the delayed modulation signal. The total accumulation time for ions is adjusted by controlling the number of accumulation windows (N+1) using a steering signal. Figure C.1 shows a block diagram of circuitry developed for ion pulse counting. The TDS Forth microcomputer sets the steering signal period by presetting a 16 bit binary counter to divide the modulation signal by N+1. Interfacing to the TDS microcomputer is undertaken by

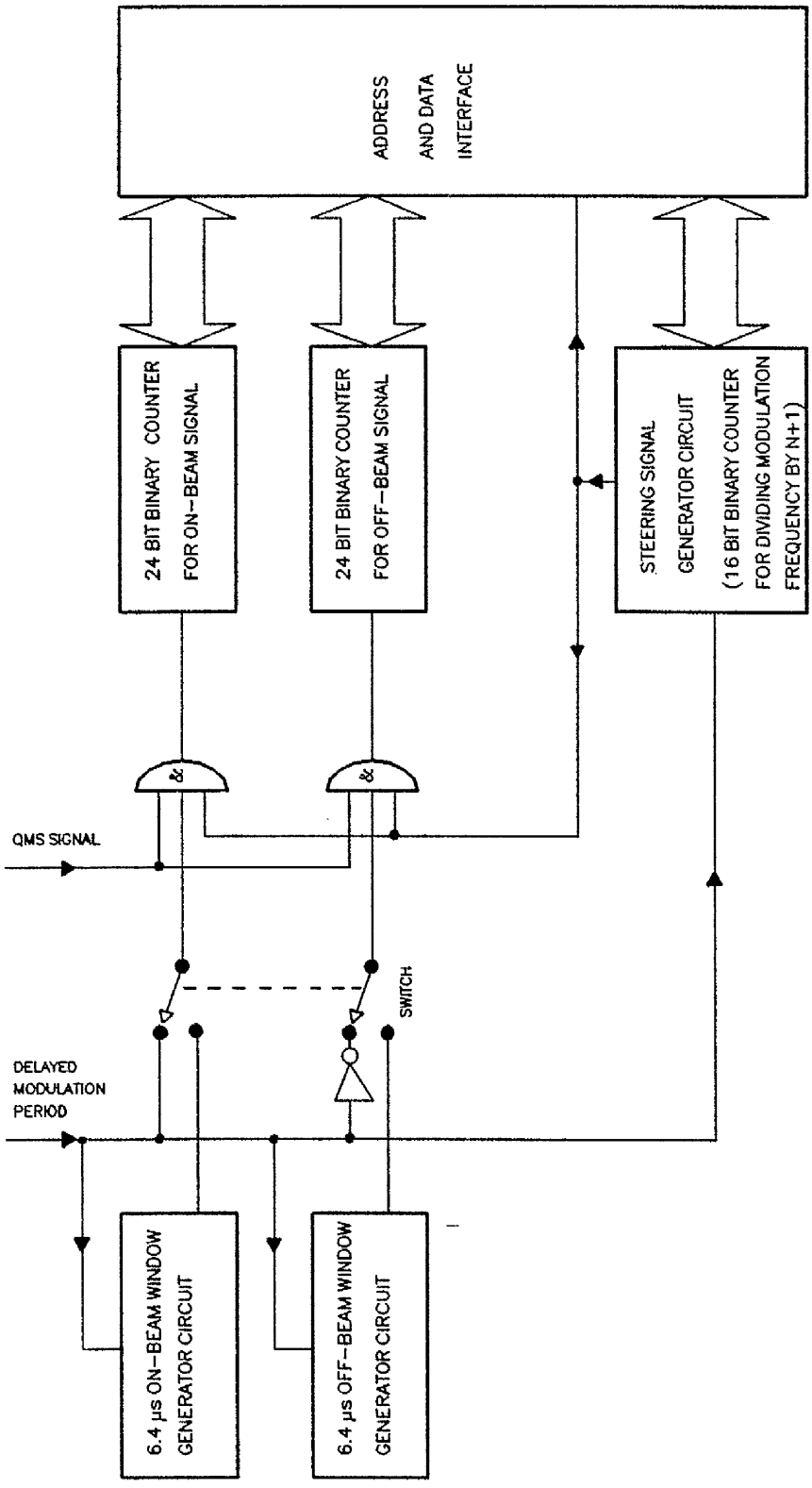

BLOCK DIGRAM FOR THE DIGITAL PULSE COUNTING CIRCUIT

FIGURE C.1

using octal tri-state buffers type 74LS244 and 8 bit latches type 74LS373 where data needs to stored for the peripheral devices as on the 16 bit counter for the steering signal.

Figure C.2 shows a detailed circuit diagram for the pulse counting circuit. The delayed modulation signal provided from the digital delay circuit is used to provide a 6.4 us window for both the on-beam and off-beam signals. A 2.5 MHz signal provided from the clock system shown on figure D.3 is used to feed the down count inputs of the 4 bit binary counters type 74LS193 (IC23 and IC24). These counters are loaded synchronously with the delayed modulation signal so that the preset count (equal to 16 in this case) is initiated through the provision of the pulses at LDon and LDoff. The 6.4 μs on-beam and off-beam windows are produced at the outputs Won and Woff respectively. These signals are shown on figure 4.12 For each of the on-beam or off beam signals, the steering signal is provided by the divide by N+1 binary counter composed of 74LS193 counters (ICs 5,6,7,8). The signals from the ion pulse amplifier, the steering signal circuit, and from either the 6.4 μs window circuit or the delayed modulation period (inverted in the case of the off beam signal) are fed to a 3 input AND gate so that the count can take place. This is carried out through a 24 bit binary counter comprising 74LS393 integrated circuits (ICs 10,12 and 14 for the on-beam signal and ICs 16, 18 and 20 for the off-beam signal). Overflow on these counters is monitored through

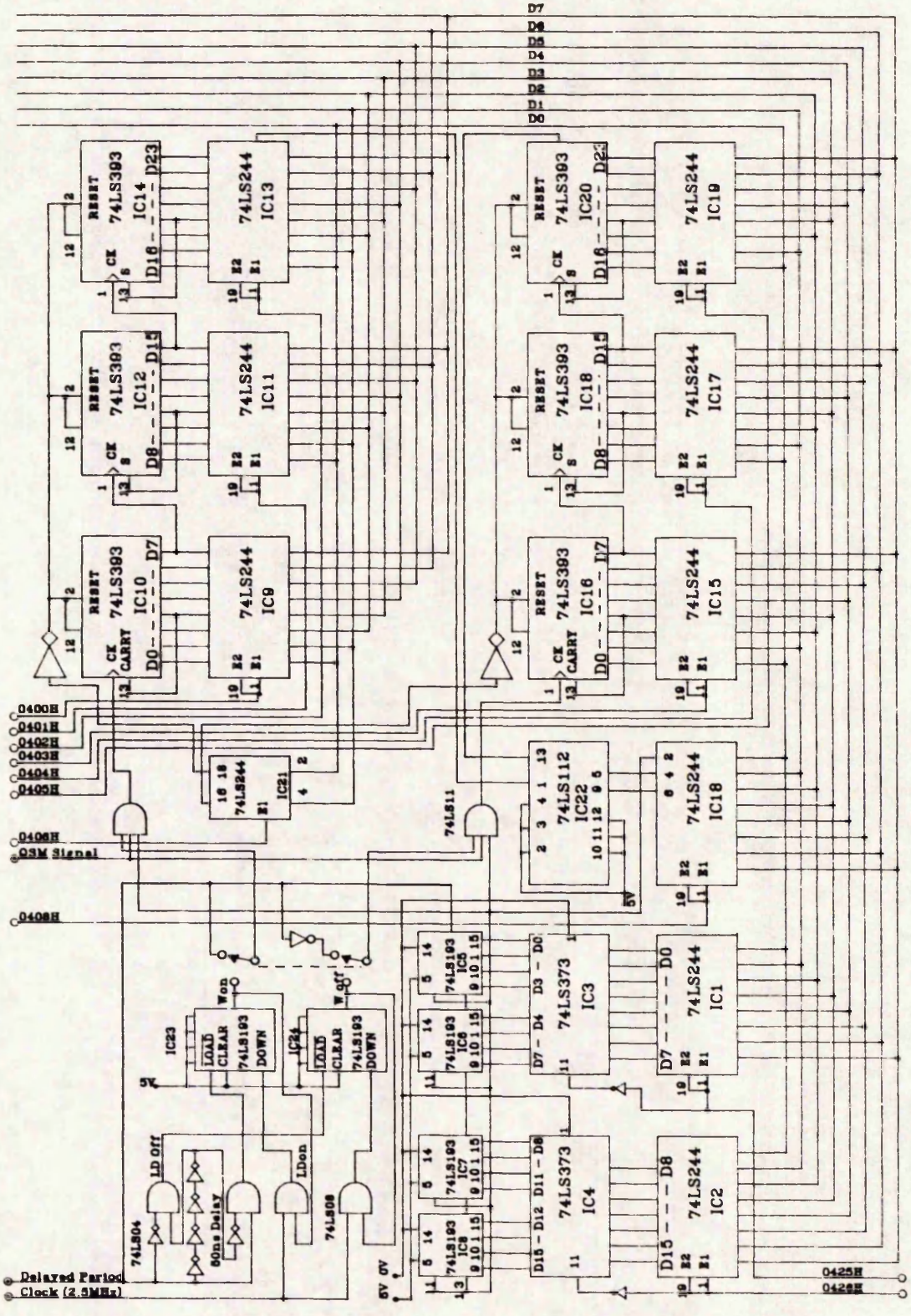

CIRCUIT DIAGRAM OF THE MASS SPECTROMETER ION PULSE COUNTING CIRCUIT

FIGURE C.2

the use of JK negative edge triggered flip-flop type 74LS112. The overflow signal is fed to the computer data bus through IC25 (type 74LS244). This is undertaken at address 0408HEX and is also used to monitor the state of the steering signal for initiating the read cycle of the TDS Forth computer as shown in figure 4.13. The 24 bit counter is reset by strobing address 0406HEX. The allocation of the addresses in the memory for controlling the pulse counting circuit is included in figure A.3.

Software control for the pulse counting circuit is undertaken by using relatively simple Forth routines. Figure 4.13 outlines the procedure executed to read and reset the counters according to the state of the steering signal. Routines have also been developed to add and substract 24 bit numbers according to the task at hand. This is mainly used for calculating the demodulated ion count and unbiased averaging on a set of individual measurements. The read cycle of the Forth microcomputer for two 24 bit numbers (one read as a 16 bit number) together with the time taken to read the overflow and steering signals and resetting the counters is found to take less than 409 μs (this is half the period of the steering signal produced with a division by 100 of a 122.2 Hz modulation frequency). This sets a lower limit on the steering signal period that needs to be produced. At a modulation frequency of 122.2 Hz, a steering signal period equal 1.636 s (200 times of the modulation period), an accumulation of 50 ns

ion pulses using windows equal to half the modulation period leads to a maximum allowable count of $8.183\ 10^{6}$ before an overflow is detected. When the 6.4 us windows are used with Fm=1018.2 HZ and a steering period equal to 1000/Fm this limit is equal to $6.4\ 10^{4}$.

APPENDIX D

THE DIGITAL DELAY CIRCUIT

The digital delay circuit has been developed in order to provide a variable time delay for the particle beam modulation signal derived from the phototransistor circuit shutter sensor[D.1]. The provision of this time delay is necessary since particles passing between the rotating shutter and the mass spectrometer electron multiplier have different transit times which affect the measurements on the particle number density. A variable delay is needed to optimize particle density measurements as well as providing important information about evaporation kinetics (chapter 7).

Circuits used for the delay of digital signal have been described by several authors [D.2, D.3, D.4] but either the precision of the time delay (or signal phase shift) or ease of instrument control poses difficulty. When the cost to performance ratio is not a primary importance commercial delay generators achieving delay steps below 3 ns can be obtained [D.5]. Recent work involving the use of custom

integrated circuits for the development of digital delay generators has been described by Mattausch et Al [D.6]. The circuit developed for the present work is dedicated to the modulated beam mass spectrometry system and simple procedures for delaying the shutter sensor signal are obtained coupled with high precision and large bandwidth.

The block diagram for the circuit developed is shown on figure D.1. The analogue signal from the phototransistor detector circuit is first made compatible with the TTL logic levels. The resulting signal is a digital form of the signal locked at the modulation frequency. The reference signal frequency at A is multiplied by 2 and this generates a signal at B which triggers a 20 bit down counter for the high frequency signal at C. The count length is set by the TDS microcomputer through interface buffers and latches which hold the preset count. A control line is also provided to enable the initialisation of the count sequence at D. The 20 bit counter underflows at the end of each preset count and the underflow signal at F is divided by 2 with reference to the signal locked at the modulation frequency. This provides the output signal for the digital delay circuit.

A detailed diagram of the circuit is shown in figure D.2. The presettable 10 bit counter is made of five 74LS193 4 bit counters (ICs 9, 10, 11, 12 and 13). The count sequence is preset by 74LS373 type 8 bit latches (ICs 2, 4 and 6) and 3 octal tri-state buffers type 74LS244 (ICs1, 3

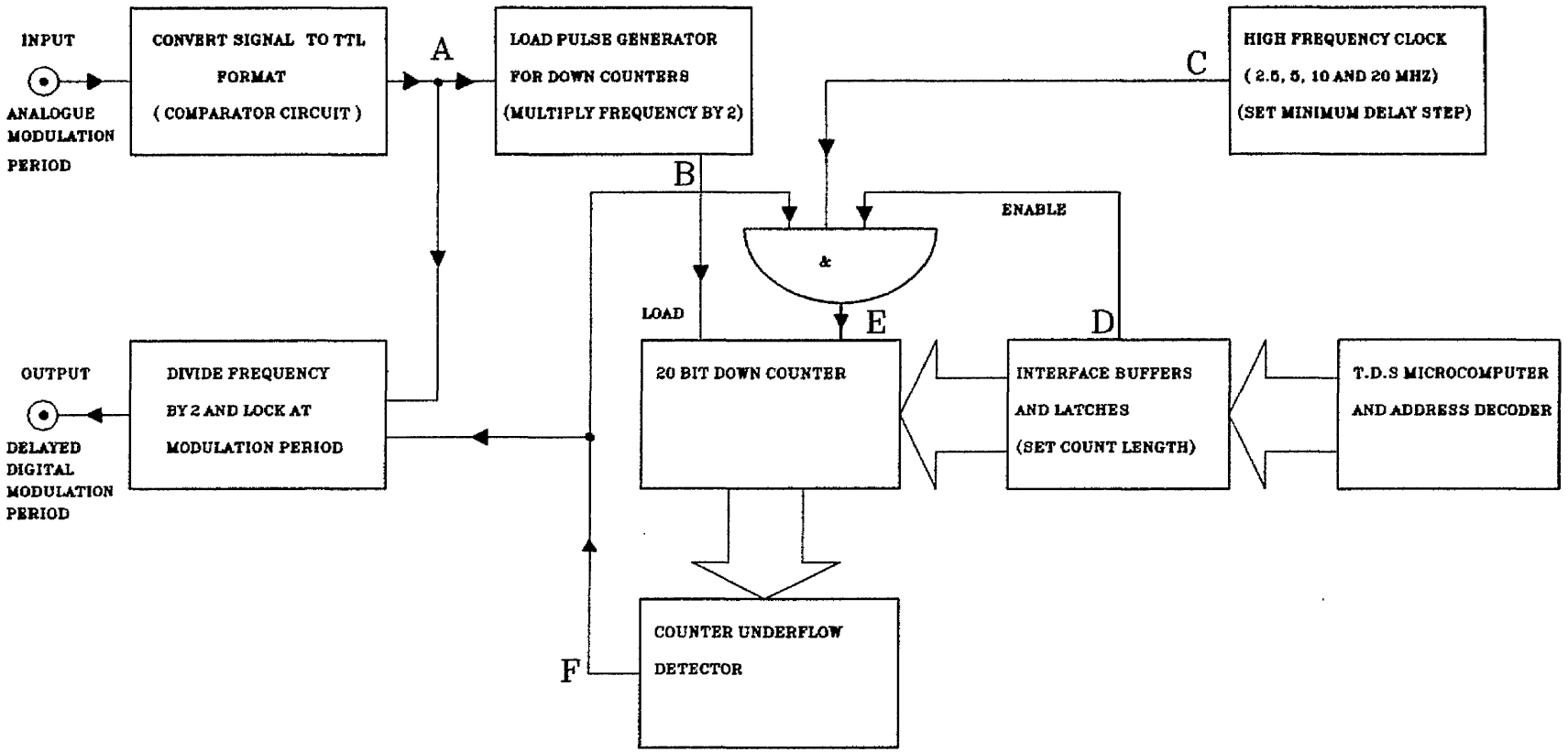

BLOCK DIAGRAM OF THE PROGRAMMABLE DIGITAL DELAY CIRCUIT

FIGURE D.1

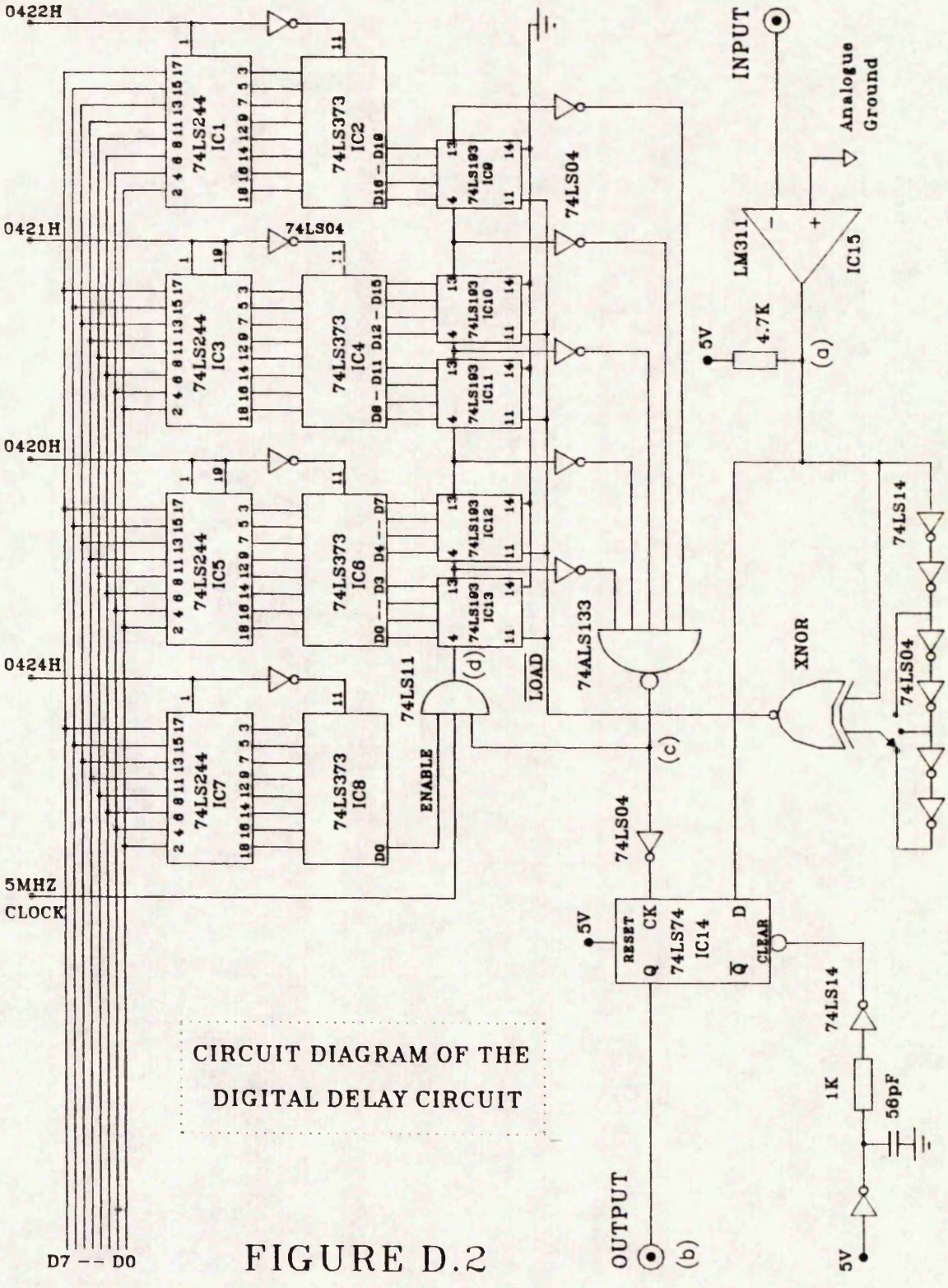

CIRCUIT DIAGRAM OF THE
DIGITAL DELAY CIRCUIT

FIGURE D.2

and 5) are used to extract the data from the data bus. These are addressed in the TDS microcomputer memory at addresses 0420HEX, 0421HEX and 0422HEX. At address 0424HEX FORTH octal buffer (IC7) driving a latch (IC8) is used to enable the initiation of the count sequence.

IC15 is an LM311 comparator and its output is a digital version of the signal locked at the modulation frequency. The 74LS193 down counters are triggered by driving their load input with a signal generated by the XNOR circuit. This signal triggers the counters on both the rising and falling edge of the modulation period with pulses which have widths that can be selected from 20 to 60 ns. These pulses occur at a rate equal to twice the modulation frequency. The NAND gate type 74ALS133 is used to detect the end of the count sequence after the occurance of each load pulse. IC 14 D type flip-flop (74LS74) with its clock input driven by the pulses which are set between the occurance of the load pulses and the end of the count sequence, is used to generate the delayed modulation period. This is equivalent to dividing the rate of these pulses by 2. False phase triggering at its output is prevented by providing a circuit which clears when the supply is switched on and also by feeding the undelayed modulation period to its set data input. The high frequency signal that is counted to produce the delay is supplied from a clock system developed for this purpose. Figure D.3 shows a detailed diagram of this circuit and Figure D.4 shows a photograph of the oscilloscope traces obtained from on the digital delay

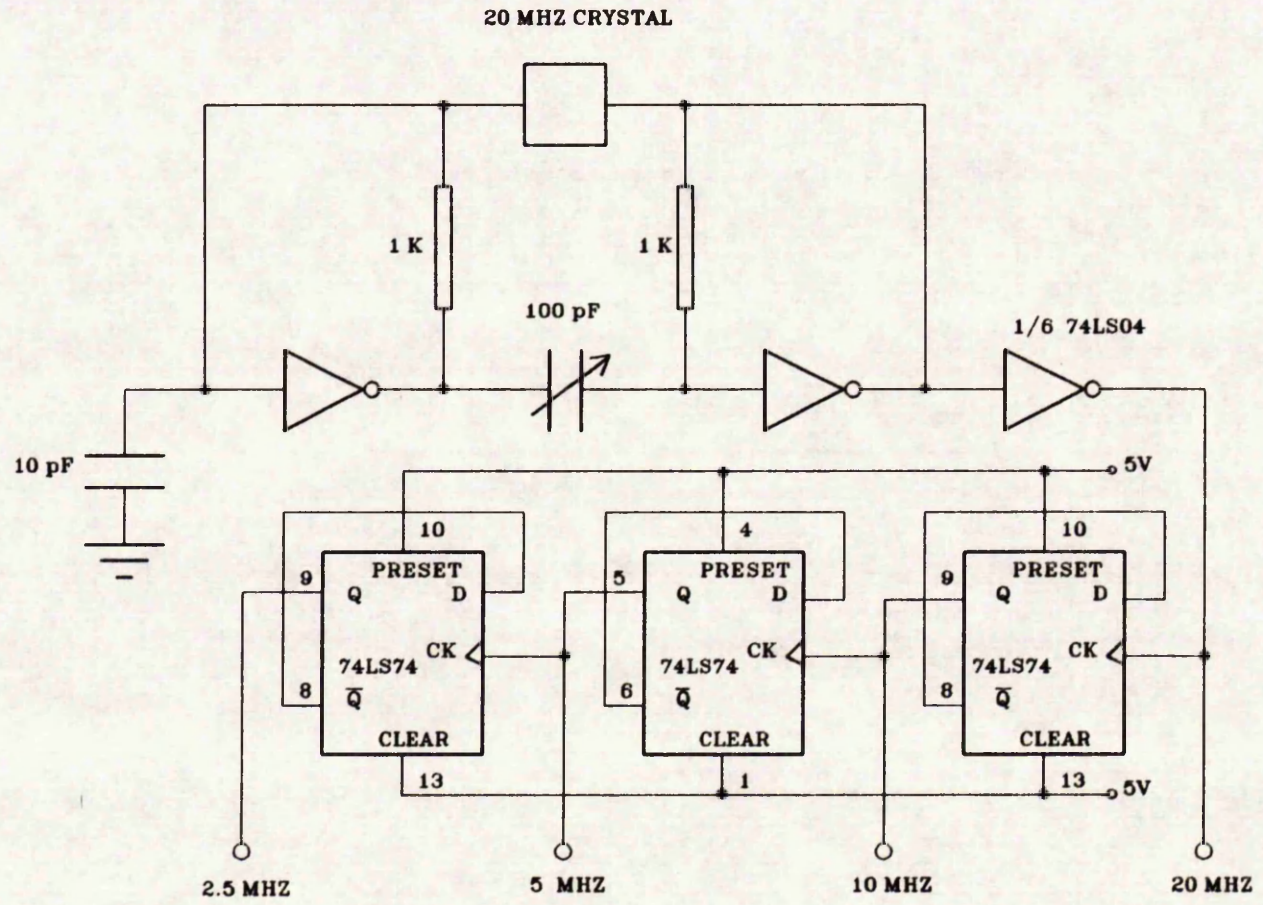

CIRCUIT DIGRAM OF THE MULTIFREQUENCY CLOCK SYSTEM

FIGURE D.3

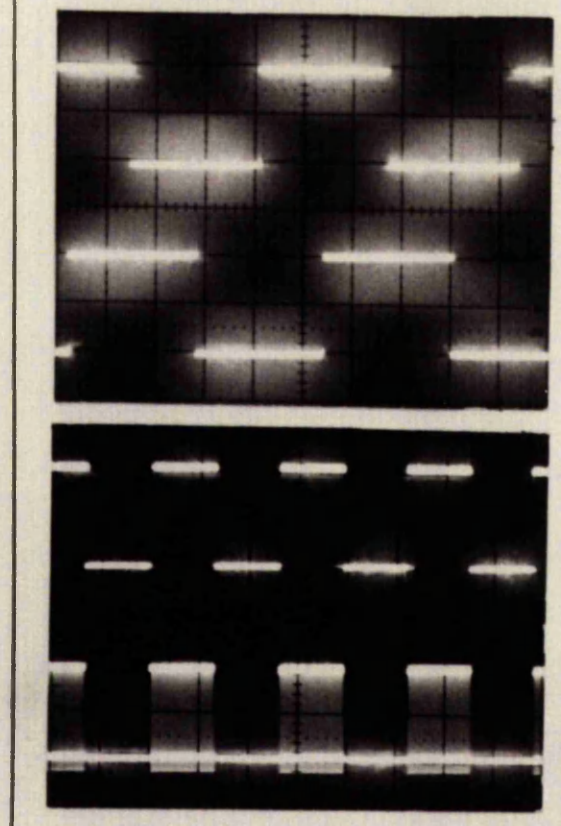

(a)
INPUT SIGNAL
(Frequency=200 Hz)

(b)
DELAYED OUTPUT SIGNAL

(c)
SIGNAL OBTAINED FROM ANDing THE COUNTERS BORROW OUTPUT

(d)
0.2μS CLOCK PULSES ANDed WITH THE SIGNAL AT (c) AND FED TO THE L.S.B BINARY COUNTER
(Delay by 6480 HF clock pulses)
(for a delay of 1296 μS)

2.2 Volts

1 mS

DIAGRAM SHOWING THE OSCILLOSCOPE TRACES OF THE SIGNALS OBTAINED FROM THE DIGITAL DELAY CIRCUIT.

FIGURE D.4

circuit at the illustrated points (a), (b), (c) and (d).

With a 20 bit counter constituted of five 4 bit 74LS193 binary counters the maximum frequency which could be used is 5 MHz. This is because of the delay inherent to each counter which can be as much as 21 ns [D.7] and a higher frequency operation leads the the underflow outputs on the counters not triggering synchronously at the end of the count sequence.

Increasing the clock frequency necessitates cutting down on the number of counters cascaded. Load pulses with widths equal to 56 ns are used. When faster devices than the TTL LS type are used the clock frequency can increased as well as the number of counters used in cascade.

The minimum delay step attainable with a clock frequency of 5 MHz is equal to 200 ns. The range of modulation frequencies is from 20 to 1040 Hz. The delay capabilities of the circuit is from 200 ns to 2.097 s. Driving the digital delay circuit through the TDS FORTH microcomputer is simple and requires loading this allocated memory addresses (figure A.3) with a number (20 bits wide) which represents the number of clock pulses by which the modulation signal will be delayed. Routines have been developed to generate continuously variable delays with a view to studying the effect of the reference signal time delay on the ion count (chapter 7).

APPENDIX E

CONTROL SOFTWARE FOR THE MASS SPECTROMETER

In mass spectrometers a choice can be considered on whether it is the peak height [E.1] or the area under the peak [E.2] which yields an appropriate measure of the peak intensity. Also, the peak position (or tuning voltage) can be considered as the tuning voltage value where the maximum intensity [D.1] or the peak centroid [E.3] occurs. In the modulated beam mass spectrometry employed, the low fluctuations observed on the ion counts for the peaks maxima and the on-line process needed for the experiments undertaken led to the choice of the peak maximum as the measure for the number density at a given mass-to-charge ratio and the peak position as the tuning voltage (or digital number from DAC) where the ion count is maximum. Recent work on mass spectrometer peak finding using Forth has been described by Kristo et al [E.4].

The QMS used is driven by a 14 bit DAC which generates 0 to 5 volts for tuning over a range of 0 to 200 a.m.u. Over 81 tuning digits (digital numbers from DAC) are therefore available for each mass-to-charge ratio. Arithmetic routines for 32 bit numbers have been developed for processing the ion counts from the spectrometer. The software developed includes a combination between calibration of the mass spectrometer tuning and a peak finding algorithm. Other features such as switching from one mass-to-charge ratio to another are also included using simple routines which rely on those used for finding the peaks.

E.1 CALIBRATION OF THE MASS SPECTROMETER TUNING

An initial calibration is undertaken using a full spectrum scan. The peaks tuning digital numbers and ion counts are recorded by examining the peaks shape. A least squares linear regression is applied to the data consisting of the obtained peaks maxima tuning digital numbers $d_{(m/e)n}$ and corresponding mass-to-charge ratios $(m/e)_n$. The relationship obtained is: $d_{(m/e)n} = A.(m/e)_n + B$ where A and B are calculated constants from the least squares fit.

For updating the calibration equation N_2^+ (m/e=28) and H_2^+ (m/e=2) peaks are used as references and

their tuning digits and mass-to-charge ratios are used to update or correct the calibration equation at the beginning of each deposition experiment. A description of a calibration equation for tuning the mass spectrometer has been included in previous research [D.1].

E.2 THE PEAK FINDING PROGRAM

The calibration equation for tuning the mass spectrometer is not exactly linear [E.5] and a further search for the peak maximum at a mass-to-charge ratios (different from those for the reference peaks) is required. Experience in using the mass spectrometer the present research has shown that the calibration equation yields tuning digits within 20 LSB (least significant bits) of the actual tuning digit required for the peak maximum. This imposed a search for the peak maxima within at least 25 LSB from the value obtained by using the calibration equation. The profiles for peaks obtained at 2 MA filament emission current setting have been considered. Of importance is rapid acquisition time of the peak maximum combined with high accuracy in the search method. A method has been chosen where the peak maximum is searched by partitioning the samples taken through a range including Rt tuning digits on both sides of the tuning digit obtained from the calibration equation. When a tuning digit, dst, for a particular mass-to-charge ratio is obtained from this

equation, samples are taken from dst-Rt to dst+Rt in steps equal to an integer Ind. In most of the present work Rt has been chosen equal to 30. Figure E.1 shows the peak profile for m/e=2 (H_2+).

It can be seen that for samples to be obtained near the peak maximum Ind has to take a small value such as 5. Figure E.2 shows the main control algorithm where subsequent scans are undertaken by calling the search routine which is shown in figure E.3. The values for Rt and Ind can be changed where appropriate. In the partitioning algorithm shown a range of 61 tuning digits is scanned (dst-30 to dst+30) but only 19 ion counts are accumulated to find the peak maximum. A threshold count Thc is introduced so that ion counts which do not differ by more than Thc are considered equal and ion counts below Thc are ignored. Thc is chosen below 1.5% of the peak intensity.

The peak finding routine is also used in time-of-flight experiments where an approximate value for the ions arrival time is used before the search routine is called.

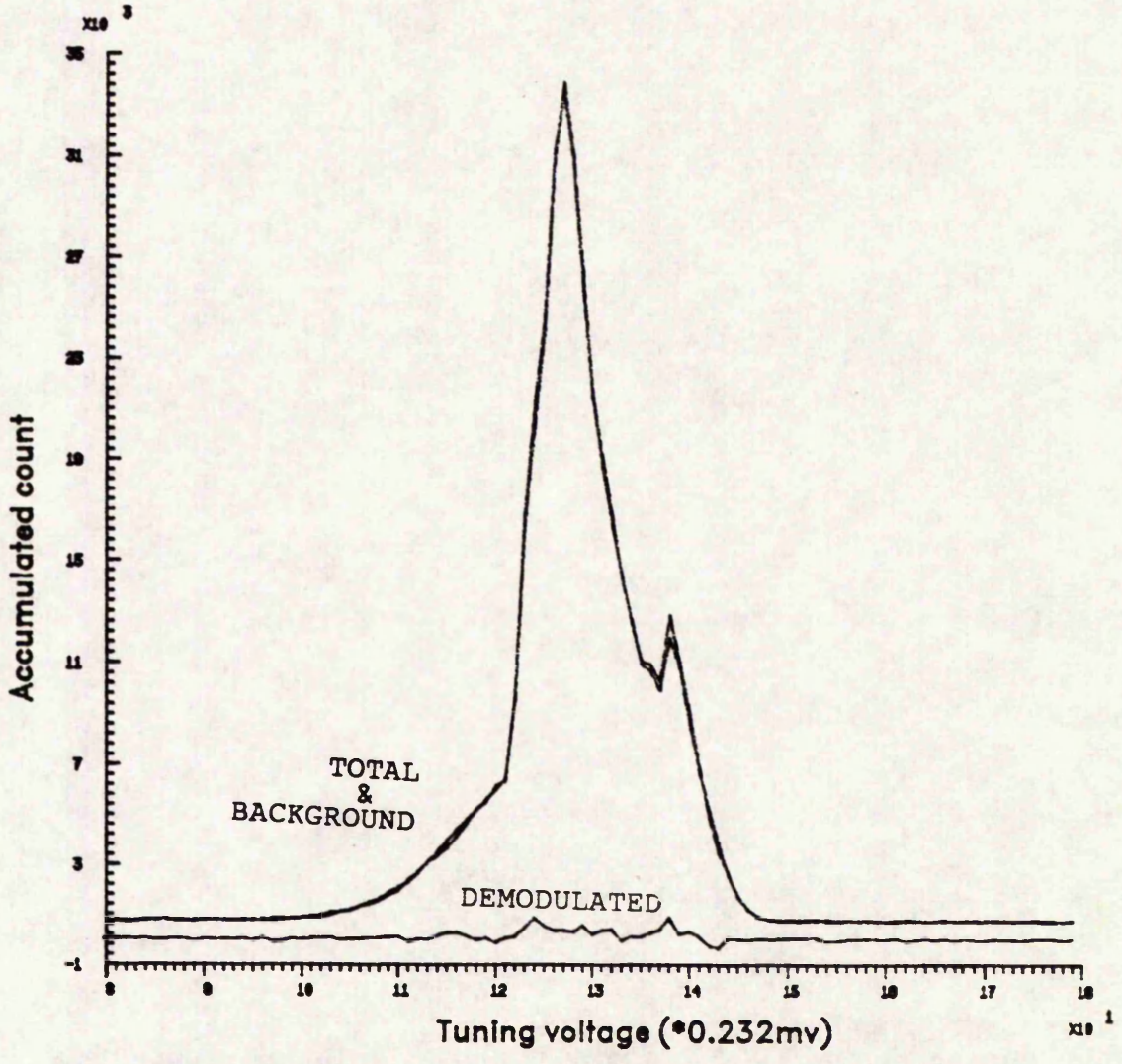

H_2^+ DIRECT, BACKGROUND AND DEMODULATED PEAK PROFILE AT 800 DEGREES CELSIUS AND 2MA EMISSION CURRENT

FIGURE E.1

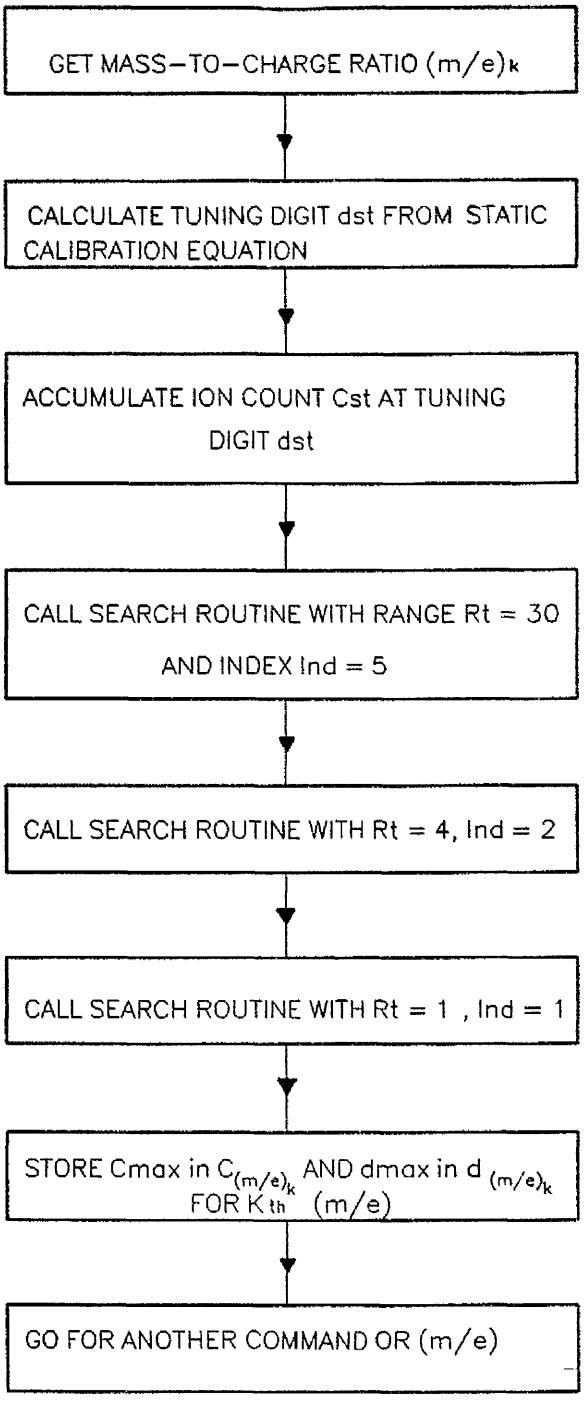

FLOWCHART OF THE PEAK FINDING ALGORITHM

FIGURE E.2

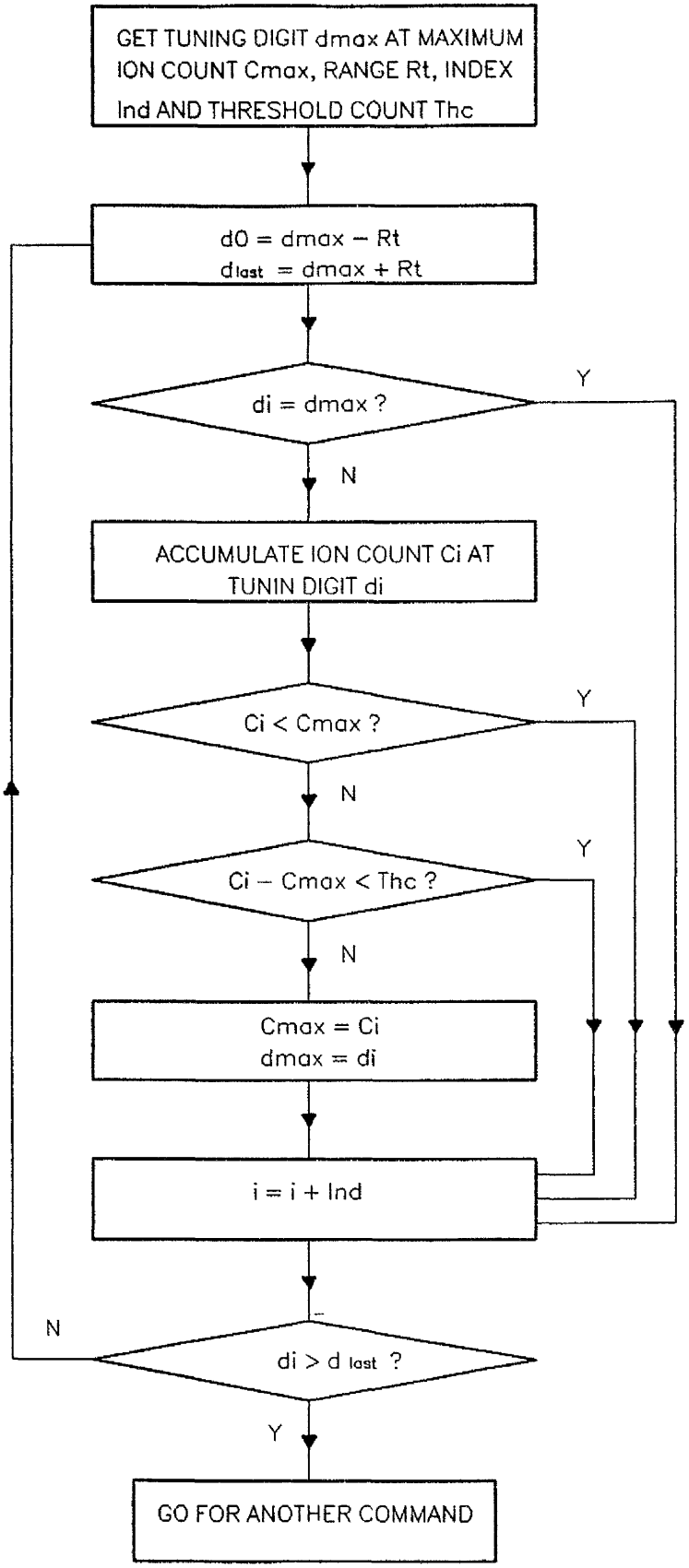

FLOWCHART OF THE SEARCH ROUTINE

FIGURE E.3

APPENDIX F

CONTROL SOFTWARE FOR THE QUARTZ CRYSTAL MICROBALANCE

Control of the quartz crystal microbalance, is performed using small Forth routines which allow the acquisition of a count proportional to the evaporant particles deposition rate over a short period of time.

The frequency of the quartz crystal is divided by N equal to 64.10^5 to produce an interrupt signal which is used to accumulate pulses from a reference clock running at a frequency f_r = 48 MHz when it is high. The oscillation frequency of the quartz crystal before material loading is 5 MHz. The control signals used for the microbalance control are included in figure A.3. The procedures undertaken for controlling the microbalance are described in figure F.1.

The minimum number of counts C_b required for a deposition rate measurement is 2. Averaging is undertaken on deposition rate measurements by recording several counts (up to 6 in the present experiments). This helps reducing

fluctuations on the measured counts. When the crystal fails to oscillate, the experiment is aborted and a new crystal is required. However, this only happens after several deposition runs (typically 4 to 5 runs) each requiring films at least 2 microns in thickness. At the end of a count sequence a strobe is produced to transfer the counts from the counting circuits to the memory of the TDS microcomputer.

An average difference $\triangle C_b$ for each two successive counts is calculated as well as an average count C_b of the two counts. The average time between two successive counts $C_{b\,n}$ and $C_{b\,n-1}$ is: $ta=(C_{b\,n}+C_{b\,n-1})/2f_r$.

The deposition rate is obtained by dividing the mass deposited by the density of the material. For ZnSe the density ρ_f= 5.42 g/cm^3 and the deposition rate in pm/s is calculated using: $5.4(C_{b\,n}-C_{b\,n-1})/ta$ deduced from equations (3.2) and (3.4).

The time taken for reading and storing counts is negligible when compared to the time taken for the accumulation of the 26 bit counts C_b (>0.64 s). The steering signal is used to initiate and halt the deposition rate measurements so that the microprocessor can be used for other tasks (ion count measurements, digital delay setting,...etc).

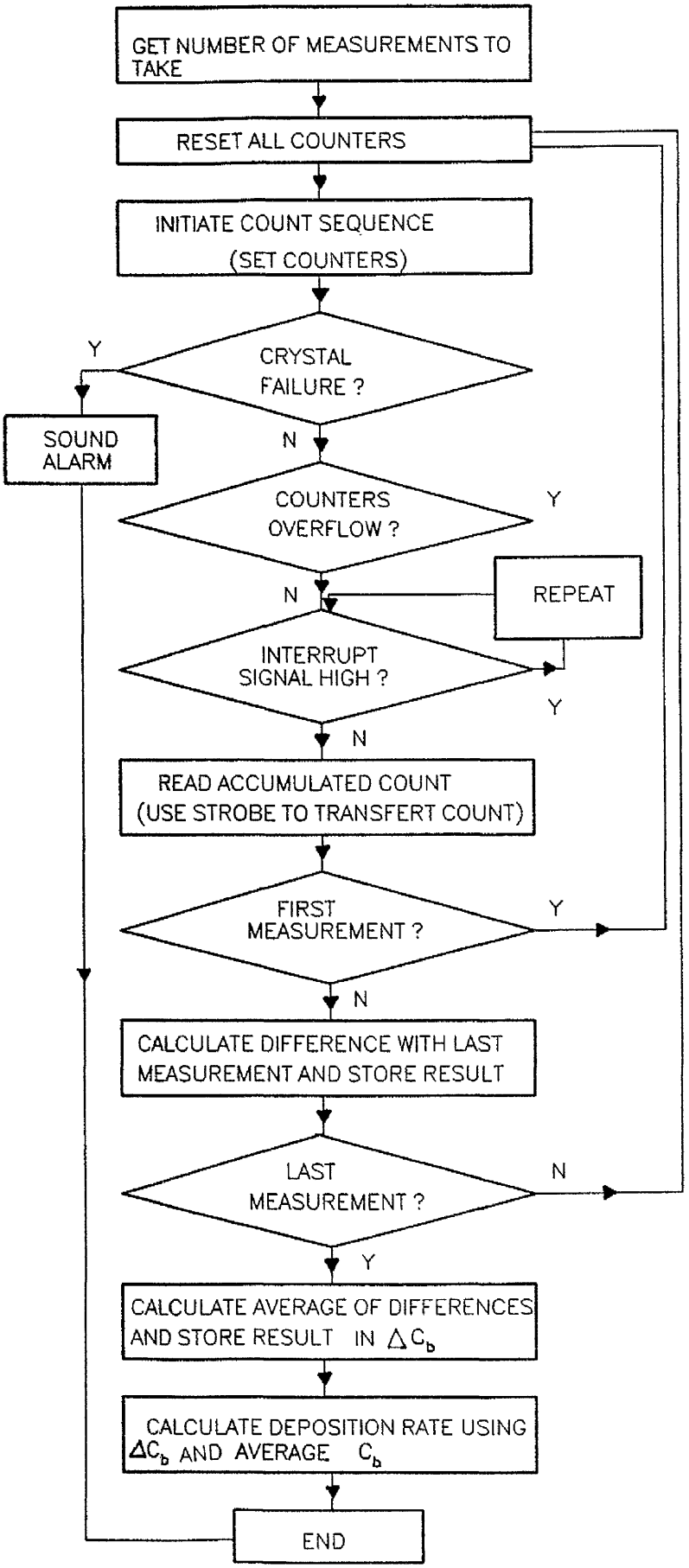

FIGURE F.1

FLOWCHART OF THE MICROBALANCE CONTROL PROGRAM

REFERENCES FOR APPENDICES A,B,C,D,E, AND F

[A.1] STAG ELECTRONICS DESIGN LTD.
Stag House Tewing Court Welwyn Garden City
Hertfordshire UK

[A.2] HEWLETT PACKARD COMPANY
16399 W.Bernardo Drive San Diego Cal. U.S.A

[B.1] ANALOG DEVICES
Two Tecnology Way, P.O. Box 280 Norwood, MA U.S.A

[D.1] M.BENYEZZAR
MSc Thesis University Of Manchester (1986)

[D.2] V.S.BATRACHENCO AND T.V.ZARUBINA
Pribory i Tekhnika Eksperimenta
No5 pp.171-172 (1978) (Plenum Pub. Press)

[D.3] F.MOMO, G.A.RANIERI, A.SOTGIU AND TERENZI
J. Phys. E: Sci. Instrum. p.1253 (1981)

[D.4] L.BRUSCHI, R.STORTI AND G.TORZO
Rev. Sci. Instrum 58(10) pp.1060-1961

[D.5] STANFORD RESEARCH SYSTEMS
"Four Channel Digital Delay Generator, Model: DG535"
1290D Reamwood Avenue, Sunnyvale CA 94089 (USA)

[D.6] H.J.MATTAUSCH, F.MATTHIESEN, J.HARTL, R.TIELERT AND E.P.JACOBS
IEEE J. SOLID STATE CIRCUITS VOL.23 (1) (1988)

[D.7] THE TTL DATA BOOK
Vol.1 and 2 Texas Instruments 9th edition (1985)

[E.1] A.S.SAHIN
MSC Thesis University of Manchester (1980)

[E.2] A.JANIK
J. Chromatogr. Sci. Vol.13 p.93 (1975)

[E.3] J.R.HALLIDAY
In "Advances In Mass Spectrometry" Ed. E.Kendrick
Vol.4 p.239 Institute Of Petroleum (1968)

[E.4] M.J.KRISTO AND CHRISTIE G.ENKE
Int. J. Mass Spectrom. And Ion Processes
Vol.87 pp.141-155 (1989)

[E.5] A.S.SAHIN
PhD Thesis University Of Manchester (1983)

APPENDIX G

PUBLICATION 1

Copy of a paper presented at the 11th International Vacuum Congress (1989)
Published in Vacuum Vol.41 p.842 (1990)

Vacuum/volume 41/numbers 4–6/pages 842 to 846/1990
Printed in Great Britain

0042–207X/90$3.00 + .00
© 1990 Pergamon Press plc

Preparation of zinc sulphoselenide alloys using MBE

M Benyezzar, D King, P L Jones and D Moore, *Electrical Engineering Laboratories, University of Manchester, Manchester, M13 9PL, UK*

A project is being undertaken to prepare single crystal zinc sulphoselenide films with a refractive index profile determined by controlling the composition of the depositing material. The apparatus developed uses controlled co-deposition of the alloy constituents from two vapour sources, one containing zinc selenide and the other zinc sulphide. Closed-loop control is exercised over the rate of vaporisation for the alloy constituents from measurements made by a quadrupole mass spectrometer having a crossed-beam ion source. Accurate measurement of vapour particle number-densities requires the use of vapour stream modulation since the background levels from some of the species, especially those of zinc, are of a significant magnitude. The results of separating Zn and S components in the vapour from ZnS are shown and the effects of noise on the signal are demonstrated.

Introduction

The work to be described in this paper is aimed at the production of zinc sulphoselenide alloy films with a controlled composition profile for use in optical waveguide structures. Several workers have recently reported[1–4] the preparation of zinc sulphoselenide material using a number of techniques but the method chosen for the present work involves the co-deposition of film constituents in a molecular beam epitaxy system. Control is to be exercised over film composition by regulating the particle flux densities of the alloy constituents impinging on the substrate surface through governing the heating power fed to the vapour sources.

A number of options available for controlling film deposition have been considered including source temperature control[5], RHEED oscillations[1,6], Bayard–Alpert gauge total flux measurement[7] and a mass spectrometer for evaporant stream analysis[8]. Of these options, source temperature control lacks reproducibility and the Bayard–Alpert gauge flux density measurements are unable to differentiate between vapour species from compound sources. RHEED oscillations provide an accurate means for controlling molecular layer deposition and would be useful as a calibration tool for the present apparatus but the technique lacks the ability to differentiate between alloy components[9] and it is not particularly suitable in the film thickness range required (a micron or more).

The use of a quadrupole mass spectrometer offers the ability to determine flux density for specific vapour species as well as supplying information about the nature of the vapour particles. Several factors contribute errors to the measurements, including the presence of substantial background pressures for the constituents, the drift in sensitivity of the spectrometer[10] and the overlapping of spectra for zinc and sulphur. Vapour stream modulation provides a means for separating the contribution of vapour particles in the evaporant stream from those present in the ambient atmosphere[11]. Drift in sensitivity of the spectrometer may be overcome by periodic calibration against a quartz crystal microbalance measuring film deposition rate. To deal with the overlapping of mass spectra a technique has been proposed[12] where isotopic abundancy information is used to calculate the proportion of various molecular species present. A major problem with this approach is the magnitude of error introduced due to the level of noise present in the height of measured mass peaks.

The aim of this paper is to describe the system developed and some of the results obtained during depositions.

The apparatus

For the work to be described apparatus has been developed from a deposition system previously reported in detail[13]. Appearing in Figure 1 is a cross-section of the apparatus with all salient features labelled. A stainless steel uhv system with a 305 mm diameter work chamber forms the basis for the equipment. On the side of the chamber is mounted a three Knudsen cell assembly made by Vacuum Generators Ltd and on the opposite side is an oven to heat the substrate. The evaporant streams emitted from the Knudsen cells converge on the substrate surface where film material is deposited. Only the two horizontal Knudsen cells are used, one for ZnSe and the other for ZnS. Control can be exercised over the rate of effusion from the cells using measurements of evaporant flux density or deposition rate and provision is made for temperature control using the Pt/Pt–13% Rh thermocouples pressed against the bases of the crucibles holding the evaporant materials. Open ended crucibles are used and the conditions inside the cells differ considerably from those of equilibrium normally associated with Knudsen cell operation. Provision is made for controlling substrate temperature during film deposition.

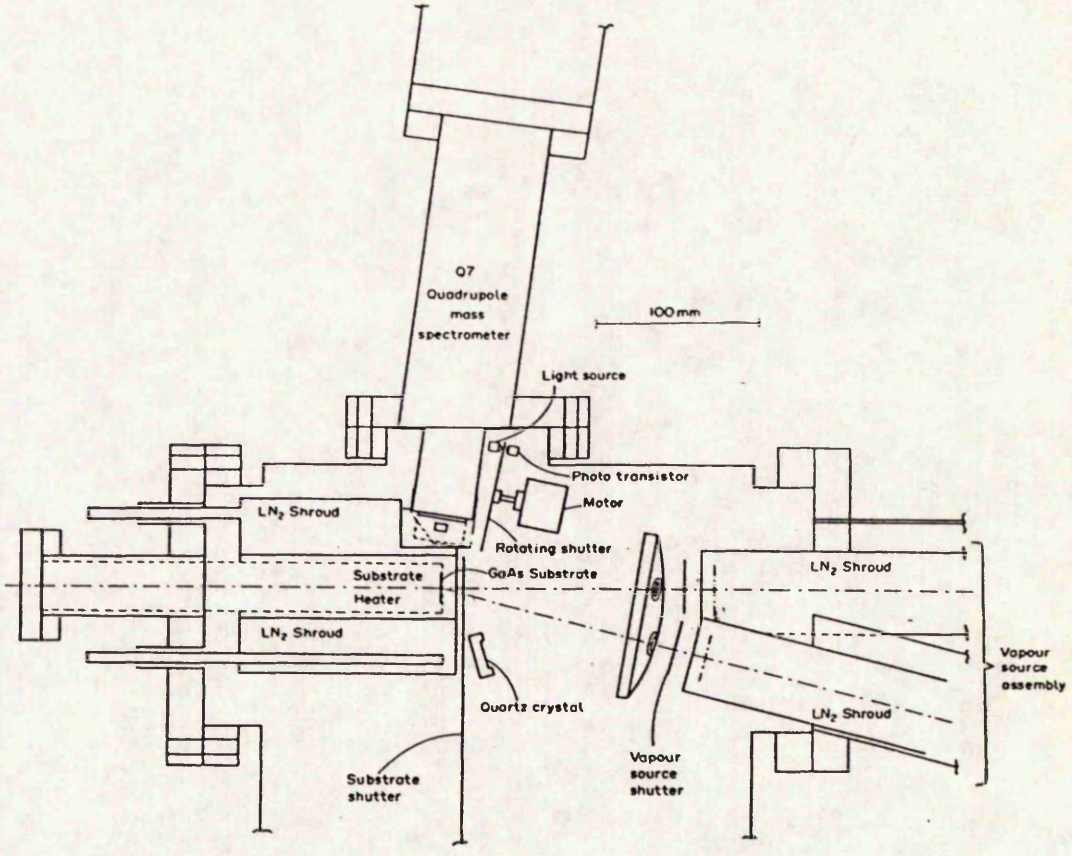

Figure 1. Cross-section of the ZnS–ZnSe deposition system.

For monitoring and controlling the deposition of film material a quartz crystal microbalance and a quadrupole mass spectrometer are installed in the system. The sensors for the measurement instruments are placed symmetrically with respect to the vapour sources and as near as practicable to the substrate surface. The water-cooled thickness-shear quartz resonator of the microbalance is in a position where it receives less vapour flux than either the substrate or the mass spectrometer and this results from the geometry of the system precluding its being mounted in an optimum position. Resolution of the microbalance in period measurement mode with a 5 MHz resonator is 6.5 fs, which represents an ability to detect changes in the thickness of ZnS films of 7.2 pm with a resolution on deposition rate of 1.4 pm s^{-1}.

The Q7 quadrupole mass spectrometer (Vacuum Generators Ltd) fitted to the system for determining the number densities of evaporant species is mounted in a cross-beam configuration to separate neutral vapour species from those that have become ionised. Vapour shielding is used to minimise contamination of the ionization chamber and quadrupole rods with evaporant material. Around the ionization chamber are extensive liquid nitrogen cooled surfaces designed to trap evaporant particles that come into contact with them. The electronic circuitry of the Q7 has been modified to provide a mass range of 200 amu, and ion-counting electronics added to overcome the effect of drift in gain inherent in secondary electron multipliers.

Modulation of the evaporant stream entering the Q7's ionization chamber is produced by shutter blades machined in the periphery of a rotating disc. The diameter of the stainless-steel shutter disc is 70 mm and the 8 shutter blades are 13.6 ± 0.05 mm wide giving effectively equal on and off periods for the modulated evaporant stream. Drive for the rotating shutter comes from a 3 phase synchronous ac motor, Ferranti type AER, with the speed of rotation governed from the frequency of the sinusoidal voltages applied to the motor windings. The speed range available from the motor is from 180 to 7800 rpm giving evaporant stream modulation frequencies from 24 to 1040 Hz respectively; although usable the high rotational speed exceeds that recommended for the motor. At low rotational speeds the motor reactances fall and damage due to overheating caused by the flow of large motor currents is prevented by adjusting the applied voltage using a frequency-based look-uptable stored in the control computer.

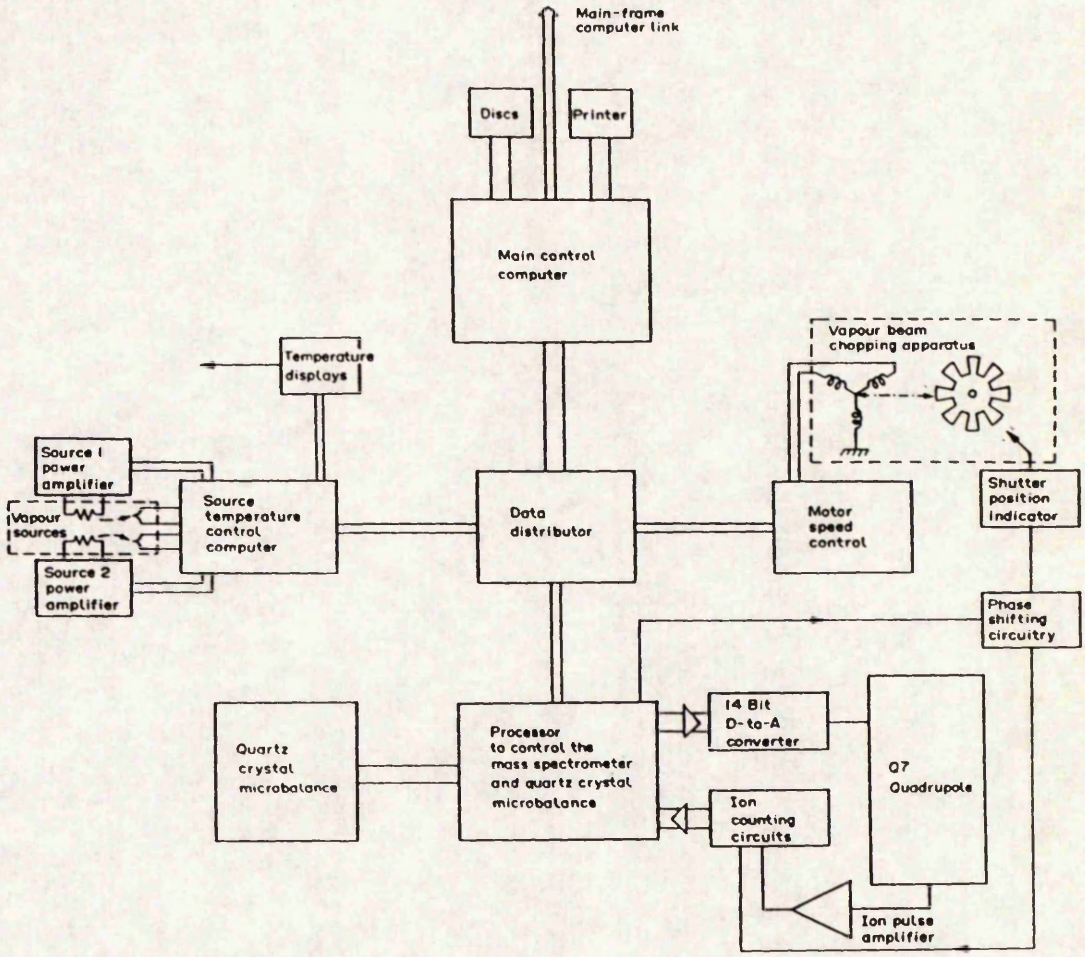

Figure 2. Schematic diagram of the electronic system used to control film deposition.

An optical sensor is used to synchronise gating of the ion counting circuits with the rotating shutter so that an indication of particle flux density for selected evaporant species can be produced. The sensor comprises of a photo-transistor and tungsten filament light source 4 mm apart and placed so that the shutter blades pass between them. Rotation of the shutter causes modulation of the photo transistor's collector current as the shutter blades periodically pass in front of the light source. A collimating slit, 300 μm wide, is placed in front of the light source and is aligned with the shutter blade edge to ensure transitions in collector current occur rapidly. At an evaporant stream modulation frequency of 244.4 Hz the transitions take 40 μs and a signal indicating the passing of a shutter edge is produced having an uncertainty of ± 1 μs.

Figure 2 shows the electronic system used with the apparatus. Almost all the facilities available are under computer control and provision is made for transferring results to external computers for analysis and display.

Number density measurements for particles in the evaporant stream

The number density for a selected vapour species is found by subtracting the density observed in the background (shutter closed) from the density obtained for the combination of evaporant stream and background (shutter open). To make the measurements it is necessary to accumulate separate counts for the open and closed phases of the shutter. Transit times for particles through the measurement system depend upon their mass and energy as well as the system geometry. The time of opening and closing the gates to the counters are specific to each vapour species and can be calculated in terms of a delay time t_d:

$$t_d = t_s + t_m + \phi/2\pi f \qquad (1)$$

where t_s is the delay introduced by the particle travelling from the rotating shutter to the secondary electron multiplier, t_m is

the response time for the multiplier and $\phi/2\pi f$ is a delay which depends upon the frequency of the evaporant stream modulation with ϕ a constant dependent on the geometry of the system and the position of the vapour source emitting the species of interest. Making some minor approximations the value fot t_s can be calcuated from:

$$t_s = m^{1/2}\left(\frac{d_1}{[2kT]^{1/2}} + \frac{d_2}{[2nqV]^{1/2}}\right) \quad (2)$$

where d_1 and d_2 are the distances from the ionisation chamber to the rotating shutter (24.3 mm) and the secondary electron multiplier (128 mm) respectively, T is the effective temperature of the particle, n the number of electronic charges q on the ion and V the acceleration potential (6.55 V) applied to ions prior to their passing through the quadrupole mass filter. Examples of t_s at a source temperature of 950°C for various ions are 71.4 μs for $^{64}Zn^+$, 79.8 μs for $^{78}Se^+$, 50.7 μs for $^{32}S^+$ and 112.8 μs for $^{64}Se^+$.

Calculating values for t_d proves difficult and, practically, the method adopted involves an experimental optimisation process to find the value of t_d maximizing the indicated number density for particles in the evaporant stream. Once determined the value of t_d for each evaporant species is stored for subsequent recall and use in tuning the measurement system. Corrections can be made to the value of t_d for changes in vapour source temperature, but for practical purposes it can be assumed constant at the modulation frequency of 122.2 Hz often used for making measurements.

Observations on ZnSe and ZnS vapour fluxes

Previous work[14], which involved controlling ZnSe depositions, without using modulated beam mass spectrometry, showed that a substantial background density of zinc particles was present and there were doubts about the materials not exhibiting congruent evaporation. Initial measurements made with the present system show that zinc particle densities in the evaporant stream can be separated from the background levels. An unexpected feature of the results is a significant background concentration of Se particles and Figure 3 shows a typical graph for $^{78}Se^+$. Observation of the background for Se using the shutter in front of the vapour source indicated that an ignorably small quantity of Se was present a short time after the shutter had been closed manually. In the case of the manual shutter a period of at least a few seconds elapsed before the measurement was made while for the rotating shutter an elapsed time of a small fraction of a second is involved The observed behaviour may be attributable to the rapid decay of Se particle concentration in the ionisation chamber when the evaporant stream ceases to flow.

Space charge accumulation effects in the ion source with high concentrations of particles were initially considered as a source of non-linearity. These effects have not proved significant in the present measurements and the presence of substantial background concentrations for particles would appear to account for non-linearity in the relationship between deposition rate and flux density observed without using evaporant stream modulation.

Determining the ratios of particle densities for species in the evaporant stream is necessary for controlling the effective composition of the vapour impinging upon the substrate. Measuring the contributions of Zn and S proves difficult because both make substantial contributions to the ion counts observed at relative ion-to-mass ratios of 32 and 64. To separate the ion counts for Zn and S the ^{64}Zn isotope has been used which has an abundancy of 27.9%[15] compared with the abundancy of 0.75% for ^{33}S. From measurements made on ZnSe vapour, which is free from overlapping spectra, the relative magnitude of peaks at 64, 33 and 32 have been found and Figure 4 shows the calculated ratios of ion counts for particle species obtained during modulated beam measurements. Noise in the signal produced by the mass spectrometer and its associated electronics leads to difficulty in measuring the ratio of $^{32}S^+/^{64}Zn^{++}$ because of the small count for $^{64}Zn^{++}$. Higher deposition rates lead to improved signal-to-noise ratio and this is critical in the determining of the concentration of sulphur in the evaporant stream. For comparison purposes the results of a ZnSe evaporation are shown in Figure 4 and the relative sensitivities for S and Se can be seen.

Conclusion

A measurement system suitable for controlling the co-deposition of ZnS–ZnSe films has been described. Modulated beam

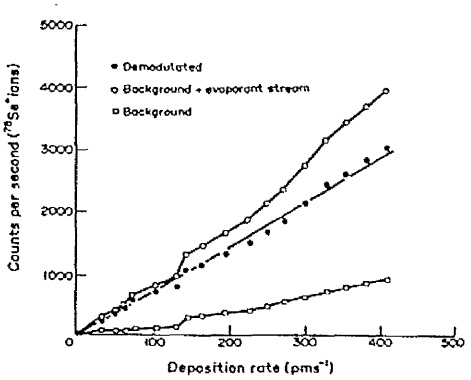

Figure 3. Particle count vs deposition rate for ZnSe.

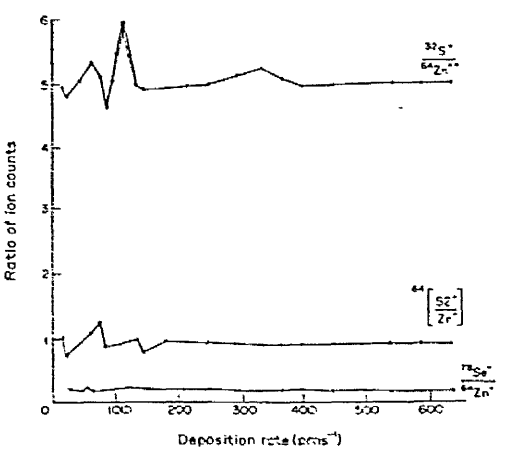

Figure 4. Ratios of ion species concentrations during the deposition of ZnS and of ZnSe.

mass spectrometry has been incorporated and it has proved necessary to use computers for controlling the measurement equipment and extracting the information needed for deposition control. Results obtained indicate the advantages of using modulated beam mass spectrometry for measuring the flux densities of constituents for ZnS–ZnSe alloys. Previous work showing variation of the selenium-to-zinc flux density ratio with changes of source temperature can be explained by the presence of significant background concentrations for the elements in the ionisation chamber of the mass spectrometer. Problems are experienced with making accurate determinations of the sulphur content in the vapour stream and this will limit the precision of deposition control during the preparation of ZnS–ZnSe alloy films.

Acknowledgements

The authors wish to thank Dr Tom Foxon of Philips Research Laboratories, Redhill for his help and encouragement at the start of the project. The work was undertaken with support from the Science and Engineering Research Council and one author (MB) has been supported by a grant from The Ministry of Higher Education (Algeria).

References

[1] H H Cornlissen, D A Cammack and R J Dalby, *J Vac Sci Technol*, B6, 769 (1989).
[2] H Kuwabara, H Fujiyasu, H Shimizu, A Sasaki and S Yamada, *J Crystal Growth*, 72, 299 (1985).
[3] H M Yates and J O Williams, *Appl Phys Lett*, 51, 11 (1987).
[4] A Yoshikawa, H Oniyama, S Yamaga and H Kasai, *J Crystal Growth*, 95, 572 (1989).
[5] P G Chilton, W S Truscott and Y F Wen, *J Vac Sci Technol*, B6, 1099 (1988).
[6] P J Dobson, B A Joyce, J H Neave and J Zhang, *Vacuum*, 38, 422 (1988).
[7] J Lilja, J Keskinen, M Hovinen and M Pessa, *J Vac Sci Technol*, B7, 593 (1989).
[8] R F C Farrow, *J Phys D*, 8, L48 (1975).
[9] D P Woodruff and T A Delchar, *Modern Techniques of Surface Science*, CUP, Cambridge (1986).
[10] C T Foxon, B A Joyce, R F C Farrow and R M Griffith, *J Phys D*, 7, 2422 (1974).
[11] R H Jones, D R Olander, W J Siekhaus and J A Schwartz, *J Vac Sci Technol*, 9, 1429 (1972).
[12] R P Gregory, P L Jones, D King and D Moore, *Vacuum*, 38, 737 (1988).
[13] A J Cooper, A S Sahin, P L Jones, D King and D Moore, *Vacuum*, 34, 925 (1984).
[14] A S Sahin, P L Jones, D King and D Moore, *Vacuum*, 37, 269 (1987).
[15] J Emsley (Ed), *The Elements*. OUP, Oxford. (1989).

APPENDIX H

PUBLICATION 2

Copy of a paper presented at the 2nd European Vacuum Conference (1990) To be published in Il Vuoto (1990) (Italian Journal Of Vacuum).

SPETTROMETRIA DI MASSA A RAGGIO MODULATO APPLICATA AL MONITORAGGIO DELL 'EVAPORAZIONE DI LEGHE DI SOLFOSELENIATO DI ZINCO

M Benyezzar, D King, P L Jones e D Moore
Laboratori di Ingegneria Elettrica
Universita di Manchester, Inghilterra

E'in corso di svolgimento un processo per la produzione di pellicole in una lega di solfoseleniato di zinco usando epitassi a raggio molecolare. La composizione della pellicola dovrà essere determinata dalla deposizione controllata dei componenti della lega provenienti da vapori di Zns e ZnSe. Le misurazioni della densità di flusso per le specie in evaporazione sono fatte con uno spettrometro di massa a quattro poli la cui fonte è uno ione a raggio incrociato ed i risultati ottenuti sono usati per controllare gli indici di evaporazione delle sostanze di partenza allo stato di vapore. La modulazione della corrente evaporante è resa necessaria per superare il problema delle alte pressioni dei materiali evaporanti.

Ci sono incertezze riguardo alle specie molecolari di selenio e zolfo presenti nella corrente evaporante ed all'effetto che le particelle di vapore multiatomico hanno sulla crescita della pellicola. Sono descritti due metodi per la misurazione del tempo di fuga (TOF) delle particelle. La combinazione tra la misurazione TOF e la regolazione dell'energia di ionizzazione consente l'identificazione delle specie molecolari presenti nella corrente evaporante. Sia il Selenio che lo Zolfo sono presenti principalmente sotto forma di dimeri, nonostante spettri di massa presi con un energia di ionizzazione di 70 eV sembrino suggerire la presenza principalmente di monomeri.

La sovrapposizione degli spettri di massa per lo zinco e lo zolfo rende difficile la separazione tra le densità delle particelle dei due elementi. Per superare il problema, si propone un metodo semplice di controllo di composizione a circolo chiuso per leghe di solfoseleniato di zinco.

MODULATED BEAM MASS SPECTROMETRY APPLIED TO MONITORING THE EVAPORATION OF ZINC SULPHOSELENIDE ALLOYS

M Benyezzar, D King, P L Jones and D Moore
University of Manchester, Electrical Engineering Laboratories
Manchester. M13 9PL. United Kingdom

Introduction

A project has been running for some time to produce zinc sulphoselenide alloy films with controlled composition profiles for use in electro-optic applications and in a study of the alloy formation process. The method of film growth adopted is molecular beam epitaxy using two compound vapour sources, one containing zinc sulphide and the other zinc selenide. Controlled codeposition on the substrate is used to determine film composition where the vapour fluxes impinging upon the substrate from the sources are regulated from vapour-species-specific measurements made using a quadrupole mass spectrometer.

Difficulty arises with evaporant particle density measurements because of the presence of sizeable residual background vapour concentrations for the film constituents. Evaporant beam modulation has been adopted to separate the particle densities arising from the flux and the background. A relatively simple modulation system has been developed and used for film deposition control /1/. Investigations using the particle beam modulation system have shown that it is capable of making time-of-flight (TOF) measurements which can be used to analyse the nature of neutral particle species emanating from the vapour sources. Extensive literature exists on modulated beam mass spectrometry and some of the major contributions to the field are cited in references 2 to 5.

This paper describes the salient features of the system developed for modulating the evaporant stream and processing the data obtained from measurements. Also described is an investigation using the system to identify the particles present in the vapour streams produced by the ZnS and ZnSe vapour sources.

The Apparatus

The equipment used for the present work is based on a Vacuum Generator's Ltd UHV system having a work chamber of 305 mm diameter. A description of the basic system has been published elsewhere /6/ and a brief outline of the additions made to permit the measurement of vapour flux density using a simple evaporant stream modulation arrangement has been described in the literature /1/.

Two Knudsen Cell vapour sources are installed in the vacuum chamber and they are disposed symmetrically with respect to the exposed area of the substrate. The evaporant streams are emitted horizontally and converge on the centre of the substrate deposition area. A modified Vacuum Generator's Q7 quadrupole is mounted with its ionization chamber 23 mm vertically above the top edge of the substrate and a high resolution (1.4 picometer per second for ZnS) quartz crystal microbalance is installed near to the bottom edge of the substrate. The quadrupole is positioned so that it receives equal vapour flux densities from the two vapour sources. The quartz crystal microbalance is included to provide a means for calibrating the particle number density measurements made by the spectrometer as well as supplying an alternative means for controlling the deposition of film materials.

The ion source for the Q7 is organised in a cross beam arrangement to minimise contamination of the ion source structure and quadrupole rods with evaporant material as well as preventing neutral vapour particles entering the

secondary electron multiplier used for ion current amplification. Extensive cryopanelling is deployed around the vapour sources, the substrate and the mass spectrometer's ionization chamber to remove volatile vapours and provide surfaces from which the components of zinc sulphoselenide alloys will not readily escape. This proves necessary because experience has shown that significant background pressures of zinc become established in systems used to prepare films containing zinc compounds.

Modulation of the evaporant stream is achieved using a rotating shutter driven by a three phase synchronous AC motor (Ferranti type AER) over a speed range from 180 rpm to 7800 rpm (modulation frequencies from 24Hz to 1040Hz). The shutter, which is attached to the end of the motor shaft, is a 70 mm stainless steel disc with 8 shutter blades cut into its periphery to give a 1:1 mark-to-space ratio for the modulated evaporant stream. Control was exercised over the machining of the shutter blades to ensure that a series of virtually identical vapour flux pulses are produced by the shutter. A signal indicating shutter position is required for processing the data obtained from the mass spectrometer. An optical sensor consisting of a tungsten lamp, photo transistor and 300μm collimating slit is mounted diametrically opposite to the point on the shutter which cuts across the path of vapour particles travelling between the vapour sources and the entry aperture of the spectrometer. Performance of the optical sensor and associated electronic circuitry is such that the passing of a shutter blade edge is indicated with an uncertainty of less than ± 1 μs at a rotation speed of 1833 rpm.

Determining the nature of particles in the evaporant flux requires the temporal analysis of the ion stream emerging from the quadrupole ion filter. A display of flux density for specific particle species is built up by sampling the pulses resulting from the stream of ions entering the secondary electron amplifier using an electronic window to gate the pulses into a counter circuit. The time

at which the sampling window occurs with respect to the output from the shutter position sensor is determined by a digital delay controlled by the computer programmed to gather data for TOF measurements. The duration of the sampling window can be pre-set and both the delay and width can be adjusted with a resolution of 200ns. Considerable fluctuations occur in the count accumulated during successive sample window periods and this arises from the random nature of the processes occuring in the spectrometer. As a consequence a large number of sample window counts are accumulated at each delay setting to form an average count. An example of typical working conditions with an evaporant stream modulation frequency of 812 Hz and a 6.4μs sample window is that the ion count from 1000 window periods is accumulated and a complete ion arrival curve, using 1μs delay increments, takes in excess of 6 minutes to produce. Making measurements over such extended periods requires the vapour sources are operated in thermal equilibrium to maintain constant flux density and this is easily achieved by the vapour source controllers used.

Calculation of Time-of-Flight for Vapour Particles

The time taken t_s for a particle of mass m to travel from the plane of the shutter to the input of the secondary electron multiplier in the spectrometer is:

$$t_s = \frac{d_1}{v} + d_2 \cdot \sqrt{\frac{m}{2nqV}} \qquad (1)$$

Where v is the velocity of travel for neutral particles towards the ionization chamber, n the number of electronic charges q on the ion and V the acceleration potential (6.55V) applied to ions prior to their passing through the quadrupole mass filter. The distances d_1 and d_2 are from the ionization chamber to the rotating shutter (24.3 mm) and to the secondary electron

multiplier (128 mm) respectively. Measurements are made of number densities for vapour particles and these can be used to indicate flux densities. Assuming the time taken to open the shutter is ignorably small and Maxwell's equation /7/ is combined with equation 1 then ion arrival curves can be calculated and the result appears in Figure 1 for a number of ion species.

For the purpose of determining the nature of species in the evaporant stream the TOF from the shutter to the ion source ($d_{1/v}$) is of interest. The ion transit time (ITT) through the quadrupole filter ($d_2 / \sqrt{\frac{2nqV}{m}}$) is of similar magnitude to the TOF even though the particle speeds involved are higher than the thermal speeds. Summing TOF and ITT gives the ion arrival time and a measure of this, for the case when the neutral particles are travelling at the most probable speed, occurs at the 57.2% point on the ion arrival curve. A complication with interpreting results arises from the mass of particles changing due to fragmentation in the ion source.

Measured Ion Arrival Curves

Figure 2 shows measured curves for ^{64}Zn and $^{160}Se_2$ which can be compared with those calculated for Figure 1. The overall delay t_d in the measured curves can be represented as follows:

$$t_d = t_s + t_m + \Phi/2\Pi f \qquad (2)$$

where t_m is the transit time for electrons in the multiplier (often ignorably small at less than 200ns) and $\Phi/2\Pi f$ is a delay dependant upon the frequency of modulation f and the geometry of the system. A value for Φ can be determined by making measurements at two modulation frequencies but often this is not required where comparisons are being made of TOF for various vapour species.

The correlation between measured and calculated flux arrival curves is surprising since it has been assumed the shutter takes negligible time to uncover the entry aperture of the ionization chamber. In practice the entry aperture is an 8 mm by 3 mm horizontal slot to accommodate the lateral displacement of the converging vapour streams. At the maximum speed of rotation the shutter takes 340μs to uncover the aperture completely and a considerably longer rise time for the measured ion arrival curve would have been anticipated. A possible explanation for the observed result is that the volume of the ionization chamber from which ions are extracted is small so the effective entry aperture is considerably less than the actual aperture.

An Alternative Means of Ion Arrival Time Measurement

Figure 2 has been obtained using a window period of 6.4μs and the noise on the waveform is considerable even though a long pulse accumulation time was used. Another way of obtaining TOF information involves using a sampling window equal to the open period for the shutter. That is T/2 where T is the modulation repetition period for the evaporant stream. Figure 3(a) shows the result of scanning the T/2 sampling window in 1μs steps through a complete modulation cycle and 3(b) shows the result of calculating the T/2 window behaviour from the 6.4μs sampling window results appearing on the same graph. For making individual measurements the T/2 window curve is easier to use but interpreting results is somewhat more difficult than the straightforward ion arrival curve. The maximum on the curve occurs when the flux density reaches 50% of the final equilibrium value and for a Maxwellian velocity distribution this represents particles having a speed some 8.8% higher than for those possessing the most probable speed. For the investigations on the vapourisation of ZnSe and ZnS, described in the following sections, the T/2 window curves have been used to measure ion arrival time and TOF.

Determining of the Nature of Selenium Vapour Produced from ZnSe

Mass spectra taken during the deposition of ZnSe films indicate the presence of zinc as a monomer and selenium as both a dimer and a monomer. The most abundant isotopes of zinc and selenium occur at atomic mass numbers of 64 and 80 respectively. Direct observation of selenium species containing more than two atoms is not possible because the tuning range of the mass spectrometer only extends up to a mass-to-charge ratio of 200 and peaks in the spectrum due to ^{80}Se and $^{160}Se_2^+$ may arise from fragmentation of larger molecules during the ionization process /8/. To determine the nature of the neutral atom giving rise to Se_2^+ in the spectrum ion arrival time measurements have been made over a range of ionizing electron energies from 12.5 eV up to 30 eV (appearance potential of Se_2, measured by the extrapolation method suggested by Reed /9/, is 13.25V). The ion arrival time observed for the species remains constant at 117μs while the calculated time for particles emitted from a source at 900^{o}C is 114μs. This result suggests the ion Se_2^+ originates from ionizing neutral Se_2 particles and that higher order selenium atoms are not present since the TOF would be considerably longer. Furthermore, the range of ionizing electron energies used could be expected to produce a range of fragments and changes would have been seen in the TOF if this had occurred.

Repeating a similar type of experiment on the Se^+ ion produces a measured ion arrival time of 108μs which is near to that expected for a particle travelling as a dimer between the shutter and ion source and as a monomer through the quadrupole filter. The experimentally measured time difference for Se_2^+ and Se^+ ions is 10μs and the calculated value is 12μs. Further evidence to support the proposition that Se^+ in the spectrum originates from Se_2 neutral particles is that the ratio of observed particle densities for Se_2^+ to Se^+ falls as the

ionizing energy of the electrons increases, the fragmentation process being favoured at higher energies. From the evidence gathered the vapourisation of ZnSe in the present system produces vapour species as follows:-

$$2\ ZnSe\ (solid) \rightarrow 2\ Zn\ (gas) + Se_2\ (gas)$$

Determining the Nature of Sulphur Vapour Produced from ZnS

Repeating the measurements made for ZnSe on ZnS is complicated by the overlap of spectra for zinc and sulphur. The most abundant isotopes for zinc and sulphur are at atomic mass numbers 64 and 32 respectively. Doubly ionized zinc atoms contribute to the sulphur peak at a mass-to-charge ratio of 32 and S_2 molecules add to the peak for zinc at 64. A further difficulty arises because the transit times for zinc and sulphur particles through the system are either quite similar or identical. Searches for sulphur molecules with an atomic mass number greater than 64 failed but there is the possibility of the sulphur peaks arising from fragmentation of larger molecules. Differentiating between S^+ and Zn^{++} ions proves relatively simple because the measured appearance potentials for the ions are 12.75V and 18.75V respectively. Measurements made at a mass-to-charge ratio of 32 with ionizing electron energies ranging from 9 eV to 20 eV yields a constant ion arrival time of 70μs at a source temperature of 1000°C. The TOF is indicative of $^{64}S_2$ being the neutral species present which fragments to give $^{32}S^+$ ions before travelling through the quadrupole ion filter.

Sulphur ions $^{64}S_2^+$ are inseparable from $^{64}Zn^+$ using mass spectrometer tuning, TOF or appearance potential measurements. The contribution of S_2 to the peak at mass-to-charge ratio 64 can be calculated using measured and published data about the relative abundancies of isotopes for the peaks at 32, 33, 64 and 66 /10/. A series of ion arrival time measurements have been made using a range of electron energies (9-20eV). It is found that the TOF remains constant while the proportion of $^{64}S_2^+$ in the spectrum falls with

increasing energy. From the observations made, it is concluded that the predominant sulphur species present in the evaporant stream is S_2 and that zinc sulphide, vapourises according to the following relationship:

$$2\ ZnS_{(Solid)} \rightarrow 2\ Zn_{(Gas)} + S_{2(Gas)}$$

Conclusions

A modulated beam mass spectrometry system has been described which was initially developed to make accurate particle flux density measurements for the deposition control of zinc sulphoselenide films. It has been found that the TOF for evaporant particles can be observed with the equipment and it is suggested that the success of the system results from the quadrupole filter only accepting ions from a very small volume of the spectrometer's ionization chamber.

An investigation performed using the equipment has shown that both ZnS and ZnSe vapour sources produce mono-atomic zinc particles while sulphur and selenium are predominantly in di-atomic form.

Films with a large range of zinc sulphoselenide alloy composition have recently been prepared and at present the structural properties are being investigated for future publications.

Acknowledgements

The authors wish to thank Dr Tom Foxon of Philips Research Laboratories, Redhill for his help and encouragement at the start of the project. The work was undertaken with support from the Science and Engineering Research Council, (U.K.) and one author (MB) has been supported by a grant from the Ministry of Higher Education (Algeria).

References

/1/ M Benyezzar, D King, P L Jones and D Moore, Vacuum, (to be published)

/2/ W L Fite and R T Brackman, Physical Review, 112 (1958) 1141

/3/ R H Jones, D R Olander, W J Siekhans and J A Schwarz, J Vac. Sci. Technol., 9 (1972) 1429

/4/ C T Foxon, J A Harvey and B A Joyce, J Phys. Chem. Solids, 34 (1973) 1693

/5/ C T Foxon, B A Joyce, R F C Farrow and R M Griffiths, J Phys. D: Appl. Phys., 7 (1974) 2422

/6/ A J Cooper, A S Sahin, P L Jones, D King and D Moore, Vacuum, 10/11 (1984) 925

/7/ J Jeans, Kinetic Theory of Gases, Cambridge University Press, 1960

/8/ M Aven and J S Prener, Physics and Chemistry of II-VI Compounds, North-Holland, Amsterdam, 1967

/9/ R I Reed, Mass Spectrometry, Academic Press, London, 1965

/10/ R P Gregory, P L Jones, D King and D Moore, Vacuum, 38 (1988) 737

FIGURE 1

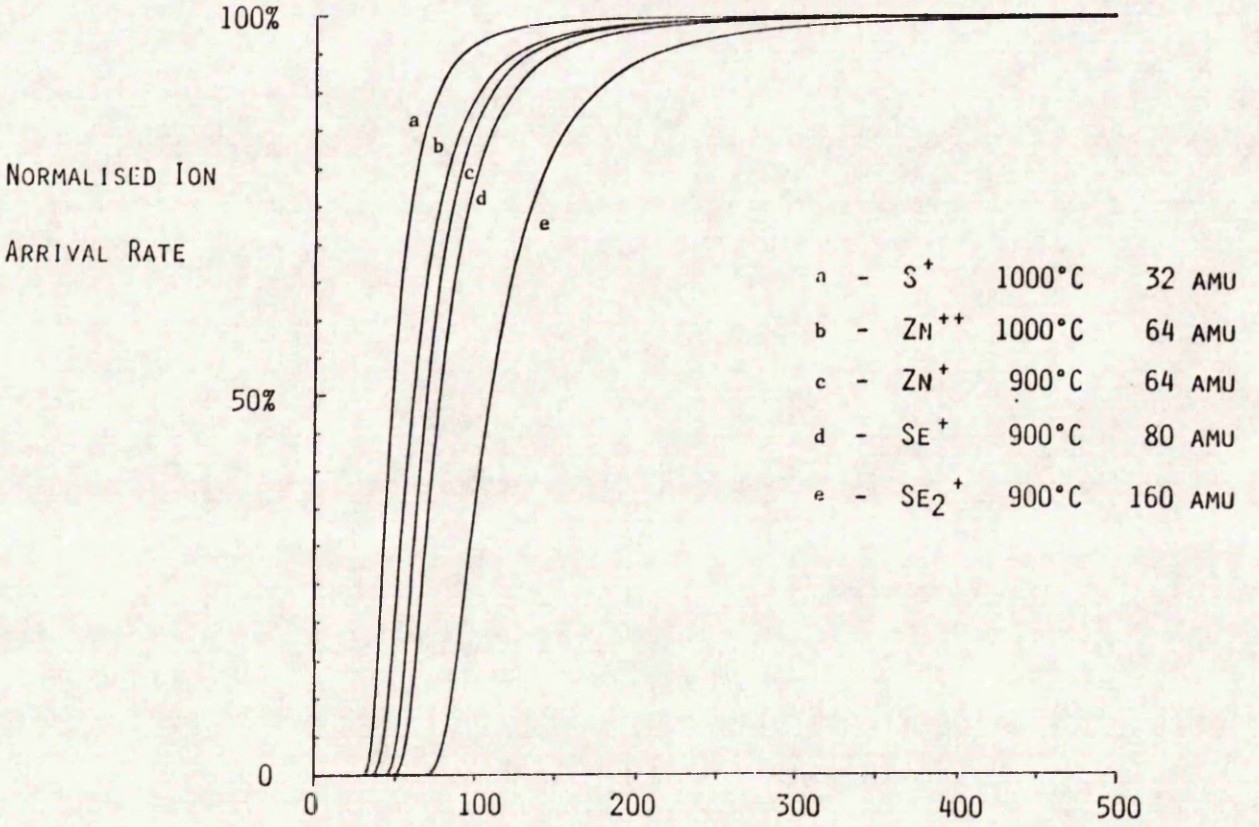

CALCULATED ION ARRIVAL CURVE

FIGURE 2

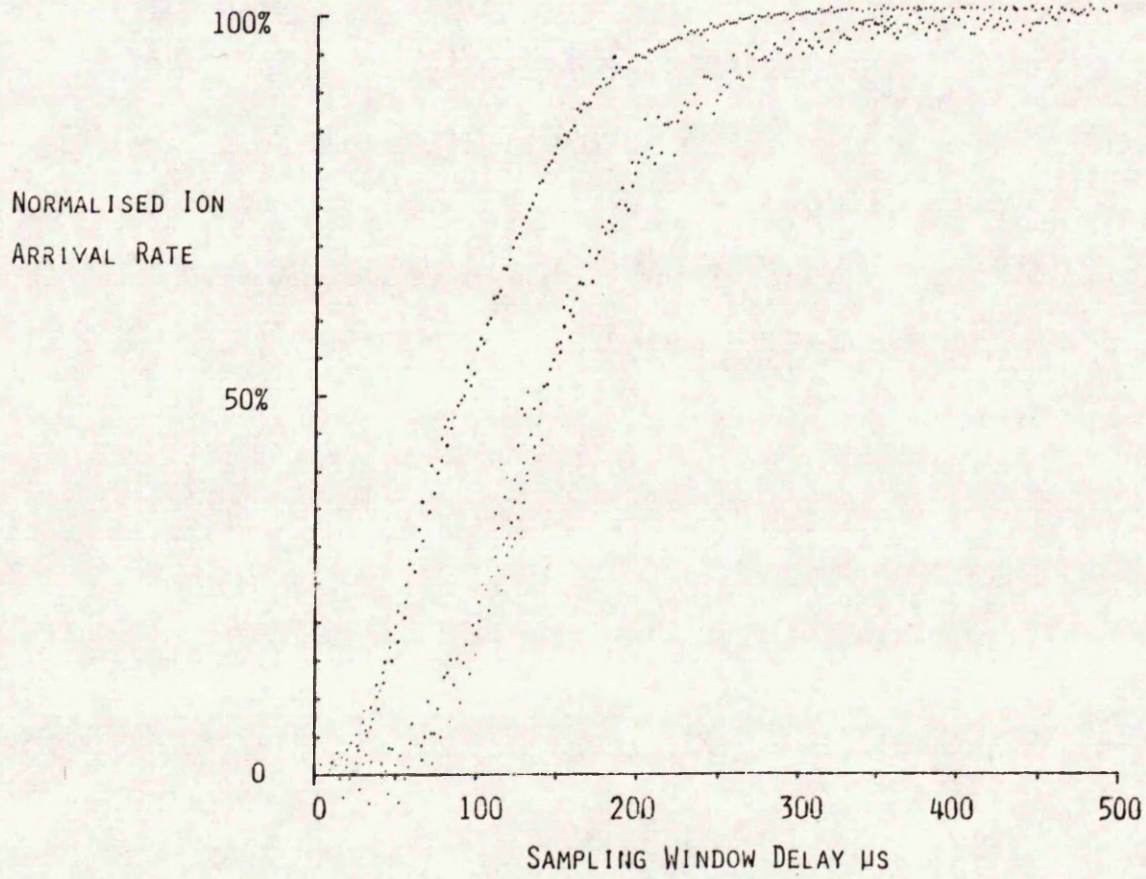

MEASURED ION ARRIVAL CURVES, SAMPLING WINDOW 6.4 µS AND SOURCE TEMPERATURE 900°C

FIGURE 3(A)

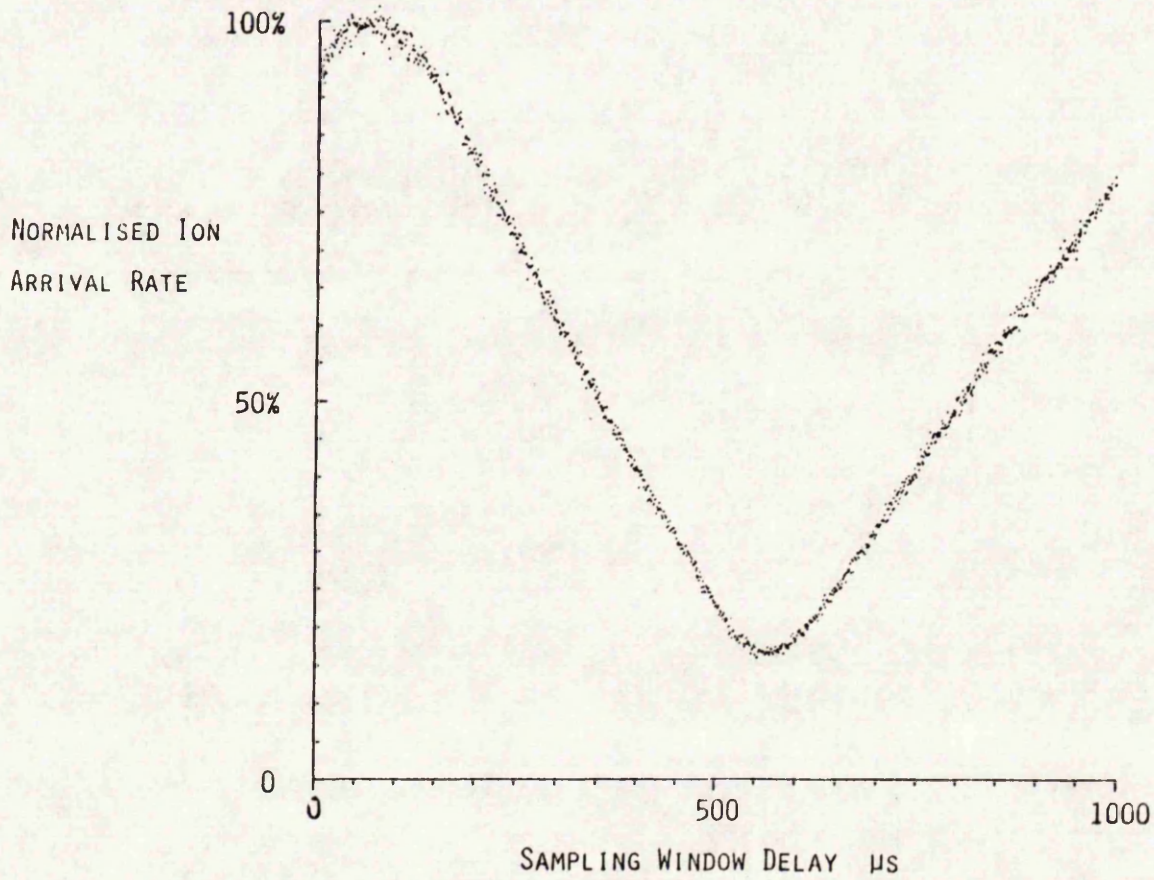

MEASURED ION ARRIVAL CURVES FOR Zn^+, T/2 SAMPLING WINDOW AND SOURCE TEMPERATURE 925°C

FIGURE 3(B)

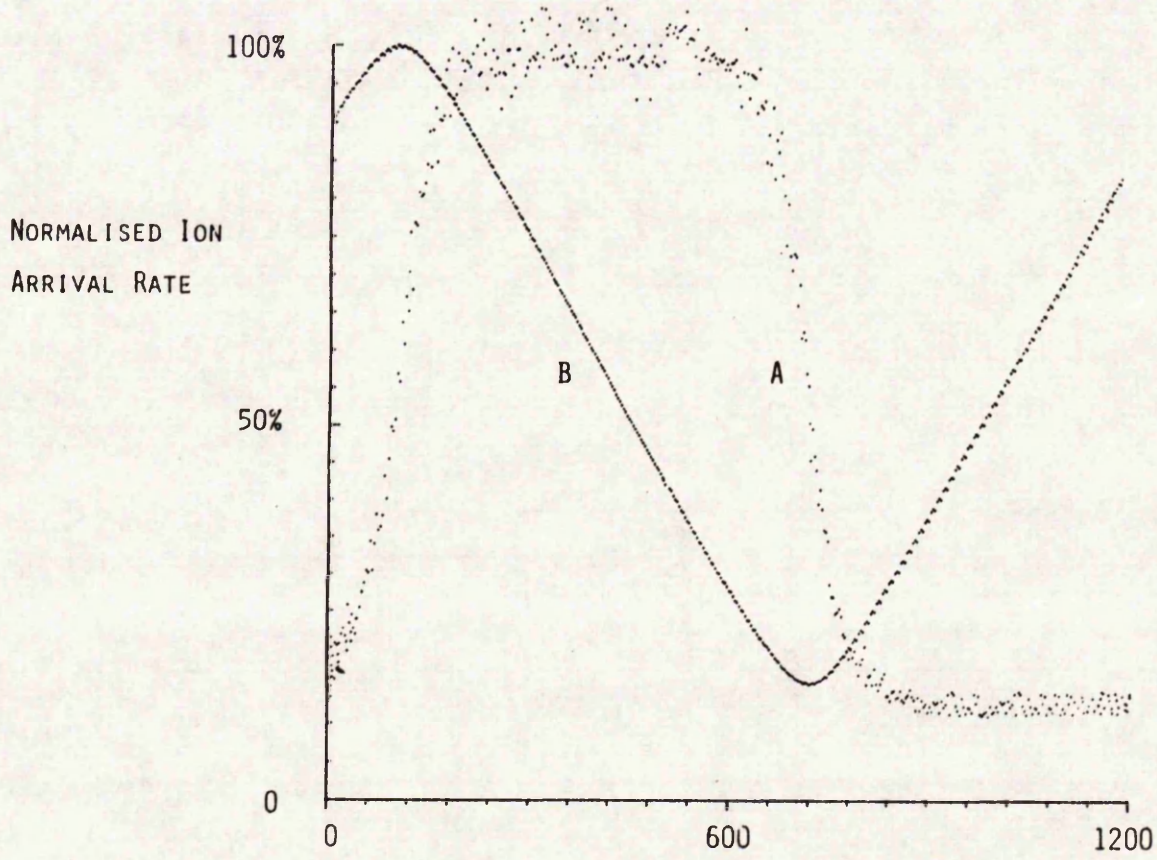

ION ARRIVAL CURVE FOR T/2 WINDOW (CURVE B) CALCULATED FROM MEASURED 6.4 μs WINDOW RESULTS (CURVE A)
SOURCE TEMPERATURE 925°C AND MEASUREMENTS ON Zn^{++}